



UNIVERSITÀ DI PISA

School of Engineering

Department of Information Engineering

MASTER'S DEGREE IN ROBOTICS AND AUTOMATION ENGINEERING

MASTER'S THESIS

DYNAMIC QUALITY ESTIMATION OF WIRELESS LINKS WITH AUTONOMOUS AGENTS

Supervisors:

Prof. Giorgio Carlo BUTTAZZO
Prof. Luis ALMEIDA

Author:

Livio BISOGNI

February 23, 2023

Abstract

Wireless Sensor Networks (WSNs) have become increasingly prevalent in various fields such as environmental monitoring, surveillance, and industrial automation. These networks consist of nodes with limited resources that wirelessly communicate to stream sensor data to a ground station. Packet Delivery Ratio (PDR) is a performance metric that evaluates a network quality of service (QoS) by measuring the proportion of successfully delivered packets to their destination among all packets sent. A high PDR value indicates efficient packet delivery, while a low PDR value indicates poor performance due to packet loss.

Relay nodes play a crucial role in Wireless Sensor Networks by forwarding data from a source node, such as a sensing node, to a destination, such as a ground station. The proper placement of these relay nodes can significantly impact the network overall performance. In particular, for the operation of autonomous agents, such as unmanned aerial vehicles (UAVs) in Flying Ad-hoc NETworks (FANETs), efficient relay placement and robust wireless communication are crucial.

This thesis investigates the online dynamic estimation of wireless link quality using autonomous agents, with a focus on detecting changes in the link models. Additionally, the thesis presents and compares various relay placement strategies in complex scenarios to optimize the network PDR. Three relay placement strategies are proposed for wireless line networks: equidistant placement, equal-PDR placement, and optimal placement, which maximizes the overall network PDR. The study also compares the strategies in different simulated scenarios. The findings show that the optimal placement strategy outperforms the others and is considered the recommended strategy for relay placement in any wireless line network.

Keywords: wireless communication, line network, channel model, packet delivery ratio, PDR, model change detection, unmanned aerial vehicle, UAV

Acknowledgements

I would like to take this opportunity to express my gratitude to everyone who has supported and encouraged me during the completion of this project.

Firstly, I am deeply grateful to my esteemed supervisors, Prof. Buttazzo and Prof. Almeida, for their invaluable guidance, expertise, and encouragement throughout the research. Their support and encouragement have been critical in shaping the direction of this work.

I would also like to extend my sincere thanks to my friends and colleagues who have supported me with their ideas, feedback, and insights. In particular, I would like to thank Miguel for his valuable contributions and insightful suggestions that have helped to shape this thesis.

I would like to express my deepest appreciation to my family for their unwavering support, love, and encouragement throughout my academic journey. Their constant encouragement, care, and support have been instrumental in achieving this milestone.

Lastly, I want to acknowledge the enduring wisdom of Monty Python and thank Brigitte for being an inspiration in more ways than one. Thank you, Brigitte.

Once again, thank you all for your support and encouragement.

Livio Bisogni, World, February 2023.

To my family

Contents

Nomenclature	xi
List of Figures	xv
List of Tables	xix
List of Algorithms	xxi
1 Introduction	1
1.1 Motivation	1
1.2 Contributions	3
1.3 Thesis Layout	4
2 Network Background	5
2.1 Relay Networks	5
2.2 Line Network Topology	6
2.3 PDR in Wireless Networks	8
2.3.1 TDMA	8
2.3.2 PDR Measurement	9
2.3.3 Wireless Link PDR Model	10
2.3.4 Weighted Line Network	13
3 Methodology	15
3.1 Problem Statement	15
3.2 Data Fitting	16
3.2.1 Non-Linear Least Squares	17
3.2.2 Fitting Weights	18
3.3 Model Change Detector	19
3.3.1 Model Change Detection	19
3.3.2 Sample Size	21
3.4 Packet Types and Payloads	22
3.4.1 Data Packet	24
3.4.2 Upstream Report Packet	24
3.4.3 Downstream Report Packet	25
3.4.4 Network Status Packet	26
3.4.5 Node Status Packet	26
3.5 Relay Placement Strategies	27
3.5.1 Equidistant Relay Placement	28
3.5.2 Equal-PDR Relay Placement	28
3.5.3 Optimal Relay Placement	30
3.6 Overview of Network Nodes	34
3.6.1 Source	34

3.6.2	Relay	34
3.6.3	Ground Station	34
4	Experimental Design and Simulation	37
4.1	Simulation Software	38
4.2	Waypoints	38
4.3	Modeling Link PDRs	43
4.3.1	Link Models	43
4.3.2	Simulation Scenarios	45
4.3.3	Estimation Error	53
5	Results and Analysis	55
5.1	Link Model Estimates	55
5.1.1	Scenario ‘a’	56
5.1.2	Scenario ‘b’	60
5.1.3	Scenario ‘c’	64
5.1.4	Scenario ‘d’	68
5.1.5	Summary	72
5.2	Network PDR Analysis	75
5.2.1	Scenario ‘a’	75
5.2.2	Scenario ‘b’	83
5.2.3	Scenario ‘c’	90
5.2.4	Scenario ‘d’	97
5.2.5	Summary	104
6	Conclusion	109
6.1	Summary	109
6.2	Future Work	110
Bibliography		111

Nomenclature

List of Symbols

α	Steepness of the link PDR curve
η_N	Reduction factor of N , the sample size
η_P	Acceptable packet loss ratio for the link from the ground station's neighbor and the ground station before activating a new relay
η_R	Reduction factor of \hat{R} , the estimated length of the link at which the PDR is 50%
λ	Node longitude
\mathbf{d}	Relay placement (vector of link lengths)
WRMSE	Weighted Root Mean Square Error
ϕ	Node latitude
Ψ	Cf. Equations (3.35) and (3.34)
ρ	Threshold factor for the model change detector
τ	Observation length of the model change detector
θ	Cf. Equations (3.35) and (3.34)
θ^{bear}	Bearing angle
ε	Residual, in the non-linear least squares fitting
ξ	Estimation error index
ζ	Network throughput
d	Link length
D_i	Model change detection indicator
E	Edge set in graph G
e	Edge in E
G	Graph
h	Node altitude
$H^{\text{in},1}$	Set of in-neighboring nodes within a 1-hop distance

$H^{\text{out},1}$	Set of out-neighboring nodes within a 1-hop distance
i	Index of the node, in $V = \{1, \dots, n\}$
k	TDMA round period index
k^A	TDMA round, as recorded by the ground station, at which the source reaches waypoint 'A'
k^B	TDMA round, as recorded by the ground station, at which the source reaches waypoint 'B'
k^C	TDMA round, as recorded by the ground station, at which the source reaches waypoint 'C'
L	Total network length
m	Index of the sample
N	Sample size
n	Number of nodes
$N^{(\text{r})}$	Number of packets received
$N^{(\text{s})}$	Number of packets sent
P	Link PDR (Packet Delivery Ratio)
P_{net}	Network PDR (also referred to as end-to-end PDR)
R	Link length at which the link PDR is 50%
r	Node position
S	Residual sum of squares, in the non-linear least squares fitting
s	Slot length
T	TDMA round period length
t_{sim}	Simulation time
V	Vertex set in graph G
v	Vertex in V
w	Weights of graph G
w_{fit}	Fitting weights

List of Subscripts

$e = \{u, v\}$ Link in E from u to v , with u, v two nodes in V

GS	Ground Station node
i	Index of the node, in $V = \{1, \dots, n\}$

List of Superscripts

$x^{\text{DRP,e}}$	Variable x obtained through the use of the dynamic relay placement strategy, with estimated parameters
$x^{\text{DRP,t}}$	Variable x obtained through the use of the dynamic relay placement strategy, with true parameters
x^{DRP}	Variable x obtained through the use of the dynamic relay placement strategy
$x^{\text{equalPDR,e}}$	Variable x obtained through the use of the equal-PDR relay placement strategy, with estimated parameters
$x^{\text{equalPDR,t}}$	Variable x obtained through the use of the equal-PDR relay placement strategy, with true parameters
x^{equalPDR}	Variable x obtained through the use of the equal-PDR relay placement strategy
x^{equi}	Variable x obtained through the use of the equidistant relay placement strategy

List of Accents

\bar{x}	Mean of the variable x (possibly weighted)
\hat{x}	Estimation of the variable x
\tilde{x}	Measurement of the variable x

List of Acronyms

DGPS	Differential Global Positioning System
DRP	Dynamic Relay Placement
EMI	ElectroMagnetic Interference
FANET	Flying Ad-hoc NETwork
GPS	Global Positioning System
GS	Ground Station (also referred to as control station, base station)
PDR	Packet Delivery Ratio
PID	Proportional–Integral–Derivative controller
PLR	Packet Loss Ratio

QoS	Quality of Service
RF	Radio Frequency
RSS	Received Signal Strength
Rx	Receiver
TDMA	Time-Division Multiple Access
TPO	Transmitter Power Output
Tx	Transmitter
UAV	Unmanned Aerial Vehicle
UID	Unique IDentifier
Wi-Fi	The IEEE 802.11 family is referred to as Wi-Fi
WSN	Wireless Sensor Network

Miscellaneous

cf.	<i>confer</i> , Latin for “compare”
e.g.	<i>exempli gratia</i> , Latin for “for example”
et al.	<i>et alii</i> , Latin for “and others”
i.e.	<i>id est</i> , Latin for “that is”
w.r.t.	with reference to

List of Figures

1.1	AR Drone 2.0 take-off	2
1.2	AR Drone 2.0 flight	3
2.1	Upstream and downstream nodes in a topology	7
2.2	Network topology example	7
2.3	Line network	8
2.4	Packet transmissions using TDMA	10
2.5	PDR measurement process	11
2.6	Packet Delivery Ratio as a function of link length	12
2.7	Weighted line network	13
3.1	Fitting weights	19
3.2	Rejection vs. non-rejection region	21
3.3	Relay placement in a dual-link line network	27
3.4	Relay placement: optimal vs. equidistant vs. equal PDR	33
3.5	Source node process flow	34
3.6	Relay node process flow	35
3.7	Source node process flow	36
4.1	Source traversal of waypoints	41
4.2	Graphical representation of waypoints	42
4.3	The simulation scenarios	46
4.4	Weighted graph of the case-study line network	47
4.5	Time evolution of the actual link models in scenario ‘a’	48
4.6	Time evolution of the actual link models in scenario ‘b’	49
4.7	Time evolution of the actual link models in scenario ‘c’	50
4.8	Time evolution of the actual link models in scenario ‘d’	51
4.9	Equidistant placement strategy in scenario ‘a’	52
4.10	Fitting comparison with estimation error index	54
5.1	Estimates of PDR model parameters for the DRP strategy in scenario ‘a’, links {4, 5} and {5, 6}	57
5.2	Estimated vs. actual link models for the DRP strategy in scenario ‘a’, links {4, 5} and {5, 6}	58
5.3	Time evolution of the estimated link models for the DRP strategy in scenario ‘a’, links {4, 5} and {5, 6}	59
5.4	Estimates of PDR model parameters for the DRP strategy in scenario ‘b’, links {4, 5} and {5, 6}	61
5.5	Estimated vs. actual link models for the DRP strategy in scenario ‘b’, links {4, 5} and {5, 6}	62
5.6	Time evolution of the estimated link models for the DRP strategy in scenario ‘b’, links {4, 5} and {5, 6}	63

5.7	Estimates of PDR model parameters for the DRP strategy in scenario ‘c’, links {4, 5} and {5, 6}	65
5.8	Estimated vs. actual link models for the DRP strategy in scenario ‘c’, links {4, 5} and {5, 6}	66
5.9	Time evolution of the estimated link models for the DRP strategy in scenario ‘c’, links {4, 5} and {5, 6}	67
5.10	Estimates of PDR model parameters for the DRP strategy in scenario ‘d’, links {4, 5} and {5, 6}	69
5.11	Estimated vs. actual link models for the DRP strategy in scenario ‘d’, links {4, 5} and {5, 6}	70
5.12	Time evolution of the estimated link models for the DRP strategy in scenario ‘d’, links {4, 5} and {5, 6}	71
5.13	Estimation error indices for different strategies and scenarios	74
5.14	UAV trajectories in scenario ‘a’ for DRP (with estimated parameters) strategy	76
5.15	UAV trajectories in scenario ‘a’ for different strategies	77
5.16	Link and network PDRs for equidistant strategy in scenario ‘a’	78
5.17	Link and network PDRs for equal-PDR (with estimated parameters) strategy in scenario ‘a’	79
5.18	Link and network PDRs for equal-PDR (with true parameters) strategy in scenario ‘a’	80
5.19	Link and network PDRs for DRP (with estimated parameters) strategy in scenario ‘a’	81
5.20	Link and network PDRs for DRP (with true parameters) strategy in scenario ‘a’	82
5.21	UAV trajectories in scenario ‘b’ for DRP (with estimated parameters) strategy	83
5.22	UAV trajectories in scenario ‘b’ for different strategies	84
5.23	Link and network PDRs for equidistant strategy in scenario ‘b’	85
5.24	Link and network PDRs for equal-PDR (with estimated parameters) strategy in scenario ‘b’	86
5.25	Link and network PDRs for equal-PDR (with true parameters) strategy in scenario ‘b’	87
5.26	Link and network PDRs for DRP (with estimated parameters) strategy in scenario ‘b’	88
5.27	Link and network PDRs for DRP (with true parameters) strategy in scenario ‘b’	89
5.28	UAV trajectories in scenario ‘c’ for DRP (with estimated parameters) strategy	90
5.29	UAV trajectories in scenario ‘c’ for different strategies	91
5.30	Link and network PDRs for equidistant strategy in scenario ‘c’	92
5.31	Link and network PDRs for equal-PDR (with estimated parameters) strategy in scenario ‘c’	93
5.32	Link and network PDRs for equal-PDR (with true parameters) strategy in scenario ‘c’	94
5.33	Link and network PDRs for DRP (with estimated parameters) strategy in scenario ‘c’	95

5.34 Link and network PDRs for DRP (with true parameters) strategy in scenario 'c'	96
5.35 UAV trajectories in scenario 'd' for DRP (with estimated parameters) strategy	97
5.36 UAV trajectories in scenario 'd' for different strategies	98
5.37 Link and network PDRs for equidistant strategy in scenario 'd'	99
5.38 Link and network PDRs for equal-PDR (with estimated parameters) strategy in scenario 'd'	100
5.39 Link and network PDRs for equal-PDR (with true parameters) strategy in scenario 'd'	101
5.40 Link and network PDRs for DRP (with estimated parameters) strategy in scenario 'd'	102
5.41 Link and network PDRs for DRP (with true parameters) strategy in scenario 'd'	103
5.42 Average network PDRs for different strategies and scenarios	105
5.43 Average link PDRs for different strategies and scenarios	107

List of Tables

3.1	Packet types	23
3.2	Packet-node mapping table	23
4.1	Source waypoints	39
4.2	The model sets used for the simulations	44
5.1	Average estimation error: simulation results	73
5.2	Average network PDR: simulation results	104
5.3	Average link PDR: simulation results	106

List of Algorithms

1	Distributed Equidistant Relay Placement Algorithm	28
2	Distributed Equal-PDR Relay Placement Algorithm	30
3	Distributed Optimal Relay Placement (DRP) Algorithm	32

1 Introduction

This chapter begins with the motivation for the research in Section 1.1. It then reviews the relevant literature and outlines the research questions and objectives. After presenting the main contributions in Section 1.2, the chapter concludes with an overview of the structure of the entire thesis in Section 1.3.

1.1 Motivation

An autonomous agent is a computational system that operates independently in a complex dynamic environment, sensing and acting on it to achieve a set of tasks on behalf of its owner. The advancement of technology has led to an increasing interest in the development of autonomous systems that can operate with limited human intervention. Autonomous agents, in particular, have become increasingly popular in various domains such as transportation, agriculture, and surveillance. In the field of wireless communications, their use has grown with the rise of unmanned aerial vehicles (UAVs).

In fact, Unmanned Aerial Vehicles (UAVs) have gained popularity for a variety of applications, ranging from leisure activities such as aerial photography and videography, to critical monitoring tasks such as search and rescue, environmental monitoring, disaster response, and inspection of large facilities [1]. These aircraft are equipped with various sensors, including gyroscopes, accelerometers, magnetometers, tilt sensors, GPS, optical cameras, multispectral cameras, thermal sensors, and more. Wi-Fi cards enable UAVs to communicate with a ground station and with each other, from a transmitter (Tx) to a receiver (Rx). When the received signal strength (RSS) decreases, communication issues may arise, and packets can be lost. This is mainly due to four possible non-mutually-exclusive causes: Tx-Rx relative orientation, Tx-Rx relative distance, packet size, and external interference.

Antenna directionality is the main cause of orientation-related RSS losses and can be addressed by knowing the relative orientations of the receiver and the transmitter and properly re-orienting them. In fact, the parallel orientation yields a higher number of received packets than the collinear orientation [2]. The received signal strength in free space is inversely proportional to the square of the distance of the receiver-transmitter antennas, which is the main factor responsible for distance-related RSS losses [3]. Also, the length of a message affects the probability of packet delivery, and smaller packet lengths increase the likelihood of successful transmissions [4]. All of these three factors can be directly controlled.

However, external interference, which is caused by a congested RF environment or physical obstructions, is beyond direct control and may cause RSS losses that limit the usable range between the transmitter and receiver. Materials such as electrical conductors, which absorb and reflect signals, and insulating materials, which do not refract them, contribute to physical obstruction-related interference.

Furthermore, interference varies in space and time, resulting in interference zones and environmental changes that affect Wi-Fi signal strength.

The quality of a network link can thus be affected by changes in transmitter power output, transmitter-receiver relative orientation or distance, and external interference, resulting in link asymmetries. As wireless network links are inherently non-symmetric, symmetric placement is generally not optimal. In fact, the maximum throughput is often achieved in positions other than the center position [5]. For the line network topology, to ensure maximum end-to-end received packets while maintaining equal total network length and number of nodes, it is crucial to determine the optimal relay placement [2, 6, 7]. Lu et al. [8] proposed a dynamic relay network deployment model that uses prediction to achieve higher communication quality with fewer UAV relays. However, open problems still exist, such as effectively estimating online, in a distributed context, and in the presence of interference, the parameters that describe the link models. Additionally, detecting changes in the link models is non-trivial [9]. This work aims to address these challenges.

Figures 1.1 and 1.2 depict two images of the Parrot AR Drone 2.0 platform, a quadrotor used in [2] to conduct wireless communication experiments between two drones. The findings of these experiments were utilized in this work. More information about the AR Drone 2 can be found on the manufacturer’s website [10].



Figure 1.1. Take-off of an AR Drone 2.0; the platform is equipped with an indoor hull [11].

Packet Delivery Ratio (PDR) represents the likelihood of a packet being successfully delivered from a transmitter to a receiver over a single-link channel. PDR decreases when packet losses occur, and it can range between 0% (no packets received) and 100% (all packets received). In [13], the single-link PDR between a transmitter and receiver on a pair of UAVs was modeled as a non-negative, strictly non-increasing curve that depends on two parameters to be estimated and the link length. For a line network, the network PDR is the product of all single-link PDRs, which are determined by the relay placement. Our goal is to achieve the optimal network PDR, which is obtained by finding the optimal relay placement that maximizes the



Figure 1.2. Flight of an AR Drone 2.0; the platform is without indoor hull [12].

network PDR. To attain this objective, obtaining accurate estimates of the two model parameters – which are necessary for the optimal placement strategy – is essential.

Efficient relay placements and robust wireless communication are crucial for the operation of autonomous agents. This thesis aims to investigate the dynamic estimation of the quality of wireless links using autonomous agents, with a focus on detecting changes in link models. Additionally, the thesis aims to design, implement, and compare various algorithms for relay placement strategies in complex scenarios.

1.2 Contributions

The primary contributions of the thesis are:

- The deployment of a reliable method for measuring link and network Packet Delivery Ratio (PDR).
- The development of a distributed relay placement strategy that ensures equal link PDRs among neighboring nodes.
- The implementation of three relay placement strategies in a distributed manner, enabled by the design of multiple packet formats that facilitate relay placement.
- The estimation of link PDR models from PDR measurements, along with the proposal of a metric for quantifying the estimation error.

- The design of a model change detector that can detect changes in the link PDR models.
- A solution for handling situations where communication between nodes ceases.
- A comparison of the presented relay placement strategies.
- The development of a C program on a Linux machine that incorporates all the aforementioned contributions.

1.3 Thesis Layout

The thesis is structured into six chapters. Chapter 2 provides background information on network topologies, specifically relay networks, and the line network topology. It also discusses packet delivery ratio (PDR) in wireless networks, time-division multiple access (TDMA), PDR measurement, wireless link PDR models, and the weighted line network. Chapter 3 presents the methodology, which includes the problem statement, data fitting techniques, a model change detector, packet types and payloads, and relay placement strategies. Additionally, it provides an overview of the network nodes. Chapter 4 details the simulation setup, the evaluation metrics, and the simulation results. Chapter 5 presents the results, including an analysis of the data fitting accuracy, the effectiveness of the model change detector, and the performance of the relay placement strategies. Chapter 6 concludes the thesis by summarizing the main findings and contributions, discussing their implications, and suggesting future research directions.

2 Network Background

This chapter provides an overview of the concepts and methodology used in this study to measure the packet delivery ratio (PDR), model transmission link behavior, and analyze the performance of wireless line networks. The chapter begins with an introduction to relay networks in Section 2.1, followed by a discussion of the graph notation adopted in Section 2.2. Then, in Section 2.3, the chapter focuses on the measurement process of PDR in wireless networks, for both a single link and an entire line network. Finally, this section presents a model for wireless link PDR and introduces the concept of weighted line networks, which is crucial for subsequent chapters.

2.1 Relay Networks

Data transfer from one or more senders to one or more recipients is made possible through networks. The data is generated by the sender, which then packs it into one or more packets for transmission over the network, using a wireless or wired communication protocol. Once the receiver receives the data, the latter decodes it before processing and consuming it. Relay networks are a type of wireless network that use intermediate nodes, called relays, to increase network performance and coverage. Relays in a relay network are in charge of forwarding data packets utilizing a multi-hop communication scheme from the source to the destination.

FANET (Flying Ad hoc NETwork) is a type of relay network consisting of a group of autonomous flying vehicles, such as UAVs. It is designed especially for dynamic and challenging environments, e.g., urban areas, remote regions, and disaster-stricken areas, where the traditional wireless infrastructure may not be available. Its main advantages are:

- High mobility: the ability of the flying vehicles to move in three dimensions enables them to effortlessly avoid obstacles.
- High flexibility: such networks can be created quickly, which is useful in response to unexpected events, such as natural disasters or emergency situations.
- Low deployment cost: as they do not require the deployment of any fixed infrastructure, FANETs are more cost-effective than traditional wireless networks.

However, given their aerial nature, there are additional challenges – less pronounced on terrestrial vehicles – to consider, such as:

- Limited energy: flying vehicles used in FANETs typically have limited energy resources, which requires careful energy management to extend the network lifetime.
- Limited stability: flying vehicles are significantly affected by the wind and weather conditions, thus impacting the stability of the network.

A Wireless Sensor Network (WSN) is a collection of low-power wireless nodes with sensing capabilities that are designed to gather and transmit environmental data for monitoring and control purposes. This data can be collected from a variety of sensors, including cameras, microphones, and temperature sensors onboard the nodes.

In our scenario, the network is a hybrid of a WSN and a FANET, where the UAVs comprise the FANET, and one of them acts as the WSN's sensor node, while others serve as relays. This configuration allows the sensor node to move around and collect data from various locations, while the other UAVs relay the data to the ground station, where it is received and processed. As a result, the environment can be monitored and controlled.

2.2 Line Network Topology

In our work, nodes are organized in a line network topology, i.e., a network where the nodes are arranged in a linear sequence, where each node is directly connected to only its immediate neighbors. More in detail:

1. The source is the sensing node, at one tip of the network (it has only one neighbor, a downstream node), responsible for generating data, e.g., a video stream.
2. The ground station, at the opposite tip of the network w.r.t. the source (it has only one neighbor, an upstream node), is a fixed remote point dedicated to receiving the data sent from the source.
3. The $n - 2$ relays are the intermediate nodes, the only ones with two neighbors: one upstream and one downstream node. Their mission is to deliver packets to – and to a lesser extent from – the ground station.

When there is only one sensing node, the majority of packets typically flow in a single direction, from the source to the ground station. Packets in the opposite direction, e.g., for network status updates, are less frequent. The scenario of a flipped line network, in which the links are reversed and flow is directed from the ground station to the source, will not be studied in detail because the main focus is on optimizing the data flow from the source to the ground station. Ultimately, although less important, it should be noted that data flow can also occur in the opposite direction.

Nodes can be identified by a univocal number i , $i \in \{1, \dots, n\}$, called Unique IDentifier (UID). This way, it is possible to model the connections in a network by using a directed graph $G(V, E)$, where $V = \{v_1, \dots, v_n\}$ is the set of n vertices representing the UIDs, and $E = \{e_1, \dots, e_m\}$, $E \subseteq V \times V$, is the set of edges representing the wireless links. A simple network made of two nodes, i and j , and one link, $\{i, j\}$, is reported in Figure 2.1. i is called the upstream node (the tail of the link), whereas j is called the downstream node (the head of the link). It should be observed that, in general, j cannot communicate with i , since $\{i, j\}$ is a direct edge; in order for j to communicate with i , the link $\{j, i\}$ must be present as well. An example of a more complex network, with $n = 10$ nodes, is reported in figure 2.2.

A hop is a single step in the data transmission process from a source device to a destination device. It occurs whenever data is transferred from one device to another. The number of hops data must take to reach its destination is called the hop count. In a directed graph, it is useful to differentiate the immediate (one-hop distant) neighbors of a node, v_i . The set of nodes that can be reached by following an outbound edge from the node is called out-neighboring nodes and represented by $H_{v_i}^{\text{out},1}$. The set of nodes that can be reached by following an inbound edge to the node is called in-neighboring nodes and represented by $H_{v_i}^{\text{in},1}$. The cardinality of $H_{v_i}^{\text{out},1}$ is known as outdegree while the cardinality of $H_{v_i}^{\text{in},1}$ is known as indegree. When not specified otherwise, the generic term "neighbor" refers to both out-neighboring and in-neighboring nodes.

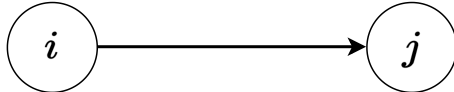


Figure 2.1. i , the upstream node, and j , the downstream node, connected by the edge $\{i, j\}$. i is the tail of the link, whereas j is the head. The link $\{i, j\}$ is an outbound link for i and an inbound link for j . Their respective one-hop out-neighboring sets are $H_i^{\text{out},1} = j$ and $H_j^{\text{out},1} = \emptyset$, and their one-hop in-neighboring sets are $H_i^{\text{in},1} = \emptyset$ and $H_j^{\text{in},1} = j$.

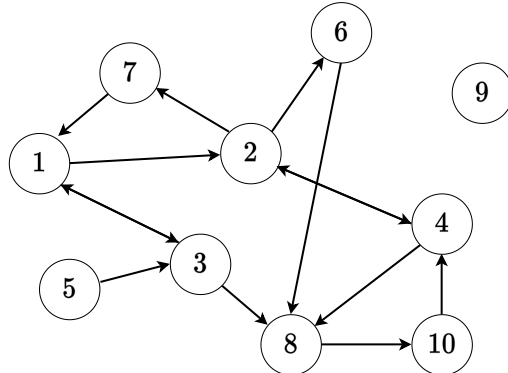


Figure 2.2. Example of a network topology created with $n = 10$ links and $m = 14$ links. $V = \{1, 2, 3, 4, 5, 6, 7, 8, 9, 10\}$, $E = \{\{1, 2\}, \{1, 3\}, \{2, 4\}, \{2, 6\}, \{2, 7\}, \{3, 1\}, \{3, 8\}, \{4, 2\}, \{4, 8\}, \{5, 3\}, \{6, 8\}, \{7, 1\}, \{8, 10\}, \{10, 4\}\}$. The one-hop out and in-neighbors of the node 2 are $H_2^{\text{out},1} = \{4, 6, 7\}$ and $H_2^{\text{in},1} = \{1, 4\}$, respectively.

Without loss of generality, we can assign the UIDs as depicted in Figure 2.3: 1 to the source, $2, \dots, n - 1$ to the relays, and n to the ground station. Following this convention, in a line network, the one-hop neighbor sets are outlined in Equations (2.1) and (2.2), respectively.

$$H_i^{\text{out},1} = \begin{cases} \{i + 1\}, & \text{if } i = 1, \dots, n - 1 \\ \emptyset, & \text{if } i = n \end{cases} \quad (2.1)$$

$$H_i^{\text{in},1} = \begin{cases} \{i - 1\}, & \text{if } i = 2, \dots, n \\ \emptyset, & \text{if } i = 1 \end{cases} \quad (2.2)$$



Figure 2.3. In a line network, packets flow from the source (node 1) to the ground station (node n) via $n - 2$ relays (nodes $2, \dots, n - 1$).

It is worth noting that the graph G is dynamic; in fact, nodes can be added to or removed from the network. In a typical situation:

1. At the beginning, the network is constituted of only $n = 1$ nodes, the ground station.
2. Then, the source is added.
3. When deemed appropriate, as discussed in more detail in Subsection 3.4.2, a relay is added.

2.3 PDR in Wireless Networks

In networking, Packet Delivery Ratio (PDR) is a performance metric that measures the proportion of packets successfully delivered to their destination among all the packets sent. It is used to evaluate a network quality of service (QoS), specifically in wireless networks. PDR is calculated by dividing the number of packets delivered by the total number of packets sent. A high PDR value indicates that the network is performing well and delivering packets efficiently, whereas a low PDR value indicates that the network is experiencing packet loss and poor performance. It is typically expressed as a percentage and can be used to estimate the reliability of the link. It is worth mentioning that PDR is not a bi-directional quantity: swapping the endpoints results in a different link, hence: $P_{i,j} \neq P_{j,i}$.

The authors in [14] reviewed the most common methods for estimating PDR and proposed a new one. The approach followed in this thesis is based on counting the number of received hello/data messages¹ within a short time frame, such as less than a second. This method can provide accurate results, at the cost of being less energy-efficient, as it requires a large number of packets to be sent. The time window during which PDR is calculated can vary depending on the specific application and the requirements of the network. In general, it is calculated over a specific period to obtain a representative measurement of the network performance. A natural choice is using the TDMA period as the time window.

2.3.1 TDMA

Time-Division Multiple Access (TDMA) is a contention-free multiplexing method that enables multiple users to share a frequency band by dividing time into slots. Each transmitter (node i , $i = 1, \dots, n$) in the network is assigned a mutually-exclusive, collision-free slot s_i , identified by a unique sequential ID and a duration $s_i = \frac{T}{n}$, where T is the fixed-length duration of TDMA round periods. In order to transmit

¹PDR is affected by the packet length [15].

a packet, a node i first adds it to a queue. At regular intervals denoted by k_i , which correspond to TDMA round periods of duration T , the packets in the queue are transmitted through the air within the specified time frame of the assigned slot s_i . The TDMA layer monitors network delays that may affect incoming packets and the receiver node adjusts its TDMA slot phase to maintain a consistent sequence and minimize overlap.

A node can only send a new packet during its assigned slot s_i and only after its previous packet has been successfully transmitted. Additionally, the queued packet must be ready to be sent during the assigned TDMA time slot. The TDMA round period T remains constant, determining the regularity at which each node transmits. In this work, a round period of $T = 200$ ms was selected. Two nodes i and j can have different TDMA round indices, denoted by k_i and k_j , respectively. However, since they share the same TDMA round period T and are synchronized, their round indices are equal except for a certain offset.

Maintaining a fixed slot size s_i when links are asymmetrical results in an overflow of buffers and high rates of packet loss. To mitigate these issues, the TDMA scheme can be improved through the implementation of distributed variable slot sizes [16], based on the RA-TDMA (Reconfigurable and Adaptive TDMA) concept [17, 18]. In [19], a novel method called RA-TDMAs+ is introduced to define TDMA slots in the presence of interfering traffic without relying on a global clock. Additionally, [20] proposes a flexible approach for synchronizing UAVs in a network with a focus on reducing delays caused by buffering in the protocol stack and WiFi interface.

Figure 2.4 illustrates how packet transmissions are organized in a TDMA system with n nodes. Each node is assigned one slot per round and can transmit packets only during the assigned slot. In this figure, all slots have the same length. The figure shows three consecutive TDMA round periods, with indices $k_i - 1, k_i, k_i + 1$ and constant length T .

2.3.2 PDR Measurement

After defining the time window in which sent and received packets are counted, we can compute the instantaneous link Packet Delivery Ratio (PDR) from node i to node j . This is expressed in Equation (2.3) as the ratio of packets received at node j to packets sent by node i during a TDMA round period of length T , where the index of the round period is represented by k_j (receiver node perspective). In this equation, $N_j^{(r)}(k_j)$ represents the number of packets received by node j during the k_j -th round period, while $N_i^{(s)}(k_j)$ represents the number of packets sent by node i during the same period². $P_{i,j}(k_j)$ range between 0% (all packets sent by i are lost) and 100% (all packets sent by i are received by j).

$$P_{i,j}(k_j) = \frac{N_j^{(r)}(k_j)}{N_i^{(s)}(k_j)} \quad (2.3)$$

Its complementary is the instantaneous packet loss ratio, in Equation (2.4). It represents the proportion of packets that were not successfully delivered to their

²Receiver node perspective.

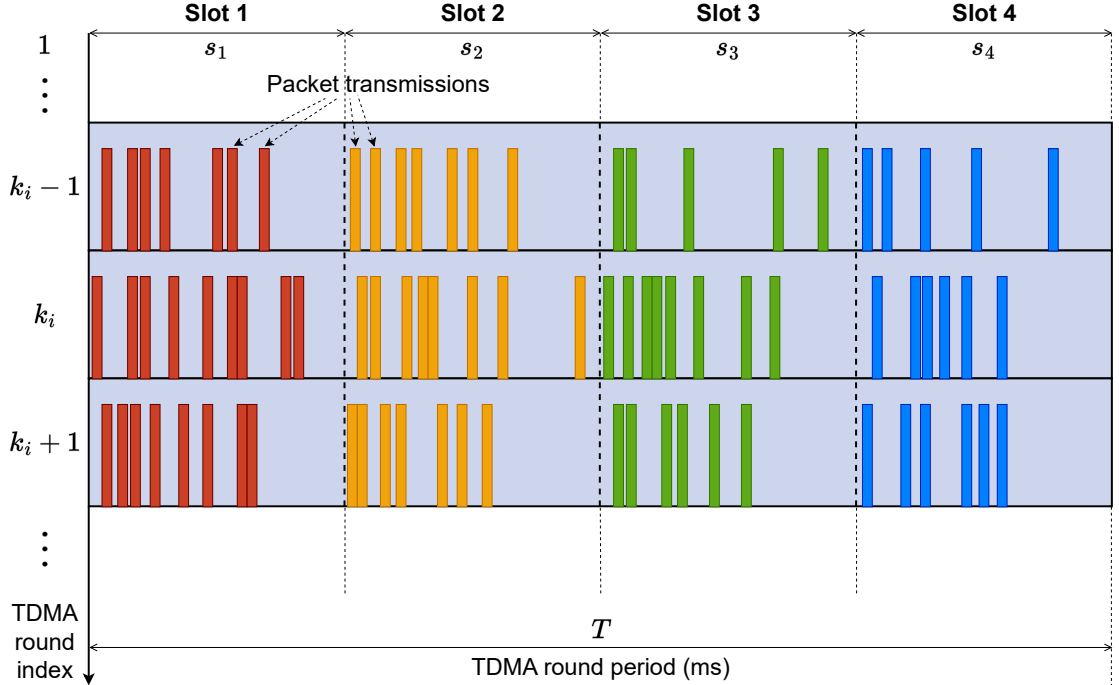


Figure 2.4. Packet transmissions using TDMA. Three consecutive TDMA round periods are shown, with indices $k_i - 1, k_i, k_i + 1$ and constant length T . Each node i ($i = 1, 2, 3, 4$) is assigned one slot per round, and packets can only be sent during the assigned slot, s_i . All slots have equal length $\frac{T}{n}$.

destination among all the packets sent.

$$1 - P_{i,j}(k_j) = \frac{N_i^{(s)}(k_j) - N_j^{(r)}(k_j)}{N_i^{(s)}(k_j)} \quad (2.4)$$

The PDR measurement process is illustrated in Figure 2.5. During TDMA round k_j , the receiver node (j) counts the packets received ($N_j^{(r)}(k_j)$) from the sender node (i). At the end of its round, the sender communicates the number of sent packets ($N_i^{(s)}(k_j)$) to the receiver. The instantaneous PDR of the link i, j at round k_j is the ratio of packets received to packets sent, $\frac{N_j^{(r)}(k_j)}{N_i^{(s)}(k_j)}$.

2.3.3 Wireless Link PDR Model

Distance plays an essential role in the quality of communication channels. To quantify this impact, the authors in [13] proposed a mathematical model that describes the packet delivery ratio (PDR) as a function of distance. If the positions of two nodes are known, they can compute the distance between themselves. Using a differential GPS (DGPS) called Piksi, developed by SwiftNav, node i can accurately determine its position with centimeter-level accuracy [21]. The node position r_i , $r_i \in \mathbb{R}^3$, can be expressed in a NED (North-East-Down) navigation frame as denoted in Equation (2.5), with the ground station serving as the reference point. In this navigation frame, the x unit vector is tangent to the meridian (north-south axis) and

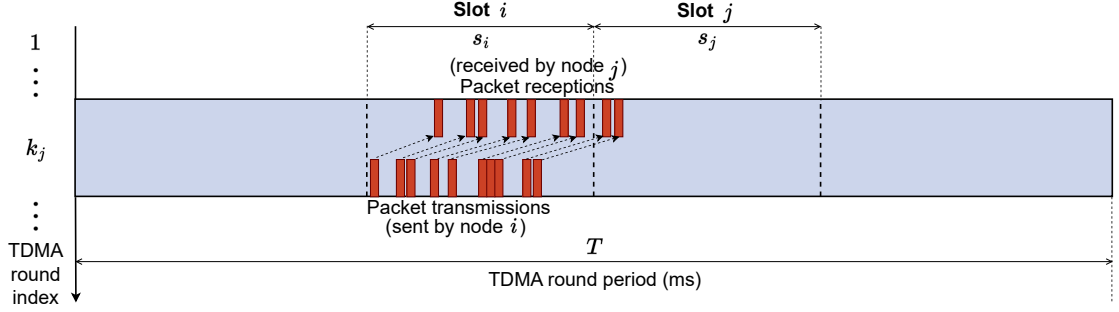


Figure 2.5. PDR measurement process, from the receiver (node j) perspective. During TDMA round k_j , the receiver node (j) counts the packets received ($N_j^{(r)}(k_j)$, drawn at the bottom center) from the sender node (i). At the end of its round, the sender communicates the number of sent packets ($N_i^{(s)}(k_j)$, drawn at the top center) to the receiver. The instantaneous PDR of the link $\{i, j\}$ at round k_j is the ratio of packets received to packets sent, $\frac{N_j^{(r)}(k_j)}{N_i^{(s)}(k_j)}$. In the figure the seventh packet sent was lost, resulting in an instantaneous PDR of $\frac{9}{10} = 90\%$ for the link $\{i, j\}$ at round k_j . This ratio can range from 0% (when all packets sent by i are lost) to 100% (when all packets sent by i are received by j). It should be noted that the reception of packets is not immediate, and the delay between sending a packet and its reception is not constant.

points towards the geographic north. The y unit vector is tangent to the parallel (east-west axis) and points towards the east. Finally, the z unit vector is normal to the WGS-84 ellipsoid of rotation (up-down axis) and points toward the ground.

$$r_i = \begin{bmatrix} x_i \\ y_i \\ z_i \end{bmatrix}, \quad i = 1, \dots, n \quad (2.5)$$

The distance between two nodes r_i and r_j on the Earth is not Euclidean. More precise distances, for example, the great-circle distance and Vincenty's formulae, can be used. However, for short distances, the distance between two points on the Earth can be approximately modeled as Euclidean (Equation (2.6)).

$$d_{i,j} = \|r_i - r_j\|_2 = \sqrt{(x_i - x_j)^2 + (y_i - y_j)^2 + (z_i - z_j)^2}, \quad i, j \in V \quad (2.6)$$

The link PDR of the link $\{i, j\}$ is the probability that a packet sent from node i will be successfully received by node j and is represented by $P_{i,j}$. The model proposed in [13], and reported in Equation (2.7), accounts for the distance between the nodes, $d_{i,j}$, as well as two link-specific parameters: $R_{i,j}$ and $\alpha_{i,j}$. $R_{i,j}$ represents the length of the link at which the delivery ratio is 50%³. Meanwhile, $\alpha_{i,j}$ is the steepness of the curve and characterizes the rate at which the PDR decreases.

$$P_{i,j}(d_{i,j}) = e^{-\log(2)\left(\frac{d_{i,j}}{R_{i,j}}\right)^{\alpha_{i,j}}} \quad (2.7)$$

³ $P_{i,j}(R_{i,j}) = e^{-\log(2)} = 0.5$

In Figure 2.6, various PDR functions are displayed for different values of the parameters R and α . By examining the curves, it is possible to understand the individual impact of each parameter on the PDR. In particular, if the distance d is held constant, a larger value of R leads to an increased PDR, while a higher value of α results in a higher PDR for distances in the range $[0, R]$.

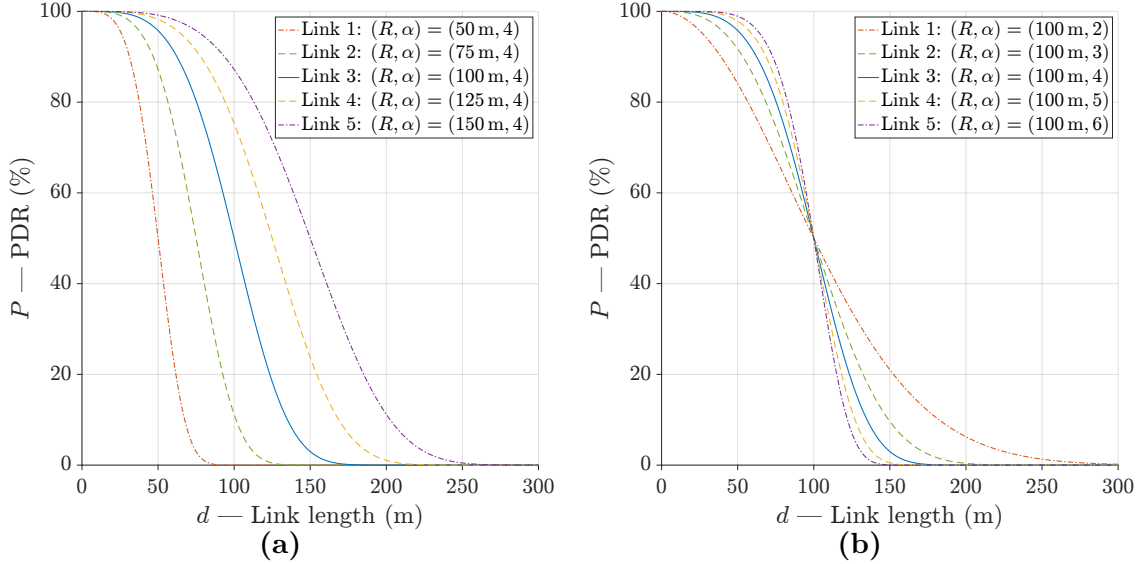


Figure 2.6. Packet Delivery Ratio P as a function of link length d for five links at different values of R , the link-length with a PDR of 50%, and α , the curve decay: **(a)** R ranging from 50 m to 150 m and constant $\alpha = 4$; the five models are $\{(50 \text{ m}, 4), (75 \text{ m}, 4), (100 \text{ m}, 4), (125 \text{ m}, 4), (150 \text{ m}, 4)\}$. **(b)** Constant $R = 100 \text{ m}$ and α ranging from 2 to 6; the five pairs PDR model parameters are $\{(100 \text{ m}, 2), (100 \text{ m}, 3), (100 \text{ m}, 4), (100 \text{ m}, 5), (100 \text{ m}, 6)\}$.

In order to define the PDR of the entire network, we need to state a few assumptions. Firstly, packets lost during the forwarding process are assumed to be unrecoverable. Secondly, we consider that these packet loss processes are independent across links, meaning that the PDR of each link ($e_j = \{j, j+1\}$, $j = 1, \dots, n-1$) is dependent only on its length ($d_{e_j} = d_{j,j+1}$) and medium characteristics ($(R_{e_j}, \alpha_{e_j}) = (R_{j,j+1}, \alpha_{j,j+1})$), and is independent of other links. Finally, a node (i , $i = 1, \dots, n$) transmits in its own time slot (s_i) only, thus without interfering with the other nodes' transmissions, by means of a global TDMA coordination scheme. With these assumptions, considering a line network with $n-1$ links e_j , $e_j \in E$, the network PDR, also called end-to-end PDR, is the product of all link PDRs, as expressed in Equation (2.8), where \mathbf{d} is the vector of $n-1$ link lengths specified in (2.9).

$$P_{\text{net}}(\mathbf{d}) = \prod_{e_j \in E} P_{e_j}(d_{e_j}) \quad (2.8)$$

$$\mathbf{d} = [d_{e_1} \quad \dots \quad d_{e_{n-1}}] \quad (2.9)$$

2.3.4 Weighted Line Network

It is possible to regard a network as a weighted graph $G = (V, E, w)$ with weight function $w : E \rightarrow \mathbb{R}_{\geq 0}$, where the weight of a link, w_{e_j} is defined in Equation (2.10).

$$w_{e_j} = \log \left(\frac{1}{P_{e_j}(d_{e_j})} \right), \quad i = 1, \dots, n - 1 \quad (2.10)$$

It is worthwhile to mention that the link lengths (d_{e_j}) and models (R_{e_j}, α_{e_j}) are not constant and therefore the weights are time-variant. This weight represents the difficulty of a packet reaching the endpoint of the link: the smaller the weight, the easier it is for a packet to reach its destination. A null weight implies 100% PDR, while an infinite weight represents a null PDR. A peculiarity of this formulation is that, by using the logarithm properties, it enables performing straightforward additions on the weights of the graph, while still being able to convert back to the PDR notation. The advantages of this approach are most apparent in more complex graphs such as meshes. Adopting the graph notation, Equation (2.8) becomes as in (2.11).

$$P_{\text{net}}(\mathbf{d}) = \left(\exp \left(\sum_{e_j \in E} w_{e_j} \right) \right)^{-1} \quad (2.11)$$

The line network depicted in Figure 2.3, considering the weights given by Equation (2.10), is as in Figure 2.7.

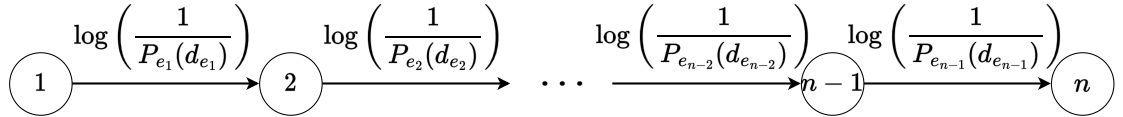


Figure 2.7. The same line network as in Figure 2.3, where the non-negative weights w_{e_j} are explicitly represented. The weight indicates the level of difficulty for a packet to reach its endpoint through the link. A smaller weight implies that it is easier for the packet to reach its destination.

3 Methodology

In this chapter, we present our methodology for a UAV to estimate its wireless link characteristics, detect a model change, communicate with its neighbors, and move according to various distributed relay placement algorithms, including an optimal one. Lastly, we introduce a metric for quantifying the error committed in the estimation process.

More in detail, after presenting the problem statement (Section 3.1), we move on to the data fitting process (Section 3.2), where we use non-linear least squares and fitting weights to model the network behavior. Next, we introduce the model change detector (Section 3.3), which helps us identify when changes occur in the network. We also explain the different packet types and payloads that are used in our simulation, including data packets, upstream and downstream report packets, network status packets, and node status packets (Section 3.4). We then delve into the relay placement strategies (Section 3.5), where we discuss the different methods we use to place relays in the network. These methods include equidistant relay placement, equal-PDR relay placement, and optimal relay placement. Finally, we provide a flowchart summary of the different types of network nodes: source, relay, and ground station (Section 3.6).

3.1 Problem Statement

The source is equipped with sensors, such as a camera, and a Wi-Fi card, which enables it to wirelessly communicate with the ground station via relay nodes. Our goal is to maintain a stable live data stream of the data generated by the sensors. However, the Packet Delivery Ratio (PDR) decreases as the network length L between the source and sink increases, as shown in Equation (2.8). In a single-hop network ($l = 1$) that has one transmitter node with a transmission speed of ν , the source transmits packets at a rate of $\nu/l = \nu$. Adding a second hop will result in a reduced maximum network throughput, as defined by Equation (3.1), where the network throughput ζ_{net} is as in Equation (3.2).

$$\zeta_{max}(\mathbf{d}) = \max_{l \in \mathbb{Z}^+} \zeta_{net}(\mathbf{d}) \quad (3.1)$$

$$\zeta_{net}(\mathbf{d}) = \frac{\nu}{l} \cdot P_{net}(\mathbf{d}) \quad (3.2)$$

Adding a relay can improve network performance beyond a certain link length, and the benefits can extend to using multiple relays. However, network delay becomes significant when using more than six relays. One major drawback of adding a relay is that the PDR model parameters depend on the link, which requires additional estimation. In [6], the authors presented an algorithm that optimizes the vector of link lengths, \mathbf{d} , for line networks to maximize the network PDR, P_{net} . At each iteration k_i (the TDMA round of the relay), the algorithm requires ten inputs for each relay i ($i = 2, \dots, n - 1$):

1. r_{i-1} and r_{i+1} , the three-dimensional positions of the two neighbors, which are measured by the neighboring nodes $i - 1$ and $i + 1$, respectively, and are affected by noise (mainly due to GPSs) and unknown to i .
2. $(R_{i-1,i}, \alpha_{i-1,i})$, the link model parameters of the upstream node, estimated by i and affected by uncertainties.
3. $(R_{i,i+1}, \alpha_{i,i+1})$, the link model parameters of the downstream node, estimated by the downstream node ($i + 1$) and unknown to i .

Moreover, when the relay i moves, the link model parameters may change, as the relay may enter or leave an interference zone, thereby influencing $(R_{i-1,i}, \alpha_{i-1,i})$ and $(R_{i,i+1}, \alpha_{i,i+1})$.

With the use of differential GPSs (DGPSs), achieving centimeter-level accuracy is possible in certain conditions [22], making r_i ($i = 1, \dots, n$) known quantities. This enables the reformulation of the problems into four parts, which are addressed in their respective sections in the rest of this thesis:

1. How to choose and fit a sample dataset adaptively online to estimate the link model.
2. How to identify a change in the model and calculate a new estimate of the link model parameters when such a change is detected.
3. How to efficiently and robustly transmit the position and model parameters to the neighbors.
4. How to compare the optimal placement with other relay placement strategies.

The first three parts are discussed in a separate section in the remainder of this chapter, namely, Sections 3.2, 3.3, and 3.4, while the last question is addressed in Section 3.5 and throughout Chapters 4 and 5.

3.2 Data Fitting

In this section, we will examine a node i with an upstream node, where i ranges from 2 to n , and we will omit the link subscripts. At each TDMA round, the node measures and records the sample (P, d) , where P is the PDR of the upstream link and d is the distance to the upstream node. If a measurement is missing, the sample is treated as void, and the node stores $(-1, -1)$. At a given round, the node has recorded at least $(P(1), d(1)), (P(2), d(2)), \dots, (P(m), d(m)), \dots, (P(N), d(N))$ data points, where N is the sample size considered.

We aim to estimate the link model parameters, R and α . If there are at least two data points, the node uses the non-linear least squares technique [23] to fit the N samples.

3.2.1 Non-Linear Least Squares

The non-linear least squares technique is named after the fact that it seeks to minimize the sum of squares of the residuals of the observations. The residual for the m -th observation, ε_m , is given by Equation (3.3), where P_m is the m -th observed value, \hat{P}_m is the m -th predicted value, d_m is the distance to the upstream node, m ranges from 1 to N , and $N \geq 2$ is the sample size¹.

$$\varepsilon_m = P_m - \hat{P}_m = P_m - P(d_m; R, \alpha) = P_m - e^{-\log(2)(\frac{d_m}{R})^\alpha} \quad (3.3)$$

Equation (3.4) [25] formalizes the non-linear least squares problem. The inclusion of the factor $\frac{1}{2}$ in the residual sum of squares S is a mathematical convenience that simplifies the expression of the gradient of S . When the gradient is equal to zero, the minimum value of S is reached, as shown in Equation (3.5). Equation (3.6) specifies the partial derivatives of the residuals with respect to the two model parameters, R and α .

$$(\hat{R}, \hat{\alpha}) = \arg \min_{(R, \alpha)} S(R, \alpha) = \arg \min_{(R, \alpha)} \frac{1}{2} \sum_{m=1}^N \varepsilon_m^2 = \arg \min_{(R, \alpha)} \frac{1}{2} \boldsymbol{\varepsilon}^\top \boldsymbol{\varepsilon} \quad (3.4)$$

$$\nabla S = \sum_{m=1}^N \begin{bmatrix} \frac{\partial \varepsilon_m}{\partial R} & \frac{\partial \varepsilon_m}{\partial \alpha} \end{bmatrix}^\top \varepsilon_m = J^\top \boldsymbol{\varepsilon} = \mathbf{0} \quad (3.5)$$

$$\begin{cases} \frac{\partial \varepsilon_m}{\partial R} = -\log(2) \frac{1}{R} \left(\frac{d_m}{R} \right)^\alpha 2^{-\left(\frac{d_m}{R} \right)^\alpha} \\ \frac{\partial \varepsilon_m}{\partial \alpha} = -\log(2) \left(\frac{d_m}{R} \right)^\alpha 2^{-\left(\frac{d_m}{R} \right)^\alpha} (\log(R) - \log(d_m)) \end{cases} \quad (3.6)$$

The Levenberg-Marquardt method [26–29] is often used for resolving nonlinear equation systems, like the one expressed in Equation (3.4). The algorithm iteratively updates the estimate of (R, α) according to Equation (3.7), where J^\top and $\boldsymbol{\varepsilon}$ are evaluated at $(\mathbf{d}; R^{(j)}, \alpha^{(j)})$, $\lambda^{(j)} \geq 0$, and I is the identity matrix of order 2.

$$\begin{bmatrix} R^{(j+1)} \\ \alpha^{(j+1)} \end{bmatrix} = \begin{bmatrix} R^{(j)} \\ \alpha^{(j)} \end{bmatrix} + (J^\top J + \lambda^{(j)} I)^{-1} J^\top \boldsymbol{\varepsilon} \quad (3.7)$$

The Levenberg-Marquardt method spans the range between two well-known optimization techniques: the Gauss-Newton method (when $\lambda^{(j)} = 0$) and the gradient descent method (when $\lambda^{(j)} \rightarrow \infty$). The choice of $\lambda^{(j)}$ is crucial for the algorithm performance, as it determines both stability through ensuring the invertibility of the approximated Hessian matrix, $J^\top J + \lambda^{(j)} I$, and the rate of convergence [30]. The damping parameter $\lambda^{(j)}$ in the Levenberg-Marquardt algorithm can be adjusted at each iteration j , as indicated by the superscript. The method for updating it can lead to improved results. A possible choice proposed in [31] is $\lambda^{(j)} = \kappa \|\boldsymbol{\varepsilon}\|_2 + (1-\kappa) \|J^\top \boldsymbol{\varepsilon}\|_2$, where $\kappa \in [0, 1]$ is a constant and $J, \boldsymbol{\varepsilon}$ are evaluated at $(\mathbf{d}; R^{(j)}, \alpha^{(j)})$. Additionally, [32] demonstrates that $\lambda^{(j)}$ can be any positive combination of $\|\boldsymbol{\varepsilon}\|_2$ and $\|J^\top \boldsymbol{\varepsilon}\|_2$.

¹If there are N data points and p fit parameters, a common assumption is that the number of degrees of freedom is $N - p$ [24].

The fitting process we implemented in our software employs the MPFIT package outlined in [33]² and is based on the Levenberg-Marquardt technique.

3.2.2 Fitting Weights

By using fitting weights $w_{\text{fit}}(m)$, it is possible to assign different levels of importance to each data point during the fitting process. To incorporate these weights into the non-linear least squares problem given by Equation (3.4), we can introduce the weighting matrix W_{fit} , as shown in Equation (3.8). The specific form of W_{fit} is given by Equation (3.9).

$$(\hat{R}, \hat{\alpha}) = \arg \min_{(R, \alpha)} S(R, \alpha) = \arg \min_{(R, \alpha)} \frac{1}{2} \sum_{m=1}^N w_{\text{fit}}(m) \varepsilon_m^2 = \arg \min_{(R, \alpha)} \frac{1}{2} \boldsymbol{\varepsilon}^\top W_{\text{fit}} \boldsymbol{\varepsilon} \quad (3.8)$$

$$W_{\text{fit}} = \begin{bmatrix} w_{\text{fit}}(1) & 0 & \cdots & 0 \\ 0 & w_{\text{fit}}(2) & \cdots & 0 \\ \vdots & \vdots & \ddots & \vdots \\ 0 & 0 & \cdots & w_{\text{fit}}(m) \end{bmatrix} \quad (3.9)$$

Common weight functions include constant, logarithmic, rooted, linear, and squared weights, as shown in Equations (3.10), (3.11), (3.12), (3.13), and (3.14), respectively. Here, the index m ranges from 1 to N_i , the number of samples at node i with $i = 2, \dots, n$. The index of the node starts from 2, not 1, because the source does not perform any fitting since it has no upstream link. We chose to use a logarithmic weight function (Equation (3.11)) because it balances the importance of recent and older data points. This weighting approach gives more weight to recent data points to detect new model changes more easily, while still considering less recent samples to represent the significance of the data comprehensively.

$$w_{\text{fit}}(m) = c, \quad c > 0 \quad (3.10)$$

$$w_{\text{fit}}(m) = \log(m) \quad (3.11)$$

$$w_{\text{fit}}(m) = \sqrt{m} \quad (3.12)$$

$$w_{\text{fit}}(m) = m \quad (3.13)$$

$$w_{\text{fit}}(m) = m^2 \quad (3.14)$$

In Figure 3.1, we compare the effects of using different weighting functions on the fitting process for $N = 1000$ samples. The graph displays the variations of the constant (blue), logarithmic (purple), rooted (yellow), linear (red), and squared (green) weights used to assign different levels of importance to the data points. In

²The software library can be downloaded at [34]. In particular, the library used in this work is called CMPFIT, which is a C version of the library.

Figure 3.1(a), the weights are normalized with respect to their maximum value ($\max_{m=1,\dots,N} w_{\text{fit}}(m)$), whereas in Figure 3.1(b), the weights are normalized with respect to their sum ($\sum_{m=1}^N w_{\text{fit}}(m)$).

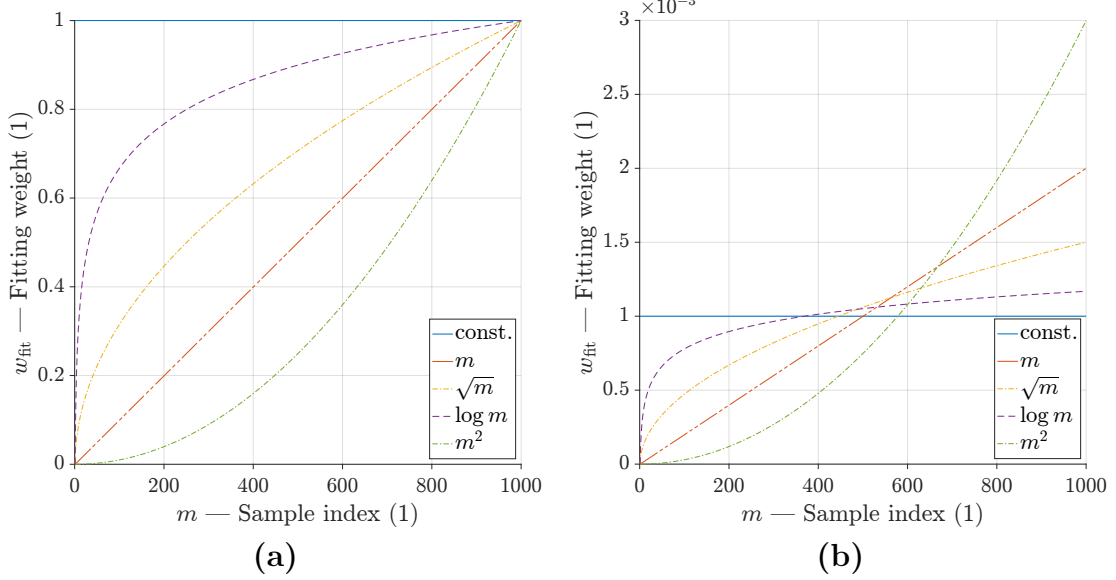


Figure 3.1. Fitting weights of $N = 1000$ samples: (a) normalized w.r.t. their maximum, $\max_{m=1,\dots,N} w_{\text{fit}}(m)$; (b) normalized w.r.t. their sum, $\sum_{m=1}^N w_{\text{fit}}(m)$.

3.3 Model Change Detector

The Model Change Detector block is implemented on each node, except for the source node³, to identify changes in the upstream link channel and make the necessary model adjustments.

3.3.1 Model Change Detection

At each TDMA round, node i ($i = 2, \dots, n$) estimates the new model parameters of its downstream node, $(\hat{R}_{i-1,i}(N_i), \hat{\alpha}_{i-1,i}(N_i))$, where (N_i) is the sample size. These N_i estimates, $\{(\hat{R}_{i-1,i}(1), \hat{\alpha}_{i-1,i}(1)), \dots, (\hat{R}_{i-1,i}(N_i), \hat{\alpha}_{i-1,i}(N_i))\}$, can be summarized by calculating weighted averages (see Equations (3.15) and (3.16)) and a weighted root mean square error (WRMSE) for each parameter (see Equations (3.17) and (3.18)). The weighted average provides an indication of the central tendency of the estimates, while the WRMSE indicates the variability of the estimates around the weighted average.

$$\bar{R}_{i-1,i}(N_i) = \frac{\sum_{m=1}^{N_i} w_{\text{fit}}(m) \hat{R}_{i-1,i}(m)}{\sum_{m=1}^{N_i} w_{\text{fit}}(m)} \quad (3.15)$$

³In fact, the source does not have an upstream link.

$$\bar{\hat{\alpha}}_{i-1,i}(N_i) = \frac{\sum_{m=1}^{N_i} w_{\text{fit}}(m) \hat{\alpha}_{i-1,i}(m)}{\sum_{m=1}^{N_i} w_{\text{fit}}(m)} \quad (3.16)$$

$$\text{WRMSE}_{\hat{R}_{i-1,i}}(N_i) = \sqrt{\frac{\sum_{m=1}^{N_i} w_{\text{fit}}(m) (\hat{R}_{i-1,i}(m) - \bar{\hat{R}}_{i-1,i}(N_i))^2}{\sum_{m=1}^{N_i} w_{\text{fit}}(m)}} \quad (3.17)$$

$$\text{WRMSE}_{\hat{\alpha}_{i-1,i}}(N_i) = \sqrt{\frac{\sum_{m=1}^{N_i} w_{\text{fit}}(m) (\hat{\alpha}_{i-1,i}(m) - \bar{\hat{\alpha}}_{i-1,i}(N_i))^2}{\sum_{m=1}^{N_i} w_{\text{fit}}(m)}} \quad (3.18)$$

The model change detector block detects significant changes in the statistical properties of a dataset with N_i samples at node i . At each TDMA round k_i , it compares the last estimate, $(\hat{R}_i, \hat{\alpha}_i)$, to their weighted averages $(\bar{\hat{R}}_i, \bar{\hat{\alpha}}_i)$ (defined in Equations (3.15), (3.16)) to check for significant deviations from the current model. If the difference for at least one of the two parameters is greater than a threshold value, ρ times the WRMSE (defined in Equations (3.17), (3.18)), a model change is triggered if the deviation is verified for τ instances. The observation length of the model change detector $\tau \in \mathbb{Z}^+$ is the number of time steps for which the condition must be satisfied before a model change is detected, and $k_i - \tau + 1, k_i$ is the detection horizon. The binary variable, $D_i(k_i)$, is set to 1 to indicate a model change at TDMA round k_i if the condition is always met during the detection horizon; otherwise, it is set to 0. We found that a value of 15 for τ and 1.96 for ρ strike a good balance in our model change detection process.

$$D_i(k_i) = \begin{cases} 1, & \text{if } |\bar{\hat{R}}_i(k'_i) - \hat{R}_i(k'_i)| > \rho \cdot \text{WRMSE}_{\hat{R}_i}(k'_i) \\ & \vee |\bar{\hat{\alpha}}_i(k'_i) - \hat{\alpha}_i(k'_i)| > \rho \cdot \text{WRMSE}_{\hat{\alpha}_i}(k'_i), \forall k'_i \in \{k_i - \tau + 1, k_i\} \\ 0, & \text{otherwise} \end{cases} \quad (3.19)$$

In Figure 3.2, the critical bounds are shown, which divide the area into two zones: the non-rejection region and the rejection region. A model change is triggered when τ consecutive estimates fall in the rejection region, which represents the unacceptable range of the estimates. Conversely, the non-rejection region represents the acceptable range of the estimates. The size of the non-rejection region tends to decrease as the rounds progress. The figure highlights the critical bounds $\hat{R}_{1,2} \pm \rho \cdot \text{WRMSE}_{\hat{R}_{1,2}}$ and $\bar{\hat{\alpha}}_{1,2} \pm \rho \cdot \text{WRMSE}_{\hat{\alpha}_{1,2}}$, where $\rho = 1.96$, for both $\hat{R}_{1,2}$ and $\hat{\alpha}_{1,2}$. It is worth noting that neither the estimated nor the actual link PDR models are included in this representation.

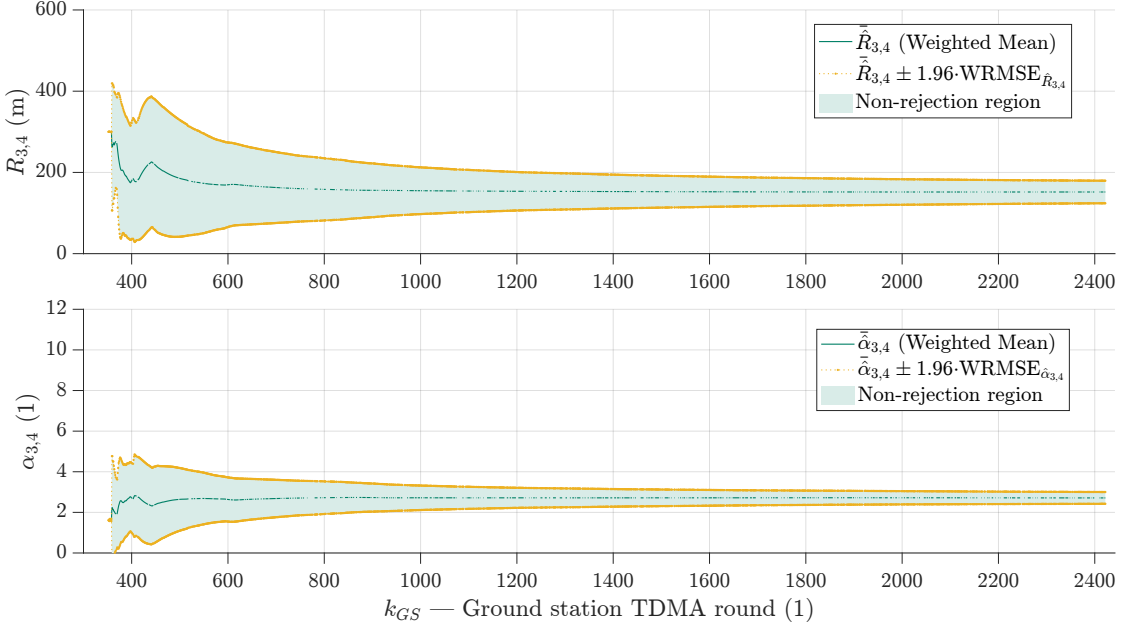


Figure 3.2. The critical bounds (highlighted in yellow) $\bar{R}_{3,4} \pm \rho \cdot \text{WRMSE}_{\hat{R}_{3,4}}$ and $\hat{\alpha}_{3,4} \pm \rho \cdot \text{WRMSE}_{\hat{\alpha}_{3,4}}$, where $\rho = 1.96$, are shown above and below the weighted averages (in dark green) and divide the area into two zones: the non-rejection region (in light green) and the rejection region (in white), for both $\hat{R}_{3,4}$ and $\hat{\alpha}_{3,4}$. When τ consecutive estimates fall within the rejection region, which represents an unacceptable range of estimates, a model change is triggered. On the other hand, the non-rejection region represents an acceptable range of estimates. It is worth noting that the size of the non-rejection regions tends to decrease as the rounds progress. Neither the estimated nor the actual link PDR models are included in this representation.

3.3.2 Sample Size

When a model change is detected, the sample size N_i is adjusted by reducing it in percentage by a factor of $\eta_N \in [0, 1]$, according to Equation (3.20). If no change is detected, the sample size is incremented by 1. The variable N_i depends on the TDMA round k_i of node i : by default, it increases by one at each round, but it is reduced in case of a model change detection at round k_i .

It is worth noting that the model change detector continues to monitor for future changes, and the sample size is adjusted accordingly. In our case, we found that a value of $\eta_N = 0.20$ works well. When η_N is set to 0, all previous data samples are discarded if a model change is detected. Conversely, when η_N is set to 1, the model change detector is disabled, and the sample size is never reduced, even if a change is detected. The equation for N_i is given by Equation (3.20).

$$N_i(k_i) = \begin{cases} \lceil (1 - \eta_N) N_i(k_i - 1) \rceil, & \text{if } D_i(k_i) = 1 \\ N_i(k_i - 1) + 1, & \text{otherwise} \end{cases} \quad \eta_N \in [0, 1] \quad (3.20)$$

3.4 Packet Types and Payloads

In this section, we will delve into the different types of packets that nodes in the network can transmit. Packets are the fundamental unit of data transmission in a network, carrying the information needed for communication between nodes. Packets are composed of two parts: a payload and a header. The payload can include any type of data, including text, audio, images, and video frames. The header, on the other hand, contains essential information that is necessary to route the packet through the network and ensure that it reaches its intended destination. Some typical fields are the source and destination addresses, packet sequence number, packet payload's length, and error-checking codes.

In our network, several types of packets were developed to serve different purposes, including data packets, upstream report packets, downstream report packets, network status packets, and node status packets. Table 3.1 provides a comprehensive overview of the different packet types, their corresponding payloads, senders, and receivers. The following subsections will describe each packet type in more detail, providing an explanation of the structure and content of its payload and ultimately its role in the functioning of the network.

Table 3.2 offers a mapping of the various packet types sent and received by the different node types in the network. The first column lists the node types, which include the source, relay, and ground station nodes. The second and third columns show the packet types sent and received by each node type respectively. The mapping in Table 3.2 complements the information presented in Table 3.1 and provides an alternative way of interpreting the data. It should be noted that when the node is the first relay (i.e., $i = 2$), a downstream report packet type is not sent since the source node does not need to execute any relay placement algorithm, and the information in the packet would be redundant.

Table 3.1. Packet types with their corresponding payloads, senders, receivers, and transmission directions in the network.

Packet type	Packet payload	$\text{Tx} \rightarrow \text{Rx}$
Data	$\begin{cases} \text{Data (e.g., video frame)} \\ N_1^{\text{s,data}} \end{cases}$	$1 \rightarrow n$
Upstream report	$\begin{cases} r_{\text{Tx}} \\ k_{\text{Tx}} \\ N_{\text{Tx}}^{(\text{s})} \end{cases}$	$1 \rightarrow 2, \dots, n-1 \rightarrow n$
Downstream report	$\begin{cases} r_{\text{Tx}} \\ (\hat{R}_{\text{Rx,Tx}}, \hat{\alpha}_{\text{Rx,Tx}}) \end{cases}$	$2 \leftarrow 3, \dots, n-1 \leftarrow n$
Network status	$\begin{cases} [r_1, \dots, r_n] \\ [\text{IP}_1, \dots, \text{IP}_n] \\ [\text{mode}_1, \dots, \text{mode}_n] \end{cases}$	$\{1, \dots, n-1\} \leftarrow n$
Node status	$\begin{cases} r_i \\ (\tilde{P}_{i-1,i}, \tilde{d}_{i-1,i}) \\ N_i \\ (\hat{R}_{i-1,i}, \hat{\alpha}_{i-1,i}) \\ (\bar{\hat{R}}_{i-1,i}, \bar{\hat{\alpha}}_{i-1,i}) \\ (\text{WRMSE}_{\hat{R}_{i-1,i}}, \text{WRMSE}_{\hat{\alpha}_{i-1,i}}) \\ \text{Other info (e.g., battery level)} \end{cases}$	$\{1, \dots, n-1\} \rightarrow n$

Table 3.2. Table that maps the packet types sent (second column) and received (third column) with the node type (first column). It complements the information in Table 3.1.

Node type	Packet type	
	Transmits	Receives
Source ($i = 1$)	Data Upstream report Node status	Network status
Relay ($i = 2, \dots, n-1$)	Upstream report Downstream report (if $i \neq 2$) Node status	Network status Upstream report Downstream report
Ground station ($i = n$)	Network status Downstream report	Data Node status Upstream report

3.4.1 Data Packet

A data packet contains the application-level data that needs to be transmitted over the network. The source, responsible for generating the data, is the only one who sends it, and the ground station, responsible for consuming the data, is the only one who receives it. The transmission time of a packet is not fixed and depends on the needs of the source generating the data. Its payload typically includes the data itself, such as a video frame, as well as the sequence number $N_1^{s,\text{data}}$, which represents the number of data packets sent in that round. In our study, the data transmitted by the source is the string “Hello, ground station.”, with an average interval of 2 milliseconds. The ground station can track the number of data-type packets received until the round k , $N_n^{r,\text{data}}(k)$. The sequence number $N_1^{s,\text{data}}(k)$ can then be used for network analysis purposes. To determine the average network PDR in a specific time window $[k^a..k^b]$, the ground station can calculate the ratio of the number of data-type packets received within that time window to the number of data-type packets sent within the same time window, as shown in Equation (3.21). This provides a measure of the overall reliability of the network during that period.

$$\bar{P}_{\text{net}}([k^a..k^b]) = \frac{\sum_{k \in [k^a..k^b]} N_n^{r,\text{data}}(k)}{\sum_{k \in [k^a..k^b]} N_1^{s,\text{data}}(k)} \quad (3.21)$$

When the node acts as the first relay (i.e., $i = 2$), there is no need to send a downstream report packet as the source node does not need to execute any relay placement algorithm, and the information in the packet would be superfluous.

3.4.2 Upstream Report Packet

An upstream report packet is a type of packet that is sent from the upstream node, at the end of its TDMA round, to its downstream neighbor. The payload of an upstream report packet includes:

- r_{Tx} , the position of the sender (i.e., the upstream node).
- k_{Tx} , the TDMA round of the sender.
- $N_{\text{Tx}}^{(s)}$, the number of packets sent by the sender during the round k_{Tx} .

The sender position is used by the receiver as an input to the relay placement strategy, while k_{Tx} is used for accurate counting of the received packets, $N_{\text{Rx}}^{(r)}$. Lastly, $N_{\text{Tx}}^{(s)}$ is used to compute the instantaneous link PDR, $P_{T_x,R_x}(k_{\text{Tx}})$ (cf Equation (2.3)).

In particular, the ground station utilizes upstream report packets also to determine when to add a new relay to the network. As the sole node responsible for the network topology, the ground station decides when to add or remove a relay. At a given time k_n , the network is represented as $G(k_n) = (V(k_n), E(k_n))$, where $V = \{1, 2, \dots, i, n\}$ and $E = \{\{1, 2\}, \{2, 1\}, \{2, 3\}, \{3, 2\}, \dots, \{i, n\}, \{n, i\}\}$. If the upstream link PDR falls below a threshold of $1 - \eta_P$ (where $\eta_P \in [0, 1]$ is the maximum Packet Loss Ratio (PLR) allowed with the upstream node) or if there are no upstream report

packets received from the current upstream neighbor, $H_n^{\text{in},1}(k_n) = i$, for at least τ_P rounds, then the ground station adds another relay node, node $i + 1$, to the network. This condition is summarized in Equation (3.22). We achieved satisfactory results with $\eta_P = 90\%$ and $\tau_P = 10$.

$$V(k_n) = \{V(k_n - 1) \cup i + 1, i + 1 \text{ relay}\} \text{ if } \{\tilde{P}_{H_n^{\text{in},1}(k_n),n}(k_n) < 1 - \eta_P \vee k_n - k_n^{\text{up}} \geq \tau_P\} \quad (3.22)$$

3.4.3 Downstream Report Packet

A downstream report packet is a type of packet that is sent from the downstream node, at the end of its TDMA round, to its upstream neighbor. The payload of an upstream report packet includes:

- r_{Rx} , the position of the sender (i.e., the downstream node).
- $(\hat{R}_{\text{Rx,Tx}}, \hat{\alpha}_{\text{Rx,Tx}})$, the link PDR model parameters estimated by the sender.

Both r_{Rx} and $(\hat{R}_{\text{Rx,Tx}}, \hat{\alpha}_{\text{Rx,Tx}})$ are used by the receiver as inputs to the relay placement strategy.

If a relay node ($i = 2, \dots, n - 1$) stops receiving packets from its upstream or downstream neighbor, it may be necessary to adjust the estimated link length, $\hat{R}_{i-1,i}$ or $\hat{R}_{i,i+1}$, in the link packet delivery ratio (PDR) model. This is because a sudden change in the link PDR can result in more lost packets at the same distance. By reducing $\hat{R}_{i-1,i}$ ($\hat{R}_{i,i+1}$, respectively), the distance between the two nodes can be decreased, leading to an increase in their link PDR. This facilitates new PDR measurements and ultimately aids in estimating the model parameters, $(\hat{R}_{i-1,i}, \hat{\alpha}_{i-1,i})$ ($(\hat{R}_{i,i+1}, \hat{\alpha}_{i,i+1})$, respectively), which is explained in Equation (3.23) (when packets from the upstream node are not received anymore) and Equation (3.24) (when packets from the downstream node are not received anymore). This technique can be useful in cases where communication between two nodes has stopped.

$$\hat{R}_{i-1,i}(k_i) = \begin{cases} \hat{R}_{i-1,i}(k_i - 1), & \text{if } k_i - k_i^{\text{up report}} < \tau_R \\ \max\{R_{\min}, (1 - \eta_R)\hat{R}_{i-1,i}(k_i - 1)\}, & \text{otherwise} \end{cases} \quad (3.23)$$

$$\hat{R}_{i,i+1}(k_i) = \begin{cases} \hat{R}_{i,i+1}(k_i - 1), & \text{if } k_i - k_i^{\text{down report}} < \tau_R \\ \max\{R_{\min}, (1 - \eta_R)\hat{R}_{i,i+1}(k_i - 1)\}, & \text{otherwise} \end{cases} \quad (3.24)$$

The last round when node i received an upstream report packet is denoted by $k_i^{\text{up,report}}$, and $k_i^{\text{down,report}}$ is the last round when node i received a downstream report packet. τ_R represents the number of rounds without an update of $\hat{R}_{i-1,i}$ ($\hat{R}_{i,i+1}$), beyond which $\hat{R}_{i-1,i}$ ($\hat{R}_{i,i+1}$) is reduced. R_{\min} is the smallest allowed value for $\hat{R}_{i-1,i}$ ($\hat{R}_{i,i+1}$), and $\eta_R \in [0, 1]$ is the reduction factor of $\hat{R}_{i-1,i}$ ($\hat{R}_{i,i+1}$, respectively). Extreme values of η_R correspond to cases where no reduction occurs ($\eta_R = 0$) or immediate full reduction occurs ($\eta_R = 1$), which can have a significant impact on the resulting estimated link PDR model parameters. For more robust communication, we used $\eta_R = 0.05$, $R_{\min} = 20 \text{ m}$, and $\tau_R = 5$.

3.4.4 Network Status Packet

At the end of each TDMA round, the ground station sends a network status packet to all other nodes. These packets contain information on the current status of the network, including:

- $[r_1, \dots, r_n]$, the last known positions of all active nodes.
- $[\text{IP}_1, \dots, \text{IP}_n]$, the IP addresses of all active nodes, ordered from the source to the ground station.
- $[\text{mode}_1, \dots, \text{mode}_n]$, the modality of flight of each active node.

The possible values for an element in the last array are “Move normally”, “Keep position”, and “Go to ground station”.

3.4.5 Node Status Packet

During the end of each TDMA round, any other node i (from the source to the last added relay) sends node status packets to the ground station, which contain navigation data and information on the PDR measurements and link PDR estimations. The following items are included in the packet:

- r_i , the position of the node
- $(\tilde{P}_{i-1,i}, \tilde{d}_{i-1,i})$, the last link PDR measurement
- $N_i^{(s)}$, the last number of packets sent by the node
- $N_i^{(r)}$, the last number of packets received by the node
- N_i , the last sample size of the node
- $(\hat{R}_{i-1,i}, \hat{\alpha}_{i-1,i})$, the last model parameters estimated by the node
- $(\bar{\hat{R}}_{i-1,i}, \bar{\hat{\alpha}}_{i-1,i})$, the last weighted model parameters
- $(\text{WRMSE}_{\hat{R}_{i-1,i}}, \text{WRMSE}_{\hat{\alpha}_{i-1,i}})$, the last WRMSEs of the model parameters
- Other information (e.g., battery level).

The ground station stores these packets in a log file for future analysis. At the end of each TDMA round, the ground station writes the following data on the log file for each node, along with the index of the round and the time, as well as the ground station’s own data ($r_n, (\tilde{P}_{n-1,n}, \tilde{d}_{n-1,n}), N_n^{(s)}, N_n^{(r)}, N_n, (\hat{R}_{n-1,n}, \hat{\alpha}_{n-1,n}), (\bar{\hat{R}}_{n-1,n}, \bar{\hat{\alpha}}_{n-1,n}), (\text{WRMSE}_{\hat{R}_{n-1,n}}, \text{WRMSE}_{\hat{\alpha}_{n-1,n}})$, and other information (e.g., battery level)).

3.5 Relay Placement Strategies

Relay nodes are used to extend the coverage area of the wireless network by forwarding data between the source and destination nodes, such as the ground station. The placement of relays in a wireless network is the strategy used to determine the locations for the relay nodes, with the goal of enhancing a network performance metrics, such as coverage or connectivity.

The placement of relays in a wireless network is a crucial aspect that can greatly impact the overall performance of the network. A proper placement of the available relays can significantly improve the end-to-end PDR. In this section, we will investigate different relay placement strategies that can be employed in a wireless network and compare their performance. These strategies include the equidistant relay placement (Subsection 3.5.1), the equal-PDR relay placement (Subsection 3.5.2), and the optimal relay placement (Subsection 3.5.3).

Figure 3.3, using the formulation proposed in Subsection 2.3.4, displays a line network composed of a source, a relay, and a ground station ($n = 3$), and highlights the key variables involved in the optimization of the network PDR (P_{net}): network length (L), the link lengths ($d_{i,i+1}$, $i = 1, \dots, n - 1$), and the model parameters ($(R_{i,i+1}, \alpha_{i,i+1})$, $i = 1, \dots, n - 1$). More relays can be added additionally, increasing the total number of nodes n .

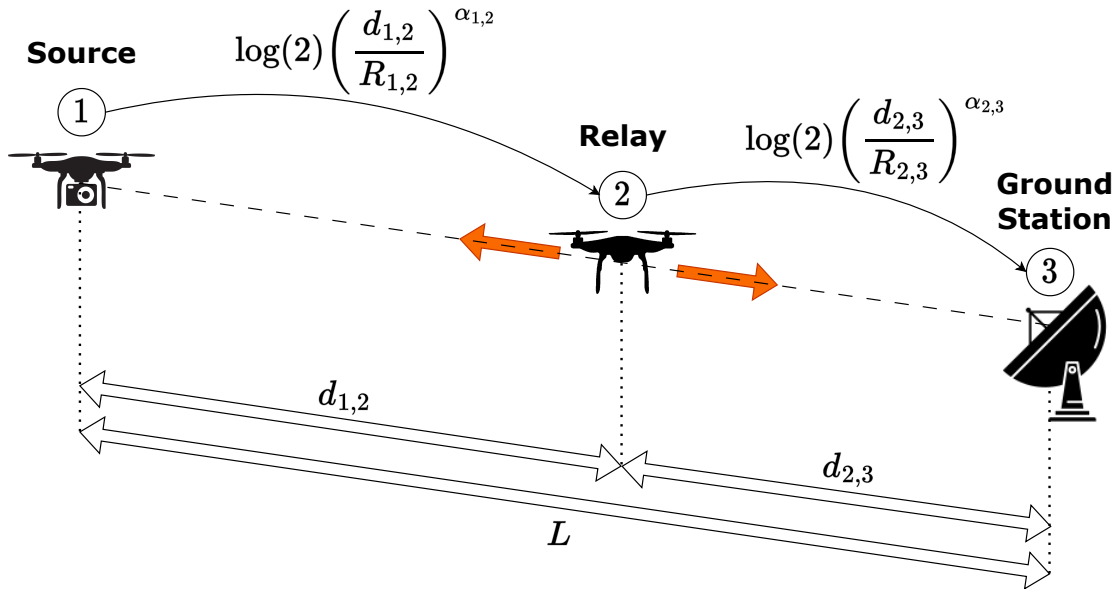


Figure 3.3. A three-node line network (source, relay, and ground station) with two links, from the source to the relay and from the relay to the ground station. The placement of the relay has a direct impact on the network PDR (P_{net}), which is why finding a good placement is crucial in improving the network performance. The optimal placement of the relay determines the maximum network PDR (P_{net}), and is based on crucial variables such as the relay's upstream and downstream distances, their sum, and the knowledge of the upstream and downstream link PDR models.

3.5.1 Equidistant Relay Placement

The first strategy that will be considered is the equidistant placement strategy, which can be considered the "naive" approach. This strategy involves placing the relay equidistant from its two neighboring nodes, as in Equation (3.25). It is immediate to implement and does not require any optimization process. However, it does not consider the different link PDR models and can result in sub-optimal performance. The achieved network PDR is as in Equation (3.26).

$$\mathbf{d}^{\text{equi}} = \begin{bmatrix} \frac{L}{n} & \dots & \frac{L}{n} \end{bmatrix} \quad (3.25)$$

$$P_{\text{net}}^{\text{equi}} = P_{\text{net}}(\mathbf{d}^{\text{equi}}) \quad (3.26)$$

The steps for determining the equidistant placement of a relay, node i , with two neighbors, nodes $i - 1$ (upstream node) and $i + 1$ (downstream node), are outlined in Algorithm 1, where T is the TDMA round period. It is worth noting that it does not depend on either of the link PDR models $((R_{i-1,i}, \alpha_{i-1,i})$ and $(R_{i,i+1}, \alpha_{i,i+1})$) but only on the neighbor positions. In fact, the equidistant position for node i is by definition at the middle point between the two neighbors, r_{i-1} and r_{i+1} .

$$r_i^{\text{equi}} = \frac{1}{2}(r_{i-1} + r_{i+1}), \quad i = 2, \dots, n - 1 \quad (3.27)$$

Algorithm 1 Distributed Equidistant Relay Placement Algorithm

```

1: for every  $T$  do
2:    $r_{i-1} \leftarrow \text{RETRIEVELASTPOSITION}(i - 1)$                                  $\triangleright$  Cf. Section 3.4
3:    $r_{i+1} \leftarrow \text{RETRIEVELASTPOSITION}(i + 1)$                                  $\triangleright$  Cf. Section 3.4
4:    $r_i^{\text{equi}} \leftarrow \text{COMPUTEEQUIDISTANTPOSITION}(r_{i-1,i}, r_{i,i+1})$ 
5:    $\text{SETWAYPOINT}(r_i^{\text{equi}})$ 
6: end for
7: function COMPUTEEQUIDISTANTPOSITION( $r_{i-1,i}, r_{i,i+1}$ )
8:    $r_i^{\text{equi}} \leftarrow \frac{1}{2}(r_{i-1} + r_{i+1})$                                           $\triangleright$  Cf. Eq. (3.27)
9:   return  $r_i^{\text{equi}}$ 
10: end function

```

3.5.2 Equal-PDR Relay Placement

Equal Power Relay Placement (EPRP) is a technique that aims to distribute the power of the relays evenly to ensure that each relay contributes equally to the network overall performance. This concept is demonstrated in [35], which presents a wireless power repeater system for long-distance applications that balances the power load at each repeater. Similarly, Equal Packet Delivery Ratio Relay Placement (EPDRRP) focuses on ensuring equal workload distribution among the relays, but instead of equalizing the power of the signals transmitted by each relay, it balances the load based on the ratio of successfully received packets at each relay.

On the other hand, with the equal-PDR relay placement strategy the relay positions are adjusted to maintain equal link PDRs with neighboring nodes. The strategy takes into account the different link PDR models to predict the PDR at different distances and the relays move to keep an equal PDR with their neighbors. This strategy is more complex than the equidistant placement, but it can result in improved performance. The equal-PDR distance $d_{i-1,i}^{\text{equalPDR}}$ ($i = 2, \dots, n - 1$) is the real solution in $[0, d_{i-1,i} + d_{i,i+1}]$ of Equation (3.28), where $d_{i-1,i} + d_{i,i+1}$ is the sum of the upstream and downstream link lengths. Then, the relay positions are given by Equation (3.30). By utilizing the distances specified in Equation (3.31), solutions of the system in Equation (3.29), the equal-PDR relay placement strategy results in a network PDR as detailed in Equation (3.32).

$$\left(\frac{d_{i-1,i}^{\text{equalPDR}}}{R_{i-1,i}} \right)^{\alpha_{i-1,i}} = \left(\frac{d_{i-1,i} + d_{i,i+1} - d_{i-1,i}^{\text{equalPDR}}}{R_{i,i+1}} \right)^{\alpha_{i,i+1}}, \quad i = 2, \dots, n - 1 \quad (3.28)$$

$$\left\{ \begin{array}{l} \left(\frac{d_{1,2}^{\text{equalPDR}}}{R_{1,2}} \right)^{\alpha_{1,2}} = \left(\frac{d_{1,3} - d_{1,2}^{\text{equalPDR}}}{R_{2,3}} \right)^{\alpha_{2,3}} \\ \left(\frac{d_{2,3}^{\text{equalPDR}}}{R_{2,3}} \right)^{\alpha_{2,3}} = \left(\frac{d_{2,4} - d_{2,3}^{\text{equalPDR}}}{R_{3,4}} \right)^{\alpha_{3,4}} \\ \vdots \\ \left(\frac{d_{i-1,i}^{\text{equalPDR}}}{R_{i-1,i}} \right)^{\alpha_{i-1,i}} = \left(\frac{d_{i-1,i+1} - d_{i-1,i}^{\text{equalPDR}}}{R_{i,i+1}} \right)^{\alpha_{i,i+1}} \\ \vdots \\ \left(\frac{d_{n-2,n-1}^{\text{equalPDR}}}{R_{n-2,n-1}} \right)^{\alpha_{n-2,n-1}} = \left(\frac{d_{n-2,n} - d_{n-2,n-1}^{\text{equalPDR}}}{R_{n-1,n}} \right)^{\alpha_{n-1,n}} \\ d_{n-1,n}^{\text{equalPDR}} = L - (d_{1,2}^{\text{equalPDR}} + \dots + d_{n-2,n-1}^{\text{equalPDR}}) = \\ = d_{n-2,n} - d_{n-2,n-1}^{\text{equalPDR}} \end{array} \right. \quad (3.29)$$

$$r_i^{\text{equalPDR}} = \frac{d_{i,i+1}^{\text{equalPDR}} \cdot r_{i-1} + d_{i-1,i}^{\text{equalPDR}} \cdot r_{i+1}}{d_{i-1,i+1}}, \quad i = 2, \dots, n - 1 \quad (3.30)$$

$$\mathbf{d}^{\text{equalPDR}} = [d_{1,2}^{\text{equalPDR}} \quad \dots \quad d_{n-1,n}^{\text{equalPDR}}] \quad (3.31)$$

$$P_{\text{net}}^{\text{equalPDR}} = P_{\text{net}}(\mathbf{d}^{\text{equalPDR}}) \quad (3.32)$$

The steps for determining the equal-PDR placement of a relay, node i , with two neighbors, nodes $i - 1$ (upstream node) and $i + 1$ (downstream node), are outlined in Algorithm 2.

Algorithm 2 Distributed Equal-PDR Relay Placement Algorithm

```

1: for every  $T$  do
2:    $(R_{i-1,i}, \alpha_{i-1,i}) \leftarrow \text{ESTIMATEMODEL}$                                  $\triangleright$  Cf. Sections 3.2 and 3.3
3:    $(R_{i,i+1}, \alpha_{i,i+1}) \leftarrow \text{RETRIEVELASTMODEL}(i+1)$                        $\triangleright$  Cf. Section 3.4
4:    $r_{i-1} \leftarrow \text{RETRIEVELASTPOSITION}(i-1)$                                       $\triangleright$  Cf. Section 3.4
5:    $r_{i+1} \leftarrow \text{RETRIEVELASTPOSITION}(i+1)$                                       $\triangleright$  Cf. Section 3.4
6:    $r_i^{\text{equalPDR}} \leftarrow \text{COMPUTEEQUALPDRPOSITION}(r_{i-1,i}, R_{i-1,i}, \alpha_{i-1,i}, r_{i,i+1}, R_{i,i+1}, \alpha_{i,i+1})$ 
7:    $\text{SETWAYPOINT}(r_i^{\text{equalPDR}})$ 
8: end for
9: function COMPUTEEQUALPDRPOSITION( $r_{i-1,i}, R_{i-1,i}, \alpha_{i-1,i}, r_{i,i+1}, R_{i,i+1}, \alpha_{i,i+1}$ )
10:    $d_{i-1,i+1} \leftarrow \|r_{i-1} - r_{i+1}\|_2$                                           $\triangleright$  Upstream-downstream distance
11:    $d_{i-1,i}^{\text{equalPDR}} \leftarrow \text{FINDROOT}(f_{Eq(3.29)}((R_{i-1,i}, \alpha_{i-1,i}), (R_{i,i+1}, \alpha_{i,i+1}), d_{i-1,i+1})) \in [0, d_{i-1,i+1}]$            $\triangleright$  Cf. Eq. (3.29)
12:    $d_{i,i+1}^{\text{equalPDR}} \leftarrow d_{i-1,i+1} - d_{i-1,i}^{\text{equalPDR}};$ 
13:    $r_i^{\text{equalPDR}} \leftarrow \frac{d_{i,i+1}^{\text{equalPDR}} \cdot r_{i-1} + d_{i-1,i}^{\text{equalPDR}} \cdot r_{i+1}}{d_{i-1,i+1}}$             $\triangleright$  Cf. Eq. (3.30)
14:   return  $r_i^{\text{equalPDR}}$ 
15: end function

```

3.5.3 Optimal Relay Placement

The aim of this study is to maximize the end-to-end packet delivery ratio of a line network by optimizing the placement of relay nodes or, equivalently, adjusting the lengths of the network links. Our optimization problem, stated in Equation (3.33), is to identify the vector of link lengths, \mathbf{d} , that achieves the highest possible network PDR P_{net} , defined in Equation (2.8), while maintaining a fixed network length constraint, L . As mentioned in Section 2.2, the bandwidth in the other direction – for example for control signals sent from the ground station to the UAVs – is significantly lower than that of the online sensing stream and therefore will be neglected in the optimization problem. Additionally, the links in the network are assumed to be physically aligned. This is a crucial constraint as we assume that moving a relay node (i , where $i \in 2, \dots, n - 1$) results in either the upstream link length $d_{i-1,i}$ or the downstream link length $d_{i,i+1}$ to shorten while the other one to extend, keeping the total network length L constant.

$$\begin{aligned} P_{\text{net}}^{\text{opt}} = \max_{\mathbf{d}} P_{\text{net}} &= \max_{d_{e_j}, e_j \in E} \prod_{e_j \in E} P_{e_j}(d_{e_j}) \\ \text{s.t. } L - \sum_{e_j \in E} d_{e_j} &= 0 \end{aligned} \quad (3.33)$$

The optimal distance $d_{i,i+1}^{\text{opt}}$ ($i = 2, \dots, n-1$) can be found as the real solution in $[0, d_{i-1,i+1}]$ of Equation (3.34), where Ψ_i and θ_i are as defined in Equation (3.35). For a detailed mathematical proof of this solution using the method of Lagrange multipliers, the reader is referred to Section 4 in [6]. The relay positions can then be determined using Equation (3.37), based on the optimal distance obtained. The distances specified in Equation (3.38), which are solutions to the system presented

in Equation (3.36), can be used to obtain an optimal relay placement strategy that results in an optimal network PDR, as detailed in Equation (3.39).

It is worth noting that the equidistant and optimal strategies are equivalent only in the case of symmetric links, meaning when the link PDR models of the two links connecting a relay i , $i = 2, \dots, n - 1$ to its neighbors are identical. This happens when $\Psi_i = \theta_i = 1 \forall i \in \{2, \dots, n - 1\}$.

$$\Psi_i \cdot (d_{i,i+1}^{\text{opt}})^{\theta_i} = d_{i-1,i+1}, \quad i = 2, \dots, n - 1 \quad (3.34)$$

$$\begin{cases} \Psi_i = \left(\frac{R_{i-1,i}^{\alpha_{i-1,i}} \alpha_{i,i+1}}{R_{i,i+1}^{\alpha_{i,i+1}} \alpha_{i-1,i}} \right)^{\frac{1}{\alpha_{i-1,i}-1}} & i = 2, \dots, n - 1 \\ \theta_i = \frac{\alpha_{i,i+1} - 1}{\alpha_{i-1,i} - 1} \end{cases} \quad (3.35)$$

$$\begin{cases} d_{1,2}^{\text{opt}} = L - (d_{2,3}^{\text{opt}} + \dots + d_{n-1,n}^{\text{opt}}) = \\ \quad = d_{1,3} - d_{2,3}^{\text{opt}} \\ \Psi_2 \cdot (d_{2,3}^{\text{opt}})^{\theta_2} = d_{2,3} \\ \vdots \\ \Psi_i \cdot (d_{i,i+1}^{\text{opt}})^{\theta_i} = d_{i-1,i+1} \\ \vdots \\ \Psi_{n-1} \cdot (d_{n-1,n}^{\text{opt}})^{\theta_{n-1}} = d_{n-2,n} \end{cases} \quad (3.36)$$

$$r_i^{\text{opt}} = \frac{d_{i,i+1}^{\text{opt}} \cdot r_{i-1} + d_{i-1,i}^{\text{opt}} \cdot r_{i+1}}{d_{i-1,i+1}}, \quad i = 2, \dots, n - 1 \quad (3.37)$$

$$\mathbf{d}^{\text{opt}} = [d_{1,2}^{\text{opt}} \quad \dots \quad d_{n-1,n}^{\text{opt}}] \quad (3.38)$$

$$P_{\text{net}}^{\text{opt}} = P_{\text{net}}(\mathbf{d}^{\text{opt}}) \quad (3.39)$$

Algorithm 3 provides the steps to determine the optimal location for a relay (node i) in a distributed fashion. The algorithm is alternatively referred to as dynamic relay placement (DRP). The relay is positioned between two neighboring nodes, node $i - 1$ (upstream node) and node $i + 1$ (downstream node). To differentiate the variables computed in the algorithm from the previous algorithms, the superscript “DRP” will be used (instead of “opt”).

In Figure 3.4 we can observe, in an introductory example from [13], the comparison of the presented relay placement strategies in a three-node wireless line network of length $L = 100$ m. The optimal placement strategy resulted in the highest PDR of 57.09% at the distances $[d_{1,2}, d_{2,3}]^T = [57.82 \text{ m}, 42.18 \text{ m}]^T$, while the PDR of the equidistant and equal-PDR placement strategies are 52.47% and 39.23% respectively, at their corresponding distances.

Algorithm 3 Distributed Optimal Relay Placement (DRP) Algorithm

```

1: for every  $T$  do
2:    $(R_{i-1,i}, \alpha_{i-1,i}) \leftarrow \text{ESTIMATEMODEL}$             $\triangleright$  Cf. Sections 3.2 and 3.3
3:    $(R_{i,i+1}, \alpha_{i,i+1}) \leftarrow \text{RETRIEVELASTMODEL}(i+1)$      $\triangleright$  Cf. Section 3.4
4:    $r_{i-1} \leftarrow \text{RETRIEVELASTPOSITION}(i-1)$                   $\triangleright$  Cf. Section 3.4
5:    $r_{i+1} \leftarrow \text{RETRIEVELASTPOSITION}(i+1)$                   $\triangleright$  Cf. Section 3.4
6:    $r_i^{\text{opt}} \leftarrow \text{COMPUTEOPTIMALPOSITION}(r_{i-1,i}, R_{i-1,i}, \alpha_{i-1,i}, r_{i,i+1}, R_{i,i+1}, \alpha_{i,i+1})$ 
7:    $\text{SETWAYPOINT}(r_i^{\text{opt}})$ 
8: end for
9: function COMPUTEOPTIMALPOSITION( $r_{i-1,i}, R_{i-1,i}, \alpha_{i-1,i}, r_{i,i+1}, R_{i,i+1}, \alpha_{i,i+1}$ )
10:    $(\Psi_i, \theta_i) \leftarrow f_{Eq(3.35)}((R_{i-1,i+1}, \alpha_{i-1,i+1}), (R_{i,i+1}, \alpha_{i,i+1}))$        $\triangleright$  Cf. Eq. (3.35)
11:    $d_{i-1,i+1} \leftarrow \|r_{i-1} - r_{i+1}\|_2$                        $\triangleright$  Upstream-downstream distance
12:    $d_{i,i+1}^{\text{opt}} \leftarrow \text{FINDROOT}(f_{Eq(3.34)}(\Psi_i, \theta_i, d_{i-1,i+1})) \in [0, d_{i-1,i+1}]$   $\triangleright$  Cf. Eq. (3.34)
13:    $d_{i-1,i}^{\text{opt}} \leftarrow d_{i-1,i+1} - d_{i,i+1}^{\text{opt}}$ ;
14:    $r_i^{\text{opt}} \leftarrow \frac{d_{i,i+1}^{\text{opt}} \cdot r_{i-1} + d_{i-1,i}^{\text{opt}} \cdot r_{i+1}}{d_{i-1,i+1}}$            $\triangleright$  Cf. Eq. (3.37)
15:   return  $r_i^{\text{opt}}$ 
16: end function

```

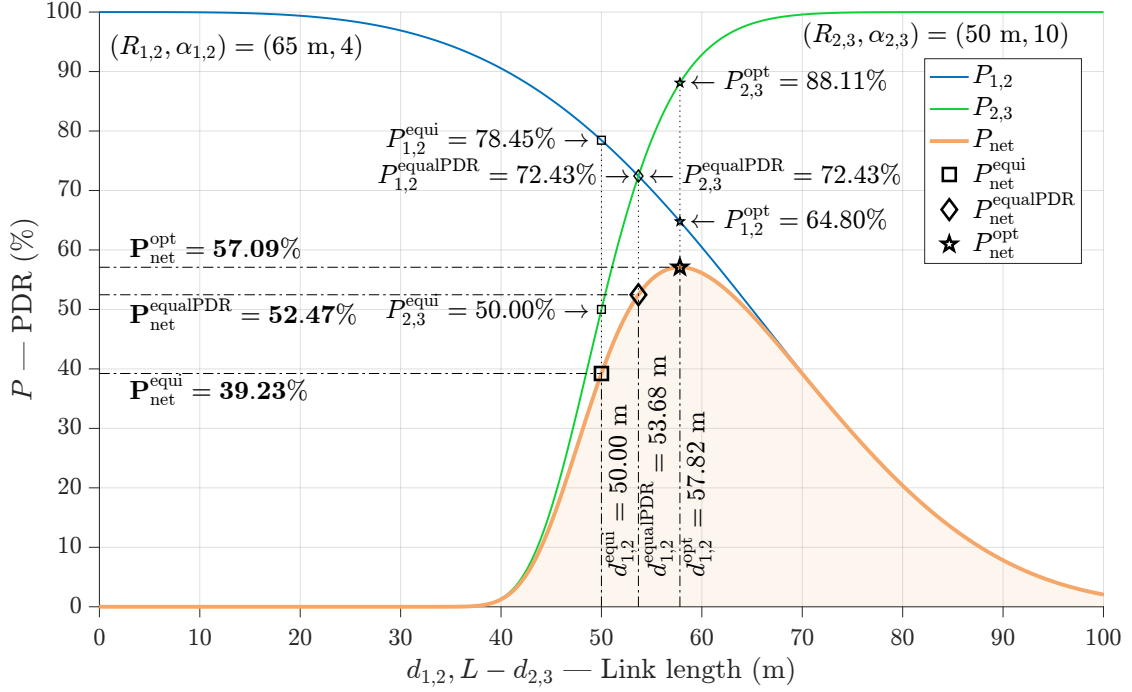


Figure 3.4. Comparison of relay placement strategies in a wireless line network of length $L = 100$ m consisting of three nodes: a source, a relay in between, and a ground station. The 2 link PDR models are represented by the blue line $(R_{1,2}, \alpha_{1,2}) = (65 \text{ m}, 4)$ and the green line $(R_{2,3}, \alpha_{2,3}) = (50 \text{ m}, 10)$, while the orange line represents their product, P_{net} . The area under P_{net} is shaded in orange.

The thicker square represents the PDR of $P_{\text{net}}^{\text{equi}} = 78.45\% \cdot 50.00\% = 39.23\%$ when the relay is placed in the middle of the network, $[d_{1,2}^{\text{equi}}, d_{2,3}^{\text{equi}}]^T = [50 \text{ m}, 50 \text{ m}]^T$. The thicker rhombus represents the PDR of $P_{\text{net}}^{\text{equalPDR}} = 72.43\% \cdot 72.43\% = 52.47\%$ using the distances where the link PDR lines intersect, $[d_{1,2}^{\text{equalPDR}}, d_{2,3}^{\text{equalPDR}}]^T = [53.68 \text{ m}, 46.32 \text{ m}]^T$. Finally, the thicker star highlights the solution with optimal placement, achieving a PDR of $P_{\text{net}}^{\text{opt}} = 64.80\% \cdot 88.11\% = 57.09\%$ at the distances $[d_{1,2}^{\text{opt}}, d_{2,3}^{\text{opt}}]^T = [57.82 \text{ m}, 42.18 \text{ m}]^T$.

The three solutions are presented in order of increasing performance. To conclude, the link PDRs for each strategy at the previously defined distances are emphasized. The smaller squares, rhombuses, and stars highlight the link PDRs obtained with the presented strategies: $P_{1,2}(d_{1,2}^{\text{equi}}) = 78.45\%$ and $P_{2,3}(d_{2,3}^{\text{equi}}) = 50.00\%$, $P_{1,2}(d_{1,2}^{\text{equalPDR}}) = 72.43\%$ and $P_{2,3}(d_{2,3}^{\text{equalPDR}}) = 72.43\%$, and $P_{1,2}(d_{1,2}^{\text{opt}}) = 64.80\%$ and $P_{2,3}(d_{2,3}^{\text{opt}}) = 88.11\%$, respectively. It is noteworthy that the distances in the equidistant strategy are uniform, and the link PDRs in the equal-PDR relay placement are consistent.

3.6 Overview of Network Nodes

This section visually illustrates how the methods described in the previous parts of this chapter interact under DRP relay placement for each node type. The variables in the following figures refer to a single TDMA round. To help with identification, the main blocks are highlighted in green, packet types (sent and received) in azure, decision blocks in blue, delays in red, and the most important data elements (stored and retrieved) in yellow.

3.6.1 Source

Figure 3.5 displays the process flow of the source node.

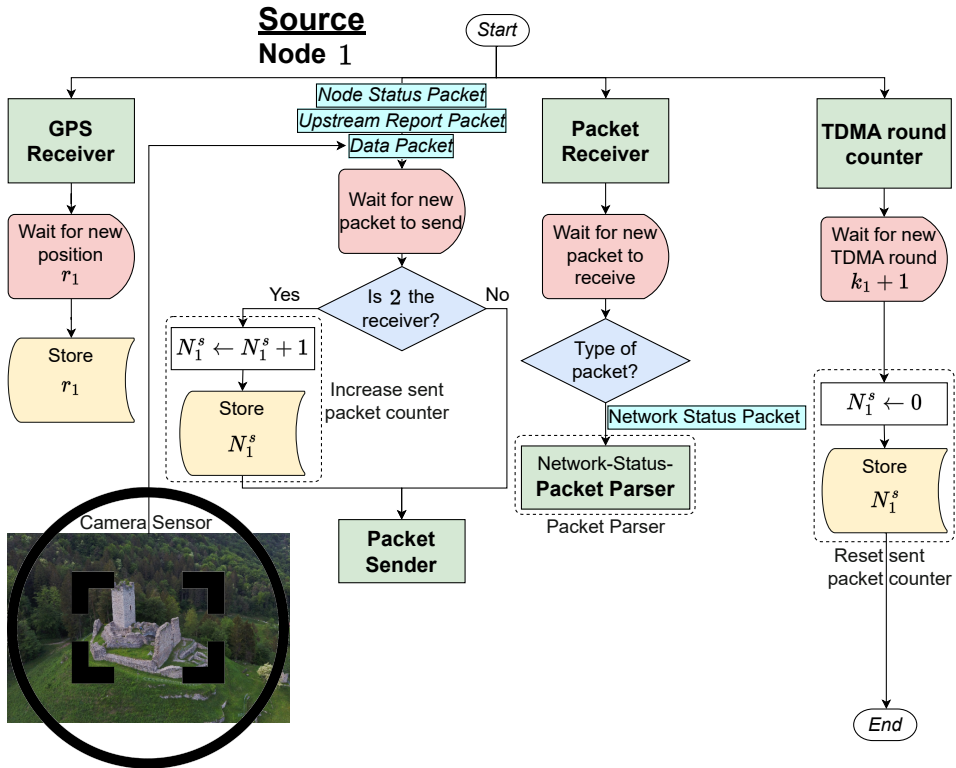


Figure 3.5. Process flow of a source node (node 1) during TDMA round k_1 . The key functional blocks are displayed in green, the packet types are in azure, the decision blocks in blue, the delays in red, and the most relevant data elements are highlighted in yellow for easy identification. The image, a drone view of the Restór castle (Comano Terme, Italy), is sourced from [36].

3.6.2 Relay

Figure 3.6 displays the process flow of a relay node.

3.6.3 Ground Station

Figure 3.7 displays the process flow of the ground station node.

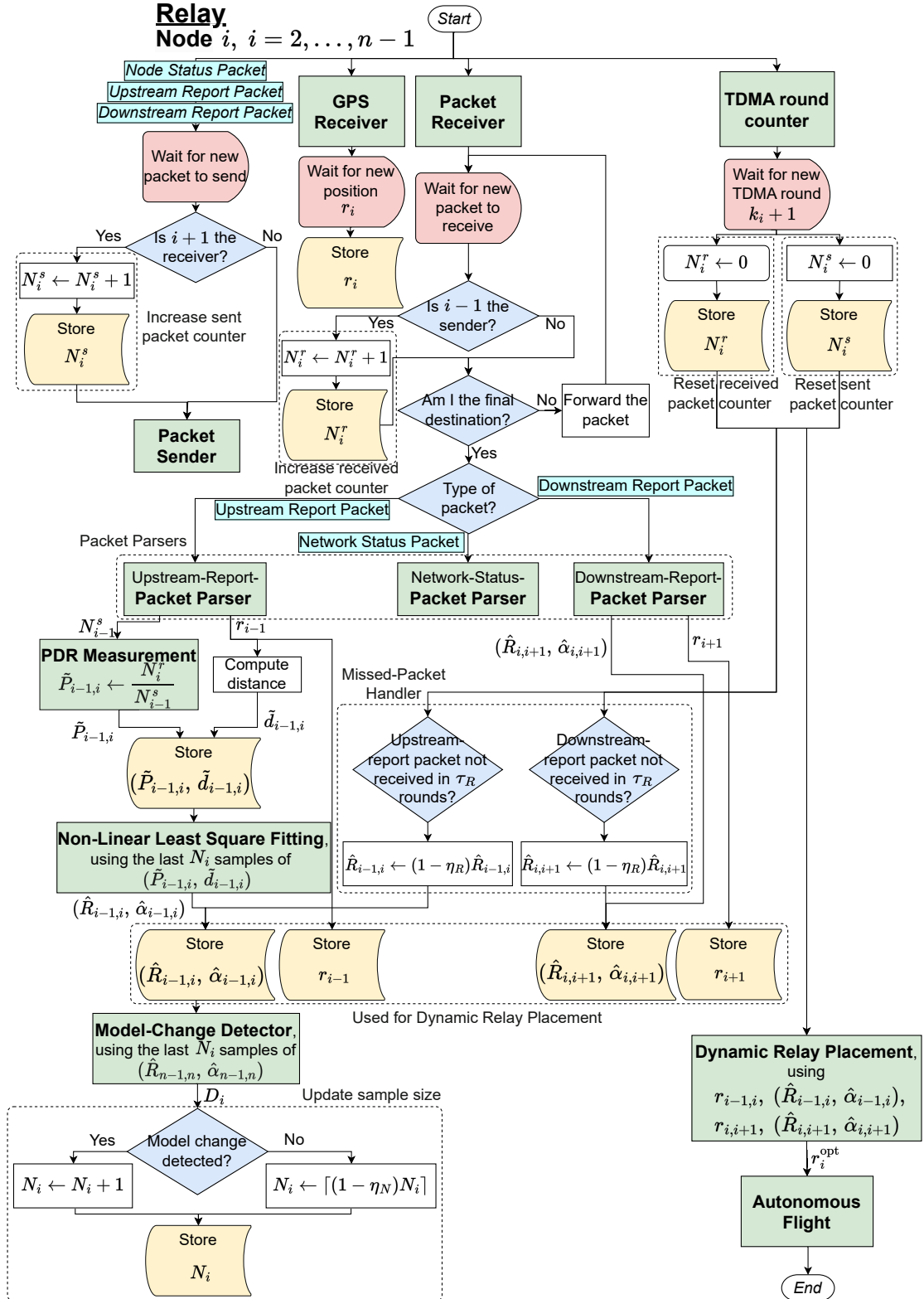


Figure 3.6. Process flow of a relay node (node i , with $i = 2, \dots, n - 1$) during TDMA round k_i . The key functional blocks are shown in green, packet types are highlighted in azure, decision blocks in blue, delays in red, and important data elements are displayed in yellow to facilitate identification.

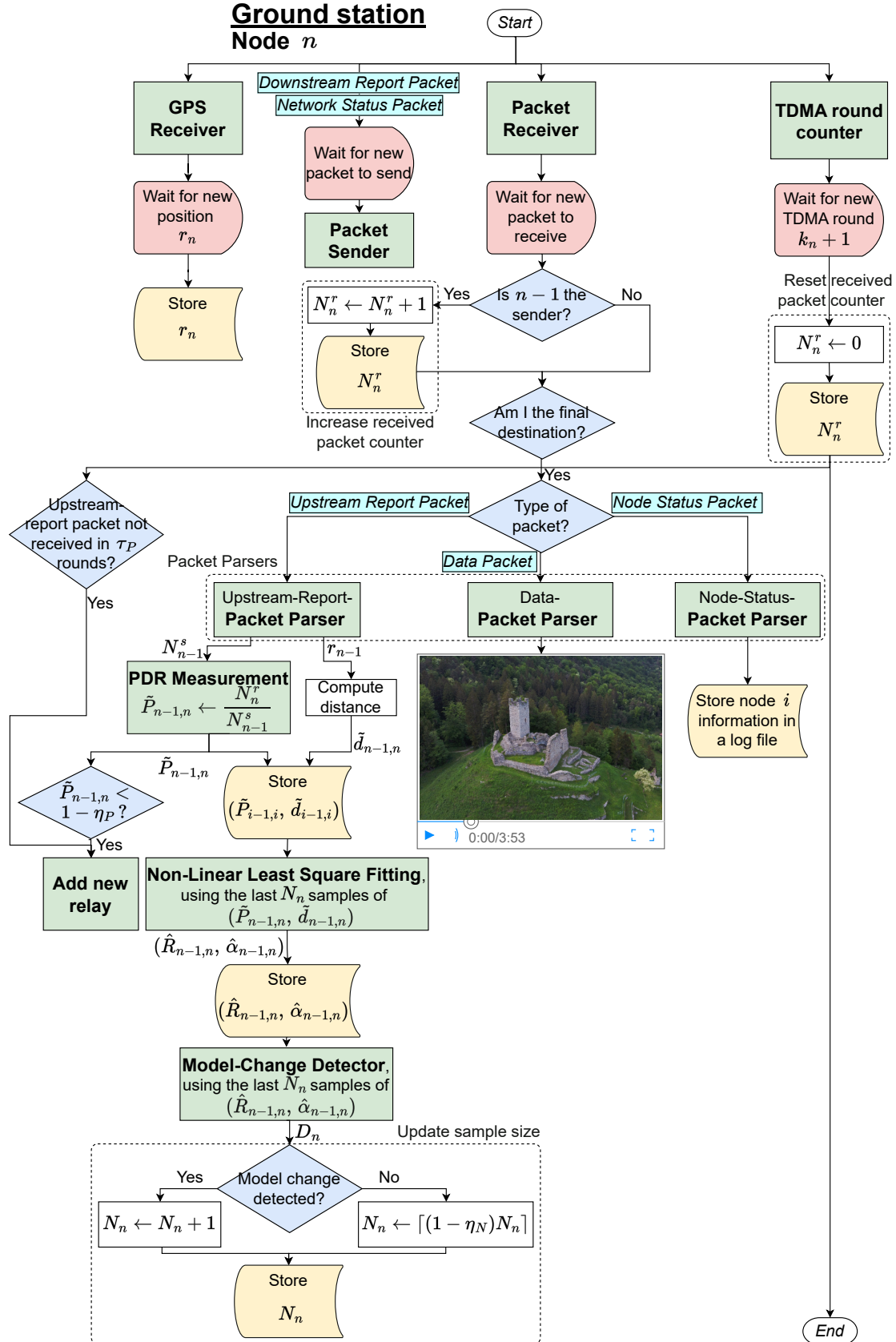


Figure 3.7. Process flow of a ground station node (node n) during TDMA round k_n . The key functional blocks are displayed in green, the packet types in blue, the decision blocks in blue, the delays in red, and the most relevant data elements in yellow to aid identification. The image is sourced from [36].

4 Experimental Design and Simulation

The simulations in this study are conducted, using the software in Subsection 4.1, on a line network consisting of seven ($n = 7$) nodes, including one source, five relay, and one ground station. The purpose of the simulations is to assess the performance of each of the strategies proposed in Section 3.5. Secondarily, we are interested in knowing the error in the estimations, to test the quality fitting in Section 3.2. Lastly, we simulate different scenarios, including some with model changes, as we are also interested in knowing the effectiveness of the model change detector discussed in Section 3.3.

The source node is the only node with designated waypoints, while the relays move according to one of the three strategies described in Section 3.5: equidistant relay placement (described in Subsection 3.5.1), equal-PDR relay placement, described in Subsection 3.5.2, and DRP relay placement, described in Subsection 3.5.3. Since we are interested in separating the performances of these strategies from the estimation process, abstracting from the estimated values, we evaluate them¹ using estimated parameters ($\hat{R}, \hat{\alpha}$) and also actual (true) parameters (R, α), adding up to five cases. The distinction between using estimated or true parameters is that in the former, the nodes lack knowledge of the link PDR models, whereas, in the latter, the models are fully known a priori. The DRP placement strategy when using true parameters can be considered the benchmark.

A generic variable x computed during a simulation is denoted as:

- (i) x^{equi} , when the relays adopt the equidistant relay placement strategy.
- (ii) $x^{\text{equalPDR,e}}$, when the relays adopt the equal-PDR relay placement strategy with estimated parameters.
- (iii) $x^{\text{equalPDR,t}}$, when the relays adopt the equal-PDR relay placement strategy with true parameters.
- (iv) $x^{\text{DRP,e}}$, when the relays adopt the DRP relay placement strategy with estimated parameters.
- (v) $x^{\text{DRP,t}}$, when the relays adopt the DRP relay placement strategy with true parameters.

The relay placement strategy is consistent for all relays within a single simulation but may vary between simulations. In this chapter, we detail in Section 4.2 the waypoints used in each simulation and in Section 4.3 the characteristics of the simulated link-PDR models. Finally, to measure the difference between the actual (simulated) parameters and the estimated parameters, a metric is introduced in Subsection 4.3.3, which calculates the error committed in an individual estimation and during an entire simulation, helping us assess the accuracy of our estimations.

¹The equidistant relay placement strategy is independent of the link models, thus it will be considered as a single strategy.

4.1 Simulation Software

This section briefly describes the software used to simulate the network and evaluate its performance. The simulation software was developed in C and implements the various components discussed in Chapter 3, including, but not limited to, a reliable PDR measurement system, a link PDR model fitting procedure based on weighted non-linear least squares², the model change detector, and the relay placement strategies under investigation. The software was based on previous work by Pinto [2] and has been designed to simulate each node as a separate process, which makes it easy to simulate the full network. Furthermore, the software has been tested and validated through successful communication tests between nodes running on separate Linux machines.

In addition to the simulation software developed in C, we also created a graphical visualizer using MATLAB® R2022a [37]. This visualizer provides a visual representation of the nodes and their movements during the simulation. It displays the position and velocity of each node in the network on a 2D map, centered at the ground station, and tracks their past trajectories. A video is generated at the end of the simulation.

To facilitate offline analysis and visualization of the data, we also developed a MATLAB® program. This program extracts data from a log file recorded by the ground station node during the simulation and provides various ways to analyze and visualize the network characteristics and performance over time. The log file contains information from node-status packets sent from all other nodes in the network to the ground station during the simulation, which was recorded using the C software mentioned at the beginning of this section. All the plots presented in this work were generated using this program.

4.2 Waypoints

The source takes off from the ground station located at (0 m, 0 m), which serves as the reference point in a NED frame. Then, it follows a path of 73 waypoints, spaced 2.5° apart, forming a semicircle with a radius of 400 m. The semicircle begins at the waypoint ‘A’, located at (400 m, 0 m), and then travels through the waypoint ‘B’ at (0 m, -400 m), and ends at the waypoint ‘C’, located at (-400 m, 0 m). The source moves through the aforementioned waypoints, ‘A’, ‘B’, and ‘C’, in successive TDMA rounds, as recorded by the ground station and identified as k^A , k^B , and k^C respectively. These TDMA rounds are shown in Figure 4.1, for a simulation. The average end-to-end PDR P_{net} is calculated in $[k^A, k^C]$, according to Equation (3.21). Additionally, some scenarios involve changes to the link PDR models when the source reaches the waypoint ‘B’, at TDMA round k^B , highlighting the significance of these three waypoints. The simulation time, t_{sim} , denotes the virtual time used in computer simulations to track the progression of the simulation and represents the elapsed time within the simulated environment.

The bearing angle from the ground station ($x_{\text{GS}}, y_{\text{GS}}$) to a waypoint ($x_{\text{waypoint}}, y_{\text{waypoint}}$), denoted as θ^{bear} , is the angle measured in the clockwise direction from the

²The MPFIT library was used for the non-linear least squares [34].

North line, with the ground station as the origin, to the line segment connecting the ground station and the waypoint. This angle has $[0, 2\pi)$ as its codomain and is defined in Equation (4.1), where $\tilde{\theta} \in (-\pi, \pi]$ is defined in Equation (4.2).

$$\theta^{\text{bear}} = \begin{cases} \tilde{\theta}, & \text{if } \tilde{\theta} \geq 0 \\ \tilde{\theta} + 2\pi, & \text{if } \tilde{\theta} < 0 \end{cases} \quad (4.1)$$

$$\tilde{\theta} = \text{atan2}(x_{\text{waypoint}} - x_{\text{GS}}, y_{\text{waypoint}} - y_{\text{GS}}) \quad (4.2)$$

An exhaustive list of the waypoints, ordered in chronological order of visiting, is reported in Table 4.1 and displayed in Figure 4.2.

Table 4.1. Source waypoints

Waypoint index	Waypoint name	x (m)	y (m)	θ^{bear} (m)
1	A (A_1)	400.00	0.00	90.00
2	A_2	399.62	-17.45	92.50
3	A_3	398.48	-34.86	95.00
4	A_4	396.58	-52.21	97.50
5	A_5	393.92	-69.46	100.00
6	A_6	390.52	-86.58	102.50
7	A_7	386.37	-103.53	105.00
8	A_8	381.49	-120.28	107.50
9	A_9	375.88	-136.81	110.00
10	A_{10}	369.55	-153.07	112.50
11	A_{11}	362.52	-169.05	115.00
12	A_{12}	354.80	-184.70	117.50
13	A_{13}	346.41	-200.00	120.00
14	A_{14}	337.36	-214.92	122.50
15	A_{15}	327.66	-229.43	125.00
16	A_{16}	317.34	-243.50	127.50
17	A_{17}	306.42	-257.12	130.00
18	A_{18}	294.91	-270.24	132.50
19	A_{19}	282.84	-282.84	135.00
20	A_{20}	270.24	-294.91	137.50
21	A_{21}	257.12	-306.42	140.00
22	A_{22}	243.50	-317.34	142.50
23	A_{23}	229.43	-327.66	145.00
24	A_{24}	214.92	-337.36	147.50
25	A_{25}	200.00	-346.41	150.00
26	A_{26}	184.70	-354.80	152.50
27	A_{27}	169.05	-362.52	155.00
28	A_{28}	153.07	-369.55	157.50
29	A_{29}	136.81	-375.88	160.00
30	A_{30}	120.28	-381.49	162.50
31	A_{31}	103.53	-386.37	165.00
32	A_{32}	86.58	-390.52	167.50

33	A ₃₃	69.46	-393.92	170.00
34	A ₃₄	52.21	-396.58	172.50
35	A ₃₅	34.86	-398.48	175.00
36	A ₃₆	17.45	-399.62	177.50
37	B (B ₁)	0.00	-400.00	180.00
38	B ₂	-17.45	-399.62	182.50
39	B ₃	-34.86	-398.48	185.00
40	B ₄	-52.21	-396.58	187.50
41	B ₅	-69.46	-393.92	190.00
42	B ₆	-86.58	-390.52	192.50
43	B ₇	-103.53	-386.37	195.00
44	B ₈	-120.28	-381.49	197.50
45	B ₉	-136.81	-375.88	200.00
46	B ₁₀	-153.07	-369.55	202.50
47	B ₁₁	-169.05	-362.52	205.00
48	B ₁₂	-184.70	-354.80	207.50
49	B ₁₃	-200.00	-346.41	210.00
50	B ₁₄	-214.92	-337.36	212.50
51	B ₁₅	-229.43	-327.66	215.00
52	B ₁₆	-243.50	-317.34	217.50
53	B ₁₇	-257.12	-306.42	220.00
54	B ₁₈	-270.24	-294.91	222.50
55	B ₁₉	-282.84	-282.84	225.00
56	B ₂₀	-294.91	-270.24	227.50
57	B ₂₁	-306.42	-257.12	230.00
58	B ₂₂	-317.34	-243.50	232.50
59	B ₂₃	-327.66	-229.43	235.00
60	B ₂₄	-337.36	-214.92	237.50
61	B ₂₅	-346.41	-200.00	240.00
62	B ₂₆	-354.80	-184.70	242.50
63	B ₂₇	-362.52	-169.05	245.00
64	B ₂₈	-369.55	-153.07	247.50
65	B ₂₉	-375.88	-136.81	250.00
66	B ₃₀	-381.49	-120.28	252.50
67	B ₃₁	-386.37	-103.53	255.00
68	B ₃₂	-390.52	-86.58	257.50
69	B ₃₃	-393.92	-69.46	260.00
70	B ₃₄	-396.58	-52.21	262.50
71	B ₃₅	-398.48	-34.86	265.00
72	B ₃₆	-399.62	-17.45	267.50
73	C	-400.00	0.00	270.00

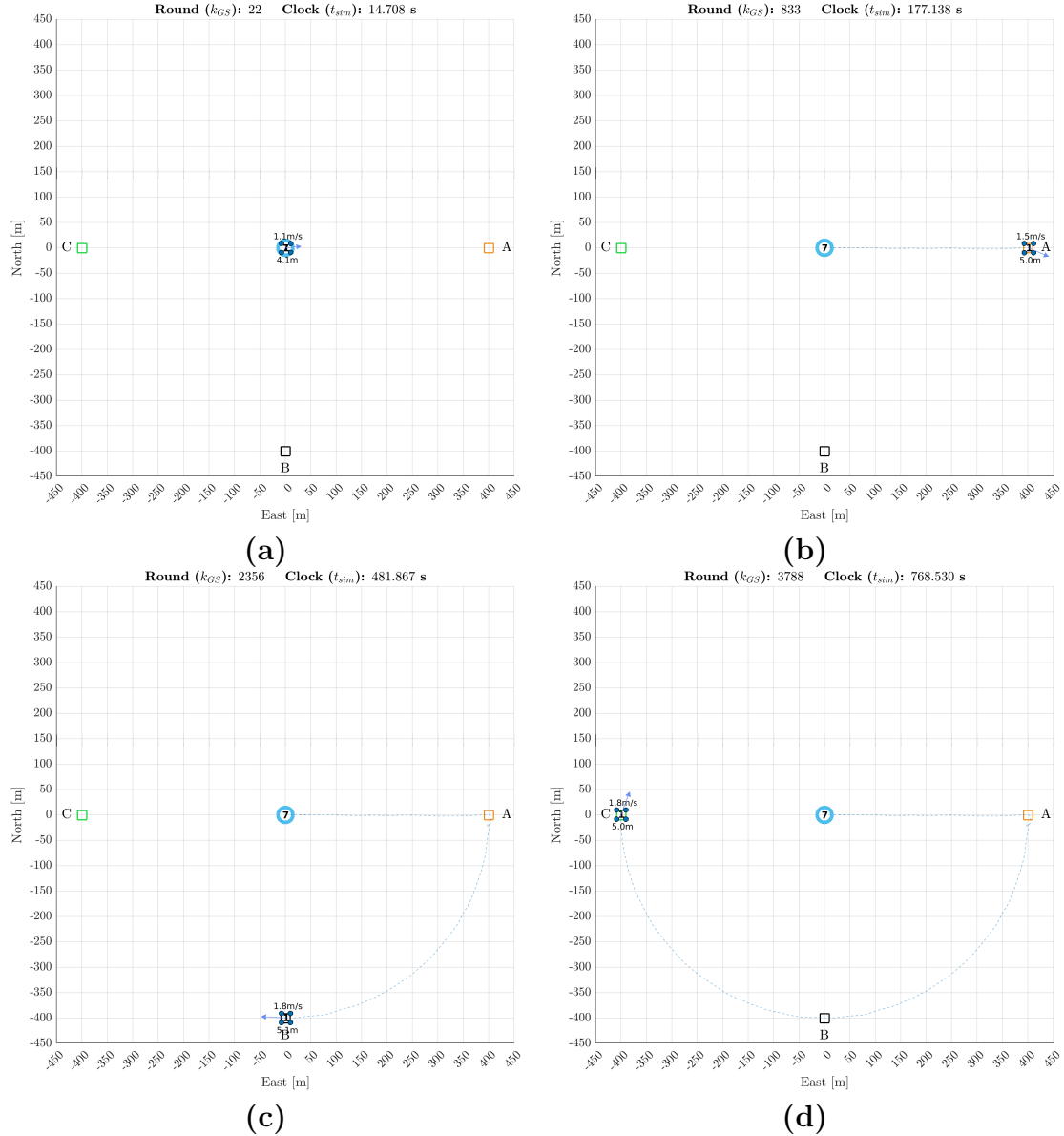


Figure 4.1. The graphical visualizer shows the main waypoints – ‘A’, ‘B’, and ‘C’ – that the source passes during successive TDMA rounds, as recorded by the ground station. The bigger, encircled values represent the node UIDs, whereas the values located above the nodes represent their speed values (in m/s), and the values located below represent their altitude values (in m). **(a)** At the start of the simulation, the source is positioned at the ground station ((0 m, 0 m)). **(b)** At TDMA round k^A , the source reaches the waypoint ‘A’ ((400 m, 0 m)) and the calculation of the average network PDR for the simulation begins. **(c)** At TDMA round k^B , the source reaches the waypoint ‘B’ ((0 m, −400 m)) and the link models may change, as detailed in Section 4.3. **(d)** At TDMA round k^C , the source reaches the waypoint ‘C’ ((−400 m, 0 m)) and the calculation of the average network PDR ends.

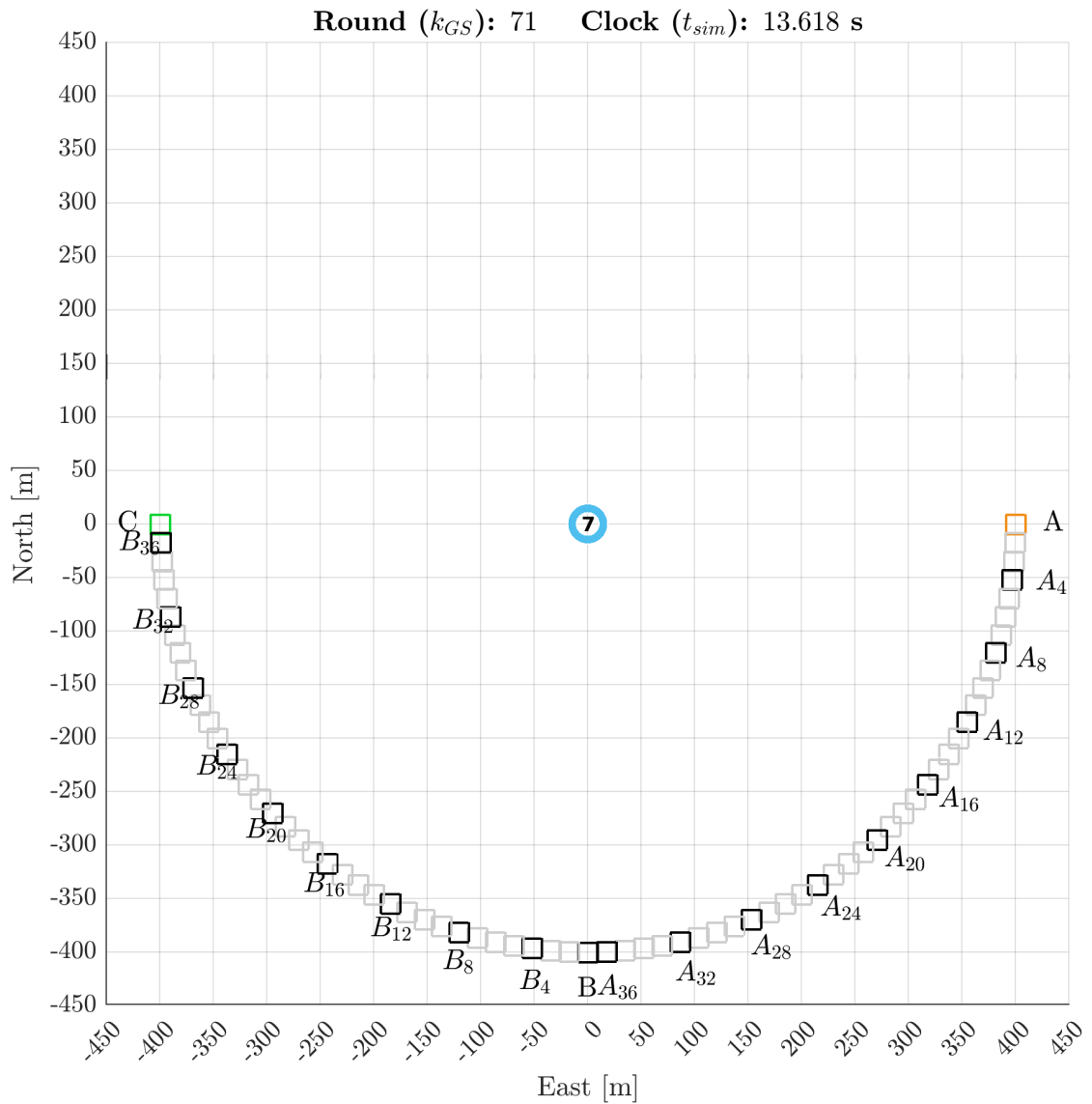


Figure 4.2. A graphical representation of the 73 waypoints traveled by the source in a NED frame centered at the ground station, starting from the ground station (located at (0 m, 0 m)). The source travels in a clockwise direction, forming a semicircle with a radius of 400 m that connects the waypoints ‘A’ (at (400 m, 0 m)) and ‘C’ (at (−400 m, 0 m)) through 71 other waypoints.

4.3 Modeling Link PDRs

With reference to the notation used in Section 2.2, the network simulated consisted of $n = 7$ nodes, $V = \{1, 2, 3, 4, 5, 6, 7\}$. The node entrance order is:

1. At the beginning there is only one node the ground station (node 7).
2. Then, the source is added (node 1).
3. Finally, the relays are added at different times, in order of UID (2; 3; 4; 5; and 6).

A relay is added every time that the link PDR between the upstream node of the ground station and the ground station becomes lower than $1 - \eta_P$, according to Equation (3.22). In our case, where $\eta_P = 10\%$, it means that whenever the PDR between the ground station upstream node becomes lower than 90%, another relay is added to the network. The 22 possible edges are in $E = \{\{1, 7\}, \{1, 2\}, \{2, 7\}, \{2, 3\}, \{3, 7\}, \{3, 4\}, \{4, 7\}, \{4, 5\}, \{5, 7\}, \{5, 6\}, \{6, 7\}, \{7, 1\}, \{2, 1\}, \{7, 2\}, \{3, 2\}, \{7, 3\}, \{4, 3\}, \{7, 4\}, \{5, 4\}, \{7, 5\}, \{6, 5\}, \{7, 6\}\}$.

4.3.1 Link Models

In the simulations, packets were dropped according to Equation (2.7), where the model parameters $(R_{i,j}, \alpha_{i,j})$ were specific to each link i, j . The simulated values for these models are listed in Table 4.2. The values for the first model set, designated as ‘1’, are based on the example in [6] (Subsection 4.2.1).³ and will be used as the first scenario, where no model change occurs. The other two model sets, labeled as ‘2’ and ‘3’, will be used in certain scenarios that will be described in the next subsection, Subsection 4.3.2. These scenarios will test the responsiveness of the model change detector, which is outlined in Subsection 3.3.1, and ultimately their impact on the network performance.

Our primary focus was optimizing the end-to-end PDR from node 1 to node 7, which required estimating the PDR models for the first half of the links in the link set E . However, we still needed to assign values to the simulated PDR models for the opposite direction, which we assumed to be symmetrical: $(R_{i,j}(k), \alpha_{i,j}(k)) = (R_{j,i}(k), \alpha_{j,i}(k)) \forall k \in \mathbb{Z}$, meaning the success rate of transmitting packets in either direction is the same. This assumption was based on the idea that transmission conditions in both directions are typically similar. In Table 4.2, only the links 4 (4rev.) and 5 (5rev.) undergo changes. Specifically, in the model set ‘2’, the R of the link 4 (4rev.) is increased by 20 m while the R of the link 5 (5rev.) is decreased by 20 m, whereas in the model set ‘3’ their values are swapped. The decision was made to alter only the links 4 (4rev.) and 5 (5rev.), either suddenly (in the model sets ‘1’ and ‘2’) or gradually (in the model set ‘3’). This was done so that all the

³The only differences from the example are the values of $\alpha_{4,7}, \alpha_{7,4}, \alpha_{4,5}$, and $\alpha_{5,4}$, which were changed to 3.7 from 3.9. This allows for the links 4 (4rev.) and 5 (5rev.) to swap their pairs of model parameters – as done in the scenarios ‘c’ and ‘d’ – simply by exchanging their R values, as they have identical α values.

relays would continue to move in the same manner after a model change, except for node 5, which would experience changes in both its upstream and downstream links.

Table 4.2. The three model sets of simulated values for the PDR model parameters on each link in the network $i, j \in E$. The packet delivery ratio is determined by the specific pair $(R_{i,j}, \alpha_{i,j})$ of model parameters assigned to each link as well as the distance $d_{i,j}$ between the endpoints i and j of the considered link. The link number indicates the order of the link in the line network (up to 6), with “rev.” denoting the reversed link. The assumption of symmetrical transmission conditions is made, meaning the success rate of transmitting packets in either direction is the same. The first model set is based on an example from [6] and will be used as the reference scenario with no model changes. The values for links 4 (4rev.) and 5 (5rev.) are changed in the second and third model sets to study the efficacy of the model change detector in different scenarios, described in Subsection 4.3.2, and ultimately their impact of a model change on the network performance.

Link number	Link	Model set 1	Model set 2	Model set 3			
		$R^{(1)}$ (m)	$\alpha^{(1)}$ (1)	$R^{(2)}$ (m)	$\alpha^{(2)}$ (1)	$R^{(3)}$ (m)	$\alpha^{(3)}$ (1)
1	1,7	90	3.4	90	3.4	90	3.4
1rev.	7,1	90	3.4	90	3.4	90	3.4
1	1,2	90	3.4	90	3.4	90	3.4
1rev.	2,1	90	3.4	90	3.4	90	3.4
2	2,7	104	2.2	104	2.2	104	2.2
2rev.	7,2	104	2.2	104	2.2	104	2.2
2	2,3	104	2.2	104	2.2	104	2.2
2rev.	3,2	104	2.2	104	2.2	104	2.2
3	3,7	148	2.8	148	2.8	148	2.8
3rev.	7,3	148	2.8	148	2.8	148	2.8
3	3,4	148	2.8	148	2.8	148	2.8
3rev.	4,3	148	2.8	148	2.8	148	2.8
4	4,7	167	3.7	147	3.7	83	3.7
4rev.	7,4	167	3.7	147	3.7	83	3.7
4	4,5	167	3.7	147	3.7	83	3.7
4rev.	5,4	167	3.7	147	3.7	83	3.7
5	5,7	83	3.7	103	3.7	167	3.7
5rev.	7,5	83	3.7	103	3.7	167	3.7
5	5,6	83	3.7	103	3.7	167	3.7
5rev.	6,5	83	3.7	103	3.7	167	3.7
6	6,7	110	3.3	110	3.3	110	3.3
6rev.	7,6	110	3.3	110	3.3	110	3.3

4.3.2 Simulation Scenarios

The evaluation of relay placement strategies was conducted under four different scenarios:

- (a) Scenario ‘a’: unchanged model, defined in Equation (4.3).
- (b) Scenario ‘b’: small abrupt model change, defined in Equation (4.4).
- (c) Scenario ‘c’: large abrupt model change, defined in Equation (4.5).
- (d) Scenario ‘d’: incremental model change, defined in Equation (4.6), where q is as in Equation (4.7) and $\theta_1^{\text{bear}}(k)$ is the bearing angle from the ground station to the source at time k .

The line network simulation at various stages, where the number of active relays increases from 0 to 5, is displayed in Figure 4.4. The values of the model parameters are determined by the scenario considered: Equation (4.3) (scenario ‘a’), Equation (4.4) (scenario ‘b’), Equation (4.5) (scenario ‘c’), Equation (4.6) (scenario ‘d’). The notation used for the weighted edges is the one presented in Subsection 2.3.4.

The schematized maps of the four scenarios are depicted in Figure 4.3. The objects in the third quadrant represent areas where the models change, with red areas indicating a region where the probability of packet reception is decreased (repulsive region) and blue areas when it is increased (attractive region). The red areas represent degradation in the link PDR model, e.g., due to interference, while the blue areas represent an improvement, e.g., due to enhanced transmitter antenna gain. The shade of the color reflects the level of change in the model. In particular, it is darker in Figure 4.3c than in Figure 4.3b, and it is progressive in Figure 4.3d.

The time evolutions for the six links⁴ in the network, for each of the four scenarios, are shown in Figures 4.5 (scenario ‘a’), 4.6 (scenario ‘b’), 4.7 (scenario ‘c’), and 4.8 (scenario ‘d’). In Figure 4.9, it can be seen a simulation in the scenario ‘b’ and where the relays are using the equidistant relay placement strategy, as evidenced by their equispaced trajectories. The simulation ends with the source reaching the final waypoint, ‘C’.

$$(R_e^{(a)}(k), \alpha_e^{(a)}(k)) = (R_e^{(1)}, \alpha_e^{(1)}), \quad k \in [k^A..k^C], \quad e \in E \quad (4.3)$$

$$(R_e^{(b)}(k), \alpha_e^{(b)}(k)) = \begin{cases} (R_e^{(1)}, \alpha_e^{(1)}), & k \in [k^A..k^B] \\ (R_e^{(2)}, \alpha_e^{(2)}), & k \in [k^B..k^C] \end{cases} \quad e \in E \quad (4.4)$$

$$(R_e^{(c)}(k), \alpha_e^{(c)}(k)) = \begin{cases} (R_e^{(1)}, \alpha_e^{(1)}), & k \in [k^A..k^B] \\ (R_e^{(3)}, \alpha_e^{(3)}), & k \in [k^B..k^C] \end{cases} \quad e \in E \quad (4.5)$$

$$(R_e^{(d)}(k), \alpha_e^{(d)}(k)) = \begin{cases} (R_e^{(1)}, \alpha_e^{(1)}), & k \in [k^A..k^B] \\ q(k) \cdot (R_e^{(1)}, \alpha_e^{(1)}) + \\ \quad + (1 - q(k)) \cdot (R_e^{(3)}, \alpha_e^{(3)}), & k \in [k^B..k^C] \end{cases} \quad e \in E \quad (4.6)$$

⁴As stated in Chapter 2, the links connecting the ground station to the source, in our case the links from 7 to 12, are not studied.

$$q(k) = \frac{\theta_1^{\text{bear}}(k) - \theta_c^{\text{bear}}}{\theta_b^{\text{bear}} - \theta_c^{\text{bear}}} \quad (4.7)$$

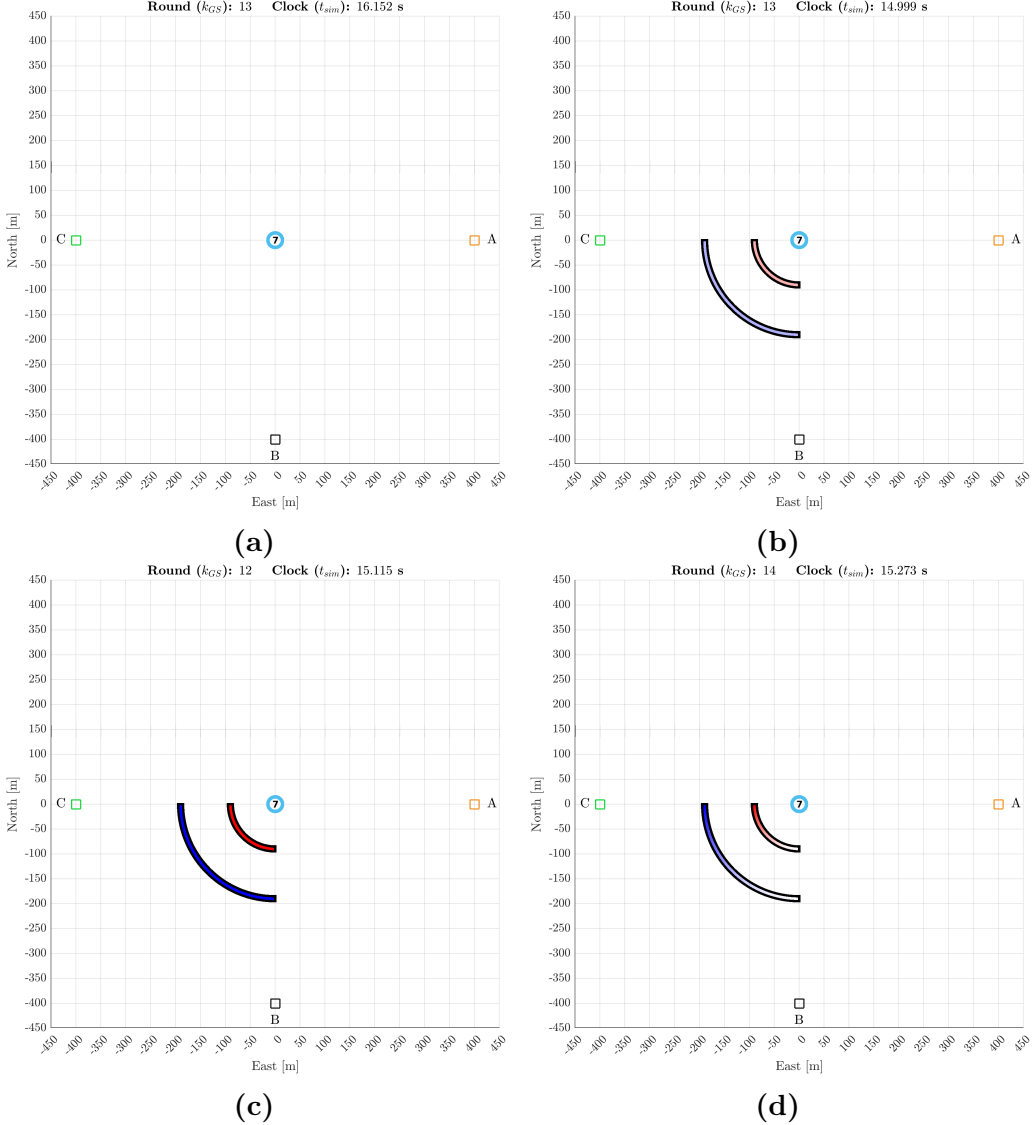


Figure 4.3. The four scenarios in which the relay placement strategies were evaluated, with the intensity of the obstacle colors indicating the magnitude of the changes in the models. **(a)** Scenario ‘a’: unchanged model. **(b)** Scenario ‘b’: abrupt model change of a small magnitude. **(c)** Scenario ‘c’: abrupt model change of a large magnitude, indicated by the full, darker colors. **(d)** Scenario ‘d’: incremental model change. The shade of the colors becomes progressively darker, reflecting an increase in the level of change in the models.

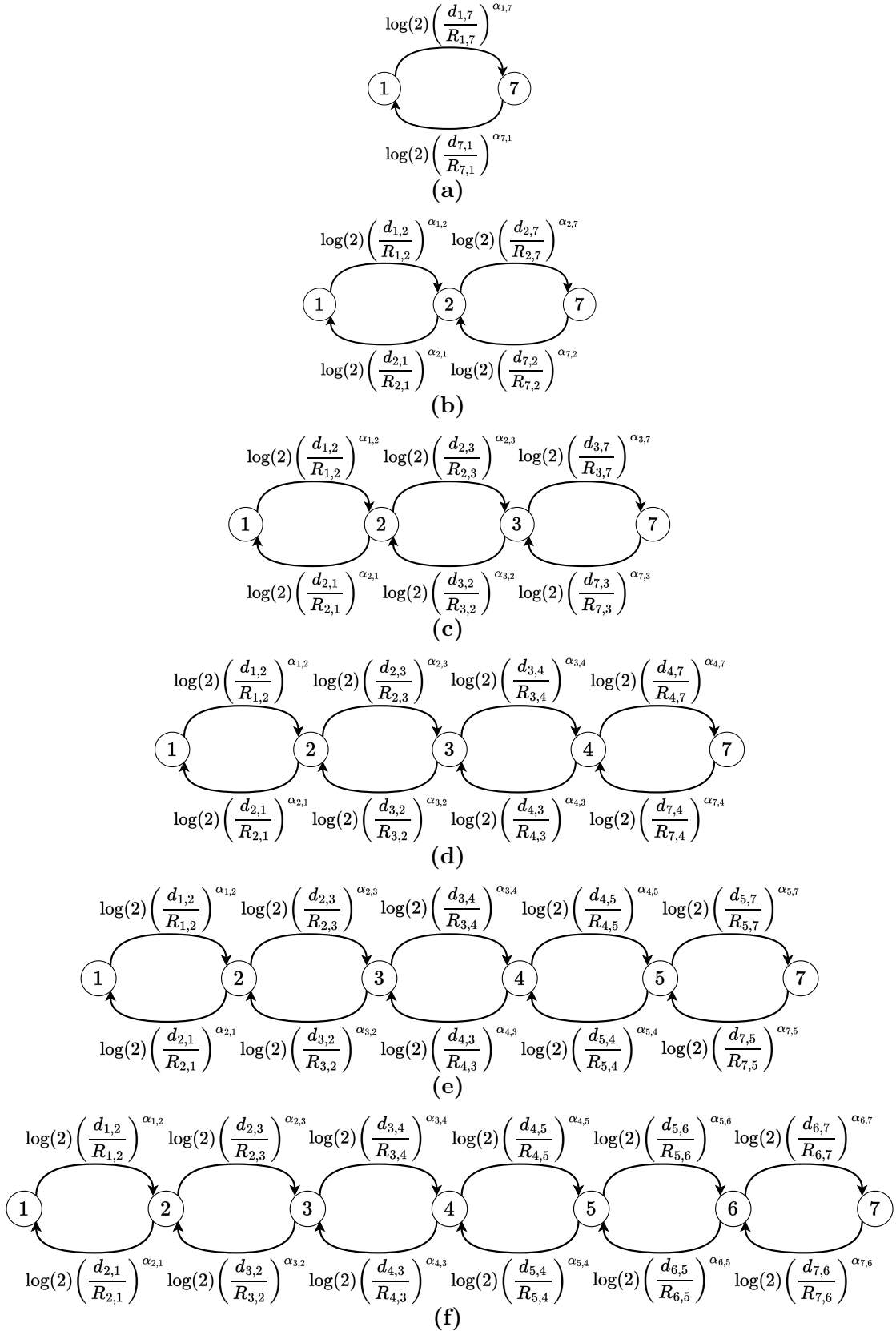


Figure 4.4. The weighted graph of our case-study line network, at different times.
 (a) $V = \{1, 7\}$; (b) $V = \{1, 2, 7\}$; (c) $V = \{1, 2, 3, 7\}$; (d) $V = \{1, 2, 3, 4, 7\}$; (e) $V = \{1, 2, 3, 4, 5, 7\}$; (f) $V = \{1, 2, 3, 4, 5, 6, 7\}$.

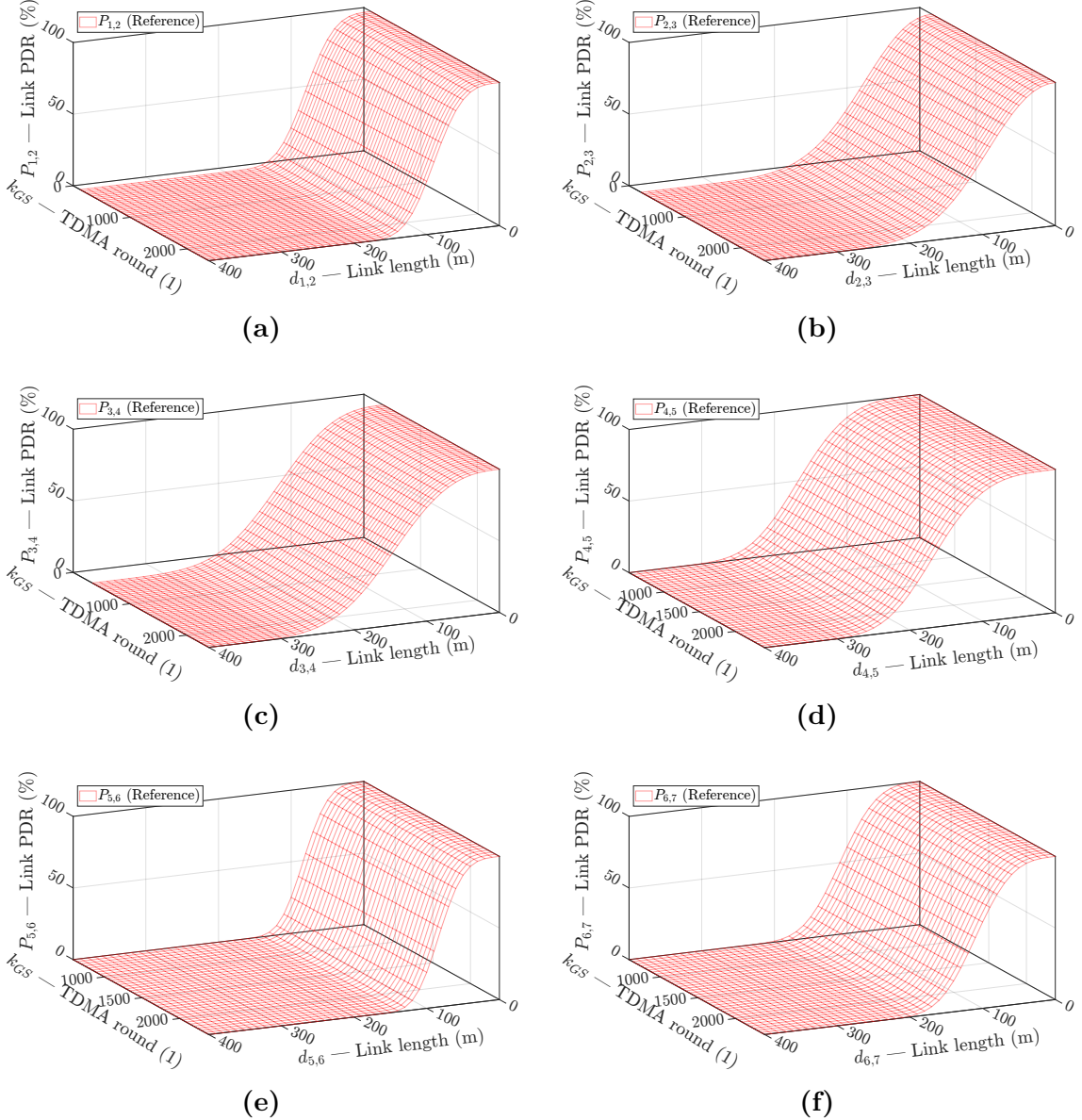


Figure 4.5. The time evolution of the actual link models in the scenario ‘a’, referred to as the ‘unchanged model’ scenario, progresses from link creation to k^A ($k_{GS} = 760$) and continues to k^C ($k_{GS} = 2422$). The models of the links remain constant throughout the simulation and their values are displayed in the model set ‘1’ section of Table 4.2. However, it is worth mentioning that the values of k^A and k^C may experience slight variations across different simulations.

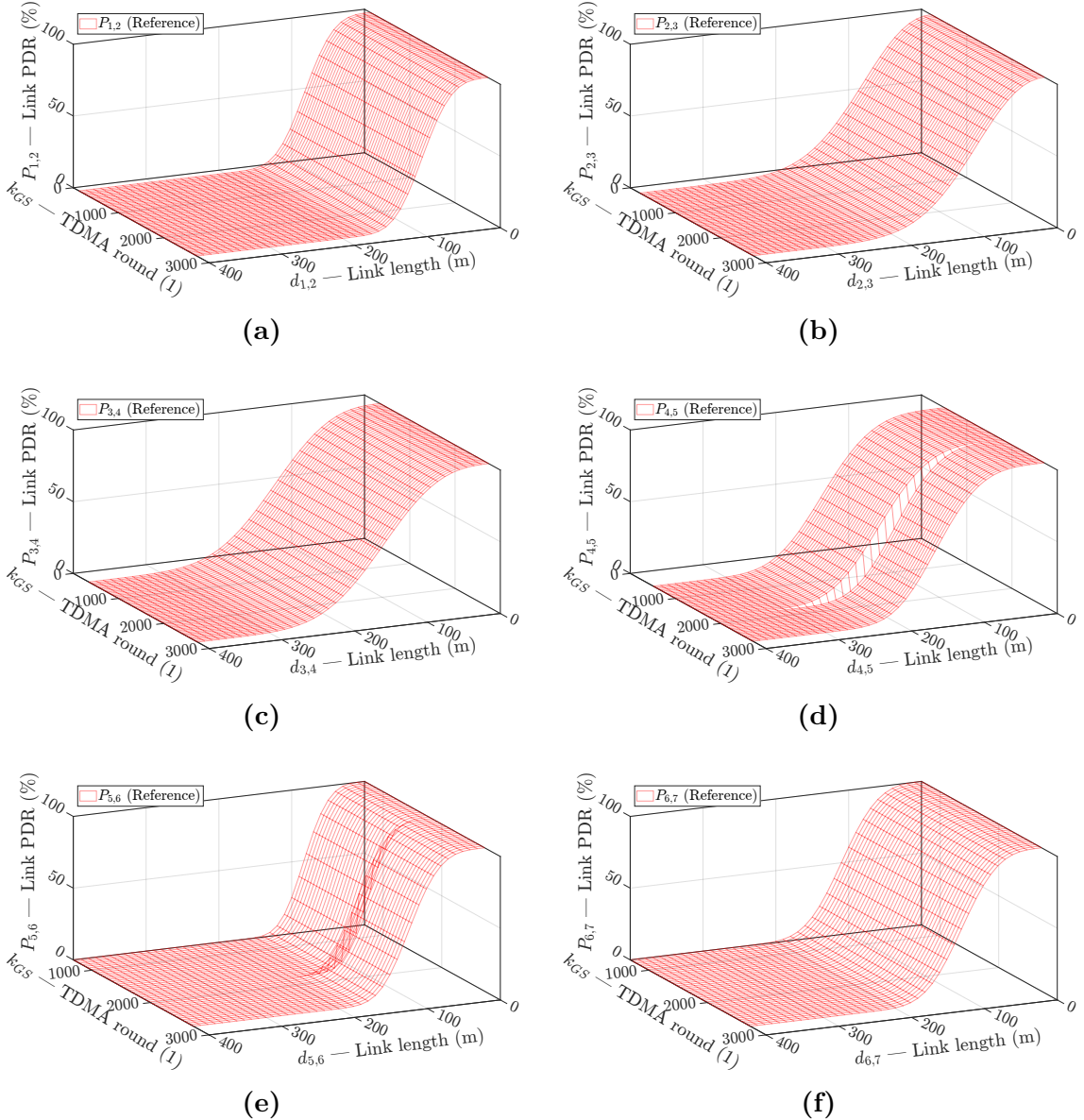


Figure 4.6. The time evolution of the actual link models in the scenario ‘b’, referred to as the ‘small abrupt model change’ scenario, progresses from link creation to k^A ($k_{GS} = 738$) and continues to k^C ($k_{GS} = 2745$). Only the models of links {4, 5}, {5, 4}, {5, 6}, and {6, 5} experience a sudden change at k^B ($k_{GS} = 1796$), switching from the model set ‘1’ to the model set ‘2’ as shown in Table 4.2. It should be noted that the values of k^A , k^B , and k^C may slightly vary from simulation to simulation.

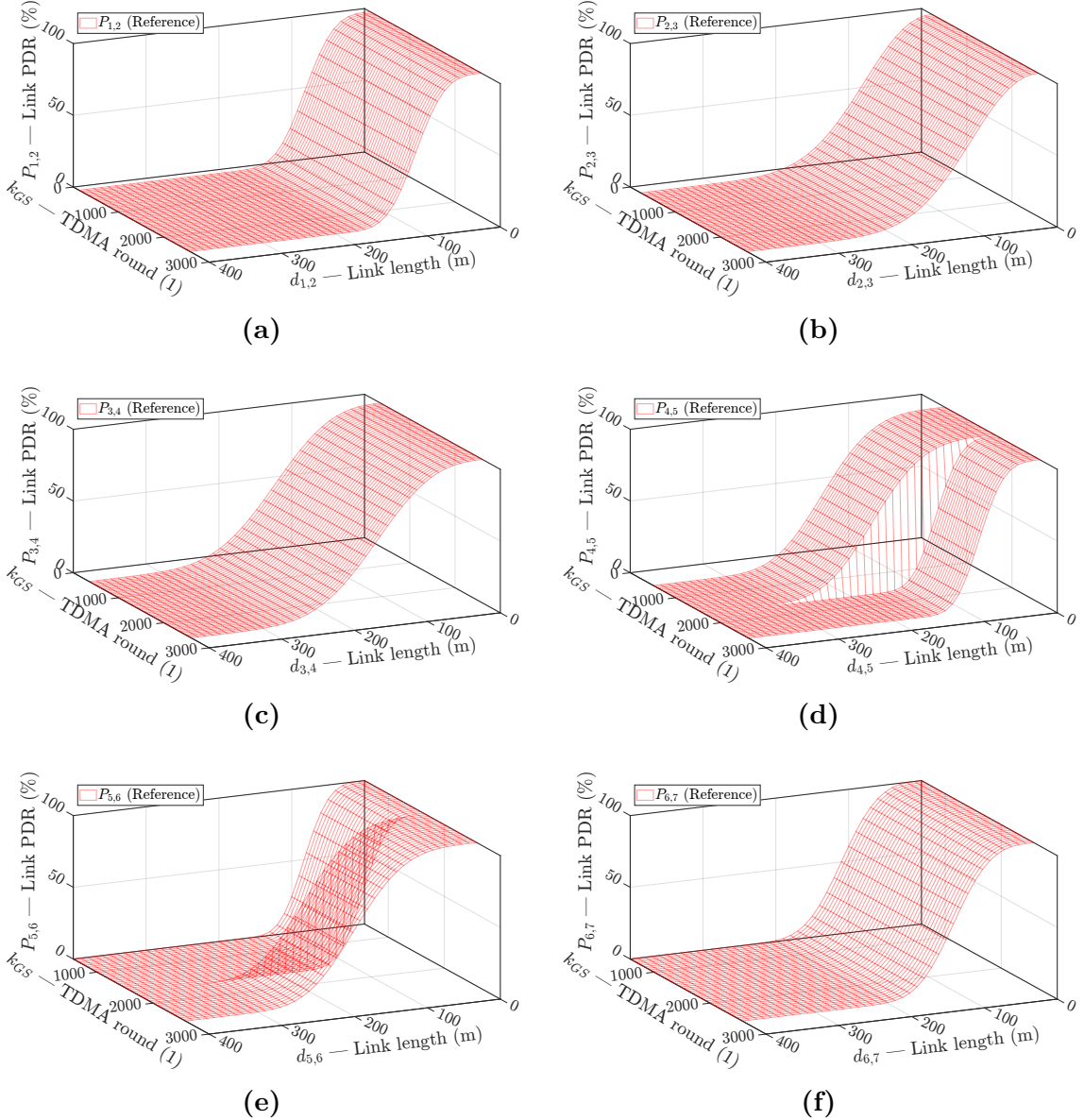


Figure 4.7. The time evolution of the actual link models in the scenario ‘c’, referred to as the ‘large abrupt model change’ scenario, progresses from link creation to k^A ($k_{GS} = 673$) and continues to k^C ($k_{GS} = 2614$). Only the models of links {4, 5}, {5, 4}, {5, 6}, and {6, 5} undergo a sudden change at k^B ($k_{GS} = 1658$), transitioning from the model set ‘1’ to the model set ‘3’ as indicated in Table 4.2. It is worth mentioning that k^A , k^B , and k^C may differ across simulations.

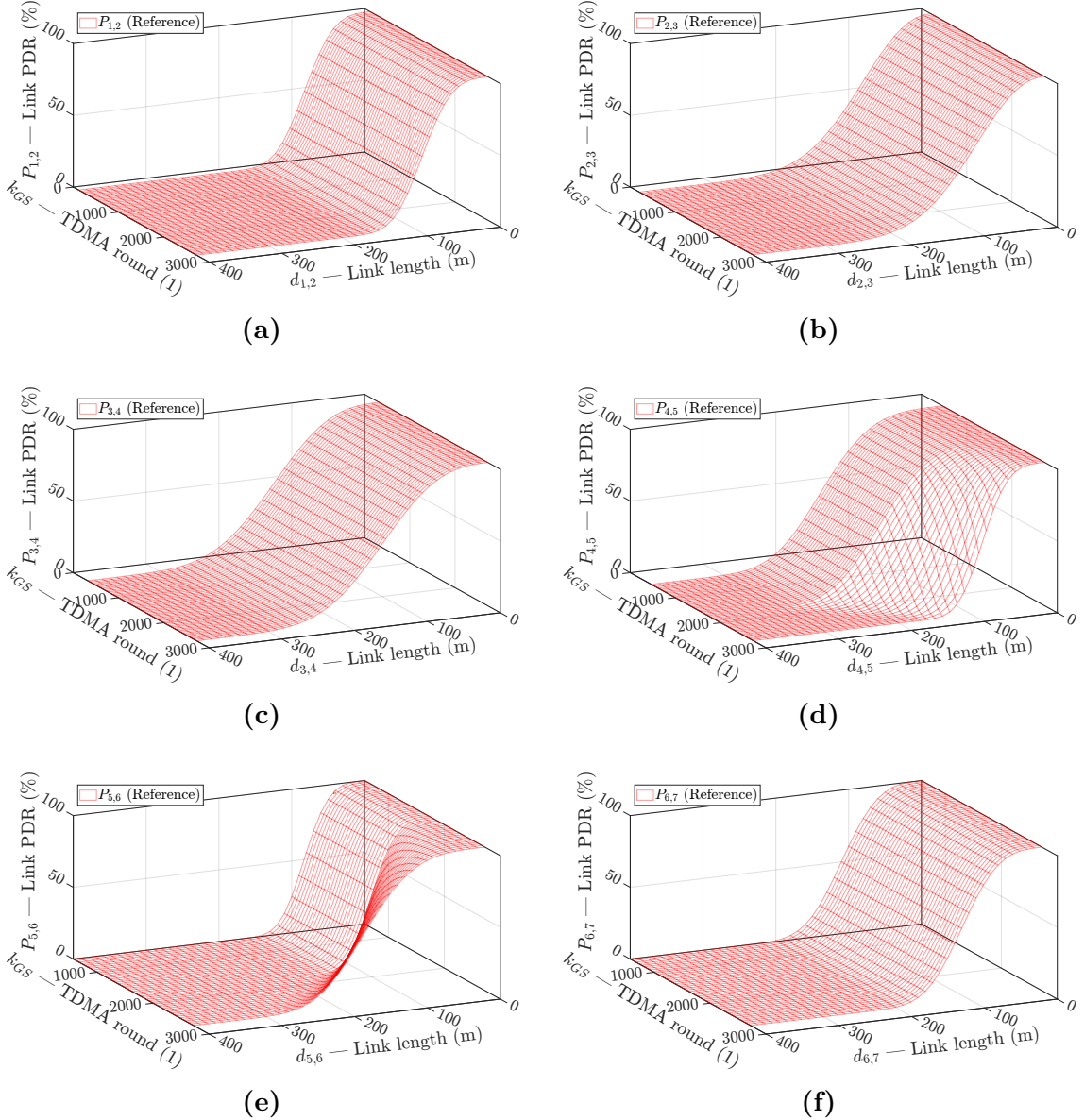


Figure 4.8. The time evolution of the actual link models in the scenario ‘d’, referred to as the ‘incremental model change’ scenario, starts with link creation at k^A ($k_{GS} = 706$) and continues until k^C ($k_{GS} = 2726$). During this time, only the models of links {4, 5}, {5, 4}, {5, 6}, and {6, 5} will change from k^B ($k_{GS} = 1774$) to k^C , transitioning from the model set ‘1’ to the model set ‘3’ as listed in Table 4.2. k^A , k^B , and k^C may have slight variations from simulation to simulation.

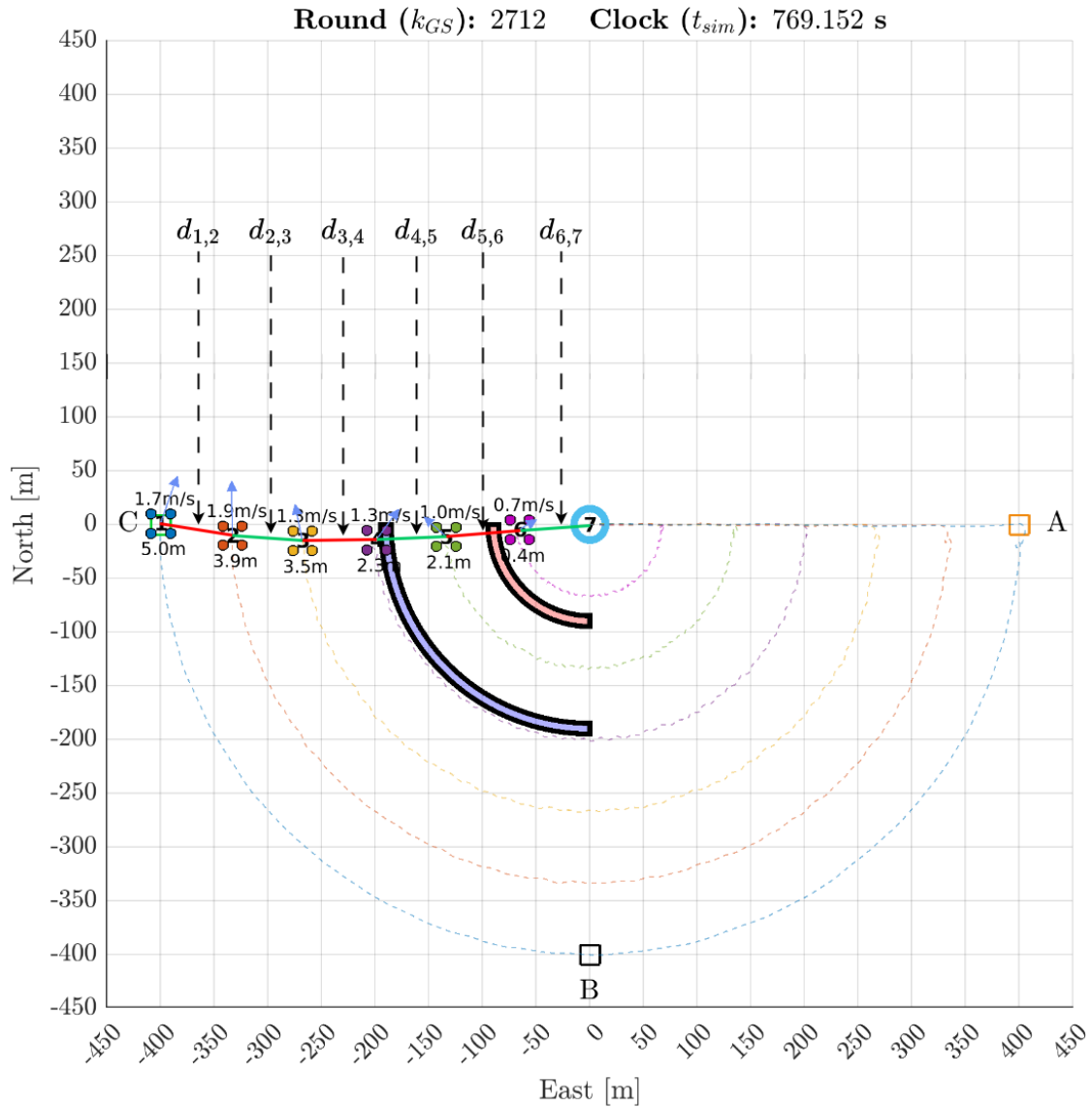


Figure 4.9. Simulation using the equidistant placement strategy in the scenario ‘b’. The simulation ends with the source reaching the waypoint ‘C’. The figure shows the trajectory of a source (in blue) moving along a set of waypoints in a 2D space, listed in Table 4.1, with the ground station in the center (in azure). The source starts at the ground station and reaches the waypoints ‘A’ (orange), ‘B’ (black), and ‘C’ (green) in succession. The equidistant placement strategy is used, as seen in the equal-length vectors (in alternated red and green) between neighboring nodes. The simulation ends with the source successfully reaching the waypoint ‘C’.

4.3.3 Estimation Error

After estimating the PDR model parameters, it is necessary to measure the distance between the estimated model and the reference model to assess how far the estimate is from the reference. The L^p distances are typical choices for measuring the distance between two functions P and \hat{P} of one real variable. For real functions on a closed, bounded interval $[a, b]$, the L^p distance is reported in Equation (4.8).

$$\|f - g\|_{L^p(a,b)} = \left(\int_a^b |f(x) - g(x)|^p dx \right)^{\frac{1}{p}}, \quad 1 \leq p < \infty \quad (4.8)$$

In our case, we are interested in comparing the estimated model, $(\hat{R}(k), \hat{\alpha}(k))$, with the actual model, $(R(k), \alpha(k))$ at each TDMA round k . To measure the difference between the two models, we use the L^1 distance, as it is less affected by outliers and is computationally more efficient than L^2 distance [38]. The estimation error index ξ over an interval from 0 to L , the network length, is defined in Equation (4.9).

$$\xi = \text{dist}(P, \hat{P}) = \int_0^L |P(d) - \hat{P}(d)| dd = \int_0^L \left| e^{-\log(2) \cdot \left(\frac{d}{R}\right)^\alpha} - e^{-\log(2) \cdot \left(\frac{d}{\hat{R}}\right)^{\hat{\alpha}}} \right| dd \quad (4.9)$$

Figure 4.10 shows an example of two different estimations for a link with $(R, \alpha) = (142 \text{ m}, 4.2)$. The estimation in Figure (b), $(138 \text{ m}, 3.95)$, is better than in (a), $(124 \text{ m}, 2.4)$, and results in a lower estimation error index ξ , 3.704 instead of 20.723. Graphically, the index in Equation (4.9) can be interpreted as the area between the estimated and the actual model, highlighted in pink in the figure.

However, as the link PDR continuously varies over time and new models are estimated at each iteration, it is useful to have a single error index for the entire simulation from k_0 to k . This index depends on two variables: d , which is continuous, and k' , which is discrete. The function domain is $[0, L] \times [k_0..k]$, where $[k_0..k] = k_0, k_0 + 1, \dots, k$ denotes an integer interval. Although time-weighted indices are a possible option, we decided to assign equal importance to each simulation. To achieve this, we introduced an average estimation error index in Equation (4.10), where the average is unweighted.

$$\begin{aligned} \bar{\xi}([k_0..k]) &= \frac{1}{k - k_0 + 1} \sum_{k'=k_0}^k \xi(k') = \frac{1}{k - k_0 + 1} \sum_{k'=k_0}^k \int_0^L |P(d, k') - \hat{P}(d, k')| dd = \\ &= \frac{1}{k - k_0 + 1} \sum_{k'=k_0}^k \int_0^L \left| e^{-\log(2) \cdot \left(\frac{d}{R(k')}\right)^{\alpha(k')}} - e^{-\log(2) \cdot \left(\frac{d}{\hat{R}(k')}\right)^{\hat{\alpha}(k')}} \right| dd \end{aligned} \quad (4.10)$$

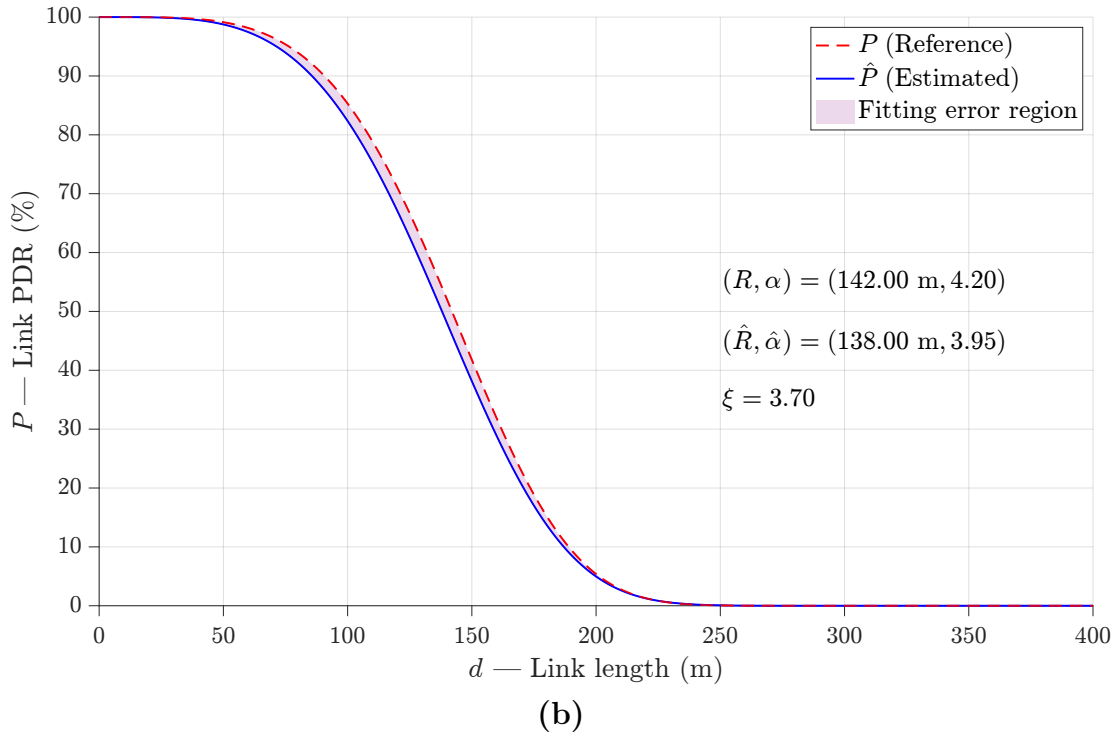
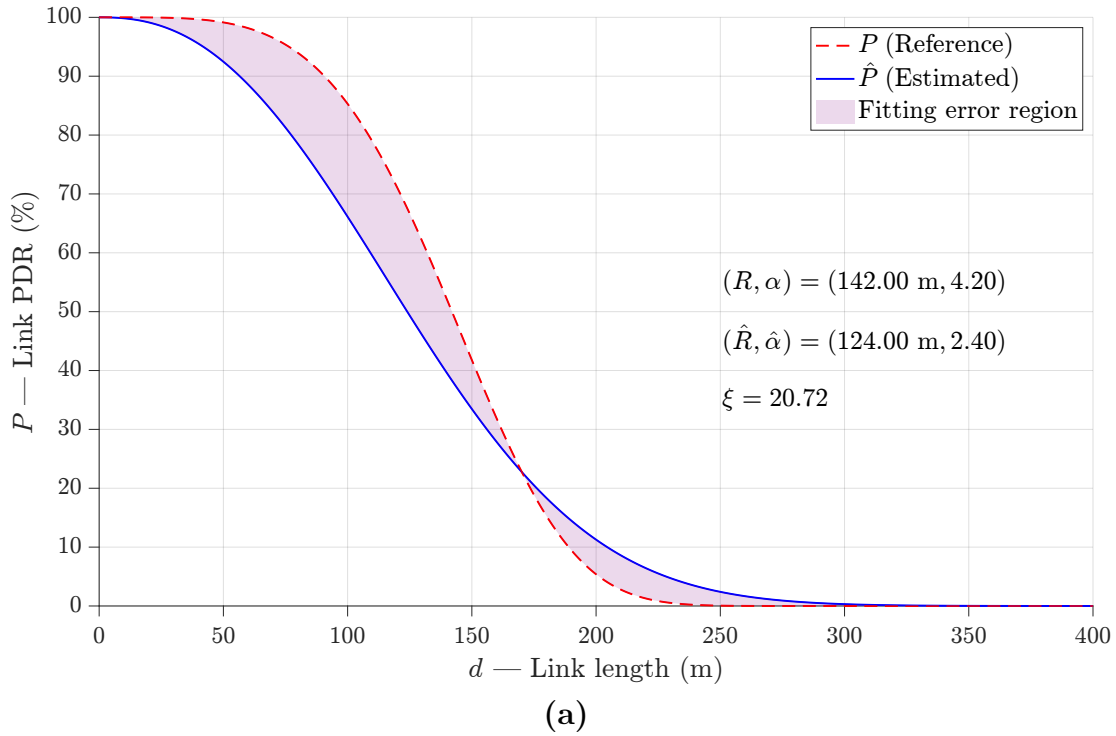


Figure 4.10. Comparison of two fittings with their estimation error indices, defined in Equation 4.9. The graphical interpretation of such an index is the area between P and \hat{P} , shaded in pink. The link PDR actual model is $(R, \alpha) = (142 \text{ m}, 4.2)$. **(a)** A poor fitting, $(\hat{R}, \hat{\alpha}) = (124 \text{ m}, 2.4)$: the error is $\xi = 20.72$. **(b)** A better fitting, $(\hat{R}, \hat{\alpha}) = (138 \text{ m}, 3.95)$: the error, $\xi = 3.70$, is more than five times lower than in (a).

5 Results and Analysis

In this chapter, we present the results of the simulations performed based on the methodology outlined in Chapter 3 and the simulation setup designed in Chapter 4. Our aim is to compare the performance of different relay placement strategies and understand how they affect the network PDR over time. Three relay placement strategies are considered: equidistant, equal-PDR, and DRP, with the last two, tested under both estimated and true parameters. The simulations are performed in four different scenarios: unchanged model ('a'), small abrupt model change ('b'), large abrupt model change ('c'), and incremental model change ('d').

We expect to observe an increase in network PDR as the relay placement strategies become more sophisticated. Specifically, we anticipate that the DRP strategy, which optimizes the placement of relays based on the link PDR models, will result in the highest network PDR. The equal-PDR strategy, which places the relays such that each link has equal PDR, is expected to result in a lower network PDR compared to the DRP strategy. Finally, the equidistant strategy, which evenly spaces the relays along the network, is expected to result in the lowest network PDR of the three strategies.

In Section 5.1, we provide a detailed comparison, including the estimation error indices, of the link model estimates for the equidistant, equal-PDR, and DRP relay placement strategies in four scenarios ('a', 'b', 'c', and 'd'). Additionally, in Section 5.2, we analyze the link and network PDRs at different time points and report the average results for each strategy – with the equal-PDR, and DRP relay placement strategies tested under both estimated and true parameters – and scenario. The two sections are concluded with summary subsections (Subsections 5.1.5 and 5.2.5, respectively) that provide an overview of our findings.

5.1 Link Model Estimates

The links $\{4, 5\}$ and $\{5, 6\}$ are the only links that undergo a change (in scenarios 'b', 'c', and 'd'); thus, they are the most interesting to analyze. Also, since the estimation process is the same across strategies, it is reasonable to consider only one strategy; we chose the DRP strategy because it has shown the most promising results. In this section, for each scenario ('a', 'b', 'c', and 'd'), for the DRP (with estimated parameters) strategy only, and for the links $\{4, 5\}$ and $\{5, 6\}$ only, we present:

- The estimates of the PDR model parameters, (R, α) , highlighting the non-rejection region.
- The estimated PDR function as well as the true PDR function, highlighting the estimation error region.
- The time evolution of the estimated PDR function, showing PDR measurements before and after model changes in different colors.

At the end of the section, the estimation error indices are summarized in Table 5.1, for each strategy, link, and scenario.

5.1.1 Scenario ‘a’

In this section, we present the model estimates for the DRP strategy in the scenario ‘a’ (cf. Equation (4.3)). Figure 5.1 displays the estimates of the PDR model parameters. The figure shows the critical bounds, weighted averages, and non-rejection region for both estimated parameters, and triggers a model change when τ consecutive estimates fall within the rejection region (cf. Equation (3.19)).

Figure 5.2 displays the estimated (in blue) and actual (in red) link models. The green dots and orange squares represent measured samples (P, d) taken after and before the most recent model change, respectively. The size and tone of the green dots indicate their fitting weights and recency, respectively. The pink shaded area represents the error region, with a smaller area indicating better performance.

Finally, in Figure 5.3 we show the evolution of the link models from the link creation to round k^C . The current estimate of the link model is based on the blue dots, which represent the measured samples (P, d) following the most recent model change. In contrast, the orange squares represent the measured samples that were utilized in previous model estimates, up until the last detected model change.

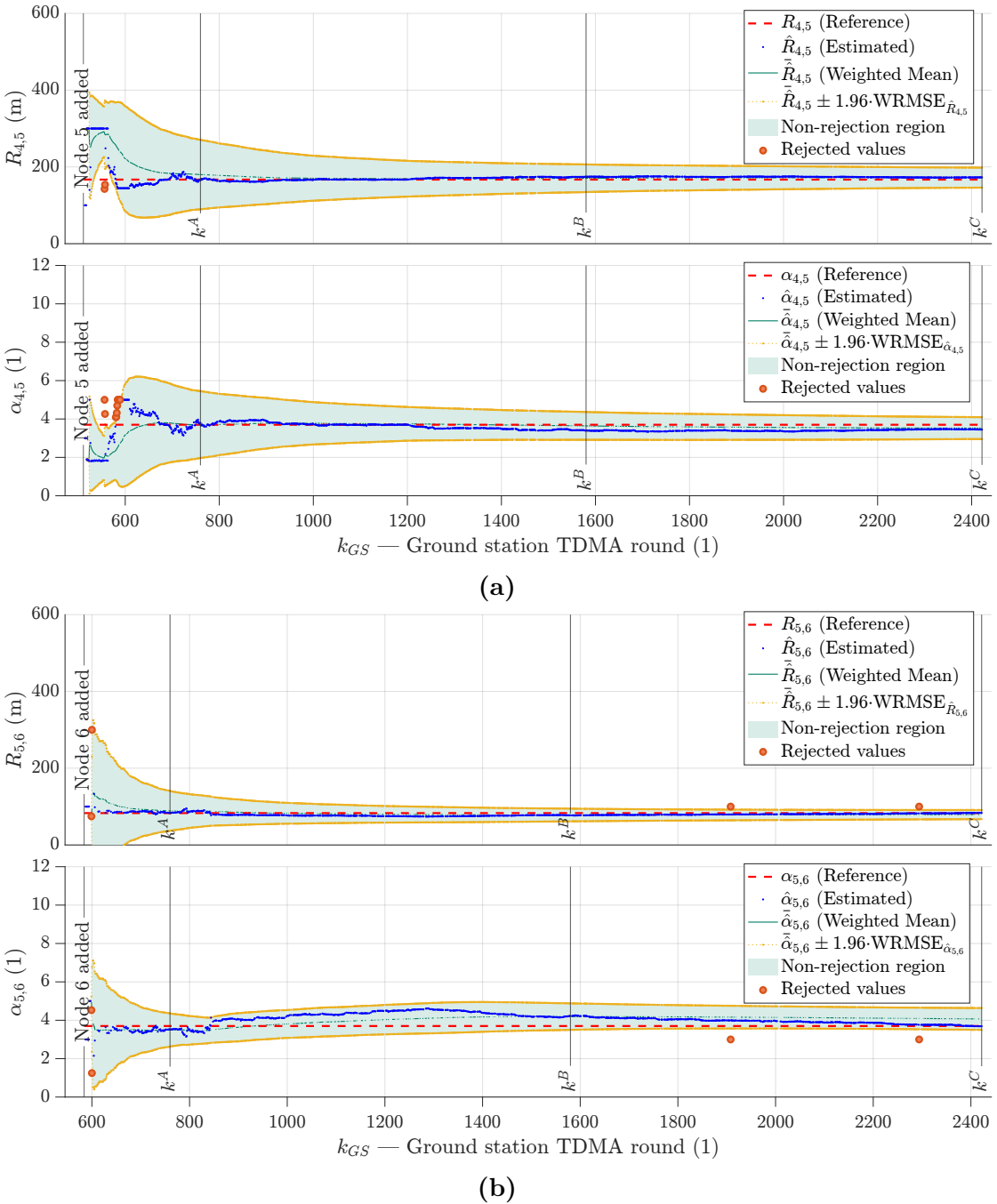


Figure 5.1. Estimates $(\hat{R}, \hat{\alpha})$ at round k^C of the PDR model parameters for the DRP strategy in scenario ‘a’, for two links: **(a)** for the link $\{4, 5\}$; **(b)** for the link $\{5, 6\}$. The critical bounds (highlighted in yellow) are shown above and below the weighted averages (in dark green) and divide the area into two zones: the non-rejection region (in light green) and the rejection region (in white), for both estimated parameters (cf. Equation (3.19)). When τ consecutive estimates fall within the rejection region a model change is triggered (by node 5 in Subfigure (a) or by node 6 in Subfigure (b), respectively). In contrast, the non-rejection region indicates an acceptable range of estimates.

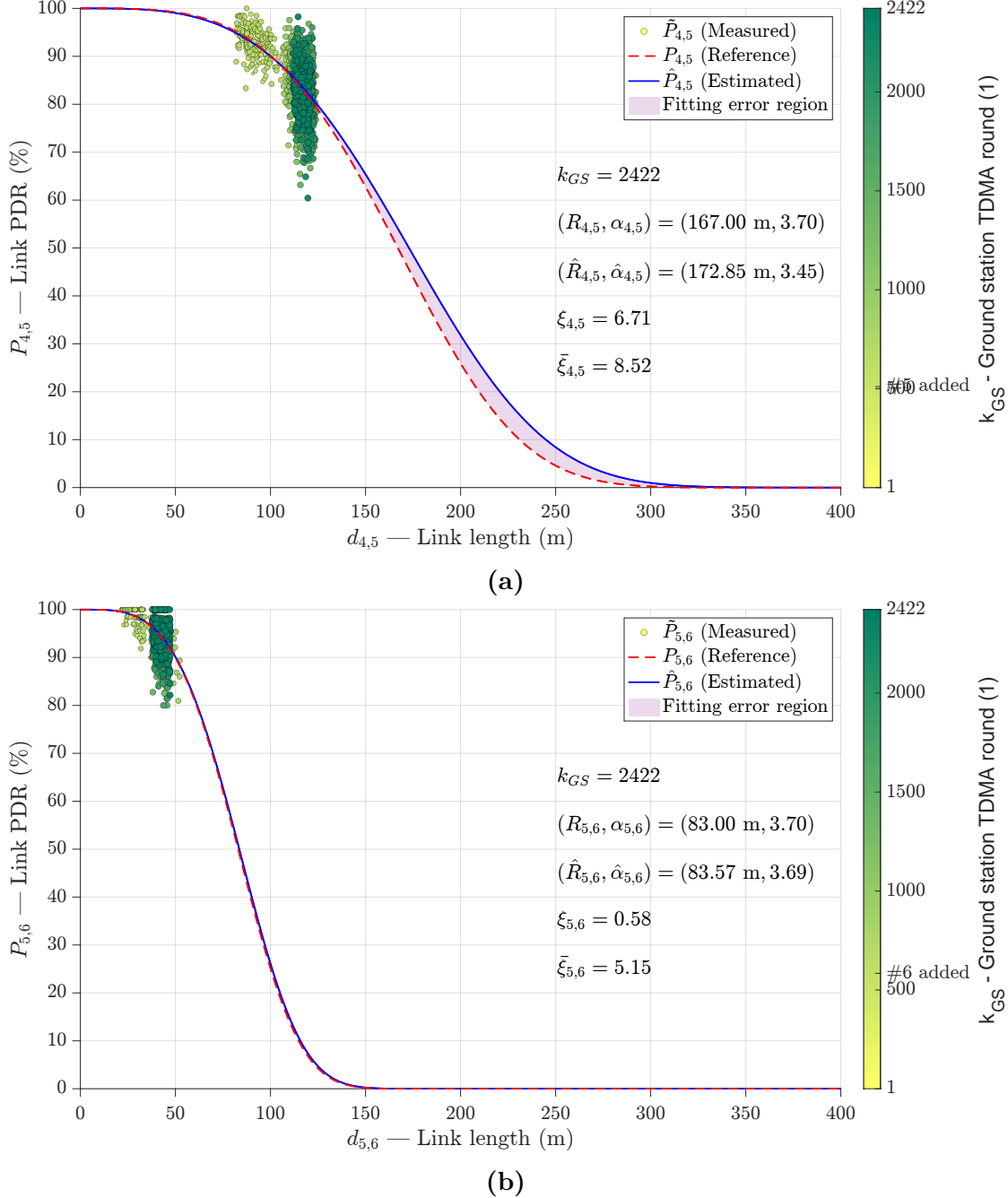


Figure 5.2. Estimated link model (in blue) versus actual link model (in red) at round k^C of the PDR model parameters for the DRP strategy in scenario ‘a’, for two links: (a) for the link {4, 5}; (b) for the link {5, 6}. The green dots represent the measured samples (P, d) taken after the most recent model change, while the orange squares represent the measured samples taken before the most recent model change (if any). The green dots are color-coded based on recency, with darker tones indicating more recent samples and lighter, yellowish tones representing older samples. The area of the green dots is proportional to their fitting weights at round k^C . The pink shaded area represents the error region (cf. Subsection 4.3.3): the smaller, the better. The TDMA round considered (k^C), the estimated $((\hat{R}, \hat{\alpha}))$ and real $(R, \alpha))$ parameters, the current error index (ξ), and the average error index throughout the simulation ($\bar{\xi}$) are reported on the figures.

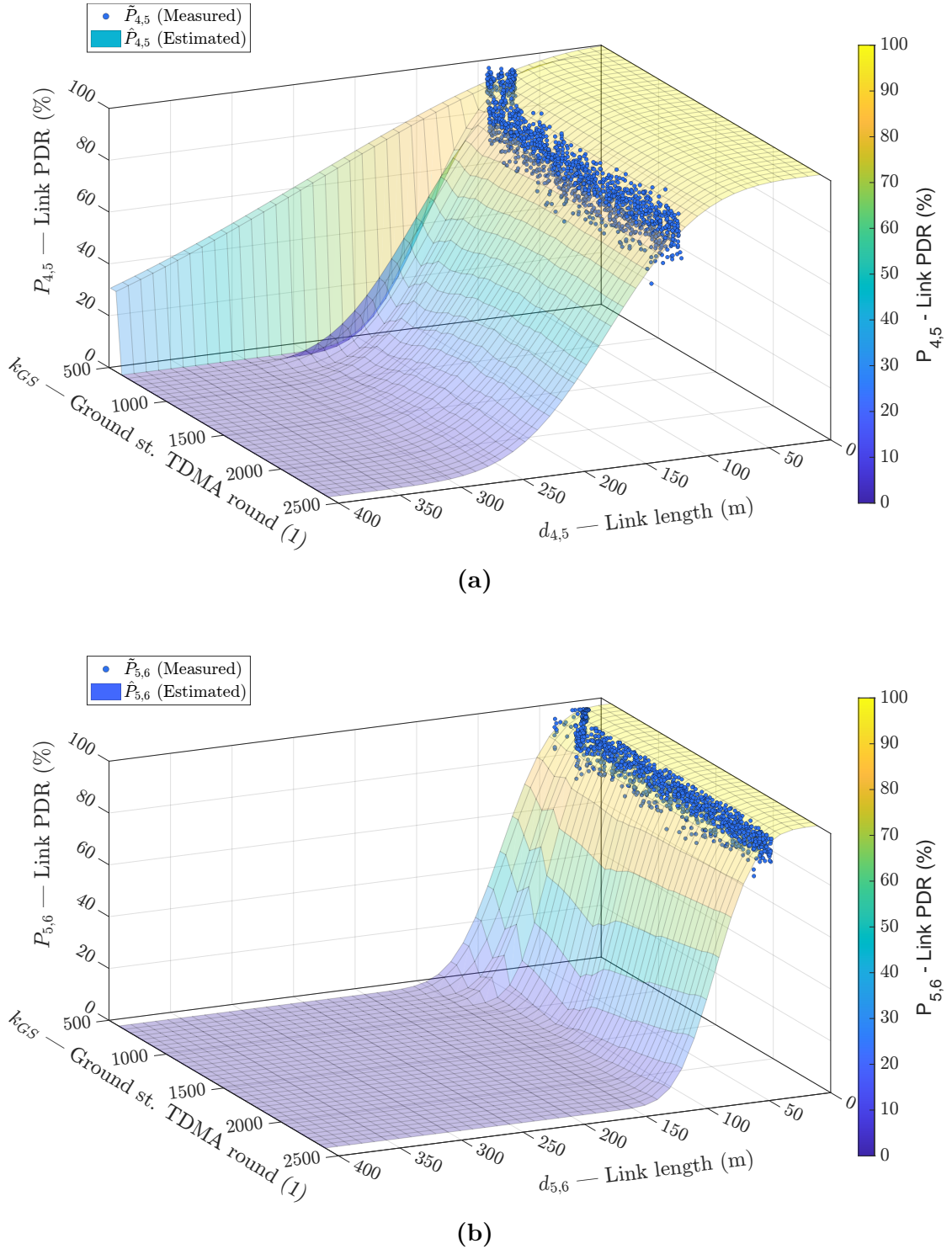


Figure 5.3. Time evolution (from the link creating until round k^C) of the estimated link models for the DRP strategy in scenario ‘a’, for two links: **(a)** for the link $\{4,5\}$; **(b)** for the link $\{5,6\}$. The blue dots represent the measured samples (P, d) that are used in the current estimate of the link model, following the most recent model change. The orange squares represent the measured samples that were used in previous model estimates, up until the last detected model change.

5.1.2 Scenario ‘b’

In this section, we present the model estimates for the DRP strategy in the scenario ‘b’ (cf. Equation (4.4)). Figure 5.4 displays the estimates of the PDR model parameters. The figure shows the critical bounds, weighted averages, and non-rejection region for both estimated parameters, and triggers a model change when τ consecutive estimates fall within the rejection region (cf. Equation (3.19)).

Figure 5.5 displays the estimated (in blue) and actual (in red) link models. The green dots and orange squares represent measured samples (P, d) taken after and before the most recent model change, respectively. The size and tone of the green dots indicate their fitting weights and recency, respectively. The pink shaded area represents the error region, with a smaller area indicating better performance.

Finally, in Figure 5.6 we show the evolution of the link models from the link creation to round k^C . The current estimate of the link model is based on the blue dots, which represent the measured samples (P, d) following the most recent model change. In contrast, the orange squares represent the measured samples that were utilized in previous model estimates, up until the last detected model change.

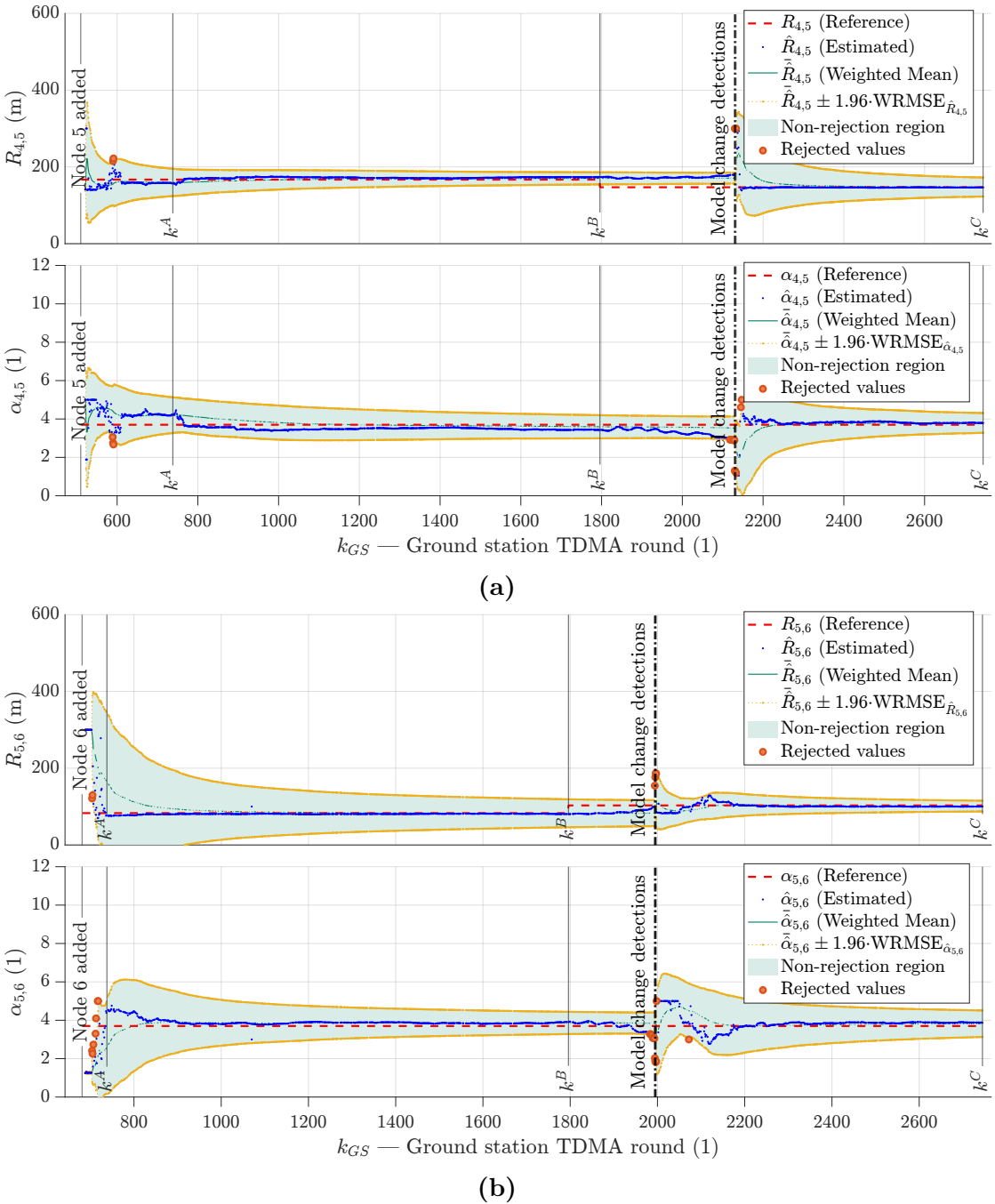


Figure 5.4. Estimates $(\hat{R}, \hat{\alpha})$ at round k^C of the PDR model parameters for the DRP strategy in scenario ‘b’, for two links: **(a)** for the link $\{4, 5\}$; **(b)** for the link $\{5, 6\}$. The critical bounds (highlighted in yellow) are shown above and below the weighted averages (in dark green) and divide the area into two zones: the non-rejection region (in light green) and the rejection region (in white), for both estimated parameters (cf. Equation (3.19)). When τ consecutive estimates fall within the rejection region a model change is triggered (by node 5 in Subfigure (a) or by node 6 in Subfigure (b), respectively). In contrast, the non-rejection region indicates an acceptable range of estimates.

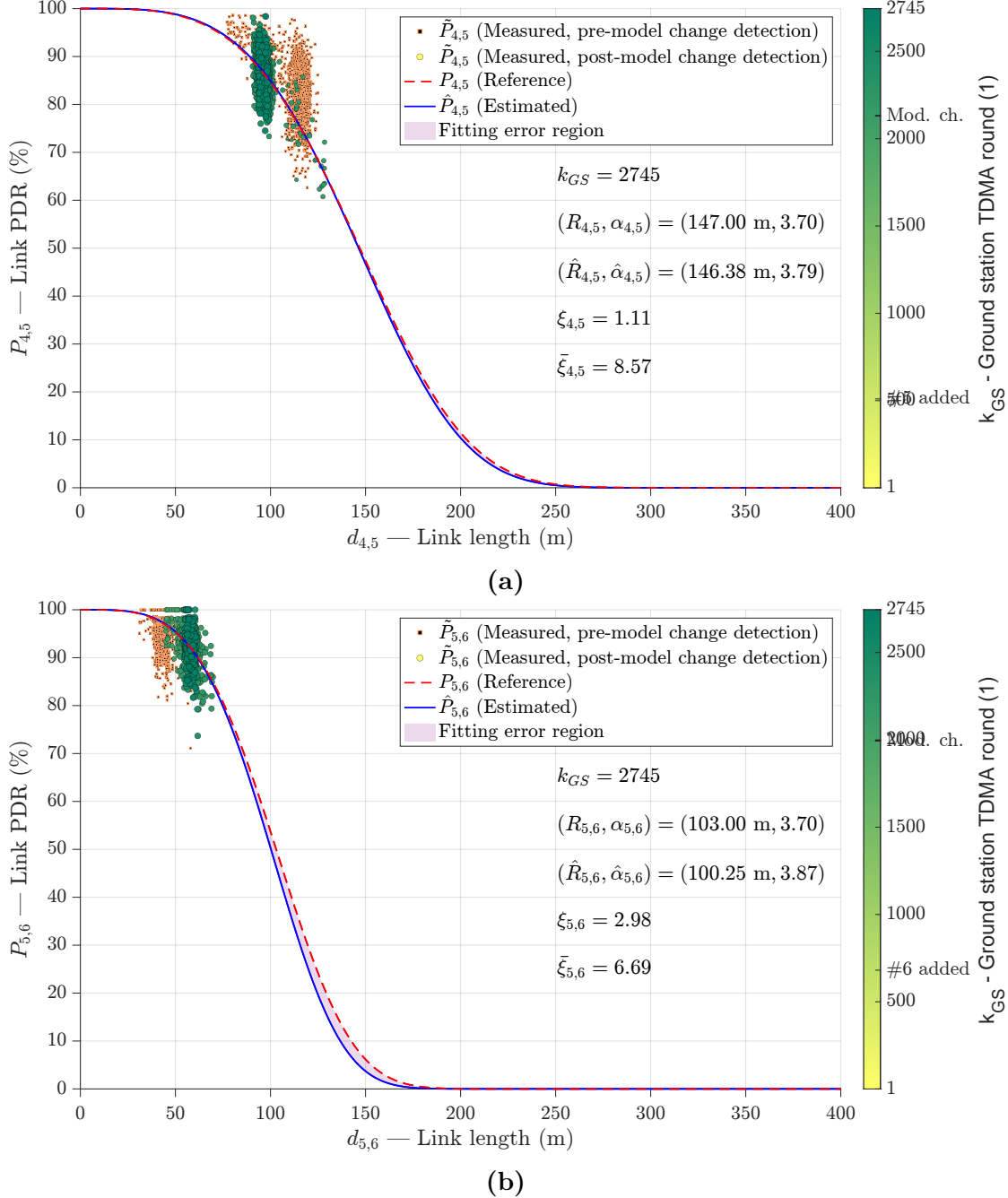


Figure 5.5. Estimated link model (in blue) versus actual link model (in red) at round k^C of the PDR model parameters for the DRP strategy in scenario ‘b’, for two links: **(a)** for the link $\{4, 5\}$; **(b)** for the link $\{5, 6\}$. The green dots represent the measured samples (P, d) taken after the most recent model change, while the orange squares represent the measured samples taken before the most recent model change (if any). The green dots are color-coded based on recency, with darker tones indicating more recent samples and lighter, yellowish tones representing older samples. The area of the green dots is proportional to their fitting weights at round k^C . The pink shaded area represents the error region (cf. Subsection 4.3.3): the smaller, the better. The TDMA round considered (k^C), the estimated $((\hat{R}, \hat{\alpha}))$ and real $(R, \alpha))$ parameters, the current error index (ξ), and the average error index throughout the simulation ($\bar{\xi}$) are reported on the figures.

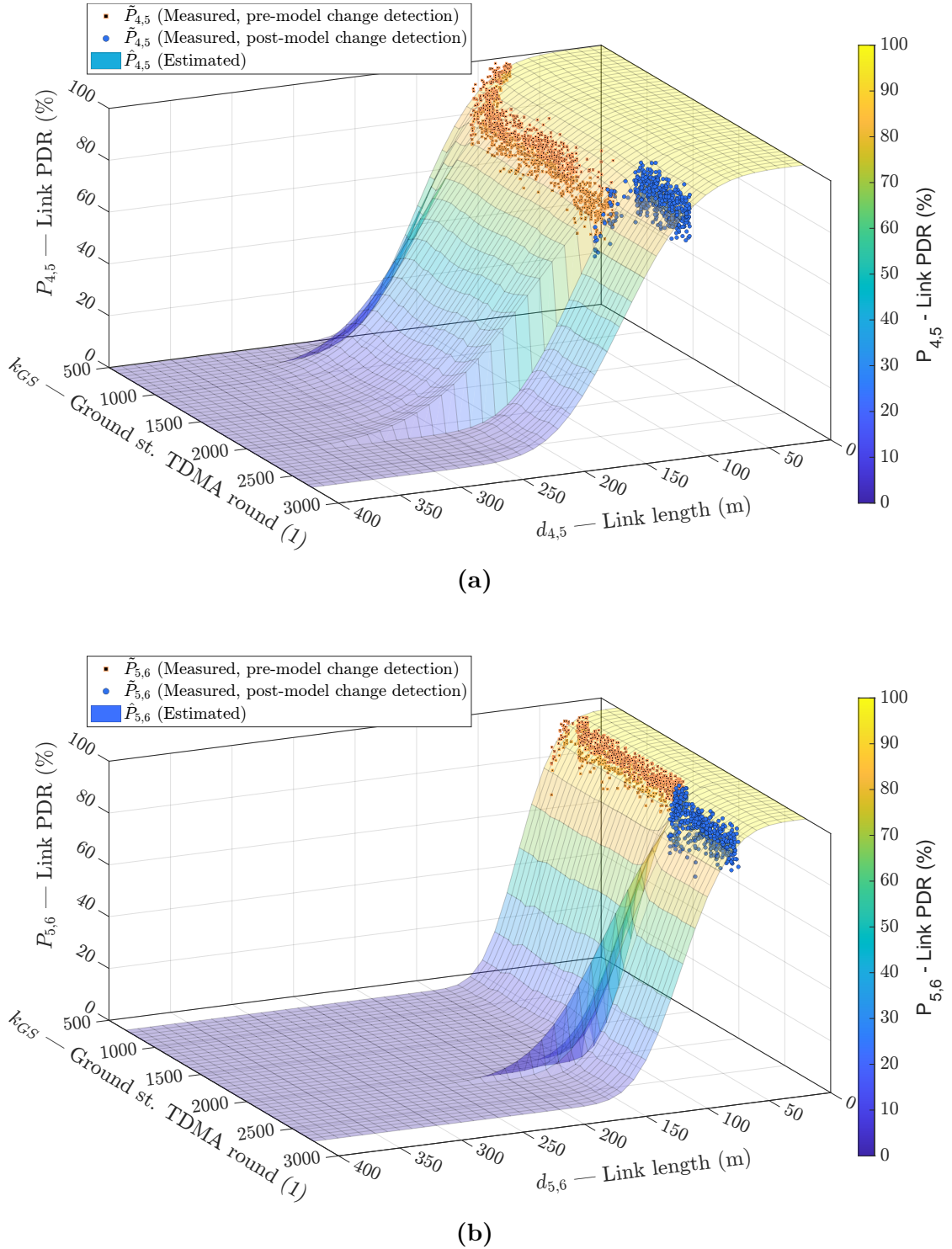


Figure 5.6. Time evolution (from the link creating until round k^C) of the estimated link models for the DRP strategy in scenario ‘b’, for two links: **(a)** for the link $\{4,5\}$; **(b)** for the link $\{5,6\}$. The blue dots represent the measured samples (P, d) that are used in the current estimate of the link model, following the most recent model change. The orange squares represent the measured samples that were used in previous model estimates, up until the last detected model change.

5.1.3 Scenario ‘c’

In this section, we present the model estimates for the DRP strategy in the scenario ‘c’ (cf. Equation (4.5)). Figure 5.7 displays the estimates of the PDR model parameters. The figure shows the critical bounds, weighted averages, and non-rejection region for both estimated parameters, and triggers a model change when τ consecutive estimates fall within the rejection region (cf. Equation (3.19)).

Figure 5.8 displays the estimated (in blue) and actual (in red) link models. The green dots and orange squares represent measured samples (P, d) taken after and before the most recent model change, respectively. The size and tone of the green dots indicate their fitting weights and recency, respectively. The pink shaded area represents the error region, with a smaller area indicating better performance.

Finally, in Figure 5.9 we show the evolution of the link models from the link creation to round k^C . The current estimate of the link model is based on the blue dots, which represent the measured samples (P, d) following the most recent model change. In contrast, the orange squares represent the measured samples that were utilized in previous model estimates, up until the last detected model change.

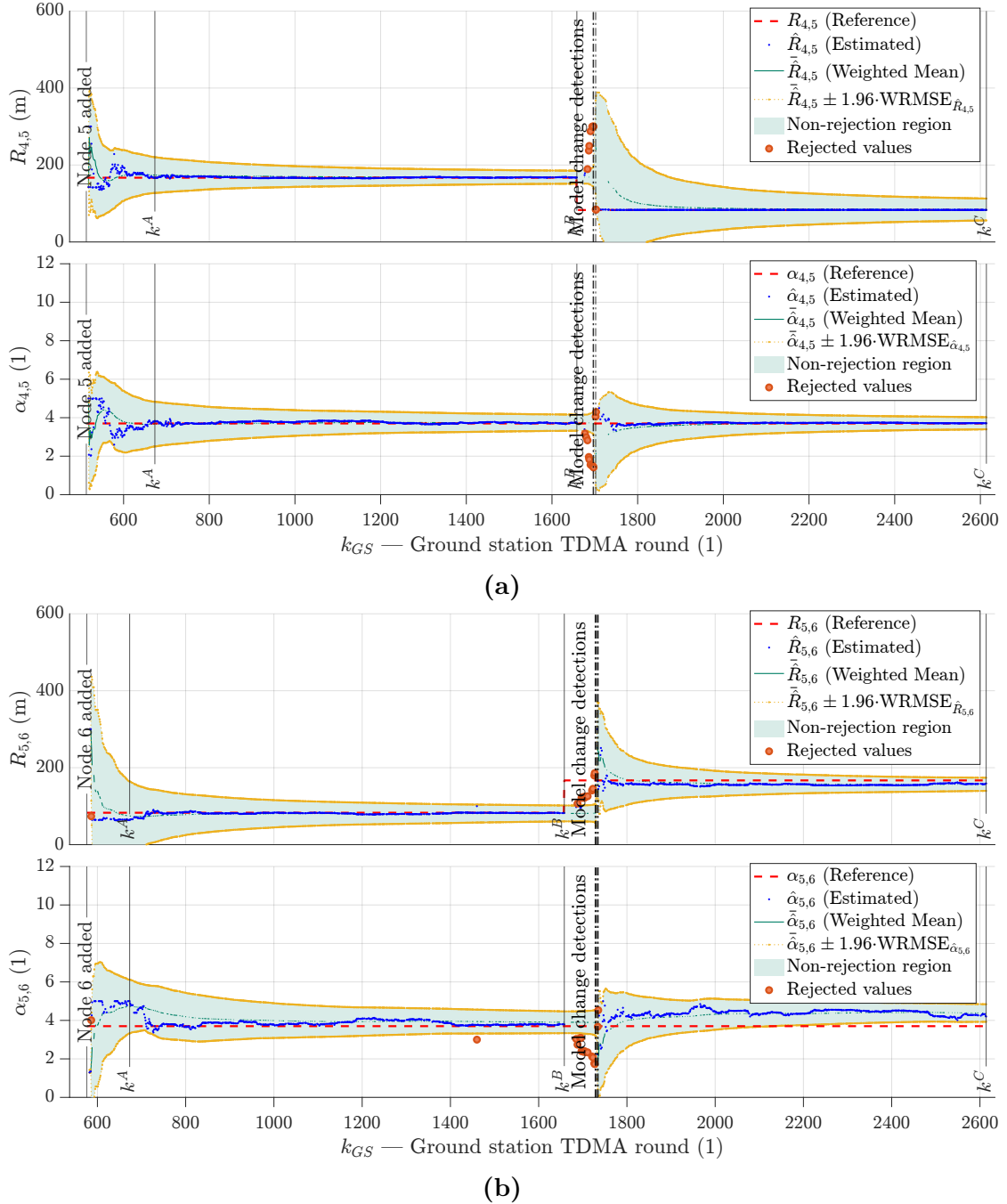


Figure 5.7. Estimates ($\hat{R}, \hat{\alpha}$) at round k^C of the PDR model parameters for the DRP strategy in scenario ‘c’, for two links: **(a)** for the link $\{4, 5\}$; **(b)** for the link $\{5, 6\}$. The critical bounds (highlighted in yellow) are shown above and below the weighted averages (in dark green) and divide the area into two zones: the non-rejection region (in light green) and the rejection region (in white), for both estimated parameters (cf. Equation (3.19)). When τ consecutive estimates fall within the rejection region a model change is triggered (by node 5 in Subfigure (a) or by node 6 in Subfigure (b), respectively). In contrast, the non-rejection region indicates an acceptable range of estimates.

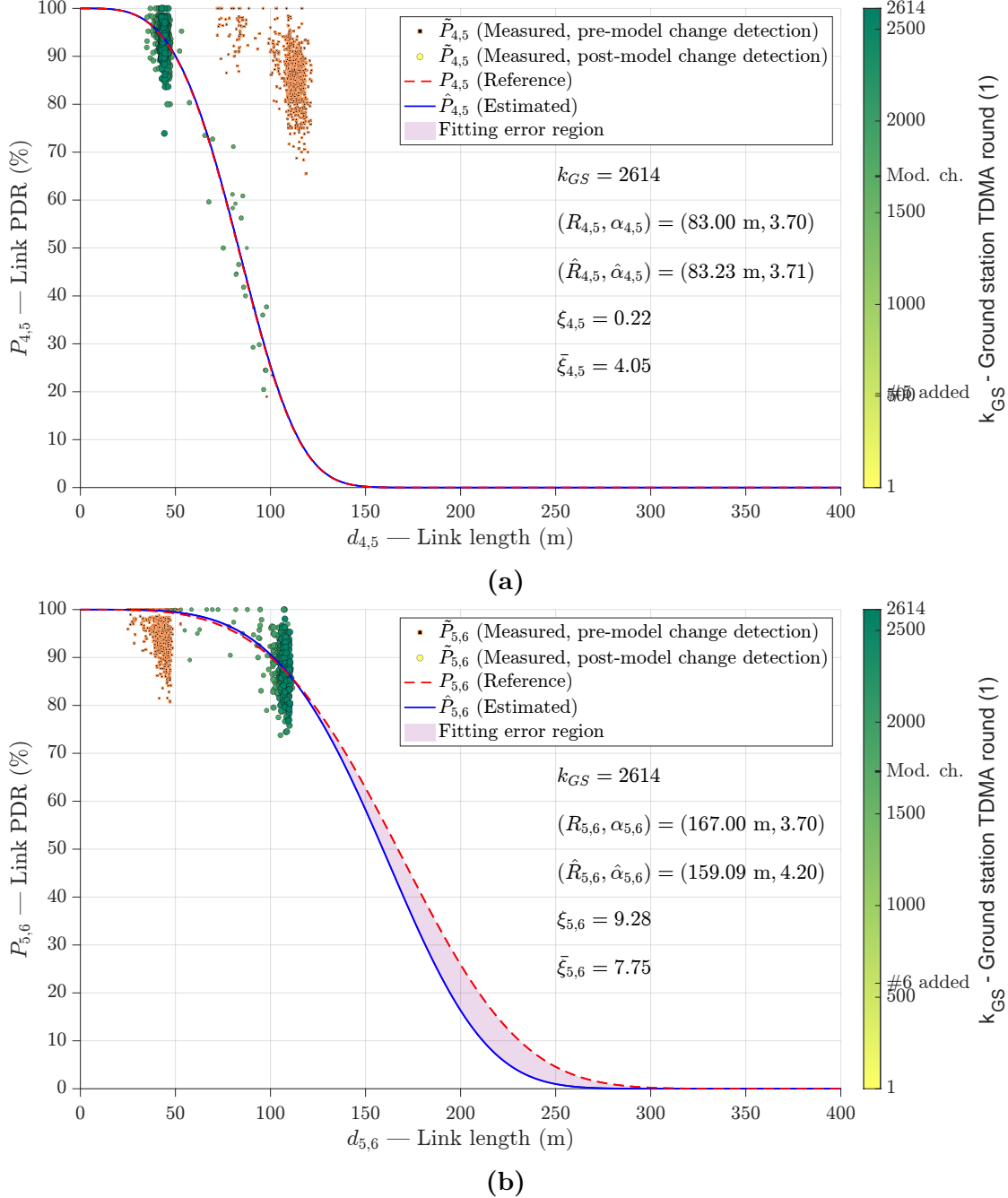


Figure 5.8. Estimated link model (in blue) versus actual link model (in red) at round k^C of the PDR model parameters for the DRP strategy in scenario ‘c’, for two links: (a) for the link {4,5}; (b) for the link {5,6}. The green dots represent the measured samples (P, d) taken after the most recent model change, while the orange squares represent the measured samples taken before the most recent model change (if any). The green dots are color-coded based on recency, with darker tones indicating more recent samples and lighter, yellowish tones representing older samples. The area of the green dots is proportional to their fitting weights at round k^C . The pink shaded area represents the error region (cf. Subsection 4.3.3): the smaller, the better. The TDMA round considered (k^C), the estimated $((\hat{R}, \hat{\alpha}))$ and real $(R, \alpha))$ parameters, the current error index (ξ), and the average error index throughout the simulation ($\bar{\xi}$) are reported on the figures.

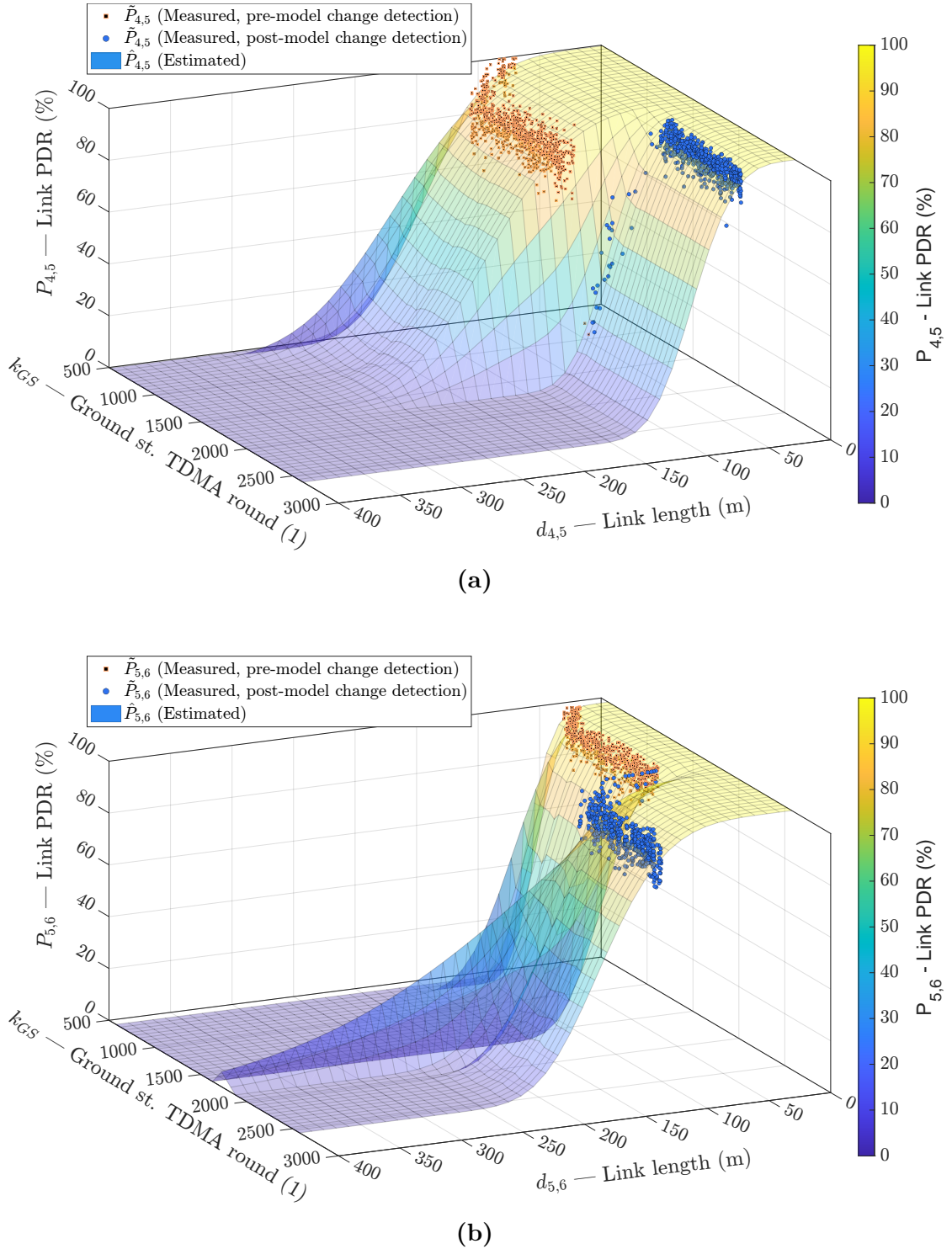


Figure 5.9. Time evolution (from the link creating until round k^C) of the estimated link models for the DRP strategy in scenario ‘c’, for two links: **(a)** for the link $\{4, 5\}$; **(b)** for the link $\{5, 6\}$. The blue dots represent the measured samples (P, d) that are used in the current estimate of the link model, following the most recent model change. The orange squares represent the measured samples that were used in previous model estimates, up until the last detected model change.

5.1.4 Scenario ‘d’

In this section, we present the model estimates for the DRP strategy in the scenario ‘d’ (cf. Equation (4.6)). Figure 5.10 displays the estimates of the PDR model parameters. The figure shows the critical bounds, weighted averages, and non-rejection region for both estimated parameters, and triggers a model change when τ consecutive estimates fall within the rejection region (cf. Equation (3.19)).

Figure 5.11 displays the estimated (in blue) and actual (in red) link models. The green dots and orange squares represent measured samples (P, d) taken after and before the most recent model change, respectively. The size and tone of the green dots indicate their fitting weights and recency, respectively. The pink shaded area represents the error region, with a smaller area indicating better performance.

Finally, in Figure 5.12 we show the evolution of the link models from the link creation to round k^C . The current estimate of the link model is based on the blue dots, which represent the measured samples (P, d) following the most recent model change. In contrast, the orange squares represent the measured samples that were utilized in previous model estimates, up until the last detected model change.

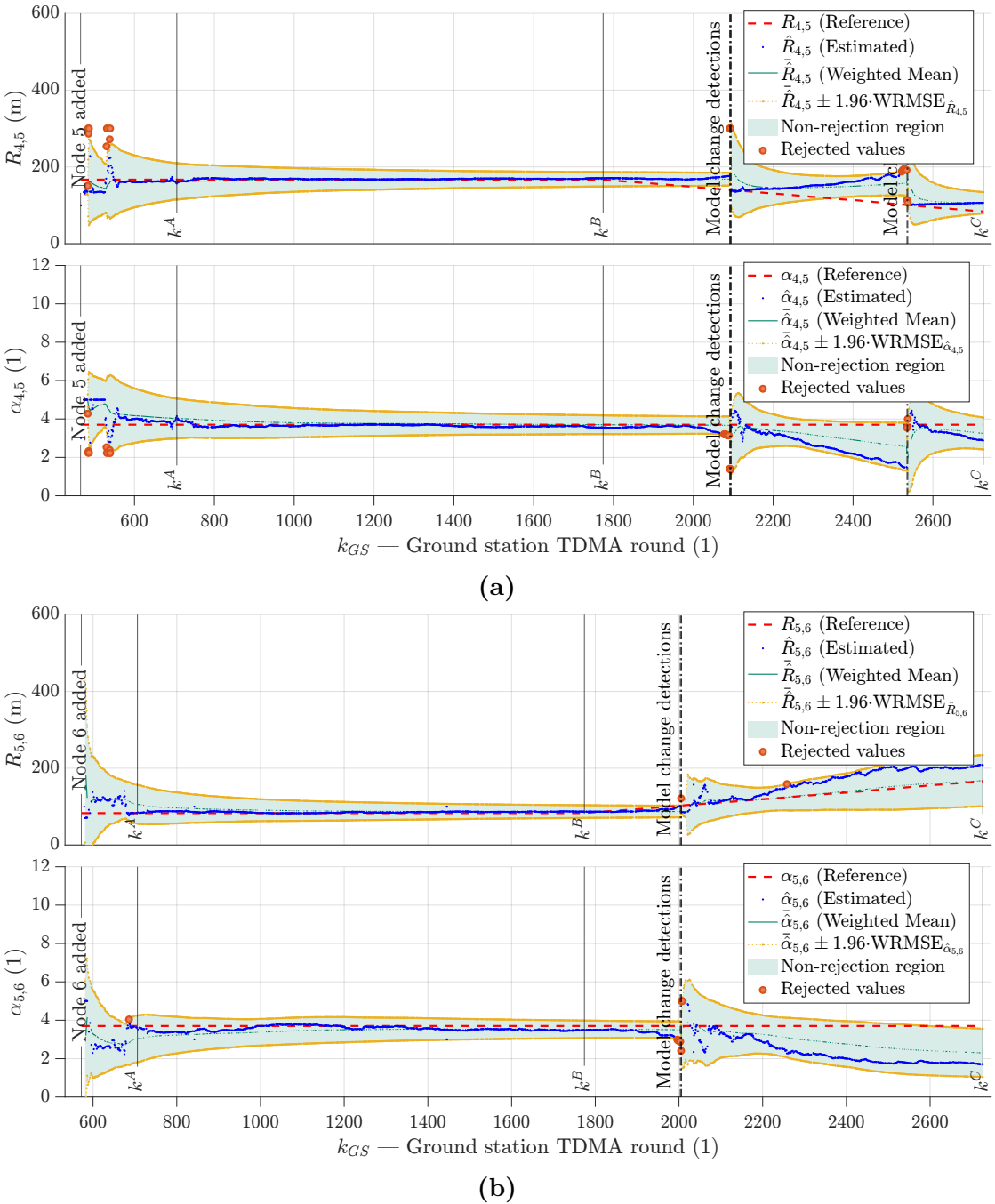


Figure 5.10. Estimates ($\hat{R}, \hat{\alpha}$) at round k^C of the PDR model parameters for the DRP strategy in scenario ‘d’, for two links: **(a)** for the link $\{4, 5\}$; **(b)** for the link $\{5, 6\}$. The critical bounds (highlighted in yellow) are shown above and below the weighted averages (in dark green) and divide the area into two zones: the non-rejection region (in light green) and the rejection region (in white), for both estimated parameters (cf. Equation (3.19)). When τ consecutive estimates fall within the rejection region a model change is triggered (by node 5 in Subfigure (a) or by node 6 in Subfigure (b), respectively). In contrast, the non-rejection region indicates an acceptable range of estimates.

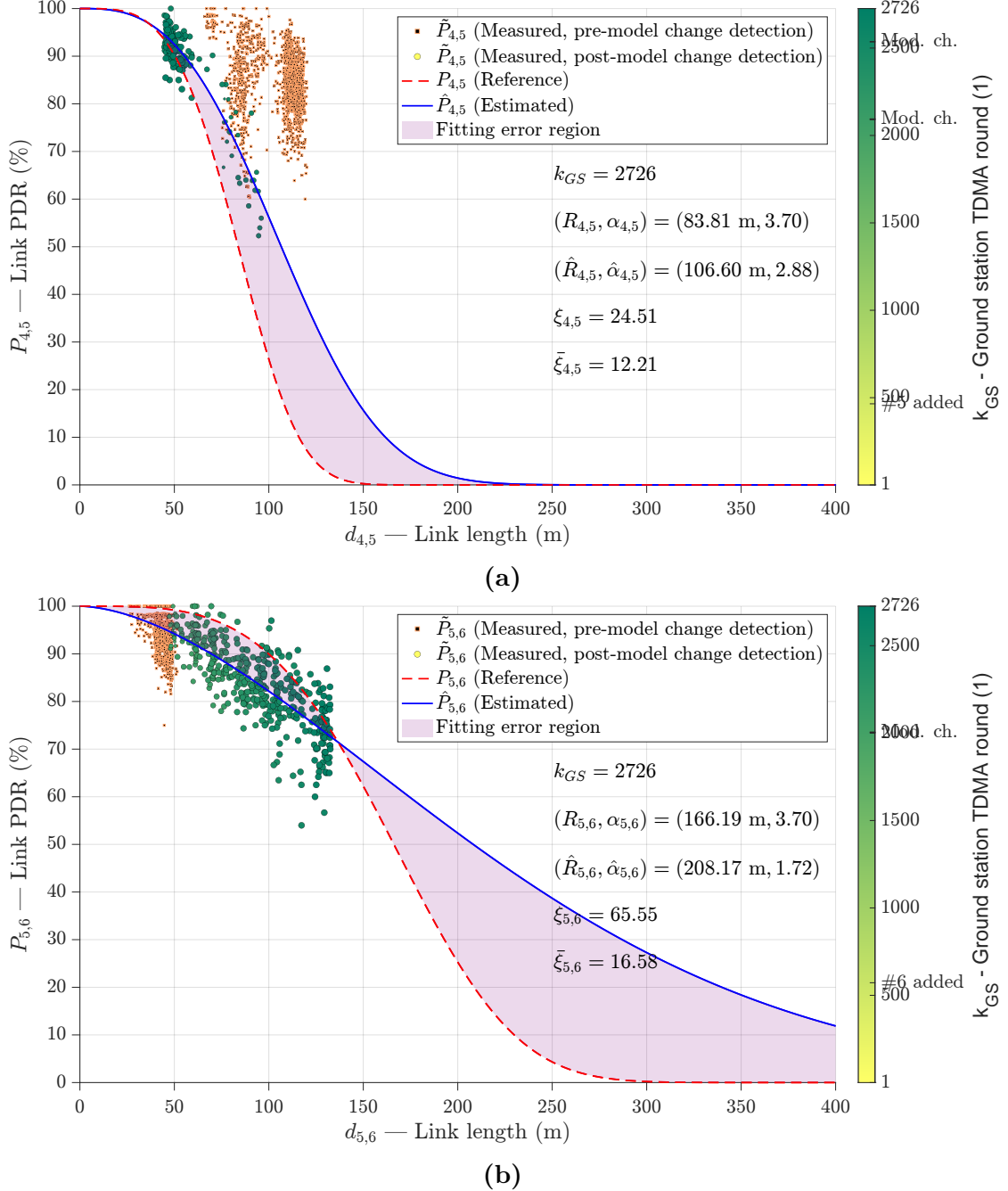


Figure 5.11. Estimated link model (in blue) versus actual link model (in red) at round k^C of the PDR model parameters for the DRP strategy in scenario ‘d’, for two links: (a) for the link {4, 5}; (b) for the link {5, 6}. The green dots represent the measured samples (P, d) taken after the most recent model change, while the orange squares represent the measured samples taken before the most recent model change (if any). The green dots are color-coded based on recency, with darker tones indicating more recent samples and lighter, yellowish tones representing older samples. The area of the green dots is proportional to their fitting weights at round k^C . The pink shaded area represents the error region (cf. Subsection 4.3.3): the smaller, the better. The TDMA round considered (k^C), the estimated $((\hat{R}, \hat{\alpha}))$ and real $(R, \alpha))$ parameters, the current error index (ξ), and the average error index throughout the simulation ($\bar{\xi}$) are reported on the figures.

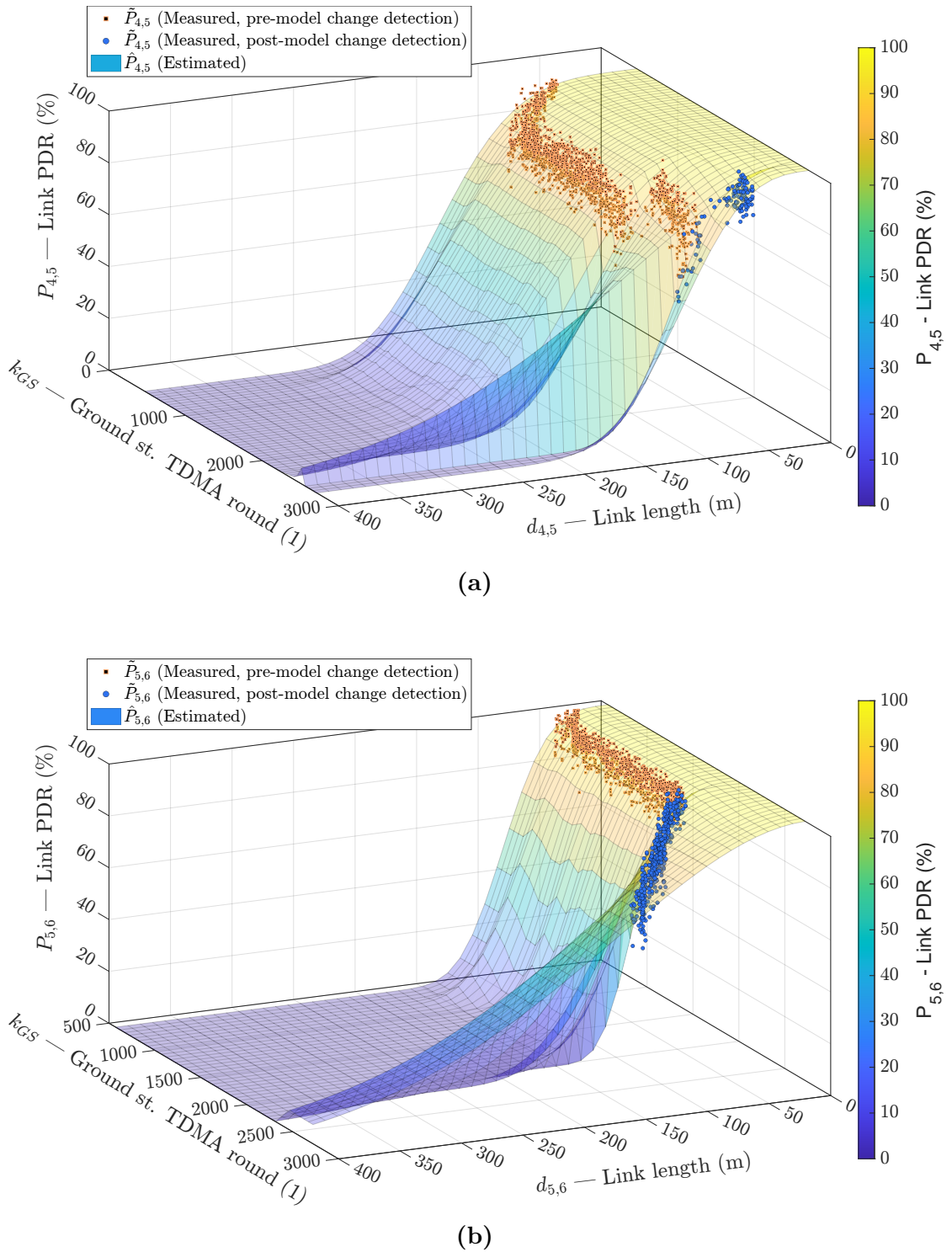


Figure 5.12. Time evolution (from the link creating until round k^C) of the estimated link models for the DRP strategy in scenario ‘d’, for two links: **(a)** for the link $\{4,5\}$; **(b)** for the link $\{5,6\}$. The blue dots represent the measured samples (P, d) that are used in the current estimate of the link model, following the most recent model change. The orange squares represent the measured samples that were used in previous model estimates, up until the last detected model change.

5.1.5 Summary

This study examined how three different relay placement strategies – equidistant, equal PDR, and DRP – performed under four scenarios: 'unchanged model' (represented by 'a'), 'small abrupt model change' ('b'), 'large abrupt model change' ('c'), and 'incremental model change' ('d'). The estimation error indices for each strategy and scenario are listed in Table 5.1 (defined in Subsection 4.3.3). The equal-PDR and DRP strategies produced null estimation error indices when using true parameters. As expected, the estimates for the fourth (4, 5) and fifth (5, 6) links were generally worse than the other links for almost all strategies and scenarios. The equidistant strategy resulted in slightly poorer estimates than the other two strategies, possibly due to relays measuring PDR at almost constant distances. However, unlike the equal-PDR and DRP strategies, the equidistant strategy does not take the model parameters as input. The estimation results obtained with the equidistant strategy were not the primary focus of this study but rather conducted for exploratory purposes. Lastly, the scenario 'd' had significantly higher estimation errors than any other scenario across all the strategies, which was at least partially expected since the models of the fourth and fifth links were changing over time during the second half of the circuit. Figure 5.13 presents the values from Table 5.1.

Table 5.1. Average estimation error outcomes for the six links in the network ($\{\{1, 2\}, \{2, 3\}, \{3, 4\}, \{4, 5\}, \{5, 6\}, \{6, 7\}\}$) when implementing one of the three strategies (equidistant, equal-PDR, and DRP, the last two of which tested with estimated and true parameters) under one of the four scenarios. The average was calculated over the period starting from the moment the source node reached the waypoint ‘A’ (at round k^A) until it reached the waypoint ‘C’ (at round k^C). The scenarios include ‘unchanged model’ (represented by ‘a’), ‘small abrupt model change’ (represented by ‘b’), ‘large abrupt model change’ (represented by ‘c’), and ‘incremental model change’ (represented by ‘d’). The green shade intensity of the cells represents the average estimation error as defined in Equation (4.10), with white cells indicating the minimum error of 0 and full green cells indicating the maximum error of 38.06.

Strategy	Average estimation error	Simulation scenario			
		a (1)	b (1)	c (1)	d (1)
Equidistant	$\bar{\xi}_{1,2}^{\text{equi}}$	1.3	1.7	2.2	1.8
	$\bar{\xi}_{2,3}^{\text{equi}}$	5.1	5.1	4.0	5.5
	$\bar{\xi}_{3,4}^{\text{equi}}$	11.2	11.2	6.3	5.8
	$\bar{\xi}_{4,5}^{\text{equi}}$	19.6	10.9	38.1	27.9
	$\bar{\xi}_{5,6}^{\text{equi}}$	2.0	9.4	13.9	13.7
	$\bar{\xi}_{6,7}^{\text{equi}}$	4.7	5.4	15.5	6.3
	$\bar{\xi}_{1,2}^{\text{equalPDR,e}}$	2.6	2.1	2.8	3.8
Equal PDR, estimated parameters	$\bar{\xi}_{2,3}^{\text{equalPDR,e}}$	4.5	3.8	6.2	7.5
	$\bar{\xi}_{3,4}^{\text{equalPDR,e}}$	6.5	11.4	5.1	6.4
	$\bar{\xi}_{4,5}^{\text{equalPDR,e}}$	3.5	10.8	6.4	37.2
	$\bar{\xi}_{5,6}^{\text{equalPDR,e}}$	2.6	5.4	8.1	17.5
	$\bar{\xi}_{6,7}^{\text{equalPDR,e}}$	3.1	8.2	4.8	5.5
	$\bar{\xi}_{1,2}^{\text{equalPDR,t}}$	0.0	0.0	0.0	0.0
	$\bar{\xi}_{2,3}^{\text{equalPDR,t}}$	0.0	0.0	0.0	0.0
Equal PDR, true parameters	$\bar{\xi}_{3,4}^{\text{equalPDR,t}}$	0.0	0.0	0.0	0.0
	$\bar{\xi}_{4,5}^{\text{equalPDR,t}}$	0.0	0.0	0.0	0.0
	$\bar{\xi}_{5,6}^{\text{equalPDR,t}}$	0.0	0.0	0.0	0.0
	$\bar{\xi}_{6,7}^{\text{equalPDR,t}}$	0.0	0.0	0.0	0.0
	$\bar{\xi}_{1,2}^{\text{DRP,e}}$	5.2	3.2	4.2	4.6
	$\bar{\xi}_{2,3}^{\text{DRP,e}}$	11.1	2.6	6.0	7.4
	$\bar{\xi}_{3,4}^{\text{DRP,e}}$	7.2	3.8	7.0	6.7
DRP, estimated parameters	$\bar{\xi}_{4,5}^{\text{DRP,e}}$	8.5	8.6	4.1	12.2
	$\bar{\xi}_{5,6}^{\text{DRP,e}}$	5.2	6.7	7.8	16.6
	$\bar{\xi}_{6,7}^{\text{DRP,e}}$	18.2	6.7	8.2	5.2
	$\bar{\xi}_{1,2}^{\text{DRP,t}}$	0.0	0.0	0.0	0.0
	$\bar{\xi}_{2,3}^{\text{DRP,t}}$	0.0	0.0	0.0	0.0
	$\bar{\xi}_{3,4}^{\text{DRP,t}}$	0.0	0.0	0.0	0.0
	$\bar{\xi}_{4,5}^{\text{DRP,t}}$	0.0	0.0	0.0	0.0
DRP, true parameters	$\bar{\xi}_{5,6}^{\text{DRP,t}}$	0.0	0.0	0.0	0.0
	$\bar{\xi}_{6,7}^{\text{DRP,t}}$	0.0	0.0	0.0	0.0

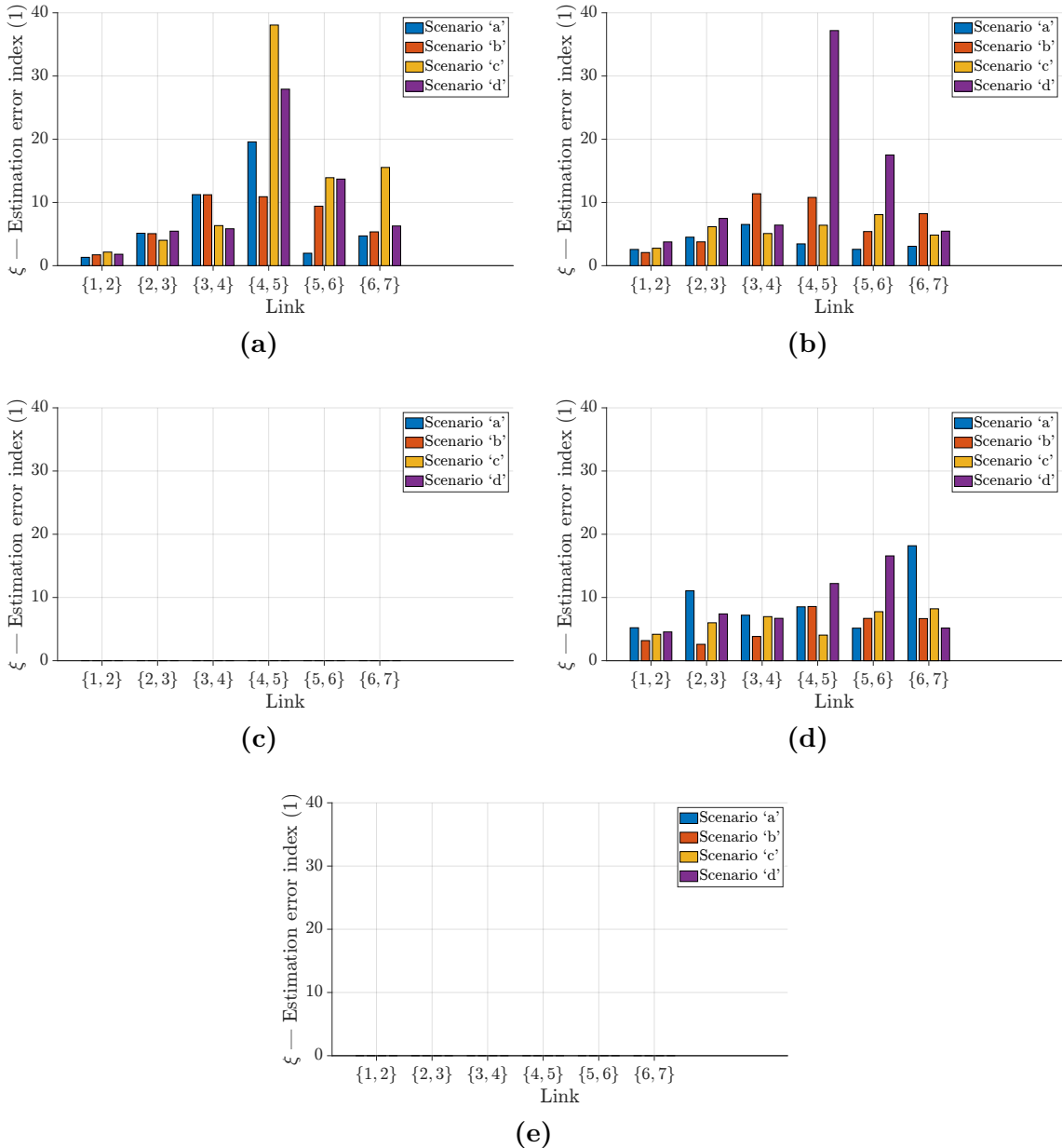


Figure 5.13. Estimation error indices for different strategies and scenarios (values from Table 5.1): (a) equidistant; (b) equal-PDR, when using estimated model parameters; (c) DRP, when using actual (true) model parameters; (d) DRP, when using estimated model parameters; (e) DRP, when using actual (true) model parameters. When using true parameters, the strategies achieve zero estimation error.

5.2 Network PDR Analysis

In this section, we analyze the PDR (Packet Delivery Ratio) of the network under three different strategies: equidistant, equal-PDR, and DRP. For the last two strategies, we tested both estimated and true parameters. For each strategy and scenario ('a', 'b', 'c', and 'd'), we present the trajectories of the UAVs, as well as the PDR evolution of all six links ($\{\{1, 2\} \{2, 3\} \{3, 4\} \{4, 5\} \{5, 6\} \{6, 7\}\}$) and the entire network from end to end, until the end of the simulation (TDMA round k^C). We visualize the instantaneous PDR for both link PDRs (in blue dots) and network PDR (in orange dots), as well as their 50-point moving average (in red line) for each PDR. Additionally, we annotate the average link and network PDRs from k^A to k^C for each strategy and scenario. Finally, we provide two tables: Table 5.3 for the average link PDRs and Table 5.2 for the average network PDRs.

5.2.1 Scenario 'a'

Figure 5.14 shows the UAV trajectories at TDMA round k^C for the scenario 'a' (unchanged model, cf. Equation (4.3)) using the DRP strategy with estimated parameters. In Figure 5.15, the UAV trajectories for the same scenario are presented for four different relay placement strategies: (a) equidistant, (b) equal-PDR with actual parameters, (c) DRP with estimated parameters, and (d) DRP with actual parameters.

The performances of the strategies with estimated parameters in the same scenario are depicted in Figures 5.16 (equidistant), 5.17 (equal-PDR with estimated parameters), 5.18 (equal-PDR with true parameters), 5.20 (DRP with estimated parameters), and 5.19 (DRP with true parameters). The figures include two subfigures each: (a) the instantaneous and average link and network PDRs, which are averaged over the pink shaded region from k^A to k^C , and (b) the instantaneous network PDR as a function of TDMA round and network length L .

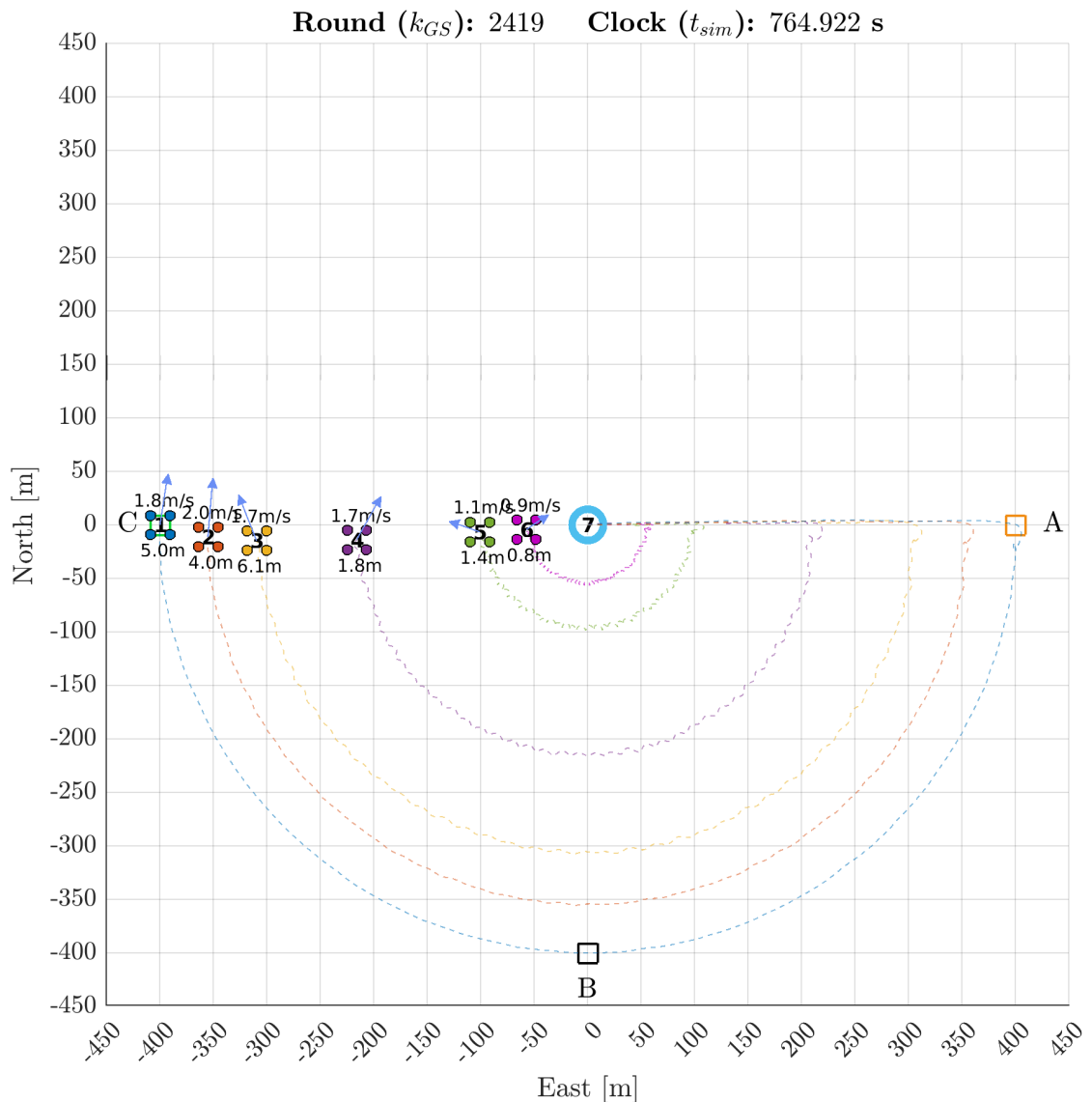


Figure 5.14. UAV trajectories at TDMA round k^C under the scenario ‘a’ using the DRP strategy (with estimated model parameters).

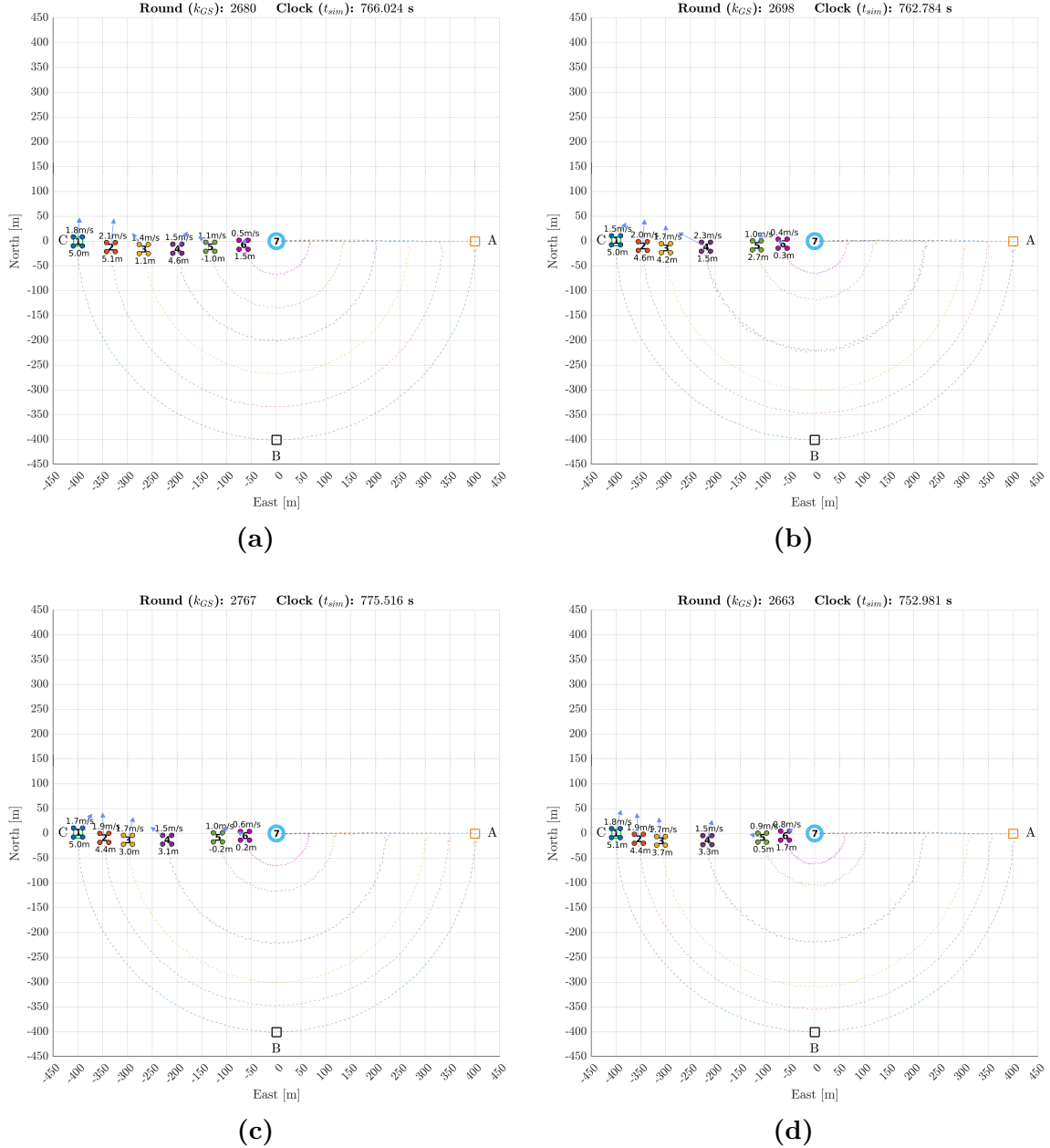
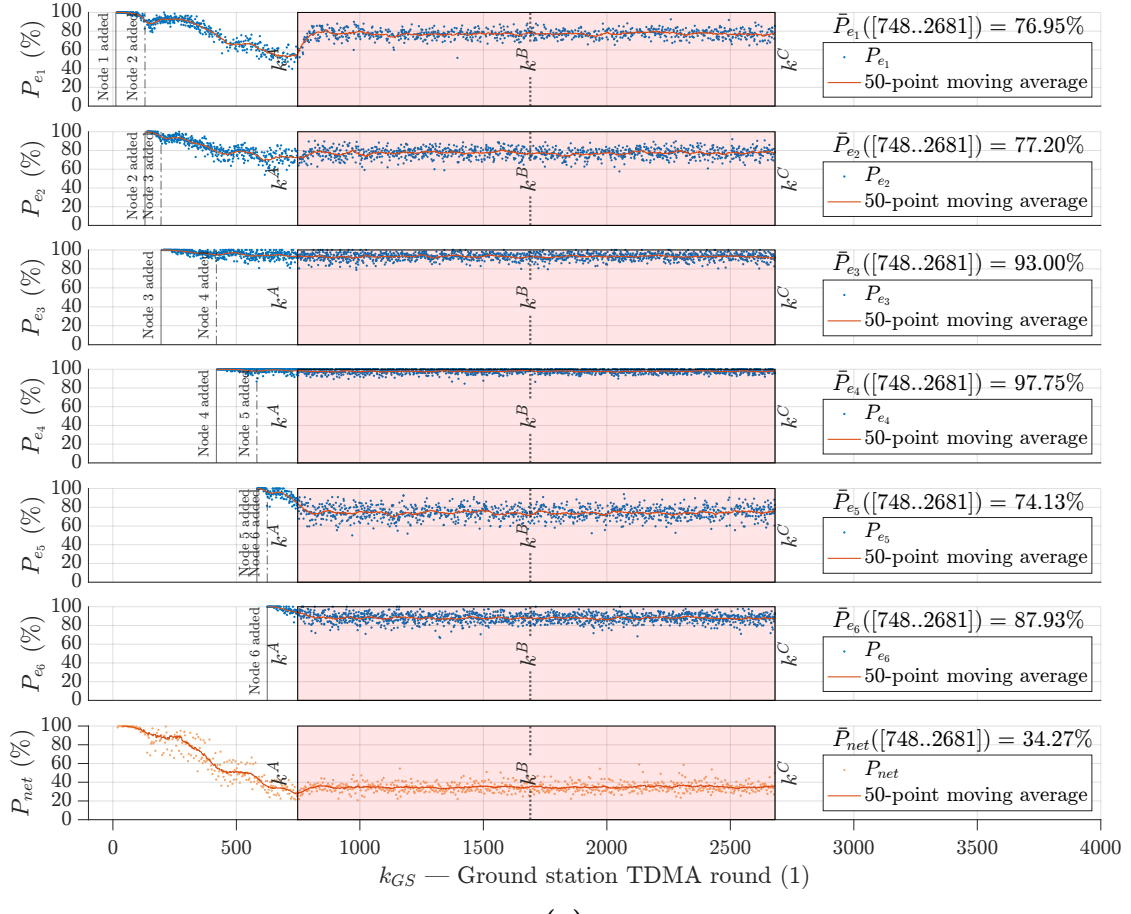
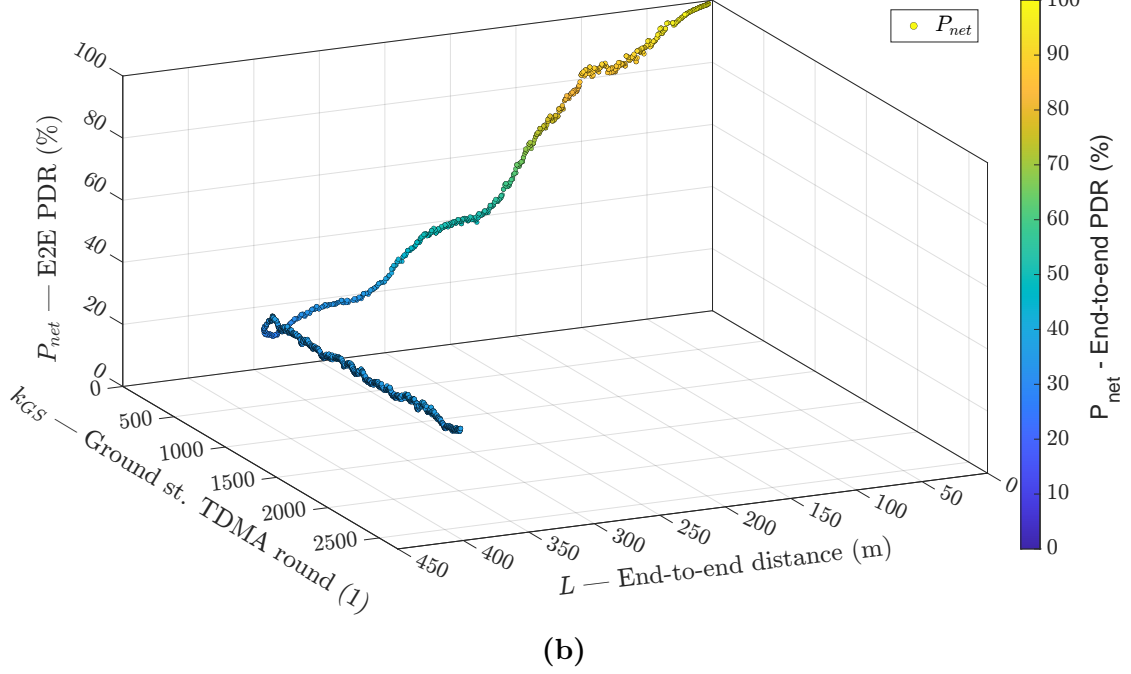


Figure 5.15. UAV trajectories at TDMA round k^C under the scenario ‘a’ using different relay placement strategies: (a) equidistant; (b) equal-PDR, when using estimated model parameters; (c) equal-PDR, when using actual (true) model parameters; (d) DRP, when using actual (true) model parameters.

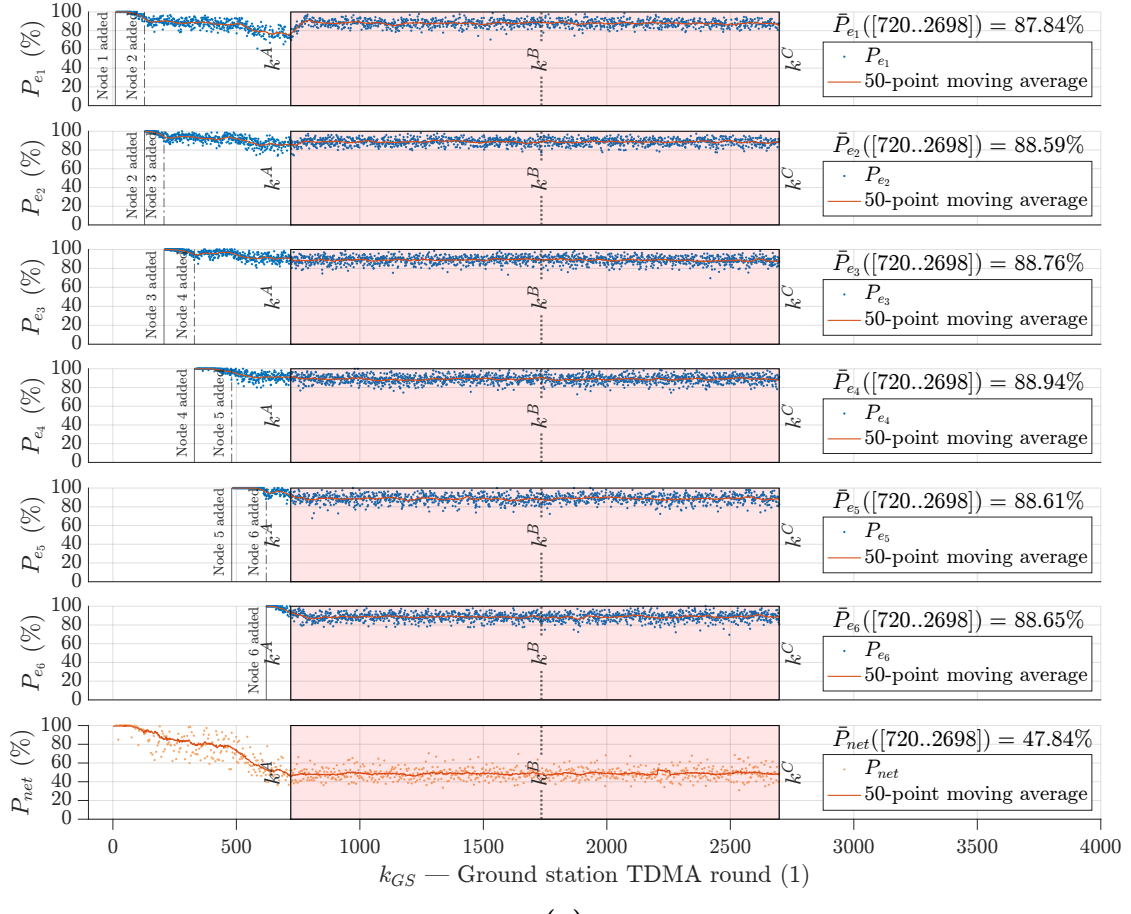


(a)

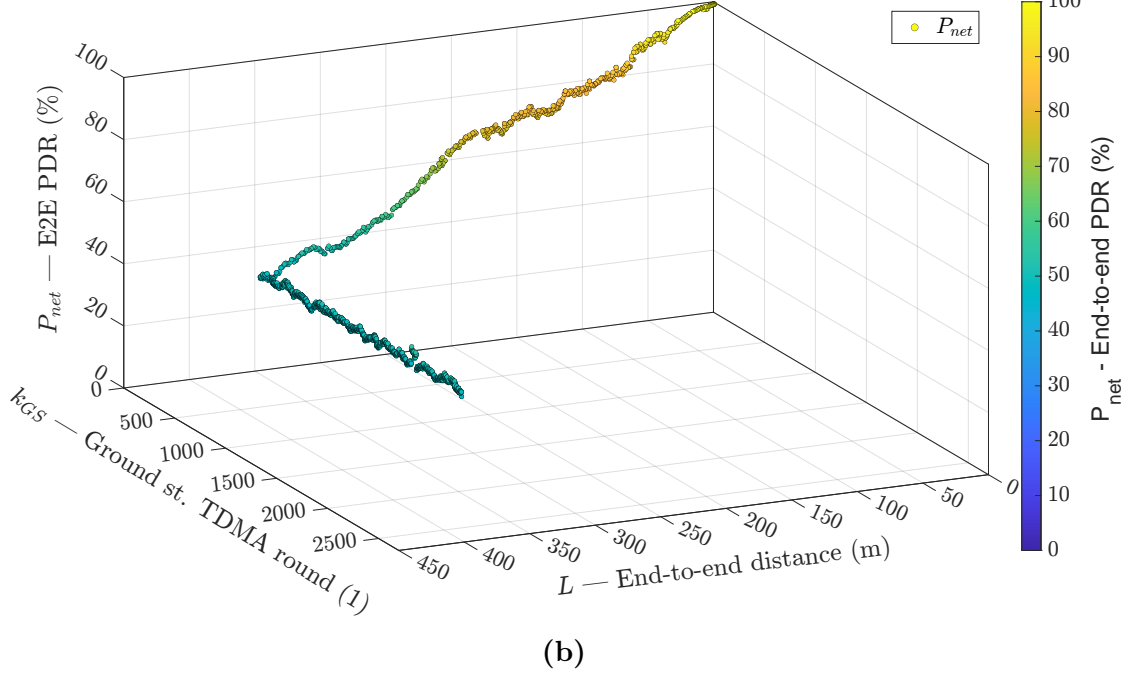


(b)

Figure 5.16. Simulation case: equidistant relay placement strategy under the scenario ‘a’. (a) Instantaneous and average link and network PDRs. The averages are computed over the region shaded in pink, which goes from k^A to k^C . (b) Instantaneous network PDR as a function of TDMA round and network length L .

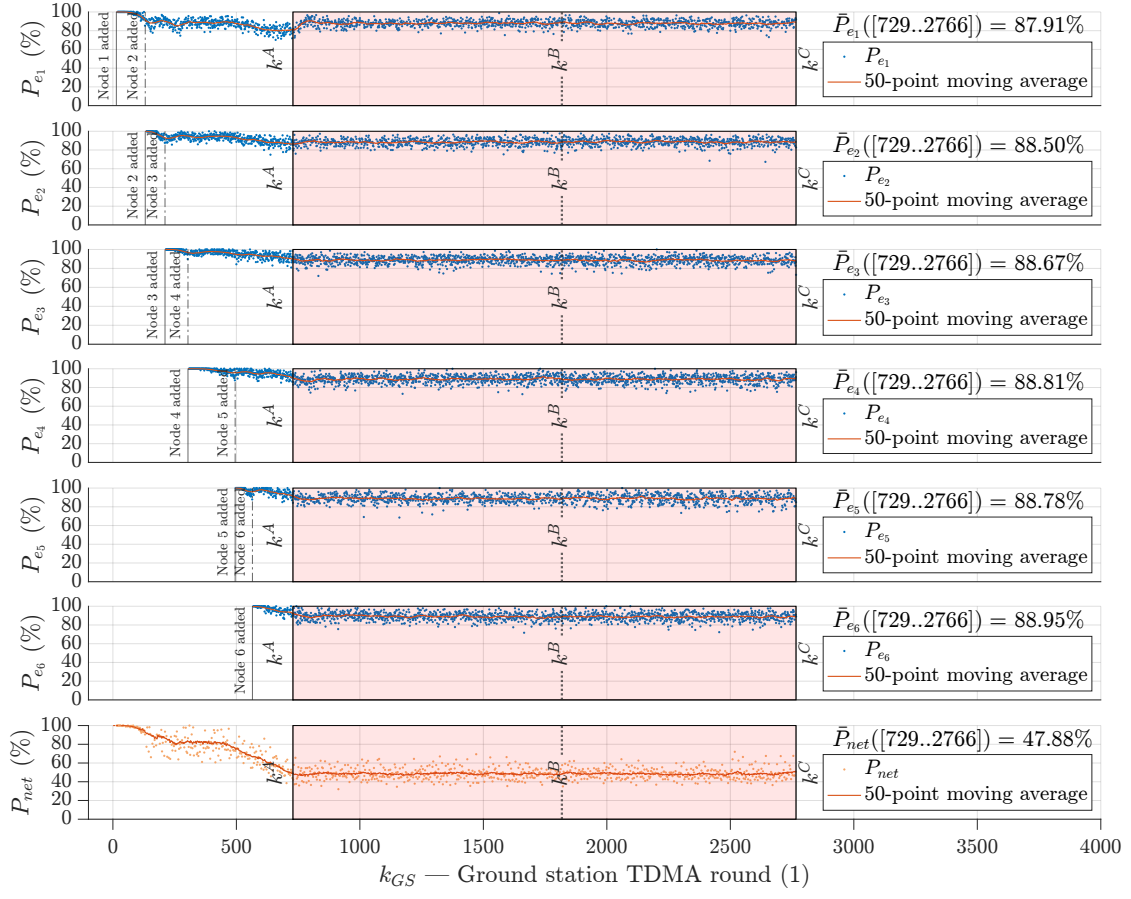


(a)

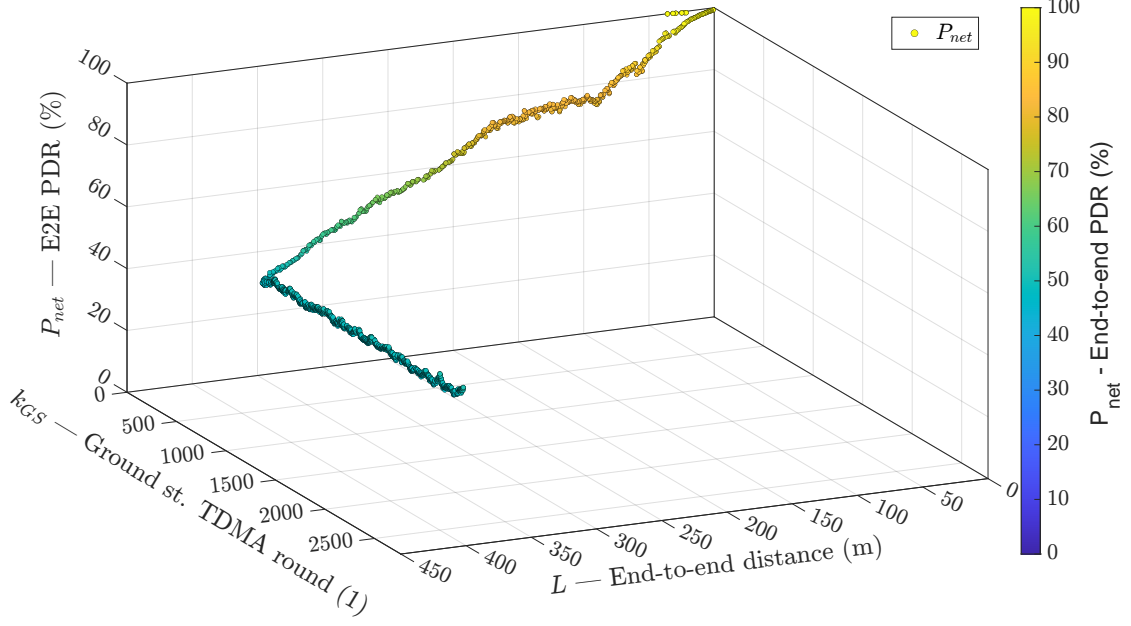


(b)

Figure 5.17. Simulation case: equal-PDR (with estimated parameters) relay placement strategy under the scenario ‘a’. **(a)** Instantaneous and average link and network PDRs. The averages are computed over the region shaded in pink, which goes from k^A to k^C . **(b)** Instantaneous network PDR as a function of TDMA round and network length L .

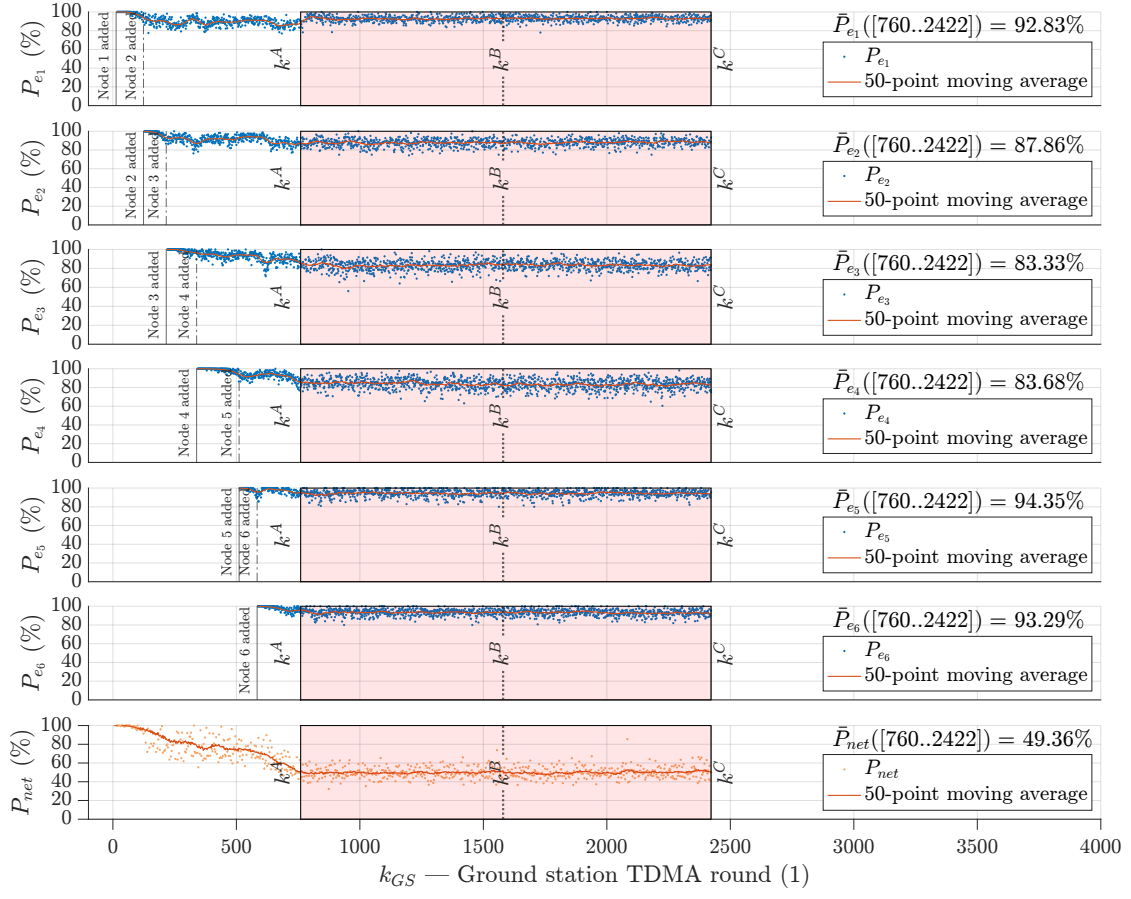


(a)

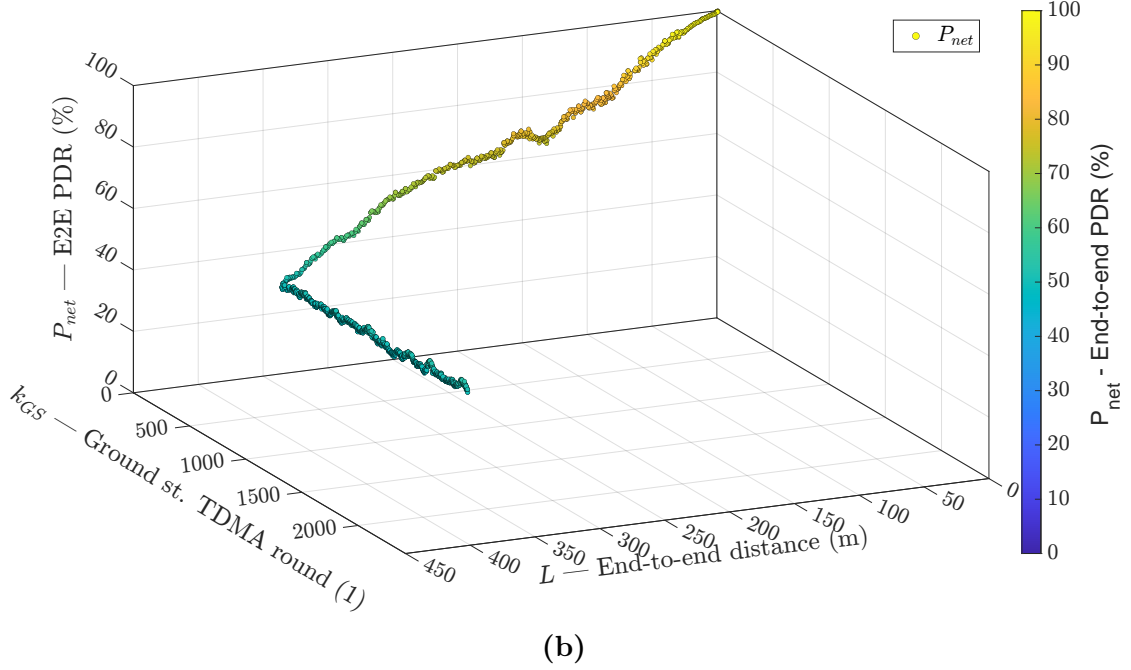


(b)

Figure 5.18. Simulation case: equal-PDR (with true parameters) relay placement strategy under the scenario ‘a’. **(a)** Instantaneous and average link and network PDRs. The averages are computed over the region shaded in pink, which goes from k^A to k^C . **(b)** Instantaneous network PDR as a function of TDMA round and network length L .

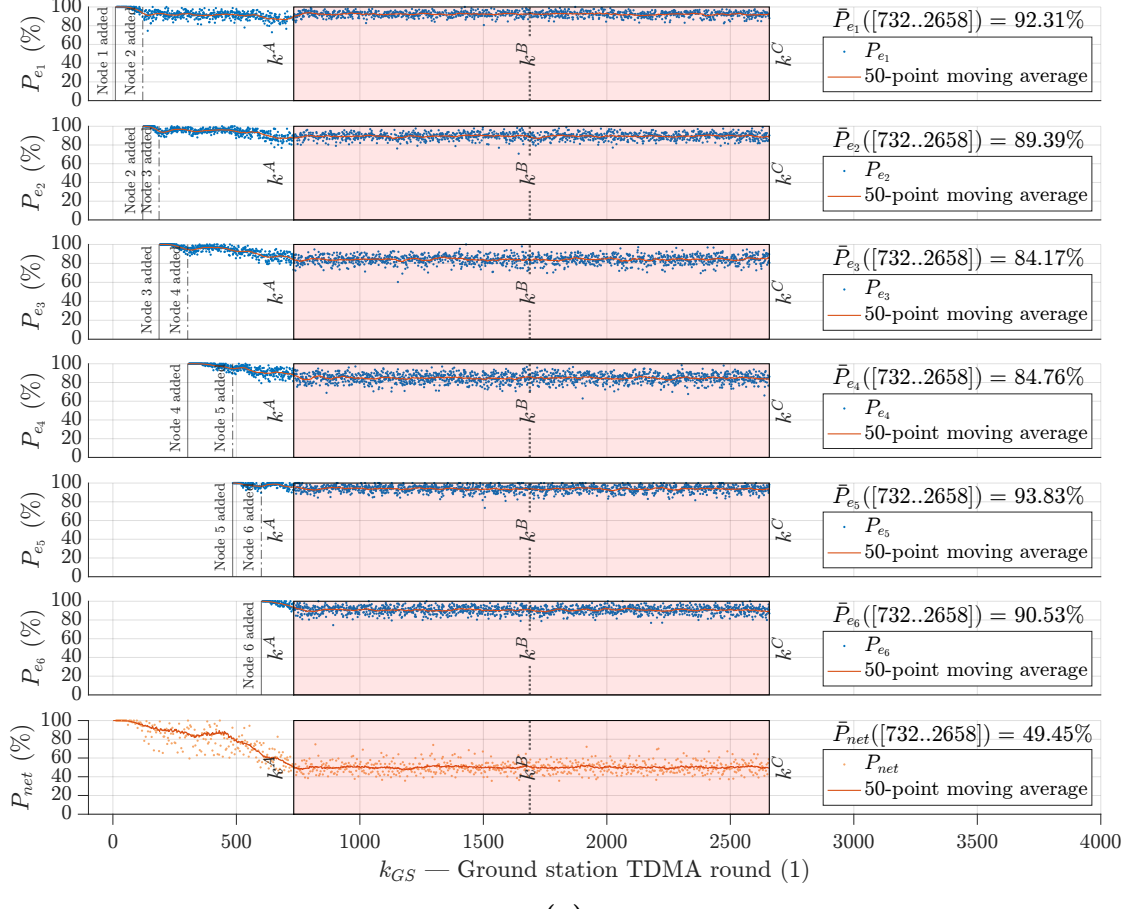


(a)

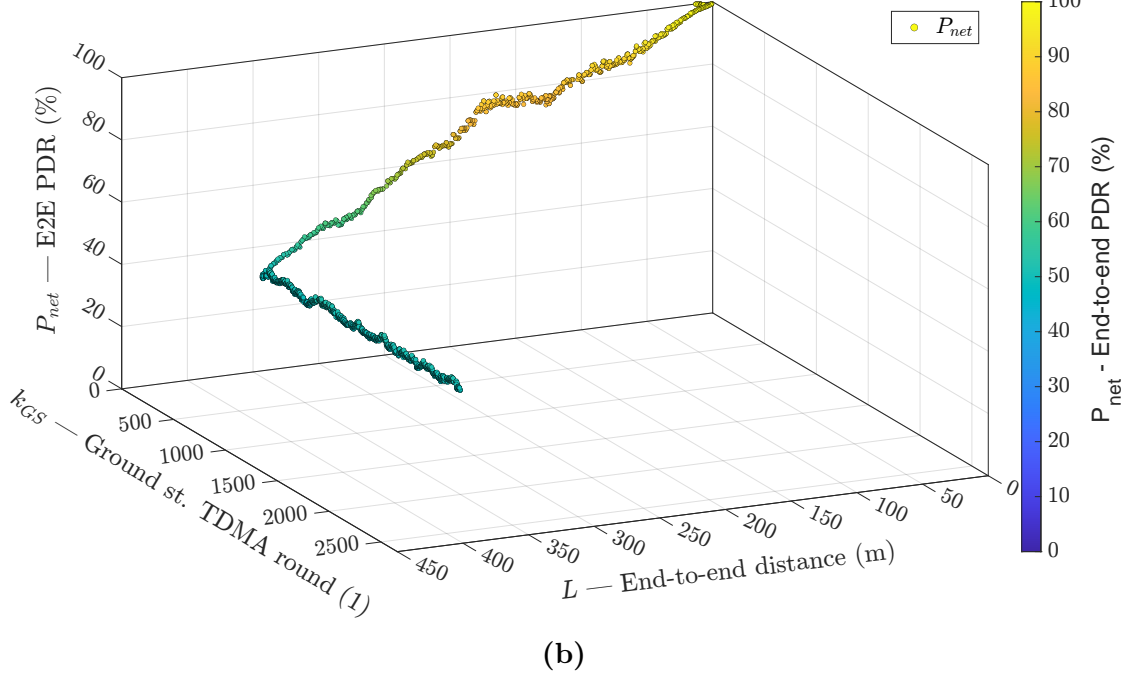


(b)

Figure 5.19. Simulation case: DRP (with estimated parameters) relay placement strategy under the scenario ‘a’. **(a)** Instantaneous and average link and network PDRs. The averages are computed over the region shaded in pink, which goes from k^A to k^C . **(b)** Instantaneous network PDR as a function of TDMA round and network length L .



(a)



(b)

Figure 5.20. Simulation case: DRP (with true parameters) relay placement strategy under the scenario ‘a’. **(a)** Instantaneous and average link and network PDRs. The averages are computed over the region shaded in pink, which goes from k^A to k^C . **(b)** Instantaneous network PDR as a function of TDMA round and network length L .

5.2.2 Scenario ‘b’

Figure 5.21 shows the UAV trajectories at TDMA round k^C for the scenario ‘b’ (small abrupt model change, cf. Equation (4.4)) using the DRP strategy with estimated parameters. In Figure 5.22, the UAV trajectories for the same scenario are presented for four different relay placement strategies: (a) equidistant, (b) equal-PDR with actual parameters, (c) DRP with estimated parameters, and (d) DRP with actual parameters.

The performances of the strategies with estimated parameters in the same scenario are depicted in Figures 5.23 (equidistant), 5.24 (equal-PDR with estimated parameters), 5.25 (equal-PDR with true parameters), 5.27 (DRP with estimated parameters), and 5.26 (DRP with true parameters). The figures include two subfigures each: (a) the instantaneous and average link and network PDRs, which are averaged over the pink shaded region from k^A to k^C , and (b) the instantaneous network PDR as a function of TDMA round and network length L .

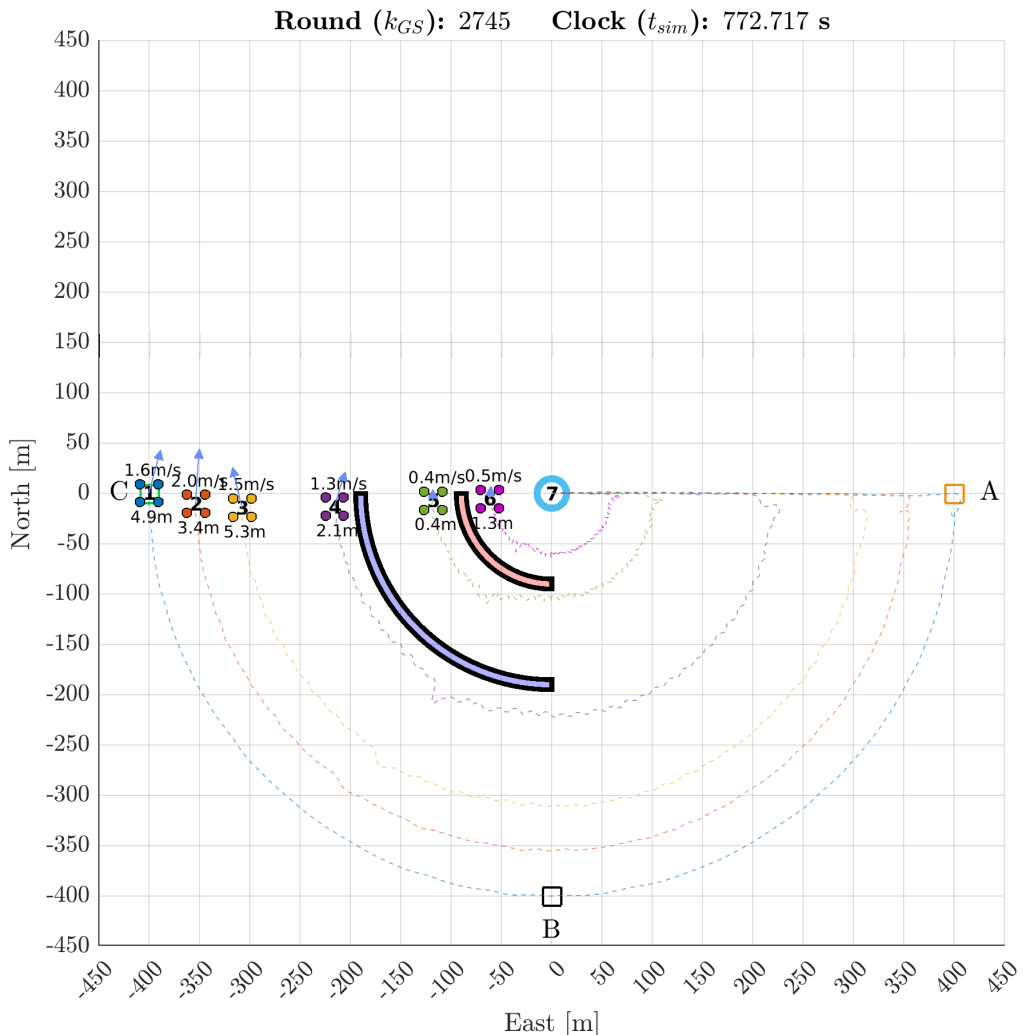


Figure 5.21. UAV trajectories at TDMA round k^C under the scenario ‘b’ using the DRP strategy (with estimated model parameters).

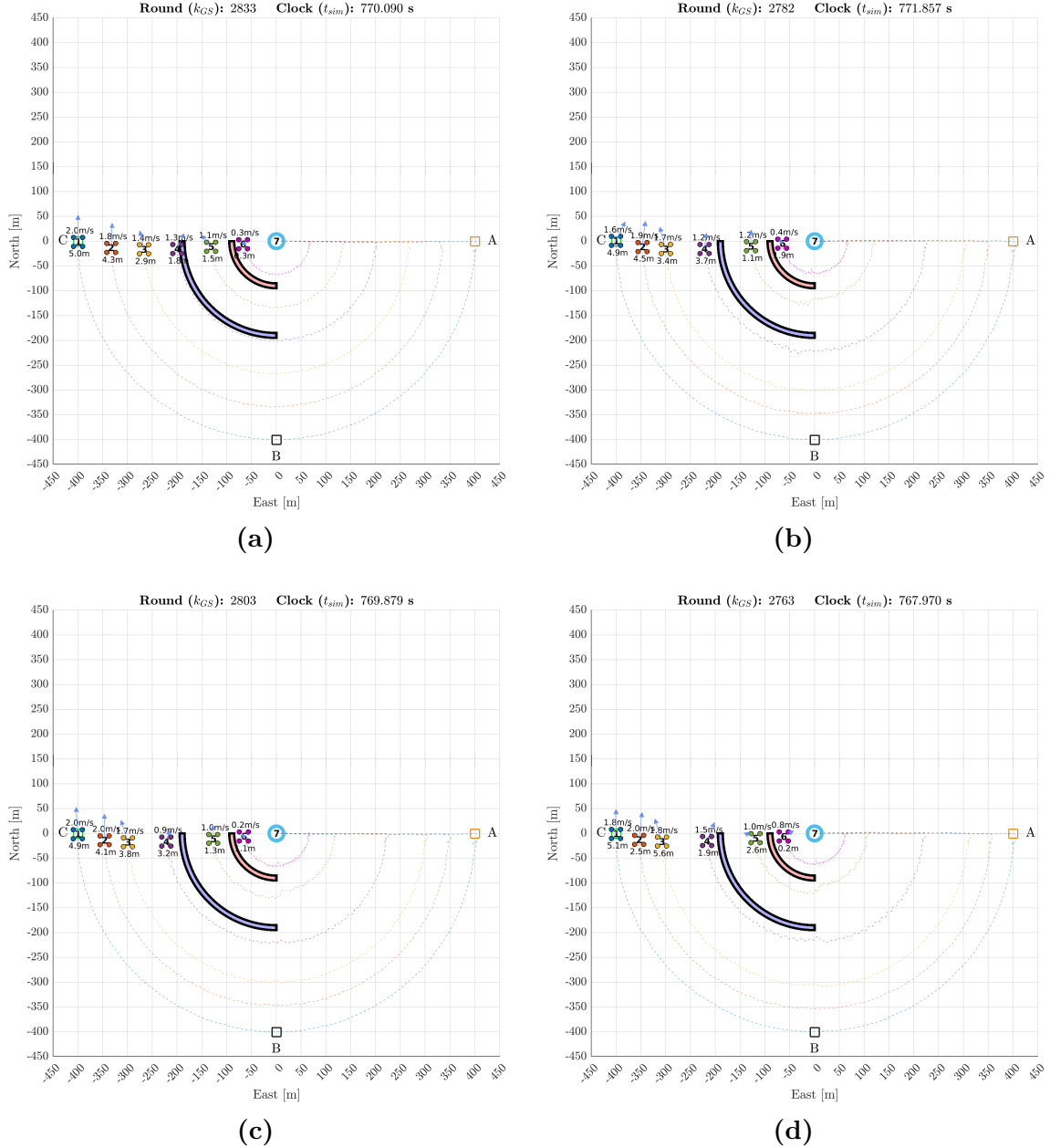
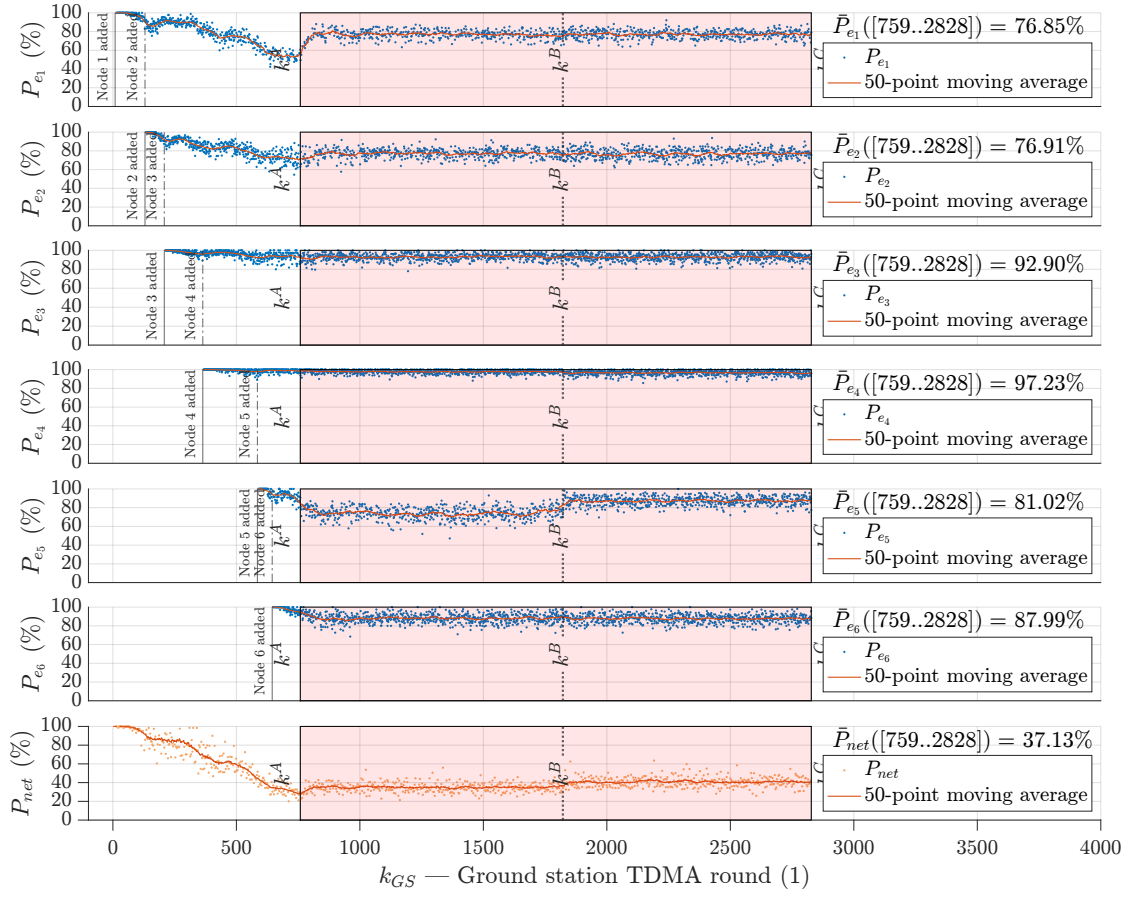
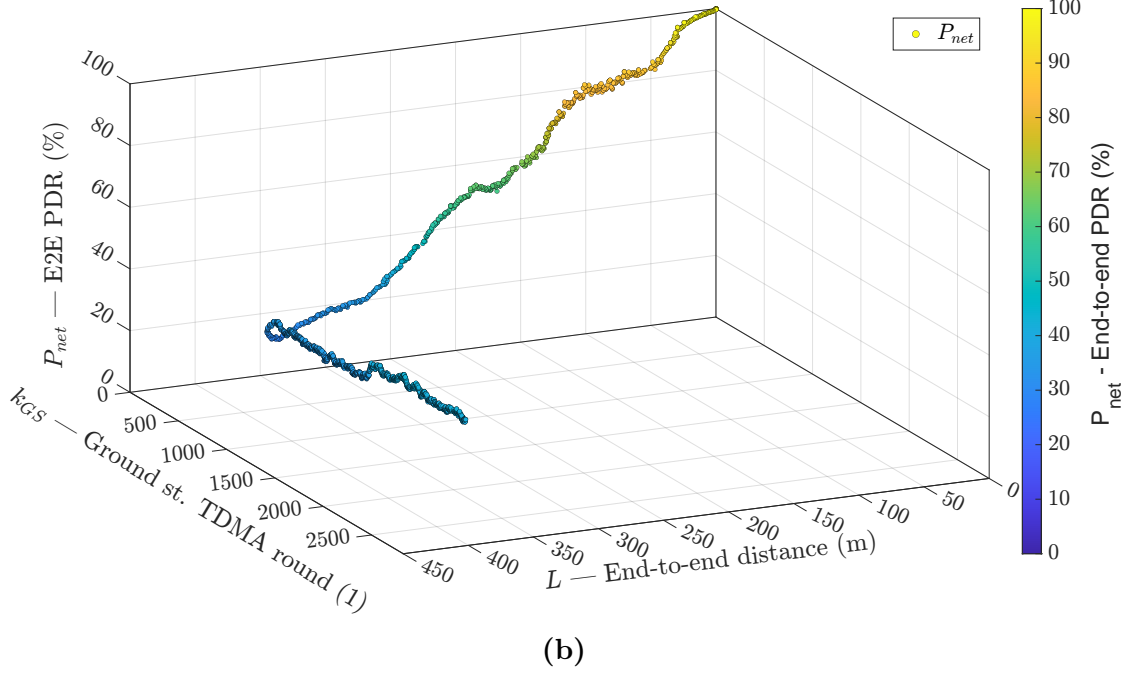


Figure 5.22. UAV trajectories at TDMA round k^C under the scenario ‘b’ using different relay placement strategies: (a) equidistant; (b) equal-PDR, when using estimated model parameters; (c) equal-PDR, when using actual (true) model parameters; (d) DRP, when using actual (true) model parameters.

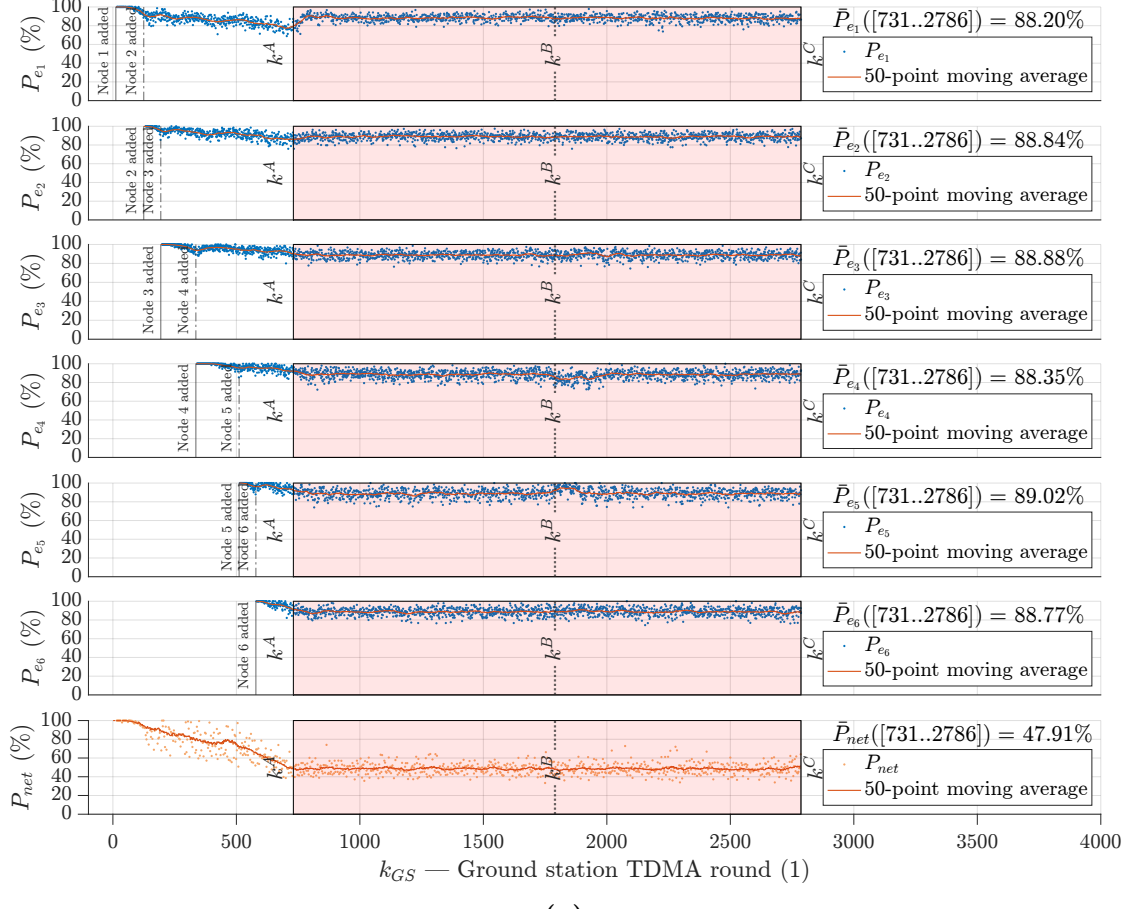


(a)

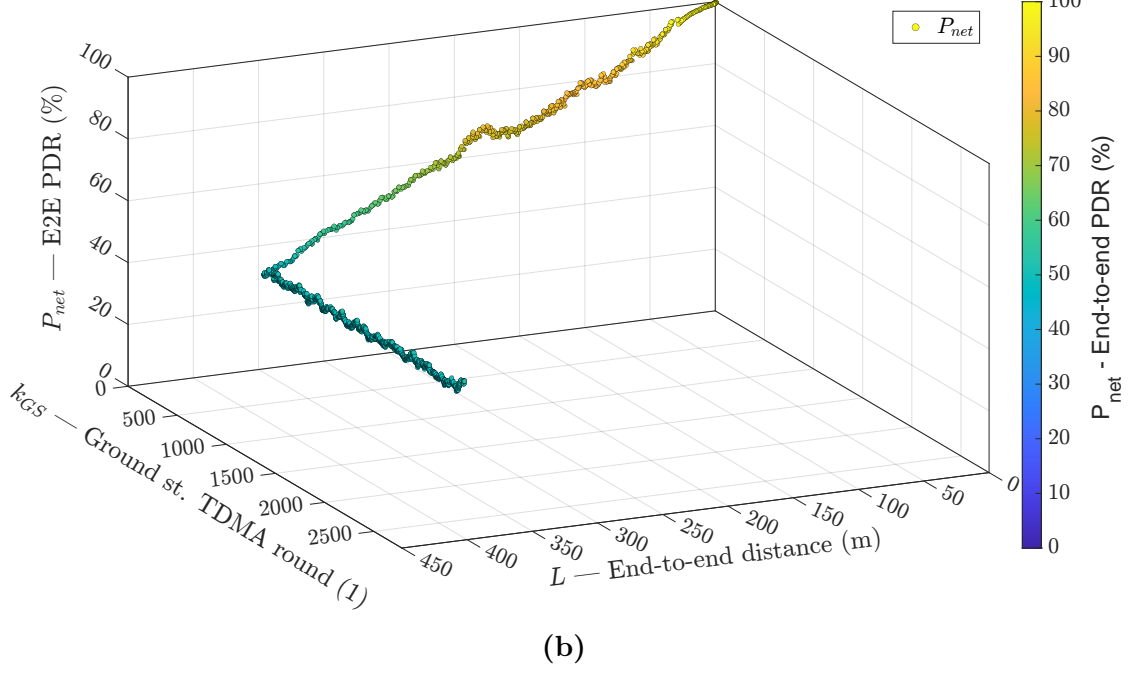


(b)

Figure 5.23. Simulation case: equidistant relay placement strategy under the scenario ‘b’. (a) Instantaneous and average link and network PDRs. The averages are computed over the region shaded in pink, which goes from k^A to k^C . (b) Instantaneous network PDR as a function of TDMA round and network length L .

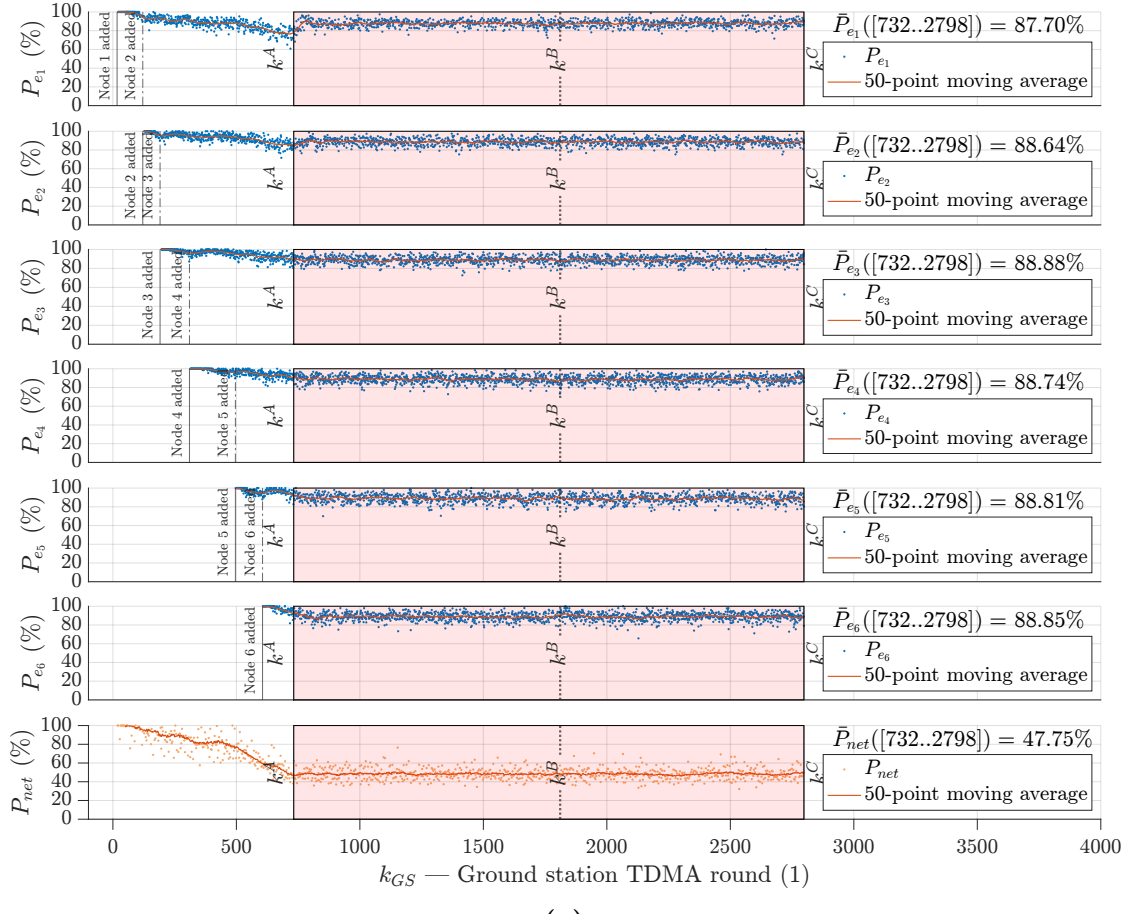


(a)

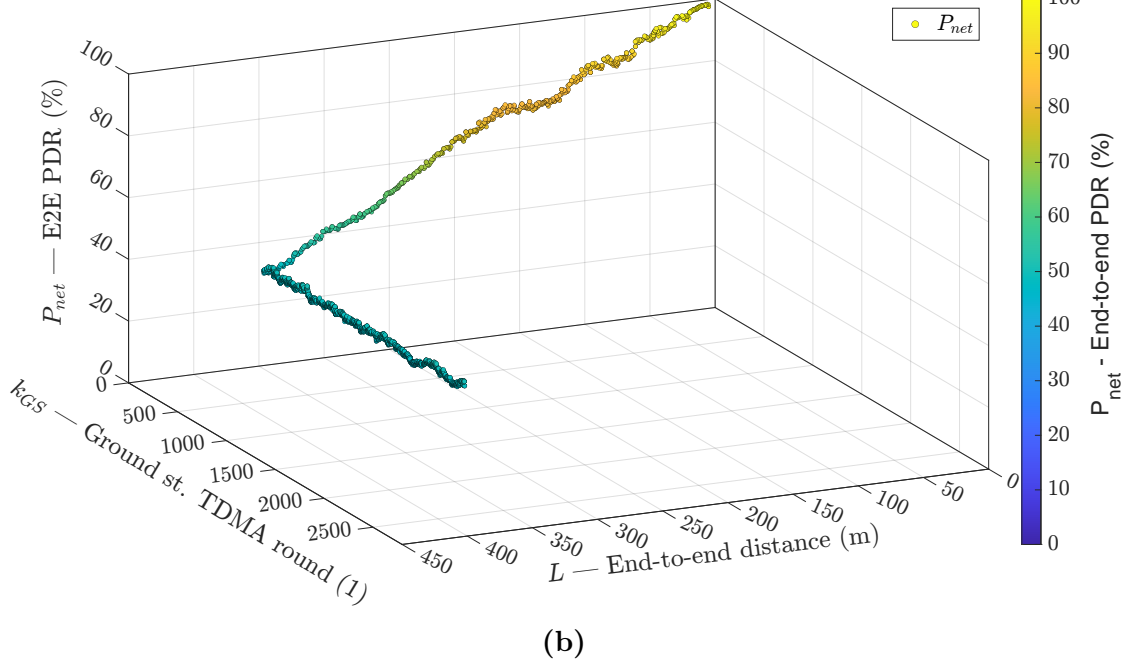


(b)

Figure 5.24. Simulation case: equal-PDR (with estimated parameters) relay placement strategy under the scenario ‘b’. **(a)** Instantaneous and average link and network PDRs. The averages are computed over the region shaded in pink, which goes from k^A to k^C . **(b)** Instantaneous network PDR as a function of TDMA round and network length L .

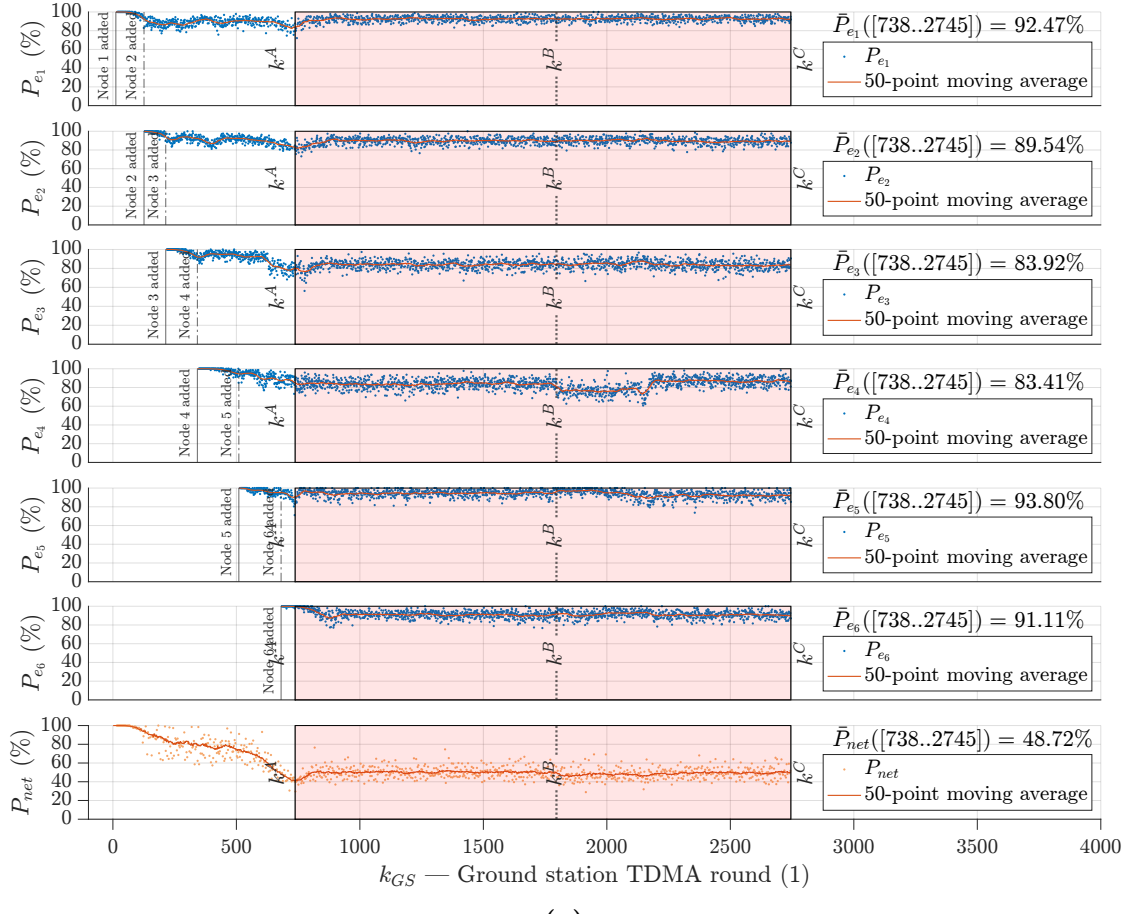


(a)

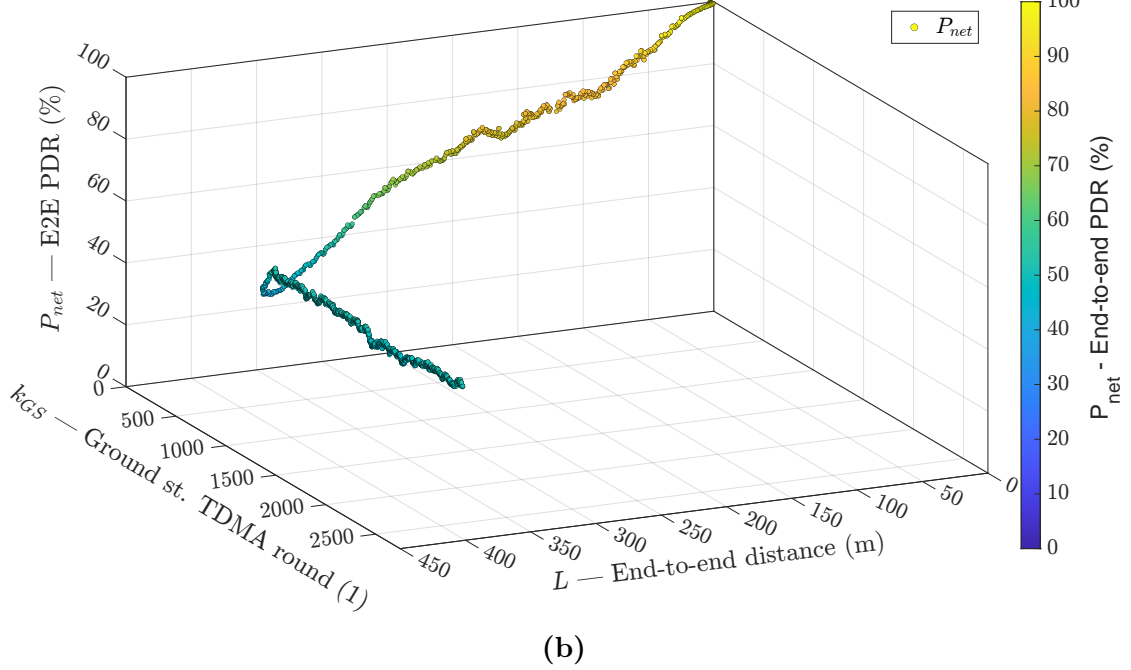


(b)

Figure 5.25. Simulation case: equal-PDR (with true parameters) relay placement strategy under the scenario ‘b’. **(a)** Instantaneous and average link and network PDRs. The averages are computed over the region shaded in pink, which goes from k^A to k^C . **(b)** Instantaneous network PDR as a function of TDMA round and network length L .

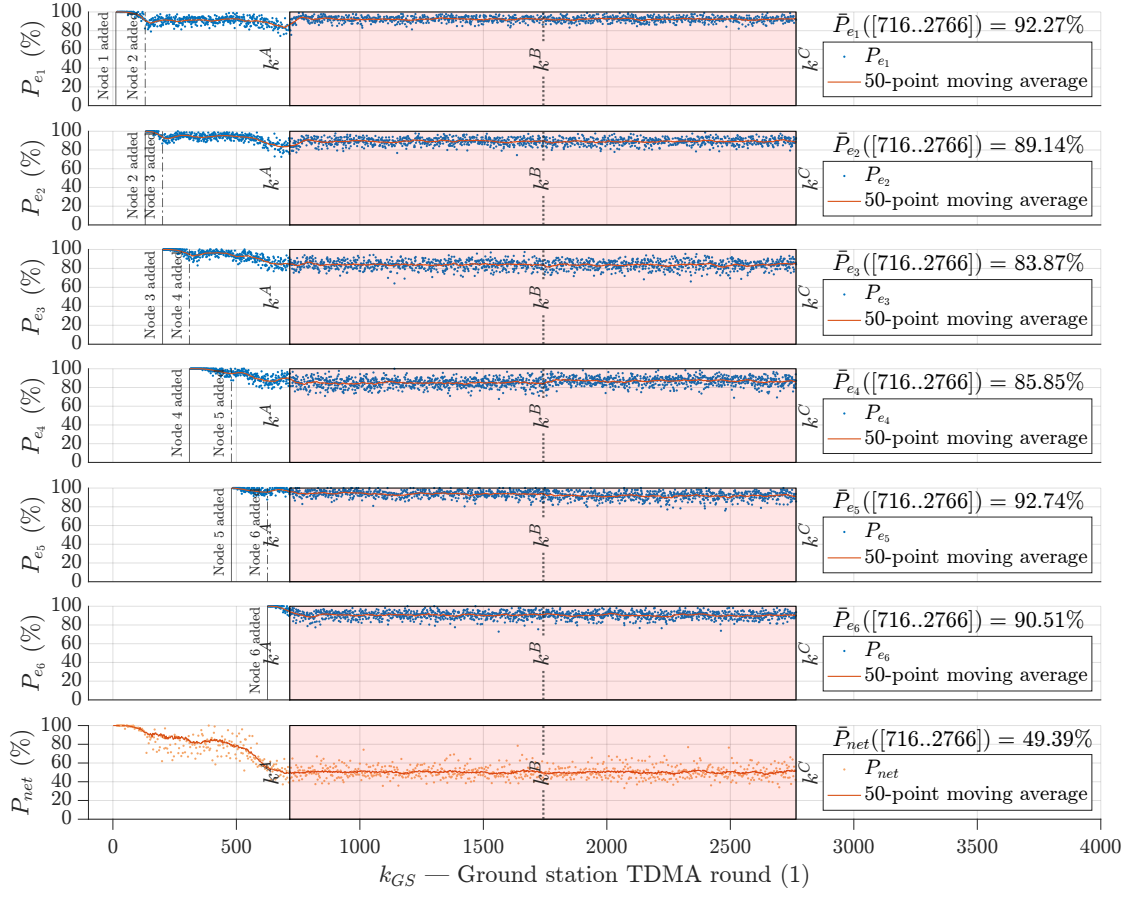


(a)

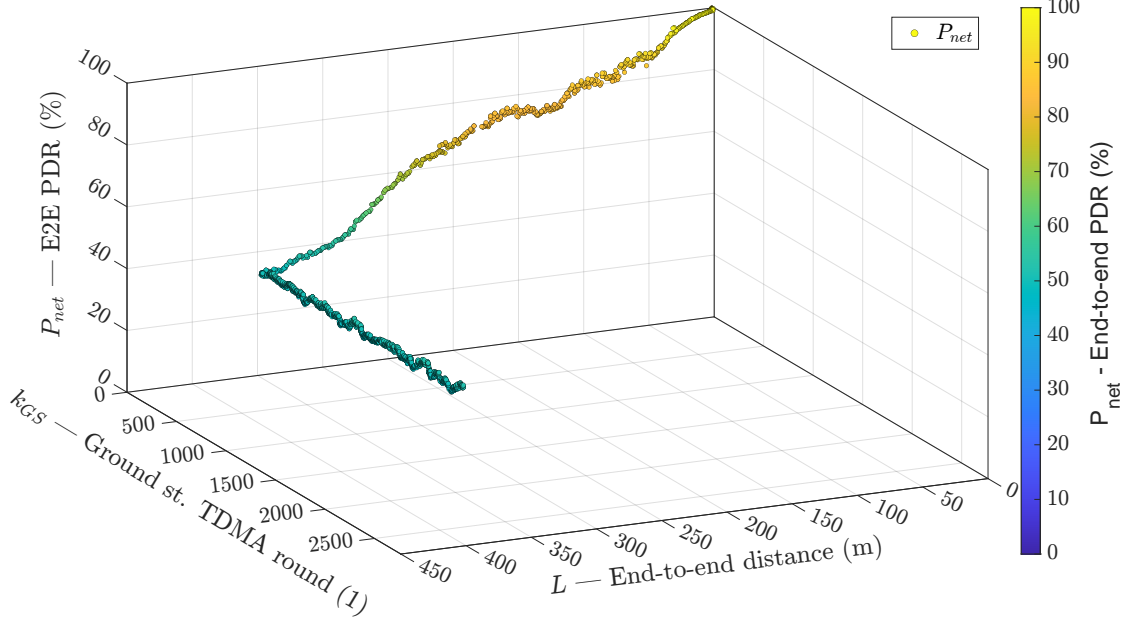


(b)

Figure 5.26. Simulation case: DRP (with estimated parameters) relay placement strategy under the scenario ‘b’. (a) Instantaneous and average link and network PDRs. The averages are computed over the region shaded in pink, which goes from k^A to k^C . (b) Instantaneous network PDR as a function of TDMA round and network length L .



(a)



(b)

Figure 5.27. Simulation case: DRP (with true parameters) relay placement strategy under the scenario ‘b’. **(a)** Instantaneous and average link and network PDRs. The averages are computed over the region shaded in pink, which goes from k^A to k^C . **(b)** Instantaneous network PDR as a function of TDMA round and network length L .

5.2.3 Scenario ‘c’

Figure 5.28 shows the UAV trajectories at TDMA round k^C for the scenario ‘c’ (large abrupt model change, cf. Equation (4.5)) using the DRP strategy with estimated parameters. In Figure 5.29, the UAV trajectories for the same scenario are presented for four different relay placement strategies: (a) equidistant, (b) equal-PDR with actual parameters, (c) DRP with estimated parameters, and (d) DRP with actual parameters.

The performances of the strategies with estimated parameters in the same scenario are depicted in Figures 5.30 (equidistant), 5.31 (equal-PDR with estimated parameters), 5.32 (equal-PDR with true parameters), 5.34 (DRP with estimated parameters), and 5.33 (DRP with true parameters). The figures include two subfigures each: (a) the instantaneous and average link and network PDRs, which are averaged over the pink shaded region from k^A to k^C , and (b) the instantaneous network PDR as a function of TDMA round and network length L .

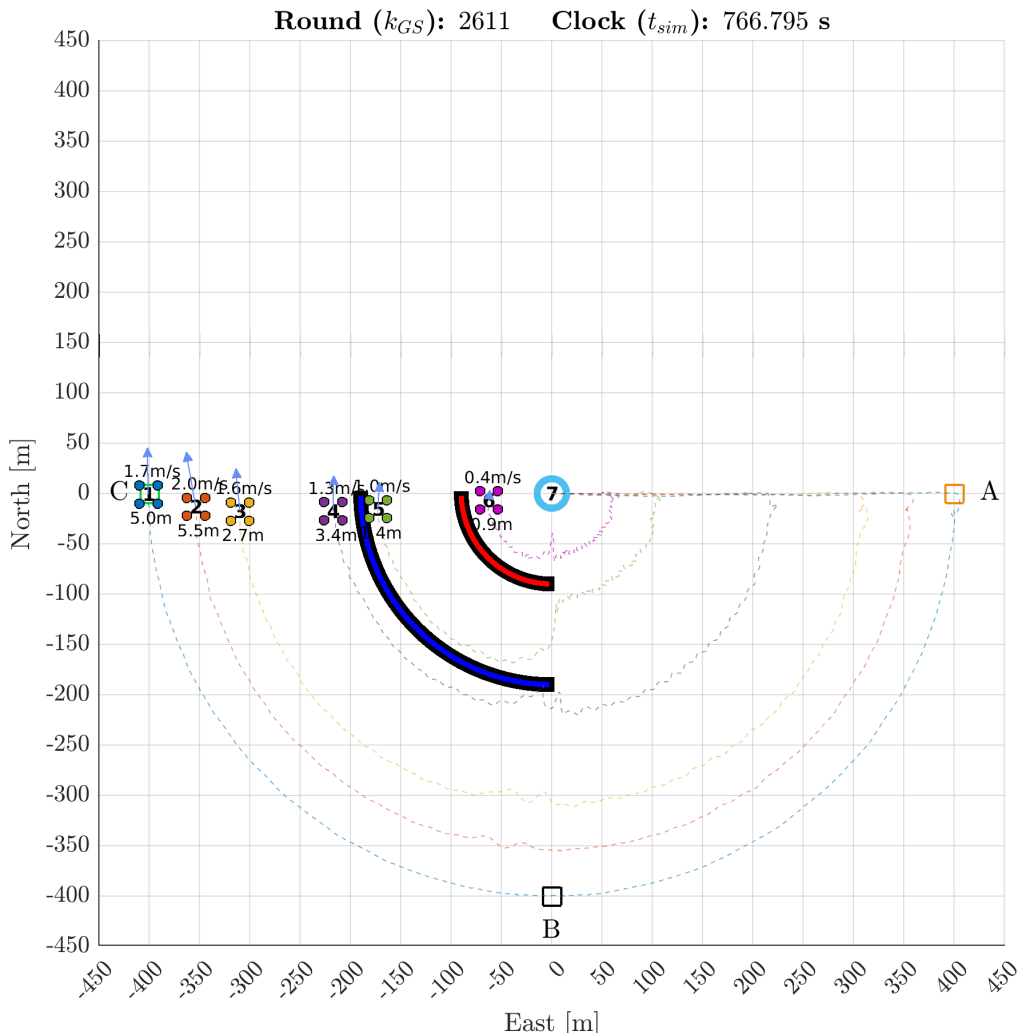


Figure 5.28. UAV trajectories at TDMA round k^C under the scenario ‘c’ using the DRP strategy (with estimated model parameters).

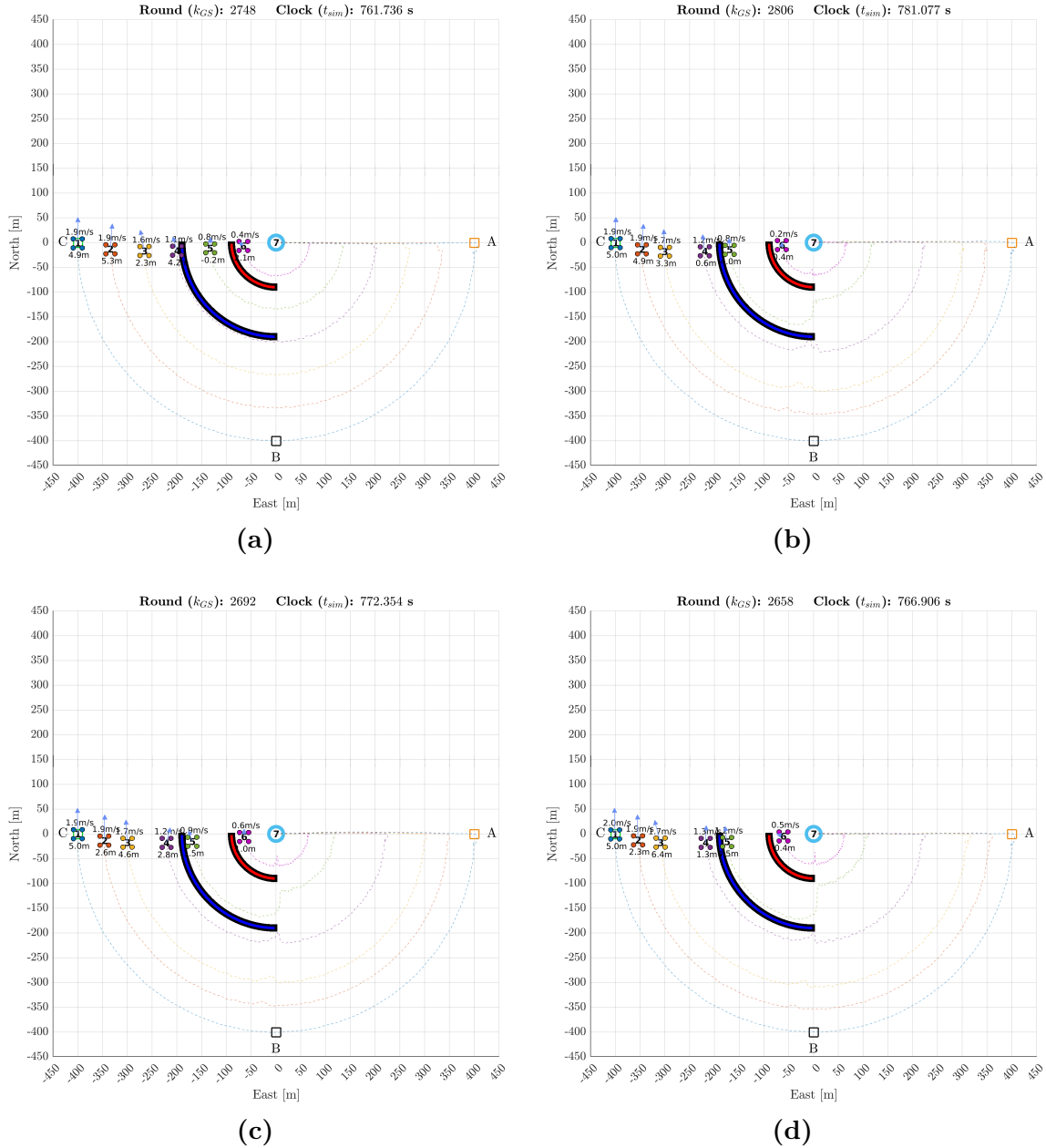
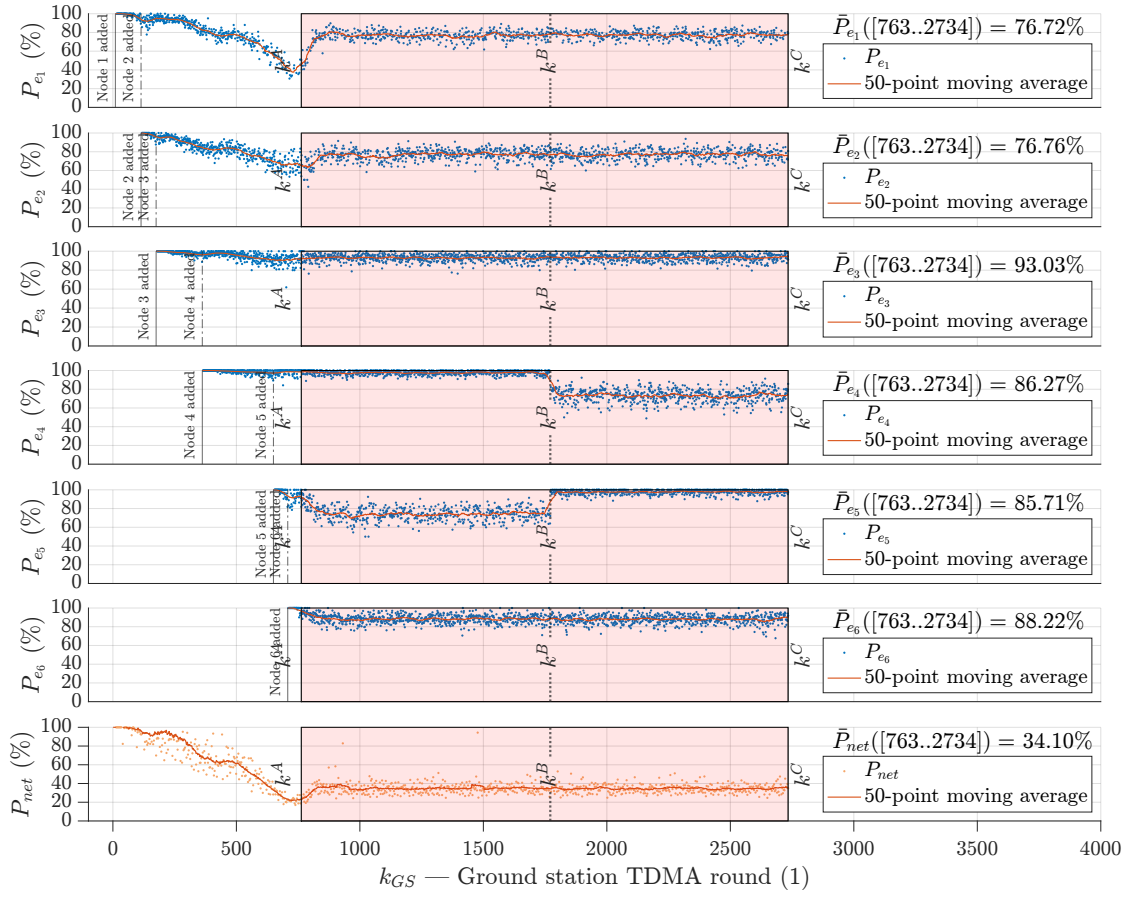
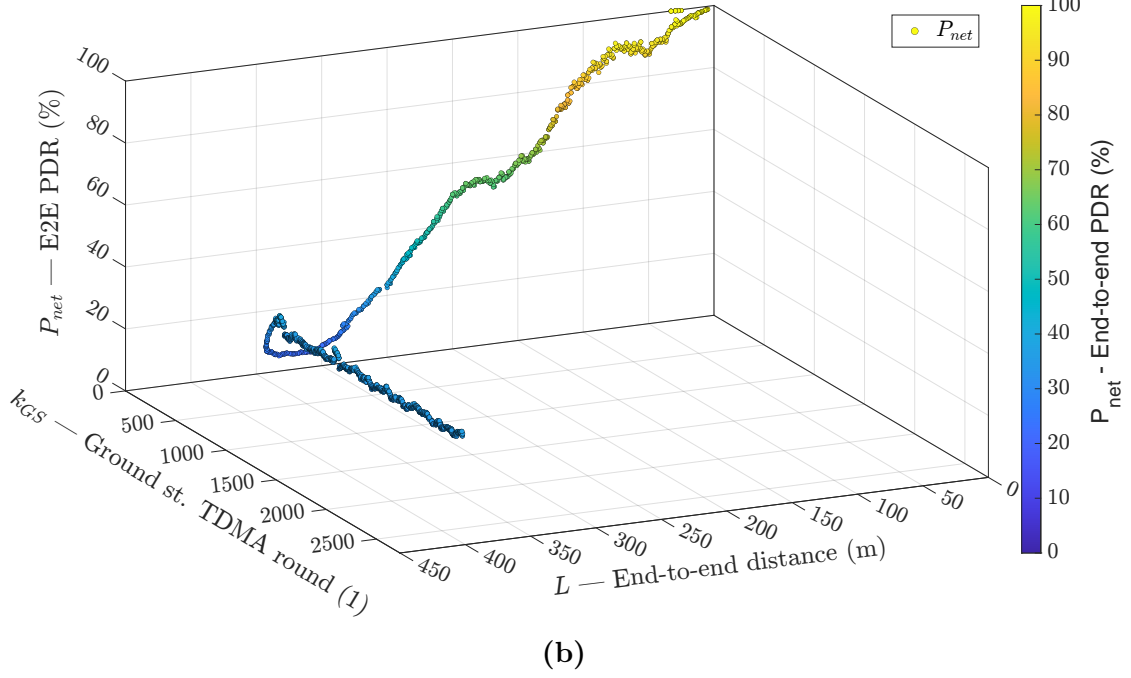


Figure 5.29. UAV trajectories at TDMA round k^C under the scenario ‘c’ using different relay placement strategies: (a) equidistant; (b) equal-PDR, when using estimated model parameters; (c) equal-PDR, when using actual (true) model parameters; (d) DRP, when using actual (true) model parameters.

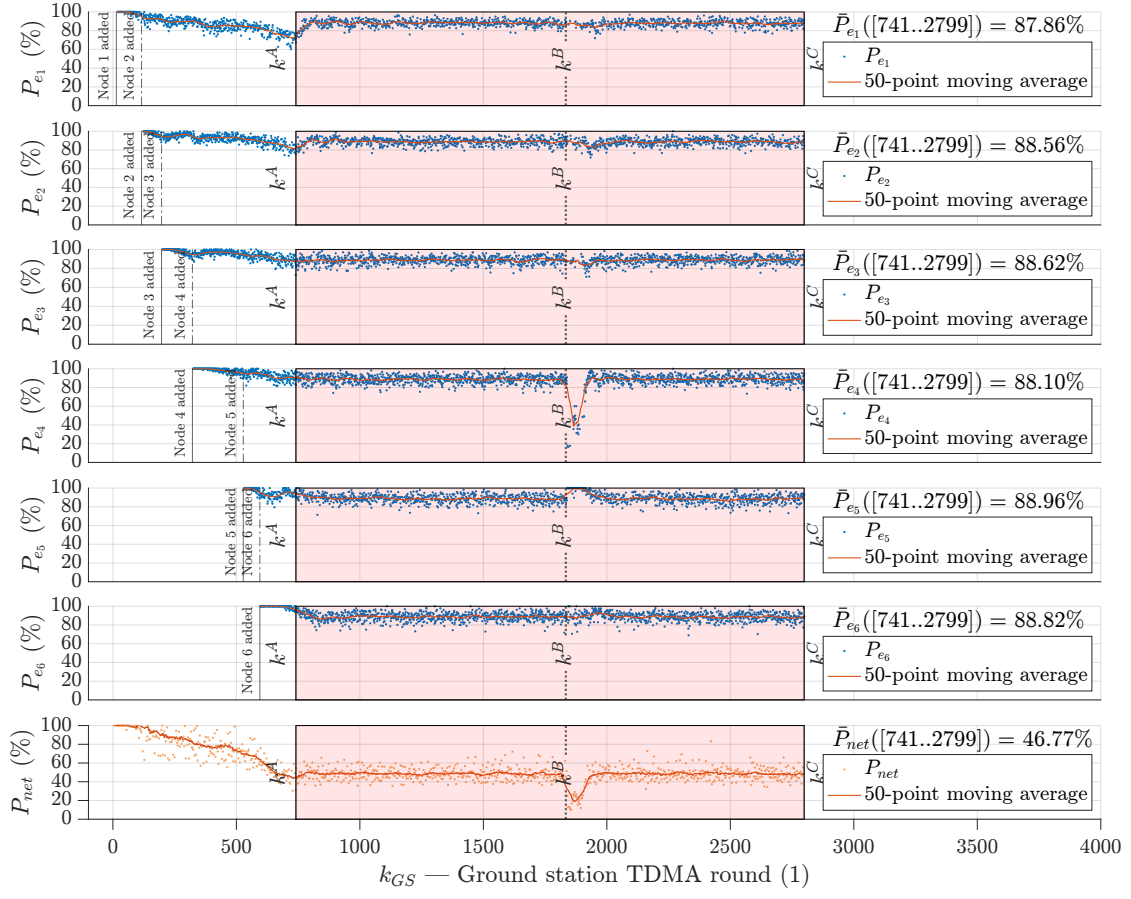


(a)

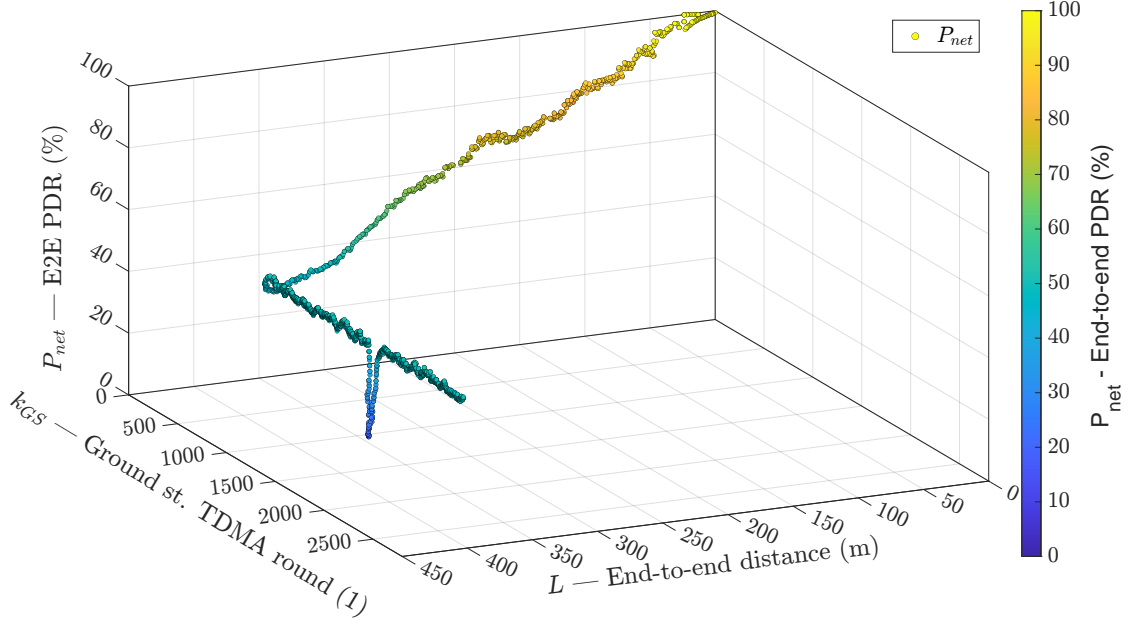


(b)

Figure 5.30. Simulation case: equidistant relay placement strategy under the scenario ‘c’. (a) Instantaneous and average link and network PDRs. The averages are computed over the region shaded in pink, which goes from k^A to k^C . (b) Instantaneous network PDR as a function of TDMA round and network length L .

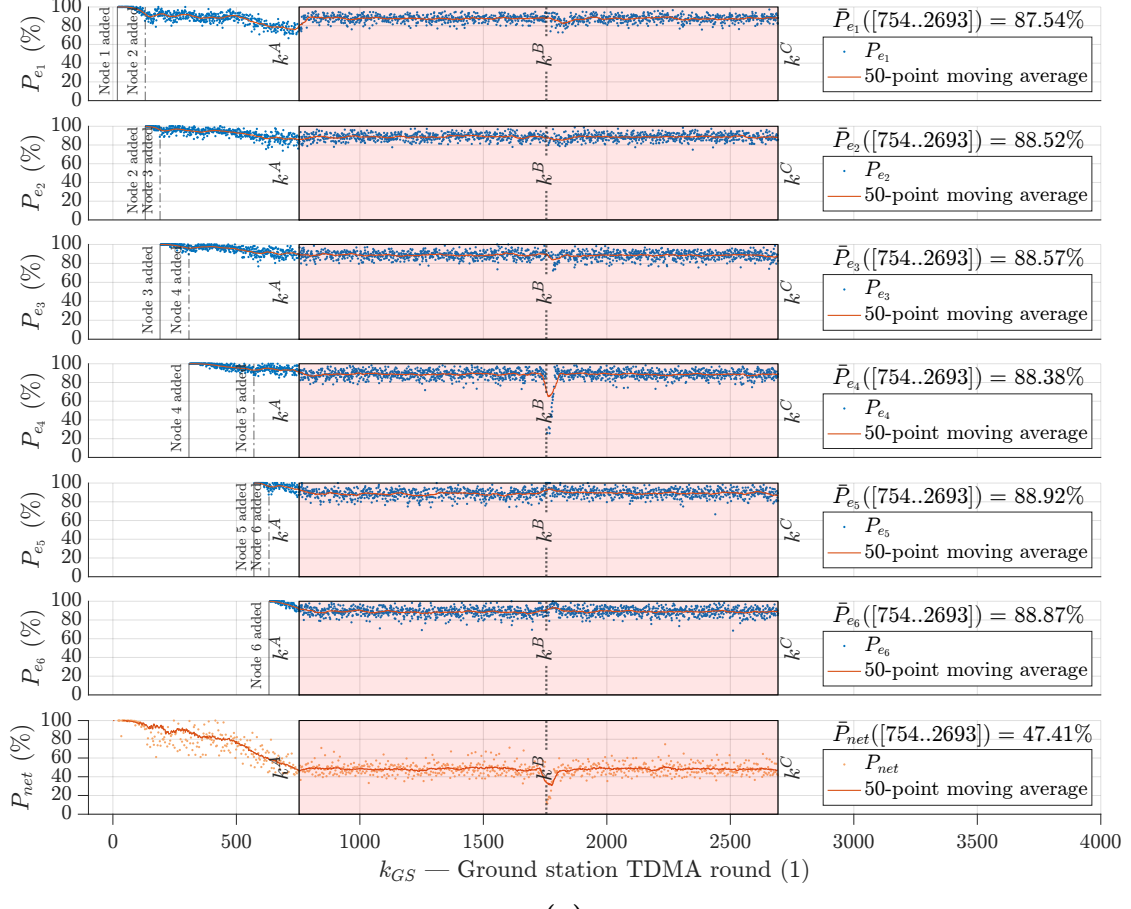


(a)

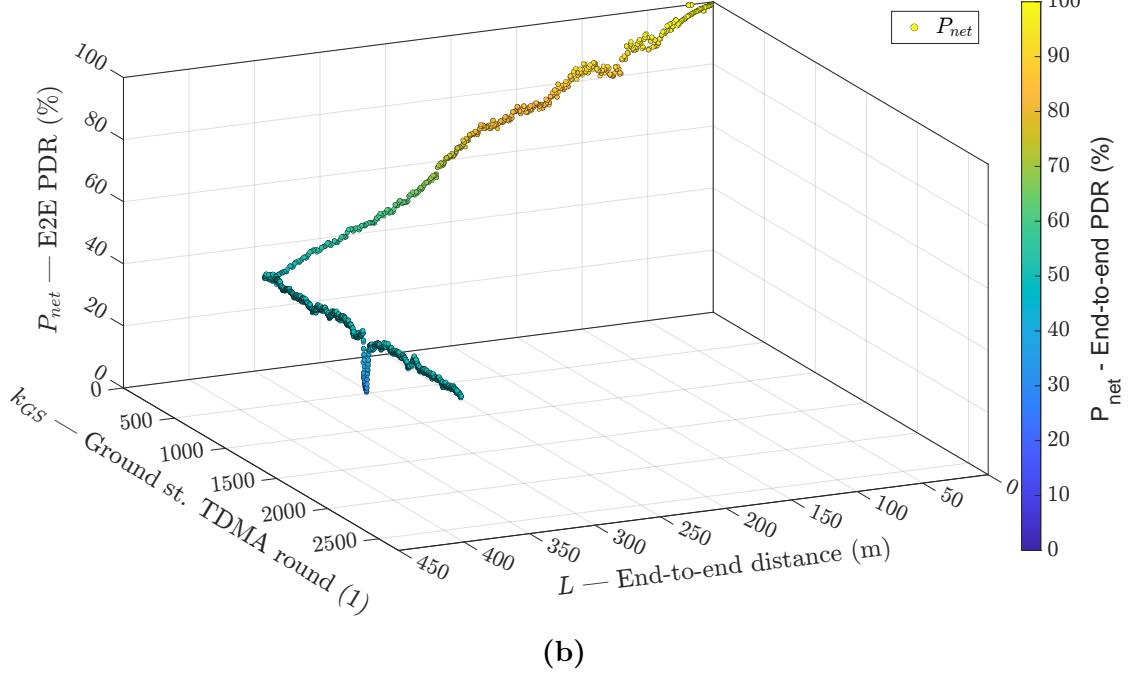


(b)

Figure 5.31. Simulation case: equal-PDR (with estimated parameters) relay placement strategy under the scenario ‘c’. **(a)** Instantaneous and average link and network PDRs. The averages are computed over the region shaded in pink, which goes from k^A to k^C . **(b)** Instantaneous network PDR as a function of TDMA round and network length L .

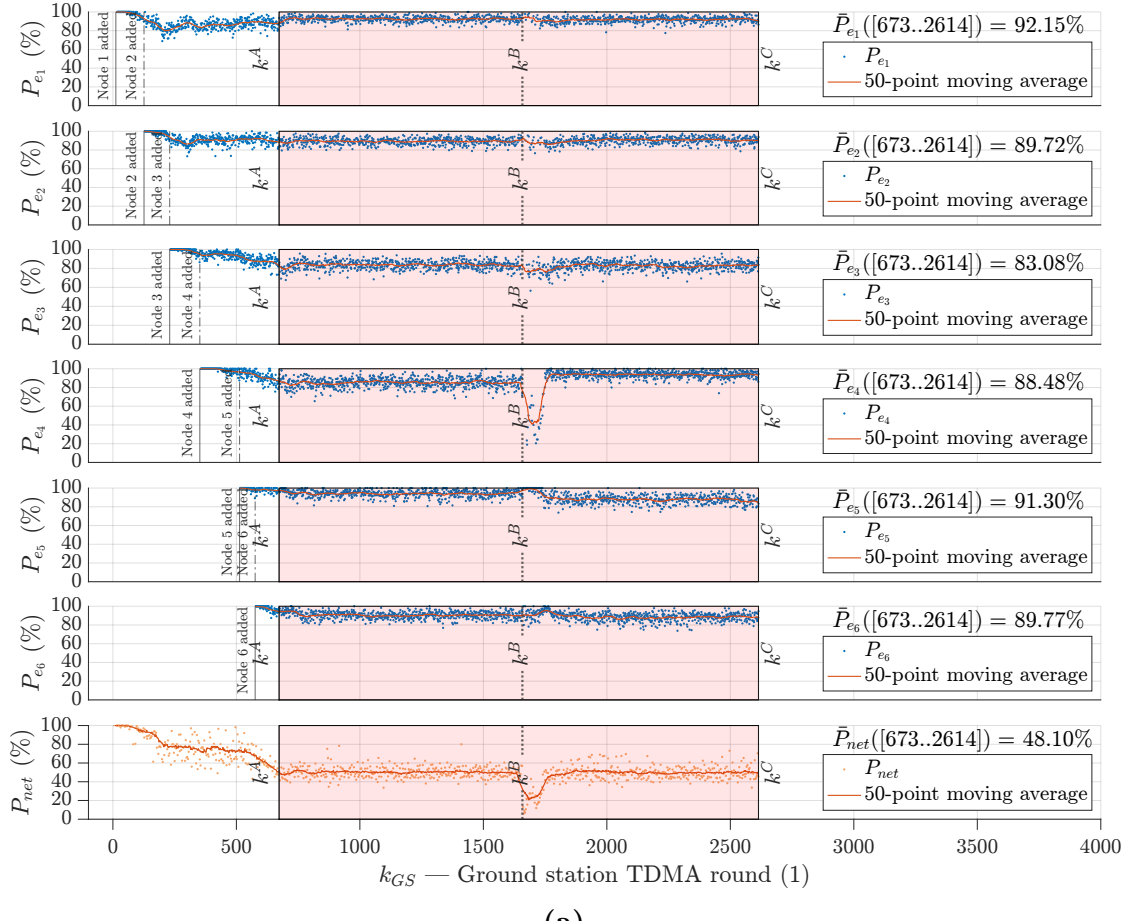


(a)

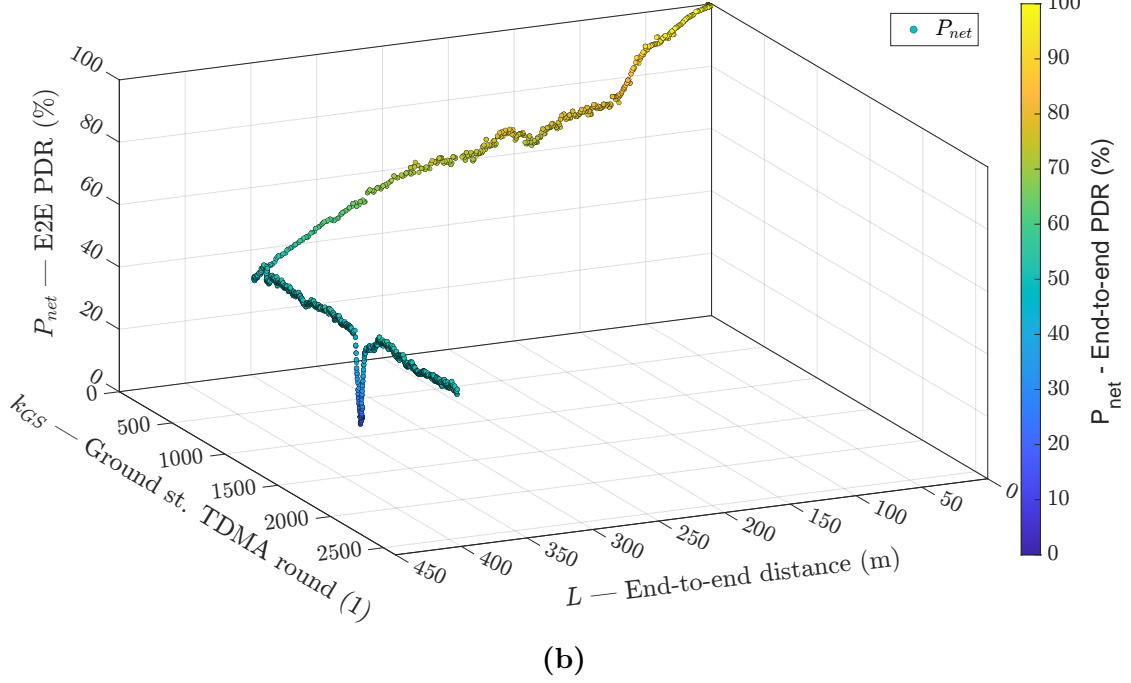


(b)

Figure 5.32. Simulation case: equal-PDR (with true parameters) relay placement strategy under the scenario ‘c’. **(a)** Instantaneous and average link and network PDRs. The averages are computed over the region shaded in pink, which goes from k^A to k^C . **(b)** Instantaneous network PDR as a function of TDMA round and network length L .

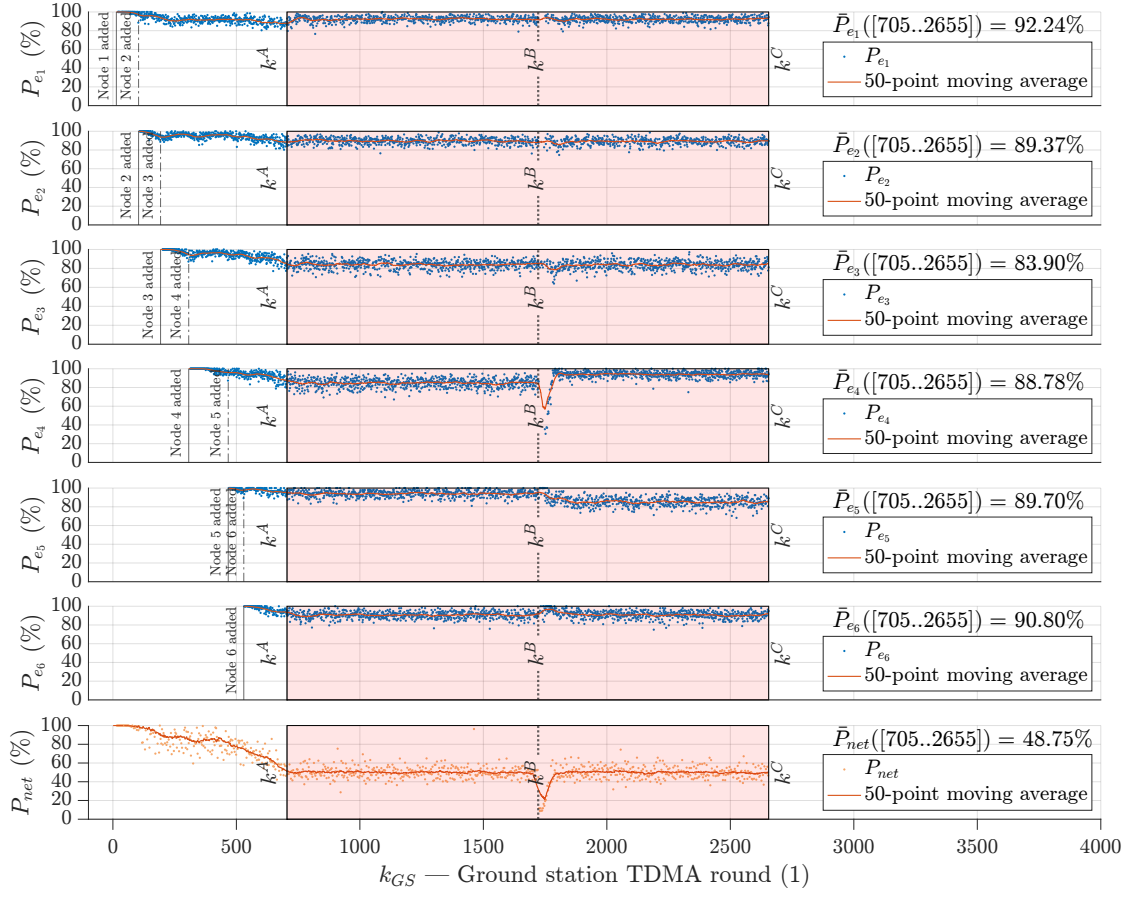


(a)

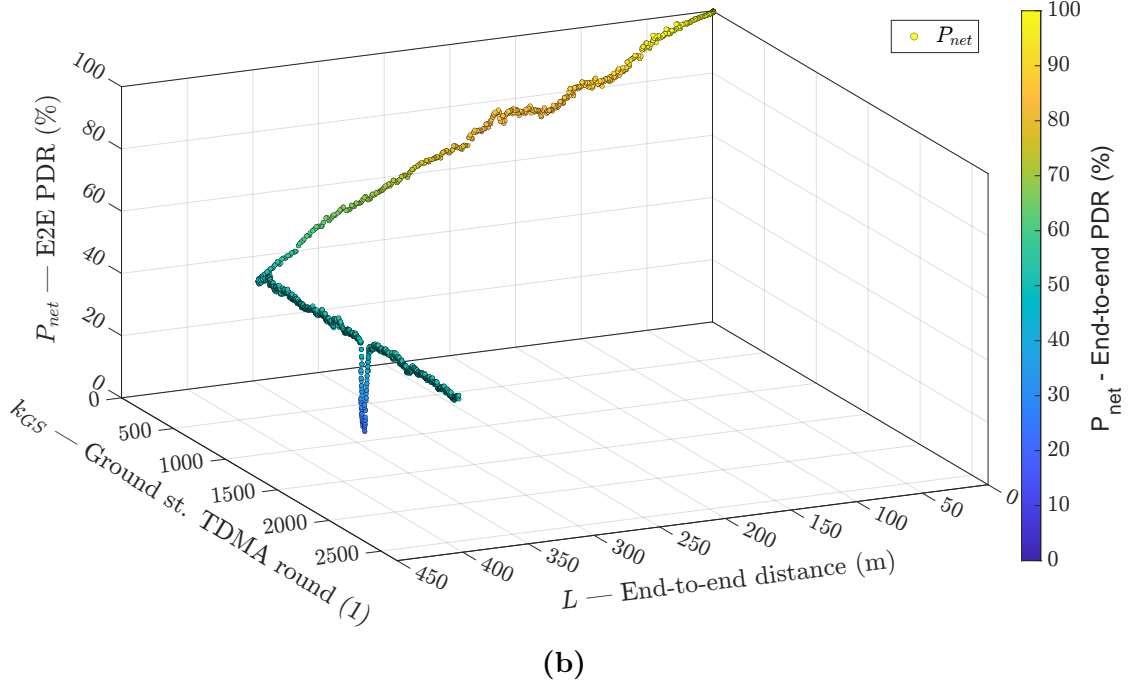


(b)

Figure 5.33. Simulation case: DRP (with estimated parameters) relay placement strategy under the scenario ‘c’. **(a)** Instantaneous and average link and network PDRs. The averages are computed over the region shaded in pink, which goes from k^A to k^C . **(b)** Instantaneous network PDR as a function of TDMA round and network length L .



(a)



(b)

Figure 5.34. Simulation case: DRP (with true parameters) relay placement strategy under the scenario ‘c’. **(a)** Instantaneous and average link and network PDRs. The averages are computed over the region shaded in pink, which goes from k^A to k^C . **(b)** Instantaneous network PDR as a function of TDMA round and network length L .

5.2.4 Scenario ‘d’

Figure 5.35 shows the UAV trajectories at TDMA round k^C for the scenario ‘d’ (incremental model change, cf. Equation (4.6)) using the DRP strategy with estimated parameters. In Figure 5.36, the UAV trajectories for the same scenario are presented for four different relay placement strategies: (a) equidistant, (b) equal-PDR with actual parameters, (c) DRP with estimated parameters, and (d) DRP with actual parameters.

The performances of the strategies with estimated parameters in the same scenario are depicted in Figures 5.37 (equidistant), 5.38 (equal-PDR with estimated parameters), 5.39 (equal-PDR with true parameters), 5.41 (DRP with estimated parameters), and 5.40 (DRP with true parameters). The figures include two subfigures each: (a) the instantaneous and average link and network PDRs, which are averaged over the pink shaded region from k^A to k^C , and (b) the instantaneous network PDR as a function of TDMA round and network length L .

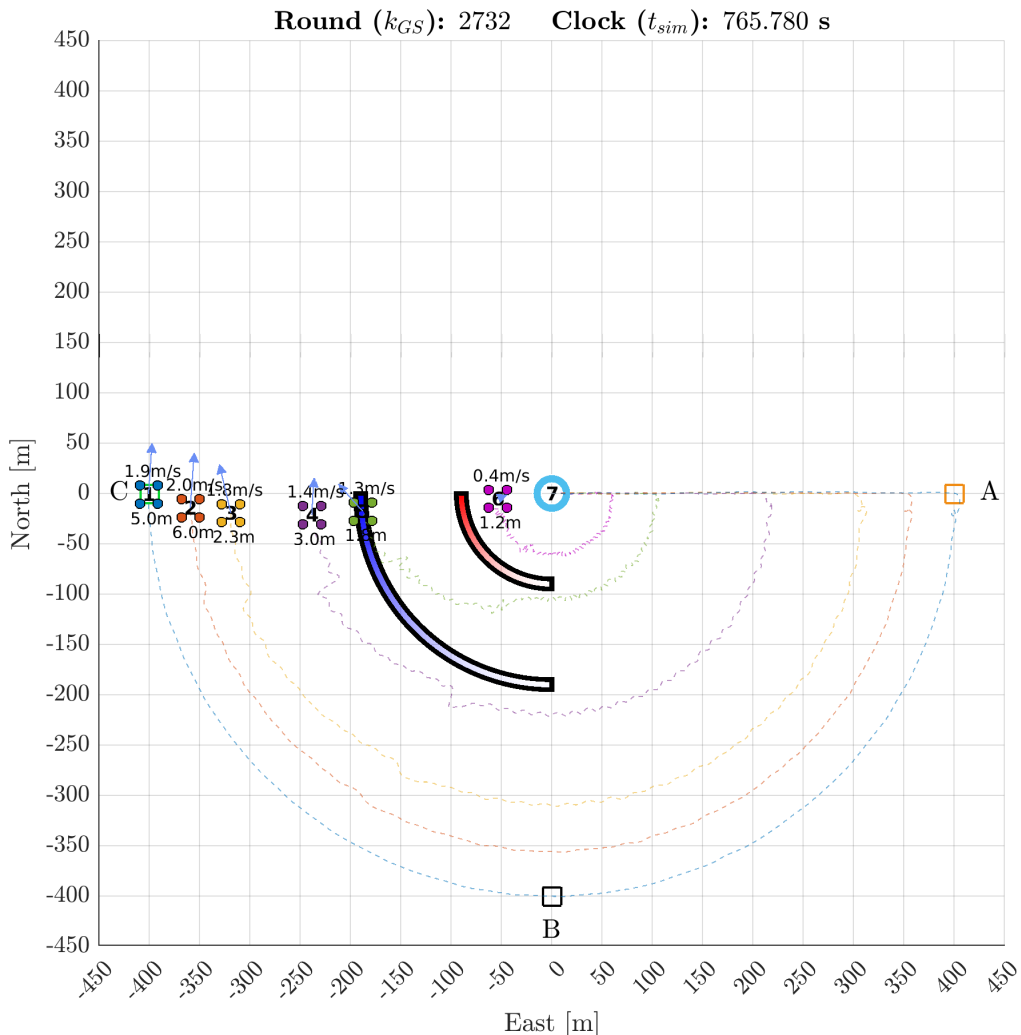


Figure 5.35. UAV trajectories at TDMA round k^C under the scenario ‘d’ using the DRP strategy (with estimated model parameters).

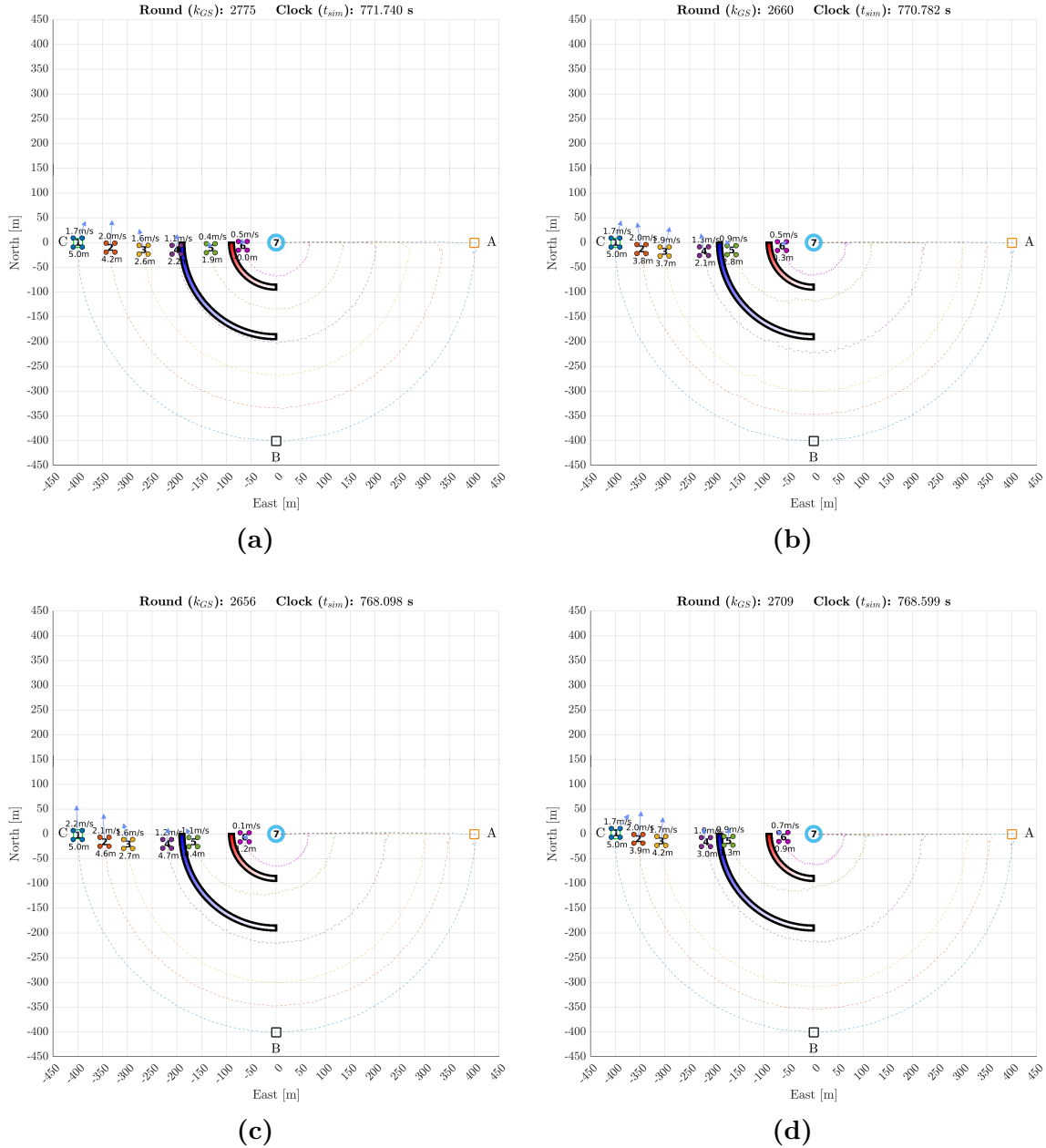
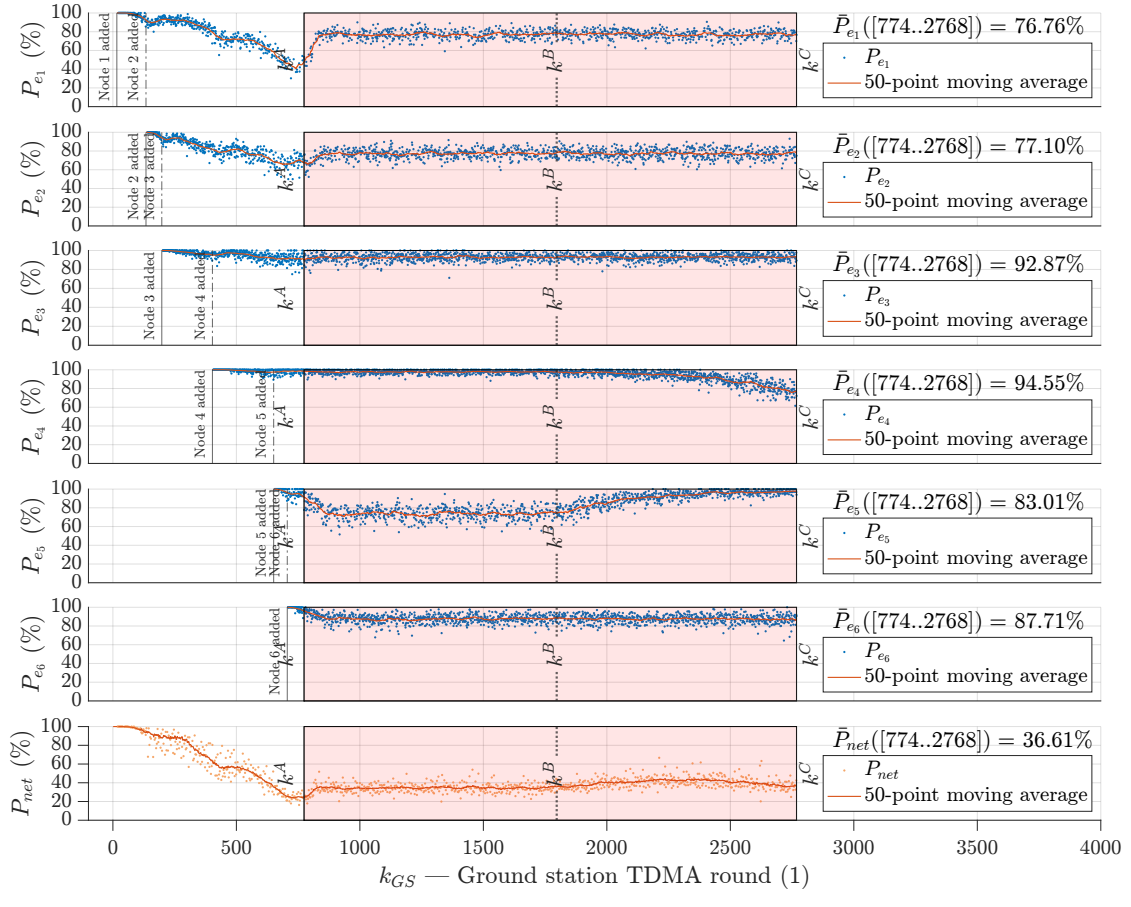
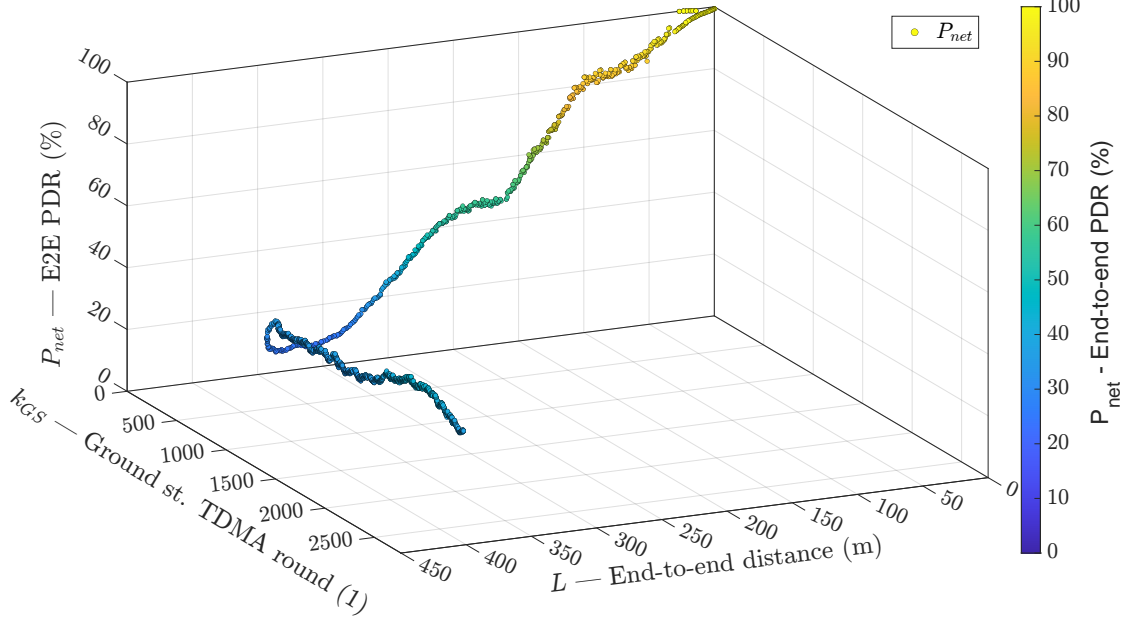


Figure 5.36. UAV trajectories at TDMA round k^C under the scenario ‘d’ using different relay placement strategies: (a) equidistant; (b) equal-PDR, when using estimated model parameters; (c) equal-PDR, when using actual (true) model parameters; (d) DRP, when using actual (true) model parameters.

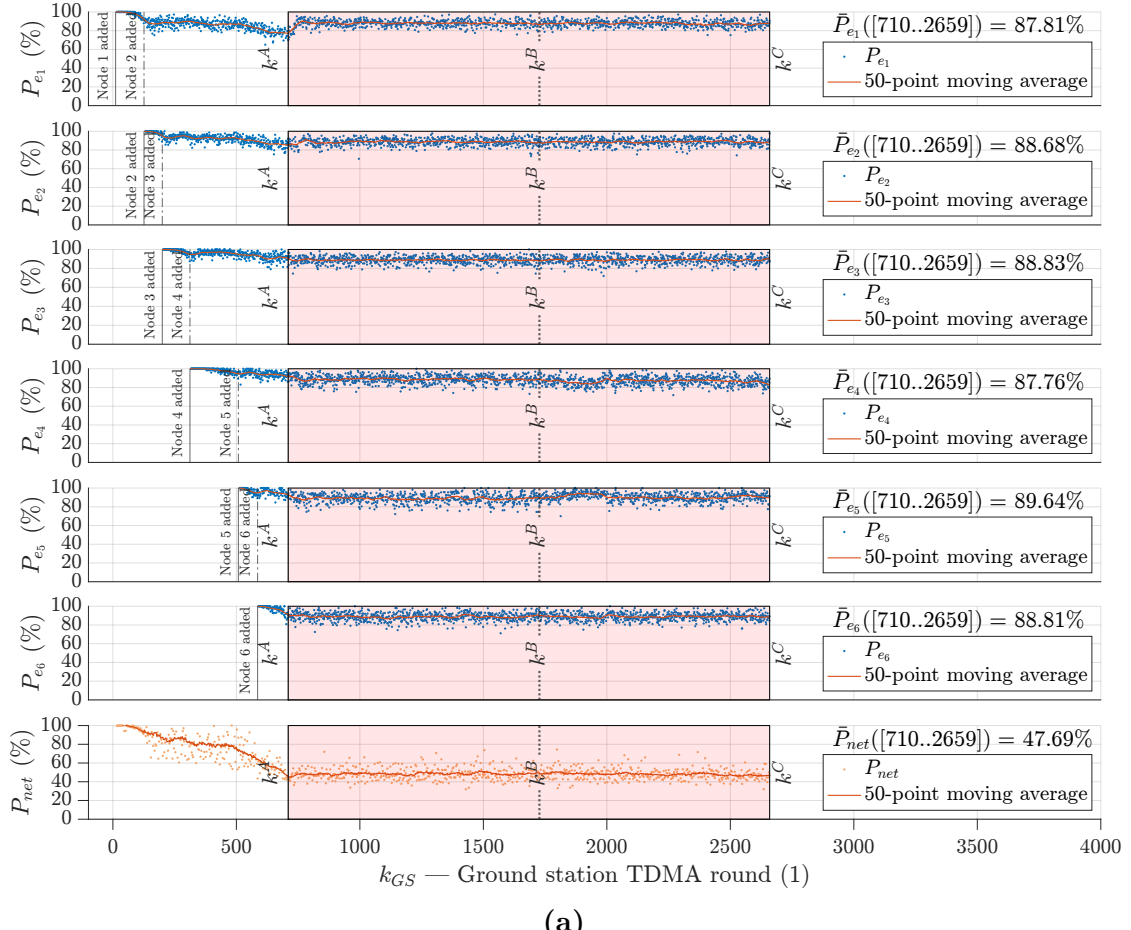


(a)

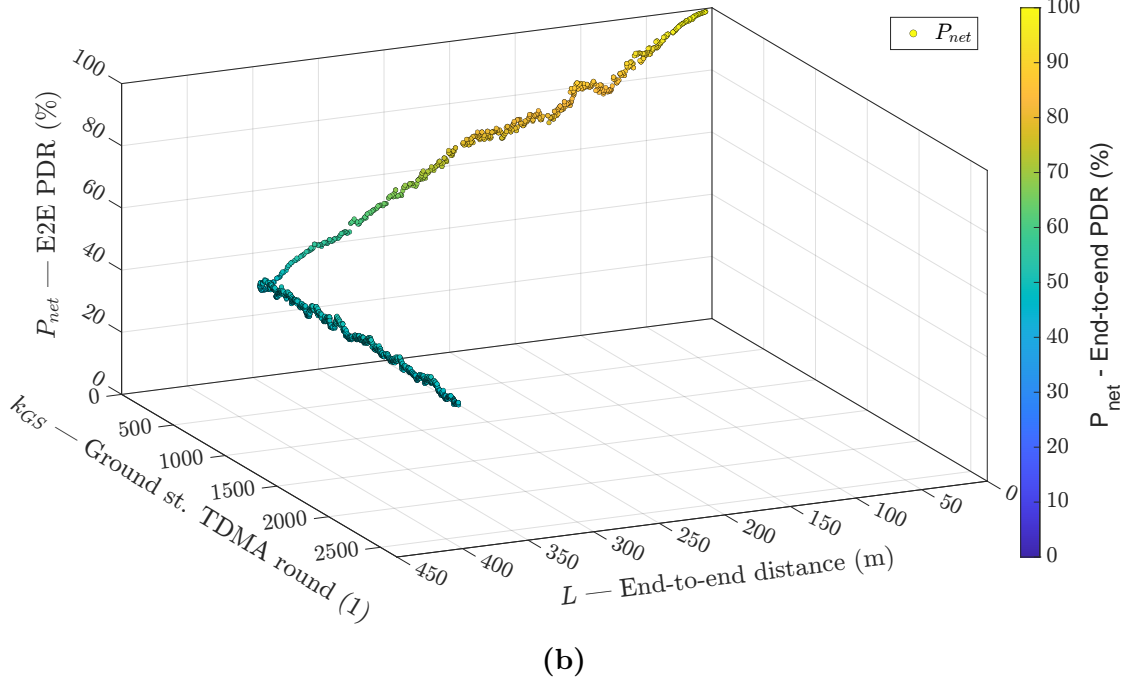


(b)

Figure 5.37. Simulation case: equidistant relay placement strategy under the scenario ‘d’. (a) Instantaneous and average link and network PDRs. The averages are computed over the region shaded in pink, which goes from k^A to k^C . (b) Instantaneous network PDR as a function of TDMA round and network length L .

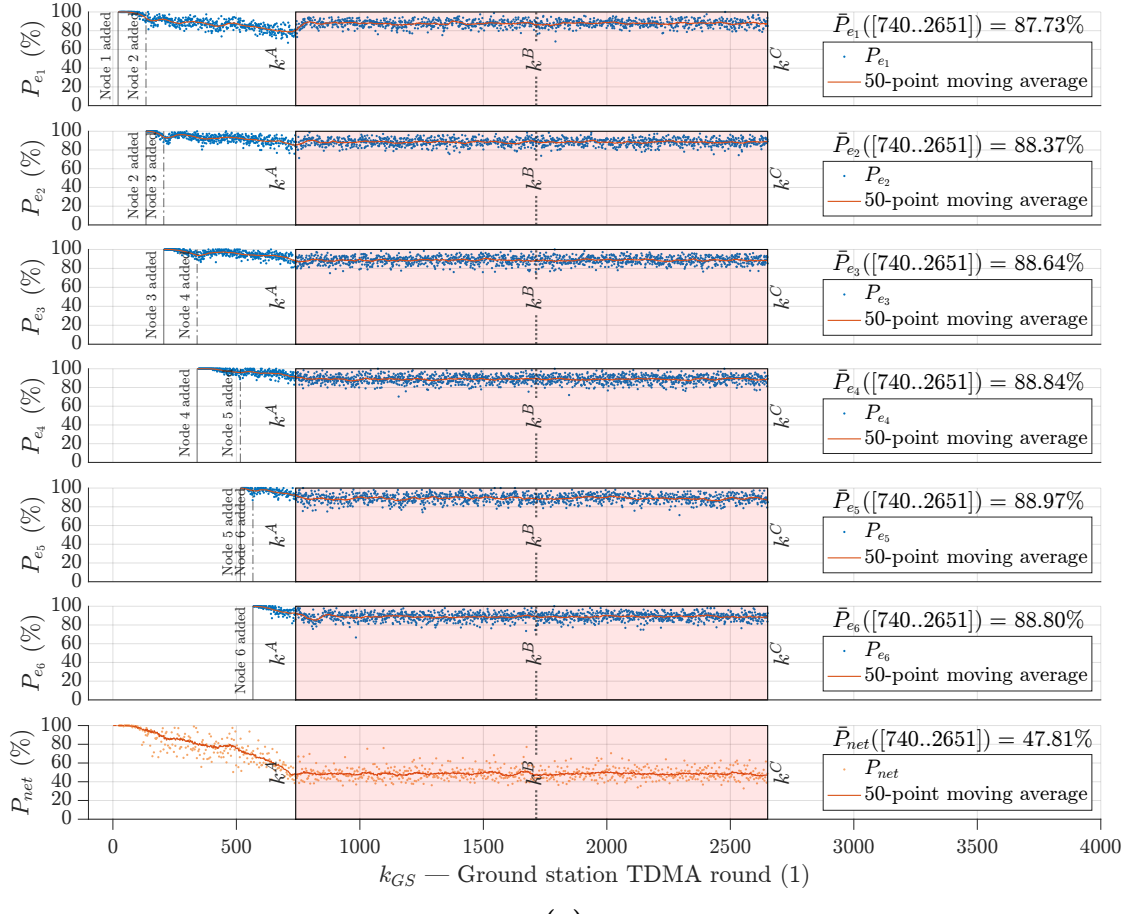


(a)

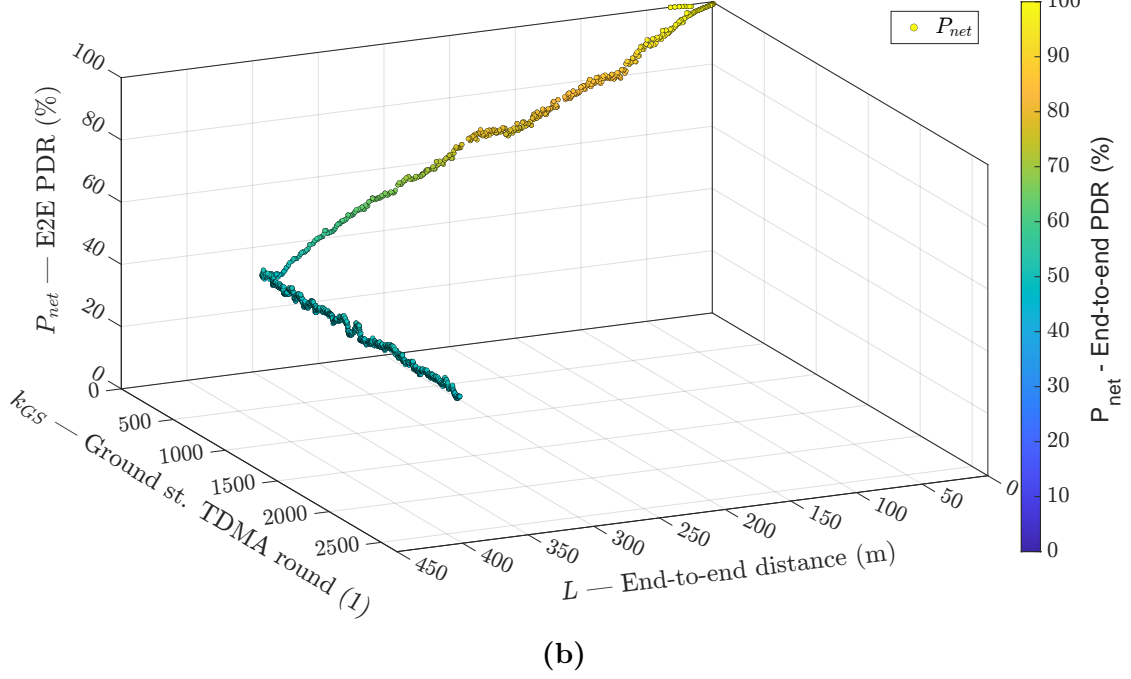


(b)

Figure 5.38. Simulation case: equal-PDR (with estimated parameters) relay placement strategy under the scenario ‘d’. **(a)** Instantaneous and average link and network PDRs. The averages are computed over the region shaded in pink, which goes from k^A to k^C . **(b)** Instantaneous network PDR as a function of TDMA round and network length L .

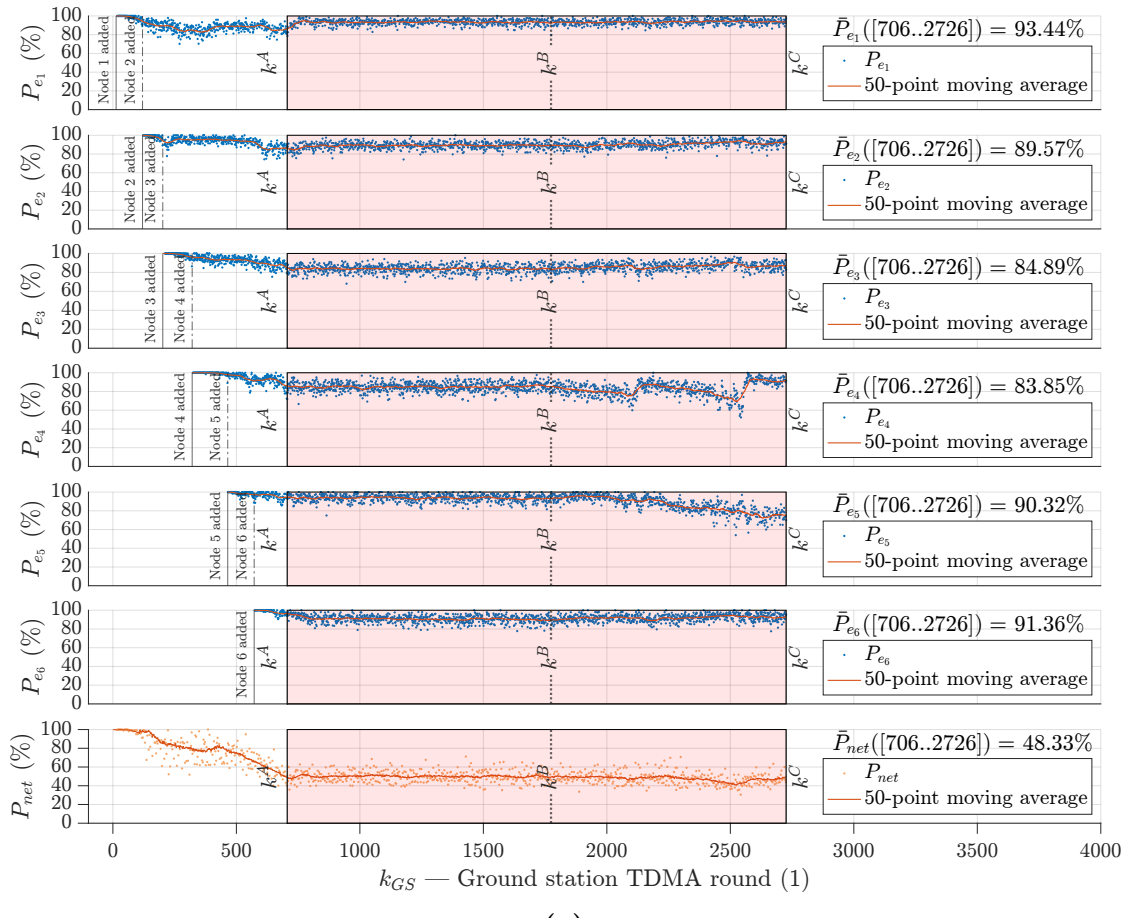


(a)

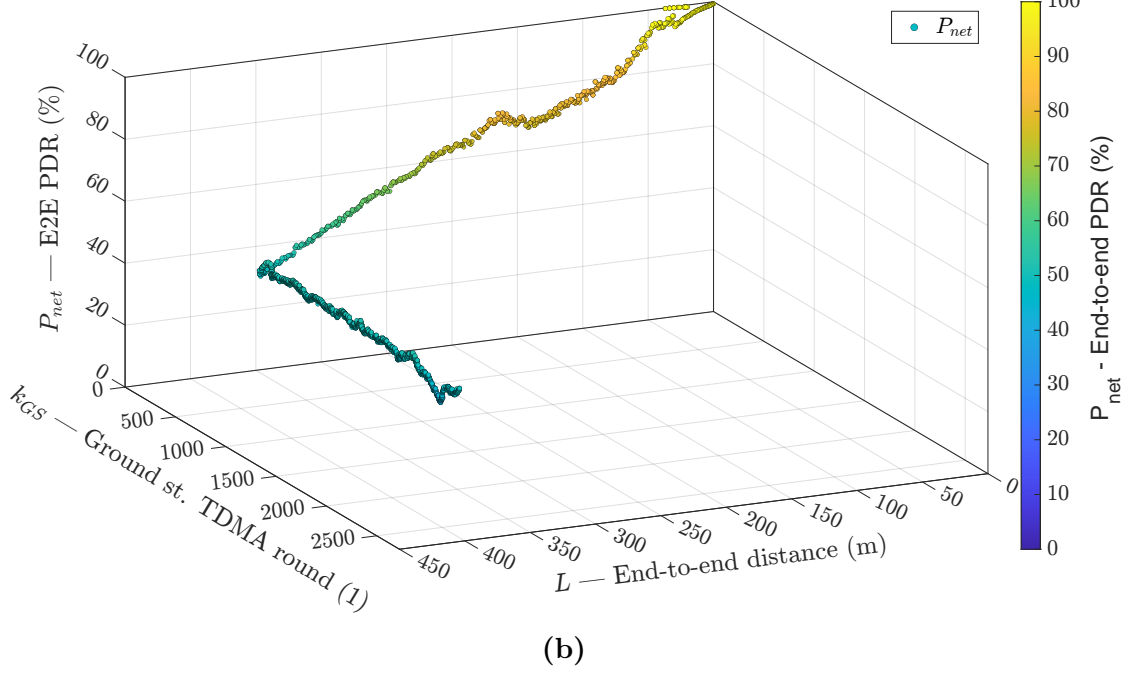


(b)

Figure 5.39. Simulation case: equal-PDR (with true parameters) relay placement strategy under the scenario ‘d’. **(a)** Instantaneous and average link and network PDRs. The averages are computed over the region shaded in pink, which goes from k^A to k^C . **(b)** Instantaneous network PDR as a function of TDMA round and network length L .

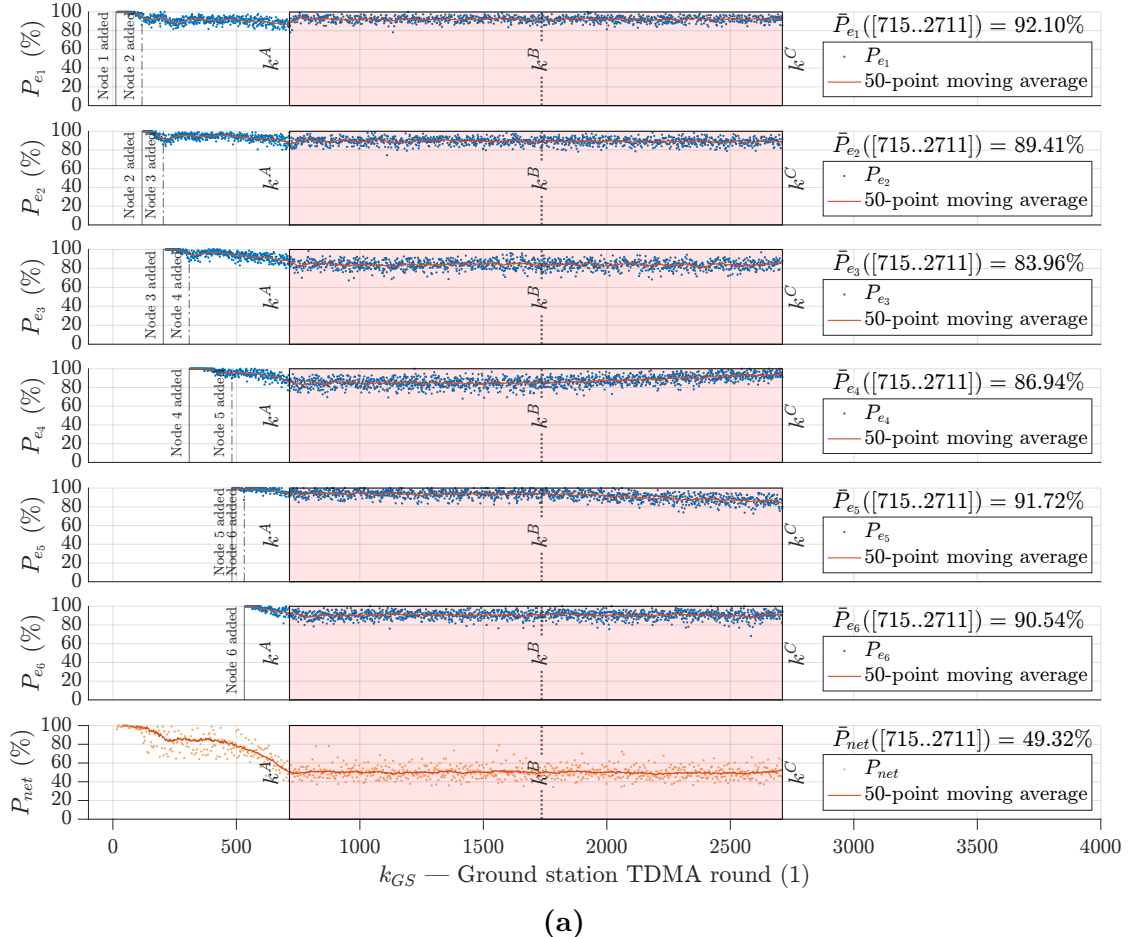


(a)

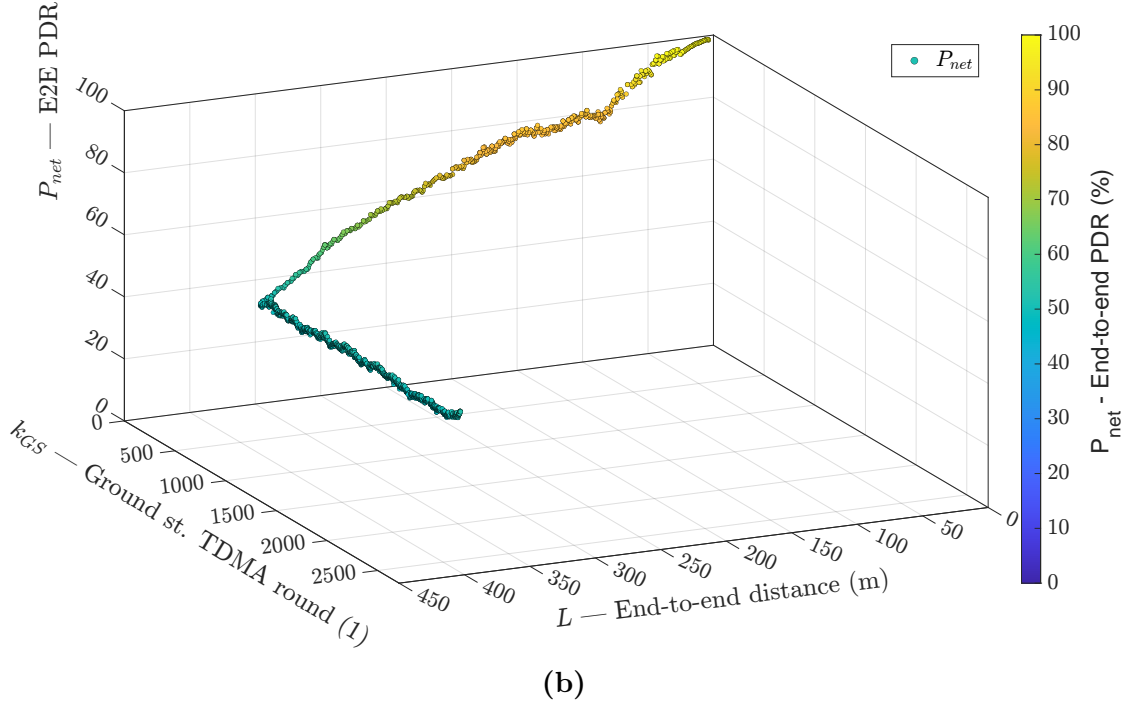


(b)

Figure 5.40. Simulation case: DRP (with estimated parameters) relay placement strategy under the scenario ‘d’. **(a)** Instantaneous and average link and network PDRs. The averages are computed over the region shaded in pink, which goes from k^A to k^C . **(b)** Instantaneous network PDR as a function of TDMA round and network length L .



(a)



(b)

Figure 5.41. Simulation case: DRP (with true parameters) relay placement strategy under the scenario ‘d’. (a) Instantaneous and average link and network PDRs. The averages are computed over the region shaded in pink, which goes from k^A to k^C . (b) Instantaneous network PDR as a function of TDMA round and network length L .

5.2.5 Summary

This study investigated the performance of three different relay placement strategies, namely equidistant, equal PDR, and DRP, under four different scenarios: 'unchanged model' ('a'), 'small abrupt model change' ('b'), 'large abrupt model change' ('c'), and 'incremental model change' ('d'). Table 5.2 displays the network PDR values for each strategy and scenario. The equidistant strategy provided the worst results in all scenarios, while the other two strategies delivered similar results. However, the DRP strategy using true parameters outperformed the other strategies slightly. Interestingly, the DRP strategy, even when using estimated parameters, consistently outperformed the equal-PDR strategy, including instances where the equal-PDR strategy employed true parameters. Overall, the results were consistent across all scenarios, indicating that the strategies responded relatively well to simulated model changes. Even though there was a slight reduction in network PDR in case of model changes, it was minimal. The results suggest that the DRP strategy is the most effective relay placement strategy, with an increase in network PDR of over 40% in the tested scenarios. Figure 5.42 displays the values from Table 5.2.

Additionally, Table 5.3 reports the average PDRs of the links, which remained fairly consistent when using the same equal-PDR strategy (with either estimated or true parameters), as expected. Figure 5.43 displays the values from Table 5.3.

Table 5.2. Average network PDR for different strategies and scenarios, where the average is done over the period beginning when the source node reaches the waypoint 'A' (at round k^A) until the waypoint 'C' (at round k^C). This table shows the average end-to-end PDR results for three different strategies (equidistant, equal-PDR, and DRP, the last two of which tested with estimated and true parameters) under four different scenarios: 'a' corresponds to 'unchanged model', 'b' corresponds to 'small abrupt model change', 'c' corresponds to 'large abrupt model change', and 'd' corresponds to 'incremental model change'. The green shade in the cells signifies the average network Packet Delivery Ratio (PDR), where white cells indicate the lowest achieved average network PDR of 34.10%, and fully green cells signify the highest achieved average network PDR of 49.45%.

Average network PDR	Simulation type			
	a (%)	b (%)	c (%)	d (%)
$\bar{P}_{\text{net}}^{\text{equi}}$	34.3	37.1	34.1	36.6
$\bar{P}_{\text{net}}^{\text{equalPDR,e}}$	47.8	47.9	46.8	47.7
$\bar{P}_{\text{net}}^{\text{equalPDR,t}}$	47.9	47.8	47.4	47.8
$\bar{P}_{\text{net}}^{\text{DRP,e}}$	49.4	48.7	48.1	48.3
$\bar{P}_{\text{net}}^{\text{DRP,t}}$	49.5	49.4	48.8	49.3

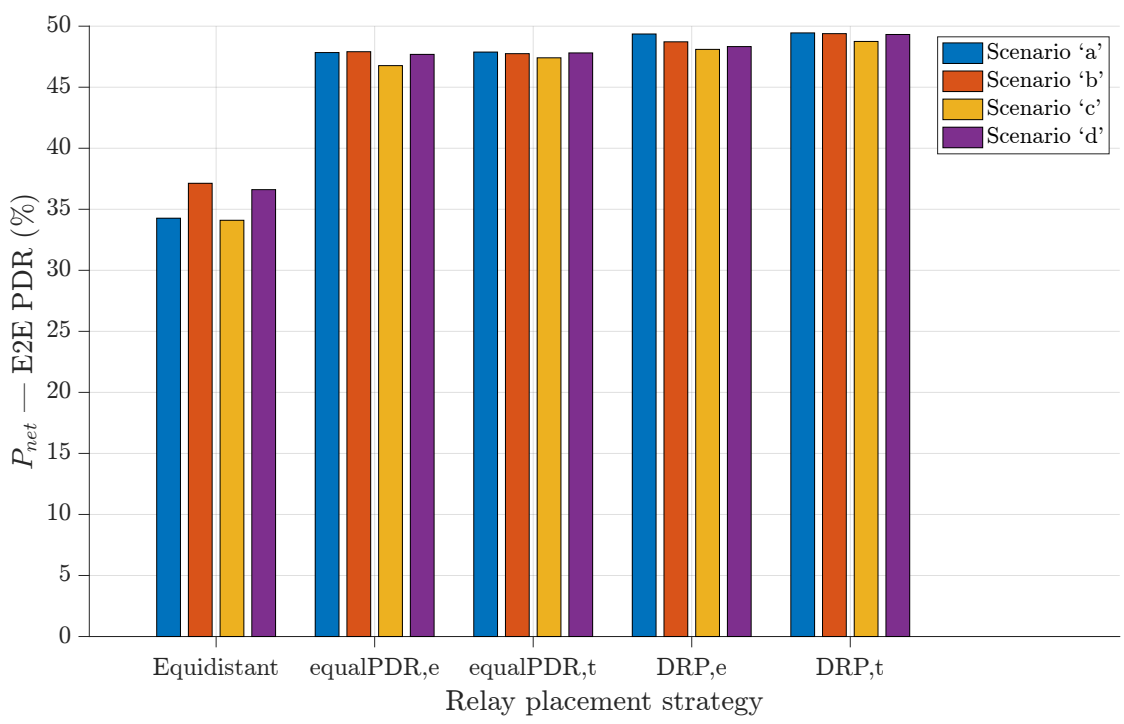


Figure 5.42. Average network PDRs for different strategies and scenarios. The values are from Table 5.2.

Table 5.3. Average link PDR for different strategies and scenarios, where the average is done over the period beginning when the source node reaches the waypoint ‘A’ (at round k^A) until the waypoint ‘C’ (at round k^C). This table shows the average link PDR results for three different strategies (equidistant, equal PDR, and DRP, the last two of which tested with estimated and true parameters) under four different scenarios: ‘a’ corresponds to ‘unchanged model’, ‘b’ corresponds to ‘small abrupt model change’, ‘c’ corresponds to ‘large abrupt model change’, and ‘d’ corresponds to ‘incremental model change’. The green shade in the cells signifies the average link PDR, where white cells indicate the lowest achieved average network PDR of 74.13%, and fully green cells signify the highest achieved average network PDR of 97.75%.

Strategy	Average link PDR	Simulation scenario			
		a (%)	b (%)	c (%)	d (%)
Equidistant	$\bar{P}_{1,2}^{\text{equi}}$	77.0	76.9	76.7	76.8
	$\bar{P}_{2,3}^{\text{equi}}$	77.2	76.9	76.8	77.1
	$\bar{P}_{3,4}^{\text{equi}}$	93.0	92.9	93.0	92.9
	$\bar{P}_{4,5}^{\text{equi}}$	97.8	97.2	86.3	94.6
	$\bar{P}_{5,6}^{\text{equi}}$	74.1	81.0	85.7	83.0
	$\bar{P}_{6,7}^{\text{equi}}$	87.9	88.0	88.2	87.7
	$\bar{P}_{1,2}^{\text{equalPDR,e}}$	87.8	88.2	87.9	87.8
Equal PDR, estimated parameters	$\bar{P}_{2,3}^{\text{equalPDR,e}}$	88.6	88.8	88.6	88.7
	$\bar{P}_{3,4}^{\text{equalPDR,e}}$	88.8	88.9	88.6	88.8
	$\bar{P}_{4,5}^{\text{equalPDR,e}}$	88.9	88.4	88.1	87.8
	$\bar{P}_{5,6}^{\text{equalPDR,e}}$	88.6	89.0	89.0	89.6
	$\bar{P}_{6,7}^{\text{equalPDR,e}}$	88.7	88.8	88.8	88.8
	$\bar{P}_{1,2}^{\text{equalPDR,t}}$	87.9	87.7	87.5	87.7
	$\bar{P}_{2,3}^{\text{equalPDR,t}}$	88.5	88.6	88.5	88.4
Equal PDR, true parameters	$\bar{P}_{3,4}^{\text{equalPDR,t}}$	88.7	88.9	88.6	88.6
	$\bar{P}_{4,5}^{\text{equalPDR,t}}$	88.8	88.7	88.4	88.8
	$\bar{P}_{5,6}^{\text{equalPDR,t}}$	88.8	88.8	88.9	89.0
	$\bar{P}_{6,7}^{\text{equalPDR,t}}$	89.0	88.9	88.9	88.8
	$\bar{P}_{1,2}^{\text{DRP,e}}$	92.8	92.5	92.2	93.4
	$\bar{P}_{2,3}^{\text{DRP,e}}$	87.9	89.5	89.7	89.6
	$\bar{P}_{3,4}^{\text{DRP,e}}$	83.3	83.9	83.1	84.9
DRP, estimated parameters	$\bar{P}_{4,5}^{\text{DRP,e}}$	83.7	83.4	88.5	83.9
	$\bar{P}_{5,6}^{\text{DRP,e}}$	94.4	93.8	91.3	90.3
	$\bar{P}_{6,7}^{\text{DRP,e}}$	93.3	91.1	89.8	91.4
	$\bar{P}_{1,2}^{\text{DRP,t}}$	92.3	92.3	92.2	92.1
	$\bar{P}_{2,3}^{\text{DRP,t}}$	89.4	89.1	89.4	89.4
	$\bar{P}_{3,4}^{\text{DRP,t}}$	84.2	83.9	83.9	84.0
	$\bar{P}_{4,5}^{\text{DRP,t}}$	84.8	85.9	88.8	86.9
DRP, true parameters	$\bar{P}_{5,6}^{\text{DRP,t}}$	93.8	92.7	89.7	91.7
	$\bar{P}_{6,7}^{\text{DRP,t}}$	90.5	90.5	90.8	90.5

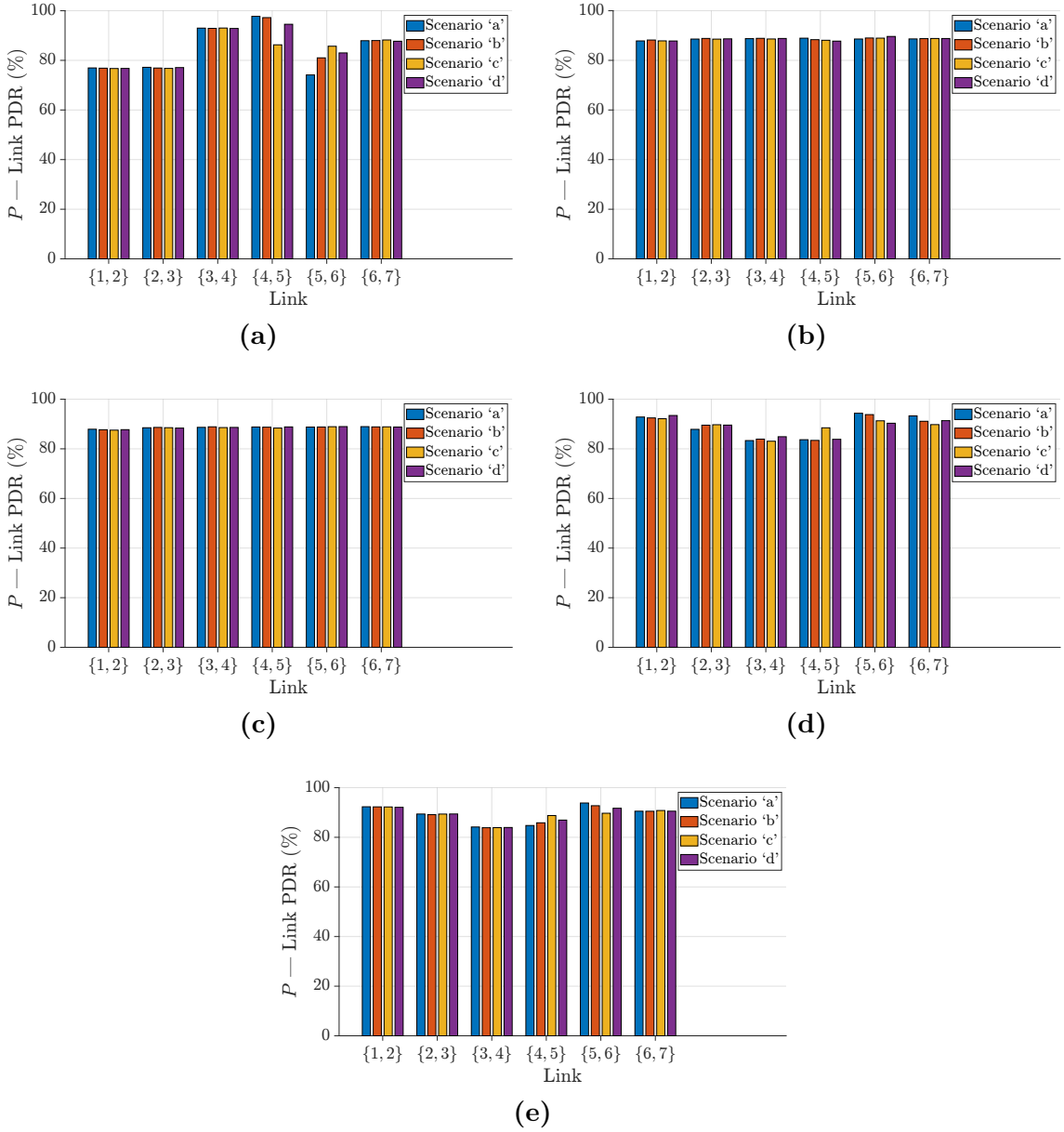


Figure 5.43. Average link PDRs for different strategies and scenarios (values from Table 5.1): **(a)** equidistant; **(b)** equal-PDR, when using actual (true) model parameters; **(c)** DRP, when using estimated model parameters; **(d)** DRP, when using actual (true) model parameters. It can be observed that when using the equal-PDR strategy (either with estimated or true parameters), the link PDRs are roughly the same (around 88%), as one would expect from the strategy.

6 Conclusion

After reporting the main findings in Section 6.1, this work concludes in Section 6.2 with suggestions for future research directions.

6.1 Summary

Referring back to the problem statement presented in Section 3.1, this section summarizes the main findings of our investigation into relay placement strategies, data fitting for link models, and model change detections. We evaluated three placement strategies (equidistant, equal-PDR, and DRP) in various scenarios and compared their performance using the average network packet delivery ratio (PDR) metric defined in Equation (3.21). In addition, we assessed the accuracy of non-linear least squares fitting for estimating link models and the effectiveness of a model change detector in detecting abrupt changes.

The low estimation error indices (Subsection 4.3.3) in Table 5.1 indicate that the fitting (Section 3.2) accurately estimates the link models, particularly in the first three scenarios ('a', 'b', and 'c'). The model change detector (Section 3.3) successfully detects abrupt model changes, as observed in Figures 5.4 and 5.5 (scenario 'b') and Figures 5.7 and 5.8 (scenario 'c'). However, in gradually changing environments, the model change detector does not estimate the model sufficiently well, as shown in Figures 5.10 and 5.11 (scenario 'd').

All the relay placement strategies used were implemented as distributed algorithms (in Algorithms 1, 2, and 3 for equidistant, equal-PDR, and DRP strategy, respectively). The average network PDR defined in Equation (3.21) is used to compare the performance of these strategies in different scenarios. The results in Table 5.2 show that the equal-PDR and DRP placements outperform the equidistant placement, with average end-to-end PDRs over 40% higher than the equidistant placement, which is considered the naive approach. The DRP placement provides the best results, even in the presence of model changes where the reductions in network PDRs are minimal.

The relays, which can communicate only with their neighbors, follow the source properly throughout the simulations, indicating that the communication system (Section 3.4) is working correctly. This is evident in Figures 5.14 and 5.15 (scenario 'a'), Figures 5.21 and 5.22 (scenario 'b'), Figures 5.28 and 5.29 (scenario 'c'), and Figures 5.35 and 5.36 (scenario 'd').

Despite the increased computational load on node processors compared to the equidistant strategy, as well as higher bandwidth requirements for transmitting upstream and downstream report packets, the DRP algorithm outperforms the other strategies and should be regarded as the go-to strategy for relays in any wireless line network.

6.2 Future Work

Overall, the proposed approach shows promising results and offers potential for future optimization and implementation in real-world scenarios.

In future work, a potential improvement is to consider the varying importance of samples. In particular, given two samples recorded at different TDMA rounds for a link $\{i, j\}$, the one with a PDR closer to 50% provides more information about the PDR model. One approach could be to temporarily move a relay away from its upstream node, increasing $d_{i,j}$ and decreasing $P_{i,j}$ to enhance the quality of the fitting. However, this would result in a temporary reduction in the end-to-end PDR.

Another potential avenue for research is exploring different regression methods to estimate the models, such as neural networks. Validating the currently implemented strategies with real drones and possibly terrestrial vehicles, using sensor fusion techniques for navigation, is another area for future exploration. To ensure safety, implementing a collision avoidance and fault detection system, such as for low battery situations, is recommended. Additionally, creating an online map of link models overlaid with a physical obstacle map would be an interesting future direction.

Bibliography

- [1] W. Jing, D. Deng, Y. Wu, and K. Shimada. Multi-uav coverage path planning for the inspection of large and complex structures. In *2020 IEEE/RSJ International Conference on Intelligent Robots and Systems (IROS)*, pages 1480–1486, 2020. [[CrossRef](#)].
- [2] L. R. Pinto. *Aerial Multi-hop Sensor Networks*. PhD thesis, Universidade do Porto - Carnegie Mellon University, 2018. [[CISTER](#)].
- [3] A. Ademuwagun. Rss-distance rationalization procedure for localization in an indoor environment. *Wireless Sensor Network*, 11(2):13–33, 2019. [[CrossRef](#)].
- [4] J. Ning, S. Singh, K. Pelechrinis, B. Liu, S.V. Krishnamurthy, and R. Govindan. Forensic analysis of packet losses in wireless networks. In *2012 20th IEEE International Conference on Network Protocols (ICNP)*, pages 1–10, 2012. [[CrossRef](#)].
- [5] E. Larsen, L. Landmark, and Ø. Kure. Optimal uav relay positions in multi-rate networks. In *2017 Wireless Days*, pages 8–14, 2017. [[CrossRef](#)].
- [6] L. R. Pinto and L. Almeida. Optimal relay network for aerial remote inspections. *Sensors*, 22(4):1391, 2022. [[CrossRef](#)].
- [7] L. R. Pinto, A. Moreira, L. Almeida, and A. Rowe. Characterizing multihop aerial networks of cots multirotors. *IEEE Transactions on Industrial Informatics*, 13(2):898–906, 2017. [[CrossRef](#)].
- [8] H. Lu, X. Wei, H. Qian, and M. Chen. A cost-efficient elastic uav relay network construction method with guaranteed qos. *Ad Hoc Networks*, 107:102219, 2020. [[CrossRef](#)].
- [9] Y. Bu, J. Lu, and V. V. Veeravalli. Model change detection with application to machine learning. In *ICASSP 2019 - 2019 IEEE International Conference on Acoustics, Speech and Signal Processing (ICASSP)*, pages 5341–5346, 2019. [[CrossRef](#)].
- [10] Ar drone 2 user guide and firmware. [<https://www.parrot.com/en/support/documentation/ar-drone>].
- [11] Wikimedia Commons. File:parrot ar.drone 2.0 take-off, nevada.jpg — wikimedia commons, the free media repository, 2020. https://commons.wikimedia.org/wiki/File:Parrot_AR.Drone_2.0_take-off,_Nevada.jpg (Accessed on January 1, 2023).

- [12] Wikimedia Commons. File:parrot ar.drone 2.jpg — wikimedia commons, the free media repository, 2020. https://commons.wikimedia.org/wiki/File:Parrot_AR.Drone_2.JPG (Accessed on January 1, 2023).
- [13] L. R. Pinto, L. Almeida, and A. Rowe. Balancing packet delivery to improve end-to-end multi-hop aerial video streaming. In Anibal Ollero, Alberto Sanfeliu, Luis Montano, Nuno Lau, and Carlos Cardeira, editors, *ROBOT 2017: Third Iberian Robotics Conference*, pages 807–819, Cham, 2018. Springer International Publishing. [[CrossRef](#)].
- [14] C. Guo, J. Zhou, P. Pawelczak, and R. Hekmat. Improving packet delivery ratio estimation for indoor ad hoc and wireless sensor networks. In *2009 6th IEEE Consumer Communications and Networking Conference*, pages 1–5, 2009. [[CrossRef](#)].
- [15] M. Jacobsson and C. Rohner. Estimating packet delivery ratio for arbitrary packet sizes over wireless links. *IEEE Communications Letters*, 19(4):609–612, 2015. [[CrossRef](#)].
- [16] L. R. Pinto, L. Almeida, H. Alizadeh, and A. Rowe. Aerial video stream over multi-hop using adaptive tdma slots. In *2017 IEEE Real-Time Systems Symposium (RTSS)*, pages 157–166, 2017. [[CrossRef](#)].
- [17] Luis Oliveira, Luis Almeida, and Pedro Lima. Multi-hop routing within tdma slots for teams of cooperating robots. In *2015 IEEE World Conference on Factory Communication Systems (WFCS)*, pages 1–8, 2015. [[CrossRef](#)].
- [18] L. Almeida and L. Santos, F. Oliveira. *Structuring Communications for Mobile Cyber-Physical Systems*, pages 51–76. Springer International Publishing, Cham, 2016. [[CrossRef](#)].
- [19] D. Almeida, M. G. Gaitán, P. d’Orey, P. M. Santos, L. R. Pinto, and L. Almeida. Demonstrating ra-tdmas+ for robust communication in wifi mesh networks. In CISTER Research Center, editor, *Demo in 42nd IEEE Real-Time Systems Symposium (RTSS 2021). 7, Dec, 2021, RTSS@Work. Dortmund*. CISTER-TR-211007, 2021. [[CISTER](#)].
- [20] L. R. Pinto and L. Almeida. A robust approach to tdma synchronization in aerial networks. *Sensors*, 18(12), 2018. [[CrossRef](#)].
- [21] Swiftnav. Piksi multi. <https://www.swiftnav.com/piksi-multi> (Accessed on January 1, 2023).
- [22] N. A. Famiglietti, G. Cecere, C. Grasso, A. Memmolo, and A. Vicari. A test on the potential of a low cost unmanned aerial vehicle rtk/ppk solution for precision positioning. *Sensors*, 21(11), 2021. [[CrossRef](#)].
- [23] S. R. Shaw and C. R. Laughman. A method for nonlinear least squares with structured residuals. *IEEE Transactions on Automatic Control*, 51(10):1704–1708, 2006. [[CrossRef](#)].

- [24] R. Andrae, T. Schulze-Hartung, and P. Melchior. Dos and don'ts of reduced chi-squared, 2010. [[CrossRef](#)].
- [25] K. Madsen, H. B. Nielsen, and O. Tingleff. *Methods for Non-Linear Least Squares Problems*. Technical University of Denmark, Lyngby, Denmark, 01 2004. [[dtu.dk](#)].
- [26] K. Levenberg. A method for the solution of certain non-linear problems in least squares. *Quarterly of Applied Mathematics*, 2(2):164–168, 1944. [[CrossRef](#)].
- [27] D. W. Marquardt. An algorithm for least-squares estimation of nonlinear parameters. *Journal of the Society for Industrial and Applied Mathematics*, 11(2):431–441, 1963. [[CrossRef](#)].
- [28] J. J. Moré. The levenberg-marquardt algorithm: Implementation and theory. In G. A. Watson, editor, *Numerical Analysis*, pages 105–116, Berlin, Heidelberg, 1978. Springer Berlin Heidelberg. [[CrossRef](#)].
- [29] J. J. Moré. *Recent Developments in Algorithms and Software for Trust Region Methods*, pages 258–287. Springer Berlin Heidelberg, Berlin, Heidelberg, 1983. [[CrossRef](#)].
- [30] H. Liu. On the levenberg-marquardt training method for feed-forward neural networks. In *2010 Sixth International Conference on Natural Computation*, volume 1, pages 456–460, 2010. [[CrossRef](#)].
- [31] C. Ma and L. Jiang. Some research on levenberg–marquardt method for the nonlinear equations. *Applied Mathematics and Computation*, 184(2):1032–1040, 2007. [[CrossRef](#)].
- [32] J. Fan and J. Pan. A note on the levenberg–marquardt parameter. *Applied Mathematics and Computation*, 207(2):351–359, 2009. [[CrossRef](#)].
- [33] C. B. Markwardt. Non-Linear Least Squares Fitting in IDL with MPFIT. In D. Bohlender, P. Dowler, and D. Durand, editors, *Astronomical Data Analysis Software and Systems XVIII*, volume 411 of *ASP Conference Series*, pages 251–254, San Francisco, 2009. Astronomical Society of the Pacific. [[CrossRef](#)].
- [34] C. B. Markwardt. *MPFIT*. [<http://purl.com/net/mpfit>].
- [35] F. Lu, H. Zhang, W. Li, Z. Zhou, C. Zhu, C. Cheng, Z. Deng, X. Chen, and C. C. Mi. A high-efficiency and long-distance power-relay system with equal power distribution. *IEEE Journal of Emerging and Selected Topics in Power Electronics*, 8(2):1419–1427, 2020. [[CrossRef](#)].
- [36] Wikimedia Commons. File:castel restor by drone 03.jpg — wikimedia commons, the free media repository, 2022. https://commons.wikimedia.org/wiki/File:Castel_Restor_by_drone_03.jpg (Accessed on January 1, 2023).

- [37] MATLAB. *9.12.0.2039608 (R2022a)*. The MathWorks Inc., Natick, Massachusetts, 2022. [<https://www.mathworks.com/>].
- [38] H. Chen, P. T. Reiss, and T. Tarpey. Optimally weighted $l(2)$ distance for functional data. *Biometrics*, 70(3):516–525, 2014. [[CrossRef](#)].